Université de Montréal

# DONNÉES NOUVELLES SUR LES INNERVATIONS CHOLINERGIQUES DE L'HIPPOCAMPE ET DU NÉOSTRIATUM, ET SUR LEUR ULTRASTRUCTURE AU COURS DU DÉVELOPPEMENT

par

**NICOLAS AZNAVOUR**

Départements de pathologie et biologie cellulaire[5] et centre de recherche en sciences neurologiques

Faculté de médecine

Thèse présentée à la Faculté des études supérieures, en vue de l'obtention du grade de Philosophiæ Doctor (Ph.D.) en sciences neurologiques

Septembre 2004

Université de Montréal

Faculté des études supérieures

Cette thèse de doctorat intitulée :

**Données nouvelles sur les innervations cholinergiques de l'hippocampe et du neostriatum, et sur leur ultrastructure au cours du développement**

présentée par

**NICOLAS AZNAVOUR**

a été évaluée par un jury composé des personnes suivantes :

**VINCENT CASTELLUCCI**
Président rapporteur

**LAURENT DESCARRIES**
Directeur de recherche

**JEAN-CLAUDE LACAILLE**
Membre du jury

**RÉMI QUIRION**
Examinateur externe



Représentant du doyen de la FES

## SOMMAIRE

Cette thèse présente une série d'études immunocytochimiques en microscopie photonique et électronique, dont le principal objectif était d'améliorer nos connaissances de la distribution et de l'ultrastructure des innervations cholinergiques de l'hippocampe et du néostriatum, particulièrement au cours du développement de ces régions cérébrales. Grâce la disponibilité d'un anticorps monoclonal à haute affinité, levé contre la molécule entière de l'enzyme de synthèse de l'acétylcholine (ACh) : la choline acétyltransférase (ChAT; courtoisie de Costantino Cozzari et Boyd K Hartman), nous avons pu d'abord examiner et quantifier, en microscopie optique, la distribution du réseau axonal cholinergique de l'hippocampe du rat et de la souris adultes, ainsi que du rat en développement, puis visualiser et analyser, en microscopie électronique, la structure fine des varicosités (ou terminaisons) axonales cholinergiques de l'hippocampe et du néostriatum en développement chez le raton.

Lors d'une première étude (publiée en 2002 dans *Hippocampus*), nous avons obtenu des données chiffrées sur la densité régionale et laminaire d'innervation cholinergique (ChAT-immunoréactive) dans trois secteurs de l'hippocampe dorsal (CA 1, CA3 et gyrus dentelé) du rat et de la souris adultes. Pour ce faire, nous avons déterminé au préalable, dans chaque couche et chaque secteur de l'hippocampe des deux espèces, le nombre moyen de varicosités par unité de longueur d'axone

immunoréactif, qui est apparu constant (4 varicosités par 10 µm d'axone). Les densités d'innervation cholinergique ont pu alors être exprimées en mètres d'axone et en millions de varicosités par $mm^3$ de tissu. L'innervation ACh de l'hippocampe s'est ainsi avérée relativement dense, avec certaines différences entre le rat et la souris, notamment dans CA1. Les données quantitatives sur sa distribution ont pu être reliées à d'autres paramètres de structure et de fonction cholinergiques, pour souligner la divergence et l'ubiquité de cette innervation en regard du rôle neuromodulateur de l'ACh dans l'hippocampe adulte.

Dans un deuxième temps (article sous presse dans *The Journal of Comparative Neurology*), nous avons employé la même méthode pour 1) examiner et mesurer, en microscopie optique, la croissance de l'innervation cholinergique de l'hippocampe dorsal en développement chez le raton, et 2) visualiser et caractériser, en microscopie électronique, ses varicosités axonales cholinergiques, à trois âges postnataux : P8, P16 et P32. En l'absence de données morphologiques antérieures, ce travail a montré que l'innervation cholinergique de l'hippocampe se développe plus précocement et plus rapidement qu'on ne le soupçonnait auparavant, et que, dès son apparition et tout au cours de sa croissance, ses varicosités axonales présentent des caractéristiques ultrastructurales intrinsèques et relationnelles comparables à celles de l'adulte. Il s'agit d'une innervation largement asynaptique, dont les varicosités sont dotées de tous les organites nécessaires à la synthèse, au stockage et à la

libération de l'ACh. La première partie de l'étude met ainsi en relief les remarquables propriétés de croissance des neurones cholinergiques qui innervent l'hippocampe, alors que sa seconde partie suggère que la neurotransmission diffuse puisse jouer un rôle prédominant dans les effets généraux exercés par l'ACh au cours du développement de cette région cérébrale, tel que précédemment constaté dans le néocortex.

Dans un troisième temps (article publié en 2003 dans *The Journal of Comparative Neurology*), nous avons examiné l'ultrastructure de l'innervation cholinergique du néostriatum du rat, aux mêmes âges postnataux : P8, P16 et P32. Ici encore, des données chez l'adulte, précédemment obtenues au laboratoire, pouvaient servir de point de référence. Dans cette région anatomique, où l'innervation cholinergique est particulièrement dense et provient essentiellement d'interneurones plutôt que de neurones de projection, nous avons à nouveau documenté des caractéristiques intrinsèques et relationnelles d'un système fonctionnel majoritairement asynaptique. Compte tenu de la très forte densité de l'innervation ACh striatale, cette constatation renforce l'hypothèse d'un niveau ambiant d'ACh, maintenu en permanence dans l'espace extracellulaire, et associé à une transmission diffuse par l'ACh, au cours du développement comme chez l'adulte. Cette hypothèse laisse prévoir que, dans le néostriatum en développement, tout comme dans l'hippocampe, la distribution subcellulaire de plusieurs sous-types de récepteurs de l'ACh sera largement extrasynaptique et intéressera une

grande variété d'éléments cellulaires, ce que laissent déjà supposer les rares données disponibles chez l'adulte. Il faudra sans doute tenir compte de cette réalité pour mieux comprendre les effets de l'ACh (et donc des interneurones cholinergiques) dans le striatum en développement.

**Mots clés**: Acétylcholine, axone, choline acétyltransférase, développement, hippocampe, immunocytochimie, innervation, néostriatum, quantification.

## SUMMARY

This thesis presents a series of light and electron microscopic immunocytochemical studies, mainly aimed at improving current knowledge of the distribution and ultrastructural features of the cholinergic innervations in hippocampus and neostriatum, particularly during the development of these brain regions. Owing to the availability of a highly sensitive antibody, raised against the whole molecule of the biosynthetic enzyme of acetylcholine (ACh): choline acetyltransferase (ChAT; courtesy of Costantino Cozzari and Boyd K Hartman), we were able, first, to examine and quantify, at light microscopic level, the distribution of the cholinergic axon network in the hippocampus of adult rat and mouse, as well as of postnatal rat, and then to visualize and analyze, at the electron microscopic level, the fine structure of cholinergic axon varicosities (or terminals) in the developing hippocampus and neostriatum of postnatal rat.

In a first study (published in Hippocampus, 2002), we obtained quantitative data on the regional and laminar density of ACh (ChAT-immunoreactive) innervation in three sectors of the dorsal hippocampus (CA1, CA3 and the dentate gyrus) of adult rat and mouse. To this end, we determined beforehand, in each layer and sector of hippocampus in both species, the average number of varicosities per unit length of immunostained axon, which turned out to be constant (4 varicosities per 10 μm of axon). It was then possible to express the density of cholinergic

innervation in meters of axon and in millions of varicosities per $mm^3$ of tissue. The ACh innervation of hippocampus was thus described as relatively dense, with some differences between the two species, notably in CA1. The quantitative data could be related to other structural and functional cholinergic parameters, to emphasize the widespread and ubiquitous distribution of this ACh innervation, in keeping with its neuromodulatory role in the adult hippocampus.

In a second study (submitted to *The Journal of Comparative Neurology*, 2004), the same method was used to 1) examine and measure, at light microscopic level, the growth of the ACh innervation in the developing dorsal hippocampus of rat, and 2) visualize and characterize, at electron microscopic level, the ultrastructure of these ACh axon varicosities at postnatal ages P8, P16 and P32. In the absence of prior morphological data, this study demonstrated that the development of the hippocampal cholinergic innervation is more precocious and rapid than was previously suspected, and that, as soon as it appears and throughout its growth, its varicosities display intrinsic and relational features similar to those in adult. It is a largely asynaptic innervation, the varicosities of which are endowed with all organelles required for the synthesis, storage and release of ACh. Thus, the first part of the study underlined the extraordinary growth capacities of the ACh neurons innervating hippocampus, whereas its second part suggested that diffuse neurotransmission may play an important role in the general

effects of ACh during the development of this brain region, as previously established in the neocortex.

In a third study (published in 2003, in *The Journal of Comparative Neurology*), we have examined the ultrastructural features of the cholinergic innervation in rat neostriatum, at the same postnatal ages: P8, P16 and P32. Here again, data from the adult, previously obtained in our laboratory, could be used as reference point. In this anatomical region, where the ACh innervation is particularly dense and emerges from a small population of local interneurons rather than projection neurons, we again documented intrinsic and relational features of a largely asynaptic functional system. In view of the extremely high density of the striatal ACh innervation, these observations reinforced the hypothesis of an ambient level of ACh, permanently maintained in the extracellular space, and associated with a diffuse transmission by ACh during development as well as in the adult. This hypothesis predicts that, in the developing neostriatum, much like in hippocampus, the subcellular localization of many ACh receptors will be found to be mostly extrasynaptic and to involve a wide variety of cellular elements, in keeping with the rare ultrastructural data already available in the adult. These observations will need to be taken into account to better understand the effects of ACh (and thus of ACh interneurons) in the developing neostriatum.

**Keywords**: Acetylcholine, axon, choline acetyltransferase, development, hippocampus, immunocytochimistry, innervation, neostriatum, quantification.

# TABLE DES MATIÈRES

# LISTE DES TABLEAUX

## Chapitre II



## Chapitre III



## Chapitre IV

## LISTE DES FIGURES

### Chapitre II



### Chapitre III

## LISTE DES ABRÉVIATIONS

| | |
|---|---|
| 5-HT | 5-hydroxytryptophane |
| ACh | acétylcholine |
| AChE | acétylcholinestérase |
| ANOVA | analyse de variance |
| BDNF | *brain-derived neurotrophic factor* |
| BSA | *bovine serum albumine* |
| ChAT | choline acétyltransférase |
| DAB | *3,3 diaminobenzidine tetrahydrochloride* |
| GABA | *gamma amino butyric acid* |
| HACU | *high-affinity choline uptake* |
| KPB | *potassium phosphate buffer* |
| NGF | *neurotrophic growth factor* |
| NHS | *normal horse serum* |
| NT3 | *neurotrophin 3* |
| Par1 | cortex pariétal (somatosensoriel) |
| PBS | *phosphate buffer saline* |
| PFA | paraformaldéhyde |
| SNC | système nerveux central |
| vAChT | *vesicular ACh transporter* |
| VIP | *vasoactive intestinal peptide* |

## REMERCIEMENTS

Je ne peux trouver de mots assez forts pour exprimer la reconnaissance que j'éprouve envers Laurent Descarries qui s'est toujours montré gentil, patient et n'a jamais cessé de me soutenir au cours des cinq années passées dans son laboratoire. J'espère avoir su m'imprégner suffisamment de son perfectionnisme et de son ardeur au travail pour me montrer un jour à la hauteur de son enseignement.

Je voudrais remercier Naguib Mechawar qui m'a initié à la recherche au laboratoire et qui m'a toujours témoigné une amitié sincère. Grâce à sa finesse et à son goût immodéré pour la recherche, il aura su me conseiller judicieusement et vaincre mes moindres incertitudes.

Merci à Mustapha Riad pour son aide indéfectible, sa générosité et son amitié.

Enfin, merci aux membres de mon jury d'avoir accepté d'évaluer ma thèse.

# Chapitre I

# INTRODUCTION GÉNÉRALE

## I.1 PRÉSENTATION DE L'OUVRAGE

Cette thèse comprend cinq chapitres. Le premier est une Introduction générale, qui présente les deux régions anatomiques du cerveau auxquelles nos travaux ont été consacrés : l'hippocampe et le neostriatum. Cette double introduction cherche à situer les résultats obtenus dans un contexte fonctionnel. Sa première partie débute par un rappel des jalons historiques pertinents, en ce qui a trait aux rôles attribués au neurotransmetteur acétylcholine (ACh) dans le système nerveux central, puis donne un aperçu de son organisation générale dans le cerveau, dont la connaissance est plus récente. Sont ensuite revues successivement i) les données actuelles sur les sources de l'innervation ACh de l'hippocampe, ii) les méthodes neuronochimiques qui permettent de visualiser cette innervation aux échelons cellulaire et subcellulaire et iii) les quelques renseignements actuellement disponibles sur la localisation cellulaire et subcellulaire des récepteurs ACh dans l'hippocampe. Une dernière section de cette première partie revoit le petit nombre de données concernant l'ontogenèse des divers paramètres et de l'innervation cholinergiques de l'hippocampe, en insistant plus particulièrement sur les rôles attribués à l'ACh au cours du développement de cette région cérébrale.

La deuxième partie de ce chapitre introductif traite de l'origine anatomique de l'innervation ACh du néostriatum, des données disponibles sur la localisation cellulaire et subcellulaire des récepteurs ACh et des rares connaissances actuelles sur l'ontogenèse des différents paramètres

cholinergiques et de cette innervation elle-même au cours du développement. Le chapitre se termine sur l'énonciation des objectifs spécifiques de la recherche.

Les trois chapitres suivants sont présentés sous forme d'articles de recherche originaux, dont les deux premiers sont déjà parus et le troisième est soumis pour publication. Le Chapitre 2 traite de la distribution de l'innervation cholinergique de l'hippocampe chez le rat et chez la souris adultes; le Chapitre 3, de la croissance et de l'ultrastructure de l'innervation cholinergique au cours du développement postnatal de l'hippocampe chez le rat; le Chapitre 4, de la croissance et de l'ultrastructure de l'innervation cholinergique du néostriatum, au cours de son développement postnatal chez le rat

Enfin le chapitre de Discussion générale rappelle les principaux résultats ainsi obtenus et les situe dans un contexte plus général, de manière à pouvoir en dégager toute la signification et la portée éventuelles, tant aux plans méthodologique que conceptuel.

Une annexe présente d'autres articles auxquels nous avons participé, qui ont exploité les avancées méthodologiques et certaines des connaissances acquises lors des travaux de cette thèse.

## I.2 JALONS HISTORIQUES

Oswald Schmiedeberg, un pionnier de la pharmacologie moderne, a démontré le premier, en 1869, que l'application d'un alcaloïde appelé "muscarine", provenant du champignon *Amanita muscaria*, avait un effet analogue à celui d'une stimulation électrique du nerf vagal sur le cœur des vertébrés (Scheindlin, 2001). Par la suite, un de ses étudiants, Reid Hunt, isola l'ACh et remarqua que cette substance induisait chez l'animal une bradycardie et une diminution de la pression sanguine (Hunt and Taveau, 1906). Durant la même période, Sir Henry Dale entreprit ses travaux sur les propriétés pharmacologiques de l'ergot du seigle. Avec l'aide de ses collaborateurs, il isola l'ACh à partir d'extraits d'ergot du seigle et put ainsi caractériser ses propriétés chimiques et sa structure (Barger and Dale, 1910-1911; Dale, 1914a; Ewins, 1914). Ces études furent possibles du fait que l'ACh isolée dans ces extraits était stable, parce que produite par la bactérie *Bacillus acetycholini*, laquelle ne synthétise pas d'enzyme de dégradation rapide de l'ACh. Par la suite, Sir Henry Dale reproduisit les résultats obtenus par Reid Hunt (Dale, 1914a) et démontra aussi des effets "parasympathomimétiques" de l'ACh sur le cœur, analogues à ceux de l'application de muscarine, alors qu'en présence d'atropine, l'ACh possédait une action "sympathomimétique" semblable à celle induite par l'application de nicotine (Dale, 1914a ; Dale 1936). Ces observations, à l'origine de la classification actuelle des récepteurs ACh, nicotiniques et muscariniques, l'amenèrent à suggérer que la courte durée

d'action de l'ACh était probablement imputable à la présence d'une estérase éliminant rapidement cette molécule du milieu (Dale, 1914a,b). Quelques années plus tard, Otto Loewi (1921) démontra expérimentalement que la substance libérée par le nerf vague, et qui fut par la suite identifiée comme étant l'ACh (Loewi and Navratil, 1926), induisait un ralentissement de l'activité cardiaque. Dans les années trente, Chang et Gaddum (1933), puis Quastel et collaborateurs (1936), mirent respectivement en évidence la présence et une synthèse de l'ACh dans le cerveau des mammifères. En 1943, Nachmansohn et Machado identifièrent l'enzyme de synthèse de l'ACh comme étant la choline acétyltransférase (ChAT). Cependant, la démonstration d'une libération d'ACh dans le cerveau ne vint qu'une décennie plus tard, par MacIntosh et Oborin (1953). Depuis ces travaux pionniers, il a été établi que l'ACh cérébrale est impliquée dans plusieurs processus cognitifs et neuropathologiques chez l'animal et l'humain.

## 1.3 ORGANISATION GÉNÉRALE DU SYSTÈME CHOLINERGIQUE CENTRAL

Selon la nomenclature introduite par Mesulam et al. (1983), on reconnaît aujourd'hui l'existence de six regroupements distincts de corps cellulaire neuronaux ACh dans le cerveau du rat et du singe. En raison de l'hétérogénéité de composition des régions qui les abritent, ces noyaux ACh ont reçu une désignation alphanumérique. Quatre de ces groupes sont télencéphaliques et deux rhombocéphaliques. Ch1 et Ch2 sont respectivement situés dans le

septum médian et dans le membre vertical de la bandelette diagonale de Broca. Leurs neurones constituent la principale source d'innervation ACh de l'hippocampe et se projettent aussi vers le cortex rhinal et le noyau interpédonculaire (Woolf et al., 1991). Chez le rat, ils représentent 30 à 50% de la population neuronale du septum médian et 50 à 75% de celle du membre vertical de la bandelette diagonale de Broca (Rye et al., 1984). Ch3 appartient au membre horizontal de la bandelette diagonale de Broca. Ses neurones représentent 10 à 20% de la population neuronale de la région (Rye et al., 1984) et leurs efférences innervent surtout le bulbe olfactif (Mesulam et al., 1983).

Le complexe substantia innominata-noyau basalis de Meynert" ou Ch4 constitue la principale source d'innervation du cortex cérébral et de l'amygdale. Chez le rat, ses neurones représentent de 65 à 90% de la population neuronale du noyau, soit 7000 à 9000 neurones de chaque côté du cerveau. Quant aux neurones ACh du tronc cérébral, Ch5-6, ils se projettent majoritairement aux différentes parties du thalamus, parmi lesquelles figurent les noyaux antérieur, latéral et réticulaire. Leurs corps cellulaires font partie des noyaux pedunculopontin, cunéiforme et de l'aire parabrachiale (Ch5), ainsi que du noyau tegmentaire dorso-latéral (Ch6).

Une seconde composante du système cholinergique est représentée par des interneurones locaux. Comme nous le verrons plus loin, ceux-ci sont à l'origine de l'essentiel de l'innervation cholinergique hyperdense du striatum,

alors que, dans le cortex cérébral et l'hippocampe, leur contribution est modeste (Johnston et al., 1981 ; Gage et al., 1986).

## I.4 INNERVATION CHOLINERGIQUE DE L'HIPPOCAMPE

### I.4.1 Origine anatomique de l'innervation cholinergique de l'hippocampe

Il est bien établi que l'innervation ACh de l'hippocampe provient majoritairement de corps cellulaire neuronaux situés dans le septum médian et le membre vertical de la bandelette diagonale de Broca (Rye et al., 1984; Amaral and Kurz, 1985; Nyakas et al., 1987; Woolf, 1991). Chez la souris, ces cellules seraient au nombre de 250 de chaque côté du cerveau (Schwegler et al., 1996), et de 385 chez le rat (Mc Kinney et al., 1983). Leurs axones s'arborisent dans toutes les régions et couches de l'hippocampe sous forme d'un réseau plus ou moins dense dont nous verrons plus loin les caractéristiques (Aznavour et al., 2002). Une deuxième source mineure d'innervation est intrinsèque et provient d'interneurones bipolaires (Houser et al., 1983; Frotscher et al., 1986; Blaker et al., 1988), dont la plupart des corps cellulaires se retrouve à proximité de la fissure de l'hippocampe, c'est-à-dire dans la couche lacunosum moleculare de CA1 ou la couche moléculaire du gyrus dentelé (DG) (Aznavour et al., 2002). Par suite de lésion des neurones cholinergiques du prosencéphale basal, il a été déterminé que ces interneurones ne contribuent que pour un faible pourcentage à l'activité de l'enzyme de biosynthèse ChAT dans l'hippocampe du rat (5-10%; Gage et al., 1983).

### I.4.2 Visualisation de l'innervation cholinergique de l'hippocampe

Malgré le nombre et la qualité des études consacrées aux rôles de l'ACh dans une région du cerveau aussi bien connue que l'hippocampe, nous n'avons trouvé aucune donnée quantitative sur la distribution de son innervation ACh avant la réalisation de nos travaux. De plus l'utilité de la très grande majorité des descriptions antérieures se trouvait limitée par leur emploi de l'acétylcholinestérase (AChE) comme indicateur d'identité de neurotransmission. Or, il est désormais reconnu que cette enzyme est exprimée par différents types de neurones non-ACh, tant au cours du développement que chez l'adulte (Butcher et al., 1975, Robertson and Gorenstein, 1987; Robertson et al., 1989; Schlagger et al., 1993). On ne saurait donc considérer l'AChE comme un marqueur fiable et rigoureux de l'identité ACh des neurones.

Ce n'est qu'il y a une vingtaine d'années que des anticorps spécifiques dirigés contre la ChAT ont pu être produits et utilisés à des fins de marquage et d'analyse immunocytochimiques. À partir de 1990 la disponibilité d'un anticorps monoclonal à très haute affinité, dirigé contre la molécule entière de ChAT (Cozzari et al., 1990), a permis la réalisation de plusieurs études dans notre laboratoire, visant à caractériser la distribution et les propriétés ultrastructurales de l'innervation ACh de plusieurs régions du cerveau (Chédotal et al., 1994; Umbriaco et al., 1994, 1995; Contant et al., 1996; Mechawar et al., 2000; Mechawar et Descarries, 2001; Mechawar et al., 2002). Ces études ont

notamment révélé que, dans toutes les régions étudiées (cortex cérébral, hippocampe, néostriatum), une très faible proportion des varicosités axonales (terminaisons) ACh, était munie d'une jonction membranaire synaptique. Dans le cortex frontal et pariétal, le cortex entorhinal, l'hippocampe et le néostriatum du rat adulte, ces terminaisons dépourvues de jonctions synaptique représentent respectivement plus de 86, 91, 93 et 91% du nombre total des varicosités ACh (voir Descarries et Mechawar, 2002). Deux principales conclusions ont été tirées de ces données. La première veut que l'ACh, comme d'autres monoamines, puisse diffuser dans le milieu extracellulaire après sa libération et agir ainsi sur une variété de cibles cellulaires situées à une distance relativement importante des sites de libération. Il s'agit ici du concept de transmission diffuse ou transmission volumique (Descarries et al., 1997). La deuxième conclusion, élaborée dans de nombreuses publications, est celle de l'existence probable d'un faible niveau ambiant d'ACh, maintenu en permanence dans les régions du cerveau densément innervées en ACh, comme le cortex, l'hippocampe et surtout le néostriatum (Descarries, 1998). Cette faible concentration ambiante d'ACh rendrait compte des mesures par microdialyse d'un niveau basal d'ACh de l'ordre du nanomolaire dans plusieurs régions du cerveau du rat (voir Descarries et al., 1997). Il s'agirait de concentrations suffisantes pour moduler l'activité de certains récepteurs cholinergiques à haute affinité dans le cerveau (Alkondon et Albuquerque, 2004), expliquant notamment le maintien de fonctions modulées par l'ACh

même à la suite de lésions ou de dégénérescences de l'ordre de 50 à 75% du système cholinergique.

### I.4.3 Les récepteurs cholinergiques de l'hippocampe

Il est aussi connu que l'ACh agit sur une variété de récepteurs nicotiniques et muscariniques largement distribués dans l'hippocampe. Les données sur la distribution cellulaire et sub-cellulaire de ces récepteurs sont demeurées fragmentaires pendant longtemps, en raison du manque de spécificité des ligands utilisés en autoradiographie, de même que de la plupart des anticorps utilisés pour l'immunocytochimie. Plus récemment, la levée d'anticorps spécifiques, du moins contre les récepteurs muscariniques, l'utilisation d'enregistrements électrophysiologiques, ainsi que le développement de la PCR pour des cellules individuelles, ont permis d'établir une cartographie fonctionnelle de la distribution des récepteurs ACh dans l'hippocampe.

Les récepteurs nicotiniques sont des récepteurs pentamériques activés par un ligand et couplés à un canal ionique perméable aux cations ($Na^+$, $K^+$, $Ca^{2+}$). À ce jour, douze sous-unités ont été identifiées ($\alpha2$- $\alpha10$; $\beta2$- $\beta4$) pouvant former une grande variété de récepteurs (McGehee, 1999; Lips et al., 2002). Toutefois, l'hétéropentamère $\alpha4\beta2$ et l'homopentamère $\alpha7$ constituent une forte majorité des récepteurs nicotiniques présents dans l'hippocampe (Sargent et al., 1993). Tels que visualisés par autoradiograghie ou immunocytochimie, ces récepteurs apparaissent principalement localisés dans le soma des cellules principales de

l'hippocampe (Séguéla et al., 1993; Hill et al., 1993; Dominguez del Toro et al., 1994), même si leur fonctionnalité n'a pas été démontrée. Des études indiquent également la présence de récepteurs nicotiniques fonctionnels sur les terminaisons glutamatergiques de l'hippocampe, où leur activation stimule la libération du glutamate (Radcliffe et Dani, 1998; Radcliffe et al., 1999). La distribution des récepteurs nicotiniques de l'hippocampe ne se limite à ses cellules principales, puisqu'une proportion importante des interneurones GABAergiques de CA1 exprimerait la sous-unité $\alpha 7$ (Sudweeks et Yakel, 2000) et que le tiers des interneurones GABAergiques, dont les corps cellulaires sont présents dans la *stratum radiatum* de CA1, exprimerait la sous-unité $\alpha 4\beta 2$ (Alkondon et Albuquerque, 2004). Ainsi, la stimulation de récepteurs nicotiniques présents à la surface des interneurones GABAergiques exercerait à la fois une action inhibitrice et désinhibitrice sur les neurones pyramidaux, la première étant directe et la seconde via d'autres interneurones GABAergiques (Alkondon et Albuquerque, 2004).

Les récepteurs muscariniques sont des récepteurs couplés aux protéines G, qui ont une activité modulatrice dans l'hippocampe. L'utilisation du clonage moléculaire à révélé l'existence de cinq sous-types m1 à m5 dont les séquences transmembranaires sont hautement conservées (Kubo et al., 1986; Bonner et al., 1987; Buckley et al., 1988). m1, m2 et m4 représentent respectivement 36, 33 et 27% des récepteurs muscariniques de l'hippocampe, tel que mesuré par immunoprécipitation quantitative chez le rat (Levey et al., 1991). m1 active la

voie de la phospholipase C, alors que m2 et m4 inhibent l'activité de l'adényl cyclase. De plus ces récepteurs contribuent à la modulation de nombreux canaux ioniques et participent à la régulation de l'activité neuronale dans l'hippocampe (voir Volpicelli et Levey, 2004). m1 se retrouve principalement sur les corps cellulaires et les dendrites des cellules pyramidales (Levey et al., 1991; Levey et al., 1995a). La distribution du récepteur m2 ressemble à celle de l'innervation ACh dans CA1 et CA3, en raison de son rôle comme autorécepteur terminal, mais ce sous-type serait également présent sur les terminaisons glutamatergiques et GABAergiques de l'hippocampe (Levey et al., 1995b; Rouse et al., 2000). m4 apparaît distribué dans tout le neuropile de l'hippocampe et présent en plus forte concentration dans le tiers interne de la couche moléculaire du gyrus dentelé, où il agirait en tant qu'hétérorécepteur terminal des voies perforante, associative et commissurale (Rouse et al., 1997; Rouse et al., 1999).

### I.4.4 Les rôles de l'acétylcholine dans l'hippocampe

Un grand nombre d'études neurophysiologiques, pharmacologiques, comportementales et cliniques concourent à démontrer un rôle crucial de l'ACh hippocampique dans des processus cognitifs comme l'attention, l'apprentissage et la mémoire.

Un des premiers indices de l'implication de l'ACh dans ces processus a été fourni par trois études indépendantes, lesquelles ont rapporté presque

simultanément, l'existence d'une perte massive de neurones ACh dans le septum médian et le noyau basalis du cerveau de patients ayant souffert de la maladie d'Alzheimer (Bowen et al., 1976; Davies and Maloney, 1976; Perry et al., 1977). Ces observations ont contribué à l'émergence d'une hypothèse ACh de la maladie d'Alzheimer (Bartus et al., 1982; Perry, 1986; Bartus, 2000), alors que de nombreuses études faisaient état d'une altération de paramètres cholinergiques dans cette pathologie : diminution de l'activité de la ChAT (Perry et al., 1977; Rossor et al., 1982; Henke and Lang, 1983) ou de l'AChE (Henke and Lang, 1983); baisse de la teneur en ACh (Richter et al., 1980); réduction du nombre des récepteurs nicotiniques et muscariniques (Banerjee et al., 2000; Guan et al., 2000; Flynn et al., 1995; Rodriguez-Puertas et al., 1997); diminution de l'efficacité du couplage des récepteurs muscariniques aux protéines G (Jope et al., 1994; Ferrari-DiLeo et al., 1995; Ladner et al., 1995; Cowburn et al., 1996).

Certaines études ont aussi suggéré que le système cholinergique puisse être déjà affecté chez les patients souffrant d'atteinte cognitive mineure (*mild cognitive impairments*) (Beach et al., 2000). Ces troubles de l'attention et de la mémoire, qui se manifestent aux premiers stades de la maladie d'Alzheimer, peuvent être reproduits chez des sujets sains avec des antagonistes muscariniques comme l'atropine (Vogel et al., 1967; Higgins et al., 1989; Caldwell et al., 1992) ou la scopolamine (Buresova et al., 1986; Givens and Olton, 1990; Bymaster et al., 1993; Wallenstein and Vago, 2001; Atri et al., 2004).

Par aillleurs, des études par suite de lésions cytotoxiques (Hepler et al., 1985; Meck et al., 1987; Riekkinen et al., 1990) ou de l'administration d'agents cholinotoxiques (Leanza et al., 1996; Johnson et al., 2002; Ikonen et al., 2002; Lamprea et al., 2003; Lehmann et al., 2003) ont permis d'établir l'importance de l'intégrité du système cholinergique septo-hippocampique pour la réalisation de nombreuses tâches d'ordre cognitif chez l'animal. De plus, des traitements avec la nicotine (Jones et al., 1992; Levin et al, 1998; Kumari et al., 2003), les antagonistes muscariniques M2 (Quirion et al., 1995) ou les inhibiteurs de l'AChE (revu par Vesey et al., 2002) améliorent les performances cognitives, du moins chez l'animal.

Divers modèles ont été développés pour tenter d'expliquer comment l'ACh hippocampique peut contribuer à l'apprentissage. La libération importante d'ACh mesurée par microdialyse dans l'hippocampe lorsqu'un rat explore son environnement (Acquas et al., 1996; Aloisi et al., 1997; Thiel et al., 1998; Giovannini et al., 2001; Bianchi et al., 2003) induirait à la fois une dépolarisation des neurones pyramidaux (Halliwell and Adams, 1982) et une augmentation de leur fréquence de décharge en réponse à une stimulation (Cole and Nicoll, 1984; Madison and Nicoll, 1984; Madison et al., 1987). Dans ces conditions, l'ACh bloquerait aussi la libération de glutamate à partir des terminaisons des boucles de rétroaction intrinsèques excitatrices (Hasselmo and Schnell, 1994).

En plus de son action sur les cellules principales, l'ACh agit sur les interneurones GABAergiques de l'hippocampe (Pitler et Alger, 1992; Behrends et

ten Bruggencate, 1993), lesquels contribueraient d'une part à affiner la réponse des neurones pyramidaux lors d'une stimulation faible, par réduction de l'activité spontanée des cellules pyramidales, et d'autre part, à augmenter la fréquence de décharge des neurones pyramidaux, en réduisant leur libération de GABA en présence d'un stimulus fort. Selon Hasselmo et al., (1999), la convergence de ces effets de l'ACh réduit sélectivement l'activité intrinsèque (décharges spontanées, boucles de rétroaction), favorise l'encodage des informations afférentes corticales et permet d'améliorer la sélectivité des réponses de l'hippocampe à un stimulus. À l'inverse, il a également été proposé que la faible libération d'ACh mesurée lors de la survenue de rythmes lents pendant le sommeil, puisse contribuer à la consolidation des informations dans les circuits neuronaux de l'hippocampe, en favorisant l'activité des boucles de rétroaction intrinsèques excitatrices (Hasselmo et al., 2004).

Par ailleurs, en synchronisant l'activité des cellules principales de l'hippocampe et des interneurones GABAergiques, l'ACh induit la genèse de rythmes dans l'hippocampe. Ces propriétés traduiraient la distribution ubiquitaire de l'innervation ACh dans l'hippocampe, dont toutes les cellules peuvent potentiellement se trouver en présence de l'ACh. L'application d'agonistes muscariniques comme le carbachol, induit la genèse des rythmes $\delta$ (0.5-2 Hz), $\theta$ (4-10 Hz), $\beta$ (10-30 Hz) et $\gamma$ (30-80 Hz) (Monmaur and Breton, 1991; Fisahn et al., 1998; Fellous et al., 2000; Shimono et al., 2000), qui se manifestent normalement dans l'hippocampe du rat lorsque l'animal se livre à différentes

tâches comme la détection de signaux, l'exploration ou encore la reconnaissance d'un stimulus (voir Tiesinga et al., 2001). Ces rythmes semblent indispensables à plusieurs formes d'apprentissage (Wetzel et al., 1977; Winson, 1978) et facilitent l'induction de la potentialisation à long terme (LTP) dans l'hippocampe du rat (Pavlides et al., 1988; Orr et al., 2001; Hyman et al., 2003).

À l'échelon subcellulaire, les enregistrements électrophysiologiques réalisés sur des tranches d'hippocampe ont permis de mettre en évidence un rôle facilitateur de l'ACh (Blitzer et al., 1990; Watabe et al., 2000; Yun et al., 2000; Leung et al., 2003) dans l'induction de la dépression à long terme (LTD) et de la LTP, auxquelles contribuent les récepteurs nicotiniques (Fujii et al., 1999; Fujii and Sumikawa, 2001) et muscariniques (Williams and Johnston, 1988; Burgard and Sarvey, 1990 ; Auerbach and Segal, 1996). Cette action facilitatrice peut être bloquée par des agents cholinotoxiques comme l'AF64A (Maeda et al., 1994)) ou certains antagonistes muscariniques (Ito et al., 1988; Hirotsu et al., 1989; Tanaka et al., 1989; Katsuki et al., 1992; Sokolov and Kleschevnikov, 1995).

### I.4.5 Le développement de l'innervation cholinergique de l'hippocampe

Les neurones ACh du septum médian et du membre vertical de la bandelette diagonale de Broca verticale sont issus de cellules de l'éminence ganglionnaire (Semba et al., 2004) qui se différencient, selon un gradient caudo-rostral, entre le 12e et le 17e jour de vie embryonnaire (E12-17) (Semba and Fibiger, 1988; Koh and Loy, 1989). Les premiers neurones AChE et

ChAT-positifs apparaissent dans ces deux régions aux jours E16 (Milner, 1983) et E17 (Armstrong et al., 1987), respectivement. Leurs projections, marquées à l'aide d'un anticorps dirigé contre le récepteur p75-NGFR ou un traceur antérograde, atteignent l'hippocampe entre E17 et P1 (Koh and Loy, 1989; Linke and Frotscher, 1993). Durant cet intervalle, l'expression de la ChAT devient détectable par hybridation *in situ* dans les corps cellulaires ACh du septum médian et de la bandelette diagonale de Broca, puis elle augmente progressivement pour atteindre un niveau comparable à celui de l'adulte vers P16 (Bender et al., 1996). Tandis que les premières fibres marquées par histochimie pour l'AChE sont visibles dans les différentes couches de l'hippocampe à P1 (Nyakas et al., 1994), il a été rapporté que les fibres ChAT-positives visualisées par immunocytochimie n'apparaissent qu'à partir de la fin de la première semaine dans l'hippocampe (Henderson, 1991; Thal et al., 1992; Gould et al., 1991). De telles inconsistances soulignent l'absence de spécificité ou le manque de sensibilité des méthodes qui étaient disponibles.

Les données portant sur l'autoradiographie des transporteurs à haute affinité (HACU) et vésiculaire (vAChT) de l'ACh dans l'hippocampe postnatal sont disparates, en raison de la diversité des âges ou des couches examinées (Shelton et al., 1979; Happe and Murrin, 1992; Aubert et al., 1996). Il semblerait toutefois que la densité de ces sites de liaison soit élevée durant la gestation, déclinerait transitoirement dans les jours suivant la naissance et augmenterait

par la suite jusqu'à l'âge adulte (Happe and Murrin, 1992; Zahalka et al., 1993; Aubert et al., 1996).

### I.4.6 Les récepteurs cholinergiques dans l'hippocampe en développement

Il a été démontré que l'hippocampe possède des récepteurs nicotiniques et muscariniques fonctionnels dès les premiers jours suivant la naissance chez le rat.

L'expression du récepteur α7 et la radioliaison de l'($^3$H)α-bungarotoxine sont maximales, entre P0 et P10, selon les différentes couches de l'hippocampe. Par la suite, le niveau d'expression de ces deux récepteurs diminue progressivement pour atteindre des valeurs comparables à celles retrouvées chez l'adulte aux alentours de P20 (Shacka and Robinson, 1998; Zhang et al., 1998; Adams et al., 2002; Tribollet et al., 2004). Malheureusement, les données disponibles provenant de plusieurs études portant sur l'expression des sous-unités β2 et α4 (Shacka and Robinson, 1998; Zhang et al., 1998) ou la radiolisaison de l'($^3$H)epibatidine aux récepteurs α4β2 (Zhang et al., 1998; Tribollet el al., 2004) sont contradictoires et ne permettent pas de tirer de conclusion sur l'ontogénie des hétérorécepteurs nicotiniques dans l'hippocampe au cours du développement. Il est intéressant de noter qu'une radioliaison transitoirement élevée de la ($^3$H)nicotine est observée dans l'hippocampe, pendant la fin de la période de gestation, tant chez le rat (Zhang et al., 1998) que l'homme (Court et al., 1997, Hellstrom-Lindhal and Court, 2000).

Contrairement aux récepteurs nicotiniques, la densité des récepteurs muscariniques chez le rat, atteint le seuil de détectabilité par autoradiographie autour de la période périnatale, puis elle augmente progressivement jusqu'à l'âge adulte (Miyoshi et al., 1987; Balduini et al., 1993; Aubert et al., 1996). Ces récepteurs sont fonctionnels dès la première semaine postnatale, car l'application d'agonistes muscariniques sur des tranches de l'hippocampe préincubées dans une solution contenant de la ($^3$H)choline induit une inhibition croissante de la libération d'ACh évoquée de P4 à P16 (Goldbach et al., 1998). Il a également été démontré que l'application de muscarine à P5 réduit de 32% la pente des potentiels post-synaptiques évoqués (EPSPs) dans CA1 (Milburn and Prince, 1993), probablement par activation de récepteurs muscariniques situés sur les terminaisons glutamatergiques (Rouse et al., 2000).

### I.4.7 Les rôles de l'acétylcholine dans l'hippocampe en développement

Plusieurs études indiquent que l'ACh joue un rôle important dans la modulation de l'activité neuronale et de la plasticité synaptique, dès les premiers jours suivant la naissance.

Pendant la première semaine postnatale, l'ensemble du réseau neuronal de l'hippocampe est parcouru par des vagues synchronisées de dépolarisation, dénommées "potentiels de dépolarisation géants" (GDPs) (Ben-Ari et al., 1989). Ces potentiels, générés par l'action excitatrice du GABA sur les récepteurs $GABA_A$ (Cherubini et al., 1991), participeraient à la consolidation des

connexions synaptiques et à la maturation des circuits neuronaux dans l'hippocampe (Shatz, 1990). L'électrophysiologie sur tranches a permis de démontrer que la stimulation des récepteurs nicotiniques (Maggi et al., 2001) et muscariniques (Avignone and Cherubini, 1999) à l'aide d'agonistes spécifiques augmente la fréquence des GDPs, et qu'à l'inverse l'application d'antagonistes les abolit.

Une seconde caractéristique du développement postnatal, observée dans plusieurs régions du cerveau dont l'hippocampe, est la présence de synapses immatures. Plusieurs hypothèses ont été avancées pour expliquer comment ces synapses inactives deviendraient fonctionnelles, parmi lesquelles figurent : l'insertion de récepteurs AMPA au niveau des densités post-synaptiques, une augmentation de la probabilité de libération du glutamate et une augmentation de la quantité de glutamate par quantum (Voronin and Cherubini, 2003). Il a été récemment démontré que l'application brève de nicotine au niveau des collatérales de Schaffer suffit à induire une libération de glutamate et permet d'activer ces synapses dîtes "silencieuses" (Maggi et al., 2003). Ces effets seraient persistants et peuvent être reproduits en stimulant la libération endogène d'ACh. Ces observations suggèrent fortement que l'ACh participe à la maturation des contacts synaptiques dans l'hippocampe en augmentant leur efficacité de transmission. La distribution ubiquitaire de l'innervation ACh dans l'hippocampe pourrait s'avérer déterminante à cet égard.

## I.5 LE DÉVELOPPEMENT DE L'INNERVATION CHOLINERGIQUE DANS LE NÉOSTRIATUM

### 1.5.1 Origine anatomique de l'innervation cholinergique du néostriatum

L'innervation ACh du néostriatum émane presque exclusivement d'un nombre restreint d'interneurones non-épineux locaux, représentant 1.2 à 1.7% de la population neuronale de cette région du cerveau (Woolf and Butcher, 1981; Phelps et al., 1985). Une projection mineure, provenant du noyau pedonculopontin tegmentaire, a également été décrite chez le rat, mais son existence reste à confirmer (Woolf and Butcher, 1986). Les corps cellulaires de des interneurones cholinergiques sont distribués de façon relativement homogène dans le néostriatum, avec une densité moyenne de 10 à 18 corps cellulaires par $mm^2$ (Schwaber et al., 1987 ). Leur taille est comparable à celle des neurones ACh de projection du prosencéphale basal, avec une surface moyenne de section de 350 $\mu m^2$ (Phelps et al., 1985).

### 1.5.2 Distribution et ultrastructure de l'innervation ACh striatale chez le rat adulte

Contrairement à la distribution homogène de ses corps cellulaires d'origine, l'innervation ACh du néostriatum se distribue selon un gradient de densité croissant dans l'axe médio-latéral. Ce réseau axonal cholinergique se distingue de celui des autres régions du cerveau par son extrême densité. Cette densité

et sa distribution ubiquitaire suggèrent à elles seules que l'ACh puisse potentiellement agir sur tous les éléments cellulaires de la région.

Une seconde caractéristique de cette innervation est la finesse apparente de ses axones et la faible dimension de leurs varicosités axonales, dont le diamètre moyen est de 0.45 µm (Wainer et al., 1987 ; Contant et al., 1996). La très grande majorité (91.2%) de ces varicosités est asynaptique (Contant et al., 1996) et les rares varicosités ACh munies d'un complexe de jonction forment, le plus souvent, des contacts symétriques avec, en ordre décroissant, les branches dendritiques, les épines dendritiques et les corps cellulaires de neurones épineux (Phelps et al., 1985; Wainer et al., 1987; Izzo and Bolam, 1988; Pickel and Chan, 1990).

### I.5.3 Ontogénie des interneurones cholinergiques du néostriatum

Les interneurones ACh du néostriatum proviennent de cellules germinales de l'éminence ganglionnaire et des aires préoptiques/antérieures entopédonculaires, qui, par suite d' une migration tangentielle par rapport au striatum (Marin et al., 2000), se différencient de E11 à E18, suivant un axe caudo-rostral et latéro-médian (Semba et al., 1988; Phelps et al., 1989). En plus de ces axes de développement, il a été démontré que les interneurones ACh situés dans les striosomes se différencient plus tôt que ceux de la matrice (van Vulpen and van der Kooy, 1996, 1998).

Aux alentours d'E13, la ChAT peut déjà être détectée par immunocytochimie dans le néostriatum (Kessler, 1986; Phelps et al., 1989). Les données biochimiques portant sur les quantités d'ACh et l'activité-ChAT (Guyenent et al., 1975; Coyle and Campochiaro, 1976) ou les démonstrations autoradiographiques du HACU (Happe and Murrin, 1992) et le vAChT (Aubert et al., 1996), indiquent que ces paramètres augmentent plus ou moins rapidement après la naissance, jusqu'à atteindre des densités de liaison comparables à l'adulte, entre P20 et P30.

### 1.5.4 Les récepteurs cholinergiques du néostriatum en développement

Telle que mise en évidence par hybridation in situ, l'expression de la sous-unité nicotinique α7 dans le striatum du rat équivaut à la naissance à celle mesurée chez l'adulte. Dans les jours suivants, elle augmente transitoirement jusqu'à P3 et retombe, à partir de P14, à sa valeur adulte, atteinte à P28 (Zhang et al., 1998). Pour sa part, l'expression des sous-unités α4 et β2 est maximale vers P0 et diminue progressivement jusqu'à l'âge adulte (Zhang et al., 1998). Cette expression précoce des récepteurs nicotiniques pourrait expliquer le fait qu'à la naissance, la radioliaison des différents ligands nicotiniques représente déjà 35 à 80% des valeurs mesurées dans le néostriatum adulte (Aubert et al., 1996; Zhang et al., 1998).

Les données autoradiographiques révèlent aussi un patron de radioliaison aux récepteurs nicotiniques hyperbolique, qui débute après la naissance

(Aubert et al., 1996; Miao et al., 1998; Zhang et al., 1998). Le sommet est atteint plus ou moins précocement : à P7 pour l'($^3$H)α-bungarotoxine (α7), P14 pour l'($^3$H)nicotine, P17 pour l'($^3$H)N-methylcarbamylcholine (α4β2) et P20 pour l'($^3$H)épibatidine (non α7). La diminution est ensuite progressive, jusqu'aux valeurs adultes atteintes entre P30 et P40.

Le patron de développement des sous-types réceptoriels m1, m2 et m4, lesquels représentent respectivement 27, 12 et 48% des récepteurs muscariniques du néostriatum (Levey et al., 1994), est en net contraste avec celui des récepteurs nicotiniques. En effet, l'expression des récepteurs muscariniques est très faible à la naissance et augmente progressivement jusqu'à l'âge adulte. Il en va de même de la densité de radioliaison de l'($^3$H)QNB (ensemble des récepteurs muscariniques), de la ($^3$H)pirenzepine (M1) et du ($^3$H)AF-DX 116 (M2) qui sont très faibles à P0 et qui augmentent progressivement par la suite pour atteindre des valeurs semblables à celles mesurées chez l'adulte entre P16 et P30 (Aubert et al., 1996) ou à P60 (Miyoshi et al., 1987) selon les études.

### 1.5.5 Les rôles de l'acétylcholine du néostriatum en développement

Les interneurones ACh du néostriatum, également nommés TANs (Neurones Toniquement Actifs), déchargent spontanément, même privés de toute afférence (Bennett and Wilson, 1999; Bennett et al., 2001). On leur attribue, d'une part, un rôle neuromodulateur dans le contrôle du mouvement volontaire

(Graybiel et al., 1994; Canales and Graybiel, 2000; Pisani et al., 2001) et, d'autre part, un rôle de régulation de la plasticité cortico-striatale (Centonze et al., 1999).

Même si les données demeurent fragmentaires, plusieurs indices laissent supposer un rôle important de l'ACh dans le néostriatum en développement, du moins chez les rongeurs. Les neurones ACh se différencient et expriment leur phénotype très précocement, et l'ACh figure parmi les premiers neurotransmetteurs qui apparaissent dans le néostriatum. Nous verrons qu'un réseau d'innervation ACh relativement dense s'y installe dès la première semaine postnatale, coïncidant avec l'augmentation de nombreux paramètres cholinergiques. Durant cette première semaine, les autorécepteurs muscariniques sont en mesure d'exercer une action inhibitrice sur la libération de l'ACh (De Vries et al., 1992). Cette étude indique également une inhibition concomitante de l'activité de l'adénylate cyclase stimulée par les récepteurs à dopamine D1. D'autre part, il a été démontré que, durant la première semaine postnatale, apparaît une modulation de la libération d'ACh par d'autres neurotransmetteurs, tels la dopamine, les opiacés, et les tachykinines (Perez-Navarro et al., 1993). L'ensemble de ces observations morphologiques et fonctionnelles indique que l'ACh pourrait exercer une puissante action neuromodulatrice à un stade relativement précoce du développement postnatal du néostriatum.

## 1.6 OBJECTIFS DE RECHERCHE

Ayant à notre disponibilité un anticorps à très haute affinité contre la ChAT purifiée à partir du cerveau du rat (Cozzari et al., 1990), nous nous sommes fixés trois objectifs de recherche visant à mieux comprendre la distribution et les caractéristiques ultratructurales de l'innervation cholinergique dans le cerveau.

Dans un premier temps, nous avons mené une étude sur la distribution de l'innervation ACh dans l'hippocampe dorsal chez le rat et la souris adultes. À cette fin, nous avons donc adapté l'utilisation d'une technique de quantification préalablement mise au point dans notre laboratoire (Mechawar et al., 2000), aux particularités morphologiques de l'hippocampe.

Grâce aux données ainsi obtenues chez le rat adulte, notre deuxième objectif fut d'étudier le croissance et la maturation de cette innervation tant au niveau de sa distribution que de son ultrastructure chez le rat.

Cette étude nous a conduit à nous demander si les caractéristiques ultrastructurales que nous avions observées au cours du développement dans l'hippocampe pouvaient s'appliquer à d'autres régions du cerveau du rat. Nous nous sommes donc fixé comme troisième objectif d'étudier les caractéristiques ultrastructurales de l'innervation ACh du néostriatum, qui est issue d'interneurones ACh locaux, au cours du développement postnatal chez le rat.

Chapitre II

# COMPARATIVE ANALYSIS OF THE CHOLINERGIC INNERVATION IN THE DORSAL HIPPOCAMPUS OF ADULT MOUSE AND RAT : A QUANTITATIVE IMMUNOCYTOCHEMICAL STUDY

Publié en 2002

*Hippocampus* 12:206-217

(N AZNAVOUR, N MECHAWAR et L DESCARRIES)

# COMPARATIVE ANALYSIS OF THE CHOLINERGIC INNERVATION IN THE DORSAL HIPPOCAMPUS OF ADULT MOUSE AND RAT: A QUANTITATIVE IMMUNOCYTOCHEMICAL STUDY

Nicolas AZNAVOUR, Naguib MECHAWAR and Laurent DESCARRIES

Départements de pathologie et biologie cellulaire et de physiologie,

and Centre de recherche en sciences neurologiques,

Faculté de médecine, Université de Montréal, Montréal, Québec, Canada H3C 3J7

(41 text pages including figure legends; 1 table and 5 figures)

Abbreviated title: **ACh innervation in mouse and rat hippocampus**

KEYWORDS acetylcholine – axons – varicosities – ChAT – distribution

immunocytochemistry

Correspondence: Laurent DESCARRIES m.d.
Département de pathologie et biologie cellulaire
Université de Montréal
CP 6128, Succursale Centre-ville
Montréal, QC, Canada H3C 3J7
tel. (514) 343-7070
fax (514) 343-5755
[redacted]

Grant sponsor: Medical Research Council of Canada; Grant number: MT-3544.

## ABSTRACT

To obtain truly quantitative data on the distribution of the acetylcholine (ACh) innervation in the dorsal hippocampus of adult mouse (C57/B6) and rat (Sprague-Dawley), a semi-computerized method was used to measure the length of immunostained axons in hippocampal sections processed for light microscopic immunocytochemistry with a highly sensitive antibody against choline acetyltransferase (ChAT). The results could be expressed in density of axons (meters per $mm^3$) for the different layers and regions of dorsal hippocampus (CA1, CA3, DG), and also in density of axon varicosities (millions per $mm^3$), after having determined the average number of varicosities per unit length of ChAT-immunostained axon (4 varicosities / 10 µm). In mouse, the mean regional densities of ACh innervation were thus measured at 13.9, 16.1 and 15.8 meters of axons, for 5.6, 6.4, and 6.3 million varicosities per $mm^3$ of tissue, in CA1, CA3 and DG, respectively. The values were comparable in rat, except for CA1, in which the densities were lower than in mouse by 40% in the stratum lacunosum, and 20% in the stratum radiatum. Otherwise, the laminar patterns of innervation were similar in the two species, the highest densities being found in the stratum lacunosum moleculare of CA3, pyramidale of both CA1 and CA3, and moleculare of DG. These quantitative data will be of particular interest to evaluate changes in mutant mice, or mice and rats subjected to experimental conditions affecting the cholinergic phenotype.

## INTRODUCTION

The neurotransmitter/modulator acetylcholine (ACh) has long been recognized as playing a role in cognitive functions involving hippocampus, such as learning, memory and attention (Olton, 1977; Becker et al., 1981; Hasselmo and Schnell, 1994; Maeda et al., 1994; Acquas et al., 1996; Kim and Levin, 1996; Fujii et al., 2000; Yun et al., 2000). ACh transmission in hippocampus is impaired in Alzheimer's disease (e.g., Davies and Maloney, 1976; Bartus, 1982), certain forms of epilepsy (Mizuno and Kimura, 1996; Bertrand and Changeux, 1999; Berkowic and Steinlein, 1999; Steinlein, 2000), and schizophrenia (Freedman et al., 1997; Lindstrom, 1997; Adler et al., 1998; Freedman et al., 1999; Breese et al., 2000; Leonard et al., 2000).

The hippocampal ACh innervation originates mainly from neuronal cell bodies in the medial septal nucleus and nucleus of the vertical limb of the diagonal band of Broca (Mc Kinney et al., 1983; Rye et al., 1984; Amaral and Kurz, 1985; Nyakas et al., 1987; Woolf, 1991). A second, intrinsic component, arises from bipolar interneurons, at least in rodents (Houser et al., 1983; Frotscher et al., 1986; Blaker et al., 1988). After selective lesions of the basal forebrain ACh neurons, it has been estimated that ACh interneurons account for 5-10% of the choline acetyltransferase (ChAT) activity in dorsal hippocampus (Gage et al., 1983). Further studies have however indicated that these interneurons are

unable to compensate for losses of extrinsic ACh input (Blaker et al., 1988; Frotscher, 1988).

ACh exerts its effects via muscarinic and nicotinic receptors that are widely distributed in hippocampus (reviewed in van der Zee and Luiten, 1999). At the single cell level, hippocampal ACh has been shown to depolarize a majority of pyramidal neurons (Cole and Nicoll, 1984; Madison et al., 1987; Benson et al., 1988) and GABA interneurons (McQuiston and Madison, 1999a, 1999b; Ji and Dani, 2000), and to modulate glutamate and GABA release (Radcliffe and Dani 1998; Radcliffe et al., 1999; Alkondon et al., 1999). These widespread effects of ACh have been shown to underlie several types of large-scale synchronous neuronal activities, such as those manifested by the characteristic hippocampal β and θ rhythms (Jones and Yakel, 1997; Williams and Kauer, 1997; Cobb et al., 1999; Chapman and Lacaille, 1999; Shimono et al., 2000; Wyble et al., 2000).

Further elucidation of the physiological and pathological roles of the ACh innervation in hippocampus would greatly benefit from the availability of truly quantitative data on its distributional features. Yet, previous descriptions have remained essentially qualitative, or at best semi-quantitative, in mouse (Kitt et al. 1994; Schwegler et al. 1996) as well as rat (Lysakowski et al. 1989; Henderson et al. 1998). This lack of information is presumably due, at least in part, to the low sensitivity of commercially available ChAT antibodies, which appear more suited for the detection of ACh neuronal cell bodies than that of their axons and

varicosities. Likewise, it remains to be demonstrated that the recently produced antibodies against the vesicular transporter for ACh provide for an integral immunocytochemical detection of this innervation (Roghani et al. 1996; Weihe et al. 1996; Arvidsson et al. 1997; Ichikawa et al. 1997; Schäfer et al. 1998; Wong et al., 1999). As for acetylcholinesterase (AChE) histo- or immunocytochemistry, it is hardly reliable for quantitative purposes, because of the widespread expression of AChE by non cholinergic neurons (Butcher et al. 1975; Robertson and Gorenstein 1987).

To fill this gap, we made use of a highly sensitive antibody against whole rat ChAT (Cozzari et al., 1990), which provides for a full light microscopic immunocytochemical visualization of ACh axon networks throughout rat brain (Umbriaco et al., 1994). In combination with a semi-computerized method for measuring the length of ChAT-immunostained axons in tissue sections, and separate counts of the average number of varicosities per unit length of ChAT-immunostained axon, it was thus possible to determine the regional and laminar densities of ACh axons and varicosities in adult and developing rat cerebral cortex (Mechawar et al., 2000; Mechawar and Descarries, 2001). In the present study, a similar approach was taken to measure and compare the density of the ACh innervation in CA1, CA3 and DG of the adult mouse and rat dorsal hippocampus. Preliminary data for the mouse have already been reported in abstract form (Aznavour et al., 2000).

# MATERIALS AND METHODS

## Tissue

All experiments abided by the policies and guidelines of the Canadian Council on Animal Care and the regulations of the Animal Care Committee at the Université de Montréal. The study was carried out on 6 adult male C57/B6 mice (body weight: 50 ± 10 g), and 6 adult male Sprague-Dawley rats (body weight : 250 ± 50 g), purchased from Charles River Canada (St-Constant, Quebec, Canada). After deep anesthesia with sodium pentobarbital (80 mg/kg, i.p.), these animals were respectively perfused through the heart with 25 or 50 ml of ice-cold phosphate buffered saline (PBS; 50mM; pH 7.4), followed by 250-300 ml or 400-500 ml of 4% paraformaldehyde (PFA) in 0.1 M sodium phosphate buffer (PB; pH 7.4; 24°C). The brain was rapidly removed, postfixed overnight in PFA at 4°C, and washed in PBS. 20-µm-thick vibratome sections were then cut across the dorsal hippocampus, at transverse levels respectively equivalent to stereotaxic planes interaural A 1.98 mm in the mouse (Franklin and Paxinos, 1997) and bregma – 3.7 mm in the rat (Swanson, 1992). The sections were then processed for light microscopic immunocytochemistry as described below, or stained with cresyl violet to delimit hippocampal regions and layers.

## ChAT-immunocytochemistry

The mouse monoclonal antibody against purified rat brain ChAT was used as previously described in detail (Umbriaco et al., 1994; Mechawar et al., 2000).

At room temperature, the free-floating sections were rinsed (3 x 10 min), pre-incubated for 2 h in a blocking solution of PBS containing 2% normal horse serum (NHS; Vector, Burlingame, CA), 1% bovine serum albumin (BSA; Sigma, St. Louis, MO) and 0.2% Triton X-100, and incubated overnight in the same solution containing 2 µg/ml of monoclonal anti-ChAT antibody.

Immunostaining was performed at room temperature with the ABC method (Shi et al., 1988). After rinses in PBS (2 x 10 min) and a 10 min rinse in 0.1 M potassium phosphate buffer (KPB; pH 7,4), sections were incubated for 2 h in biotinylated horse anti-mouse, secondary antibody (Vector), diluted 1/200 in KPB containing 2% NHS and 1% BSA, followed by the avitidin-biotin complex procedure (ABC Kit, Vectastain Elite; Vector) for 2 h. The labeling was revealed for 2.25 min in a 0.05% solution of 3,3'-diaminobenzidine (Sigma) containing 0.01% $CoCl_2$, 0.01% $NiSO_4$, 0.01% $(NH_4)_2SO_4$, to which 0.005% $H_2O_2$ was added. Sections were rinsed in KPB (3 x 10 min), air-dried on gelatin-coated slides, dehydrated in ethanol, cleared in toluene, and mounted with DPX (Fluka; Sigma).

**Length of ChAT-immunostained axons**

The length of ChAT-immunostained axons was measured in three major sectors of hippocampus: CA1, CA3 and DG. This was done with the aid of a computer-based image analysis system: Macintosh Quadra 950, connected to a light microscope (Leitz Orthoplan; 25 X PlanApo objective lens) via a video

camera (Panasonic WV-BD400; 768 x 493 pixels for 1,7 $cm^2$). For each animal, a 240 µm-wide vertical strip across the three hippocampal regions was captured as a series of images (645 X) that were assembled on the screen as a photomontage (Adobe Photoshop 5.5 software). Because of the relative thinness of the sections and depth of focus of the objective, all immunostained fibers across the sections were visible. Square sampling windows, 50 µm x 50 µm (0.0025 $mm^2$), were randomly positioned in each layer of each region, so as to fit 3 sampling windows per layer, as illustrated in Fig. 1. Using an Intuos Graphics Tablet (Wacom, Vancouver, WA), the axonal network was then drawn on the screen for each sampling window, i.e. in a total hippocampal surface of 0.0825 $mm^2$ per animal.

The length of the drawn axon networks was measured with the NIH Image software (1.61; public domain). The lines of the drawings were reduced to a uniform thickness of 1 pixel with the "skeletonize" function of the program, closed surfaces were cut open by removal of 1 pixel, and the length measurement (plus the number of removed pixels) was converted to micrometers, based on a prior calibration of the system with a microscopic scale. A correction (x 1/cos 45; Soghomonian et al. 1987) was then introduced to compensate for angulation of the fibers, assuming their random orientation in the section, and the values were extrapolated to 1 $mm^3$ of tissue, to be expressed as average density of axons (meters per $mm^3$) for each layer, interlaminar mean for each hippocampal region, and interregional mean for whole dorsal hippocampus.

**Number of ChAT-immunostained axon varicosities**

The average number of ACh axon varicosities per unit length of axon was determined for each layer and the 3 regions of hippocampus in 3 mice and 3 rats. Varicosities were defined as axon dilations greater than 0.5 μm in transverse diameter (Umbriaco et al., 1994), as such dilations have been shown to display all subcellular attributes of axon terminals in the rat hippocampus (Umbriaco et al., 1995). In each region, the number of such dilations for 25 axon segments per layer was counted directly at the light microscope (1000 X; 1650 counts). The laminar, regional and mean hippocampal densities of axon varicosities ($10^6$ per $mm^3$) were calculated by multiplying the densities of ACh axons by the average number of varicosities per unit length.

**Statistics**

The laminar densities of ChAT-immunostained axons and axon varicosities were tabulated as means ± s.d. per $mm^3$ of tissue (n = 6). The statistical comparisons among layers of one species and between layers from a given region in mouse and rat were made by one-way ANOVA ($\alpha$=0.05) followed by two-tailed Student's t test ($\alpha$=0.05).

# RESULTS

## Visualization of ACh neurons

Previous studies have shown that the present experimental conditions provide for a specific and maximal immunocytochemical labeling of ChAT-immunoreactive axons in the rat CNS (e.g. Umbriaco et al., 1994; Mechawar et al., 2000). In mouse as well as in rat hippocampus, the nickel-cobalt enhanced ChAT-immunostaining resulted in intense darkening of a few neuronal cell bodies and of a dense network of fine varicose axons against a light background (Figs. 1-3). Individual axons could be followed without discontinuity across the thickness (20 µm) of the sections, attesting to the full penetration of immunoreagents in tissue.

## Laminar distribution of hippocampal ACh innervation in mouse and rat

In both species, there were only a few small, round or ovoid, immunopositive cell bodies within hippocampus (Figs. 1A and 1B). In mouse, these neurons (2 or less per section) were mostly seen in the strata radiatum and lacunosum moleculare of CA1, and moleculare of DG but not in CA3. Their proximal dendrites were observed on rare occasions (Fig. 2C). In rat, immunostained nerve cell bodies were slightly more numerous (2-4 per section), and often typically bipolar, with their primary dendrites oriented perpendicular to the hippocampal surface (Fig. 3C). These neurons were mostly located in the stratum lacunosum moleculare of CA1, and, less often, in the strata radiatum,

oriens and pyramidale of CA1, and the strata moleculare and granulare of DG. As in mouse, they were never seen in the polymorph layer of DG or in CA3.

The more or less intricate branching network of ChAT-immunoreactive axons pervaded all layers of each hippocampal region in both species (Figs. 1-3). These varicose fibers showed no predilection for the immediate vicinity of microvessels, nor any pericellular arrangement suggestive of particular relationships with specific neuronal types. In all layers, the varicose enlargements were comparably spaced along fibers, smaller and larger varicosities were visible along the same fibers, and there were no indications of regional or laminar segregation on the basis of their size. Overall, the laminar distribution of these fibers appeared consistent with earlier descriptions in mouse (Kitt et al., 1994) and rat (Lysakowski et al., 1989).

There were many more species similarities than differences when comparing, region by region, the laminar distribution of ACh axons (Figs. 2 and 3). In CA1 (Figs. 2A and 3A), a three-layered pattern was characteristic of the stratum pyramidale, with denser bands of varicose axons on its inner and outer borders. In contrast, the three neuropil layers, oriens, radiatum and lacunosum moleculare, were more homogeneously innervated, notwithstanding some density differences (see below). A narrow band of denser innervation was also found at the border between the strata lacunosum moleculare and radiatum. In CA3 (Figs. 2B and 3B), there was no stratification in the stratum pyramidale. The confinement of immunostained fibers between the closely packed

immunonegative cell bodies in this layer produced a dark crescentic zone, riddled on its inner face with pale silhouettes outlined by varicose fibers. Inserted between this dark crescent and a stratum radiatum as densely innervated as in CA1, the less densely innervated stratum lucidum stood out as a light zone. The DG of mice and rat also displayed a layered pattern, consisting of alternating bands of lesser and higher density of ACh innervation on either side of the stratum granulare (Figs. 2A and 3A). These bands differed in thickness between the two species, resulting in a different overall apearance. Compared to mice, both dorsal and ventral lips of the rat DG displayed a much thicker light zone in the inner third of the molecular layer and dark zone immediately above the granular layer. In both species, a narrow band of dense innervation was also present immediately underneath the granular layer, delimiting the hilus. Within the molecular layer in both species, there were hints of a discreet three-sublayer pattern (Figs. 2A and 3A), as already reported for the rat (Lysakowski et al., 1989).

**Quantitative data on hippocampal ACh innervation in mouse and rat**

The densities of ACh axons and axon varicosities (laminar, regional, whole hippocampus), respectively expressed in meters of axons and millions of varicosities per cubic millimeter of tissue, are given in Table 1 for both species. The mean number of axon varicosities per unit length of axon was not significantly different among hippocampal layers or regions within and between the two species (interlaminar means of 0.41 µm ± 0.02 s.d. and 0.40 µm ± 0.02 s.d., respectively). A fixed ratio of 4 varicosities per 10 µm of axon was therefore used

to infer the densities of axon varicosities from the densities of axons, as listed in Table 1 and depicted in Figs. 4 and 5. Either parameter could indeed serve as index of ACh innervation density.

In mouse, the mean density of ACh axons and axon varicosities was significantly lower in CA1 than CA3 and DG, the latter two showing similar values (Table 1 and Fig. 4). Within each region, there were statistically significant differences between layers (Fig. 4). In CA1, stratum pyramidale was the most densely innervated (17.9 m of axons or 7.2 million varicosites per $mm^3$), and lacunosum moleculare the least (10.8 m; 4.3 x $10^6$). Radiatum and oriens displayed intermediate values. In CA3, on the contrary, stratum lacunosum moleculare had the highest density (20.2 m; 8.1 x $10^6$). Pyramidale (19.6 m; 7.8 x $10^6$) and oriens (16.7 m; 6.7 x $10^6$) followed, also more densely innervated than in CA1. Stratum radiatum was moderately innervated (as in CA1), and lucidum had the lowest density (10.4 m; 4.2 x $10^6$). In DG, stratum moleculare showed a high density (19.8 m; 7.9 x $10^6$), while those of granulare (13.6 m; 5.4 x $10^6$) and polymorph (13.9 m; 5.6 x $10^6$) were intermediate.

In rat, as in mouse, the lowest mean regional density was that of CA1, the values for CA3 and DG were similar, and there were statistically significant differences between layers in all three regions (Table 1 and Fig. 5). In CA1, stratum pyramidale was again the most densely innervated (16.9 m of axons or 6.8 million varicosities per $mm^3$), and lacunosum moleculare the least (6.4 m; 2.6 x $10^6$), the latter values being significantly lower than in mouse. The oriens

values were intermediate, as in mouse (14.7 m; 5.9 x $10^6$). Radiatum was also moderately innervated, but at lower densities than in mouse (10.6 m; 4.2 x $10^6$). In CA3, the laminar densities were very similar to those in mouse. The values for stratum lacunosum moleculare were almost three fold greater than in CA1 (18.8 m; 7.5 x $10^6$), those of pyramidale even higher (20.3 m; 8.1 x $10^6$), and those of oriens also high (17.8 m; 7.1 x $10^6$). Stratum radiatum was moderately innervated (13.2 m; 5.3 x $10^6$), and lucidum had the lowest density (10.6 m; 4.2 x $10^6$). Rat DG was also very similar to that of the mouse, with a stratum moleculare having a high density (19.5 m; 7.8 x $10^6$), whereas those of granulare (13.4 m; 5.4 x $10^6$) and polymorph (13.8 m; 5.5 x $10^6$) were intermediate. In brief, only CA1 showed a marked interspecies difference in ACh innervation, accounted for by the particularly low densities in strata lacunosum moleculare and radiatum.

## DISCUSSION

### Methodological considerations

Previous immunocytochemical descriptions with the present ChAT antibody have demonstrated its specificity throughout rat brain (Umbriaco et al., 1994), including hippocampus (Umbriaco et al., 1995; Deller et al., 1999). The fact that this antibody allows for a maximal detection of ACh axons and their varicosities under the present experimental conditions has been previously established, at least in adult rat neocortex (Mechawar et al., 2000). In the present study,

visualization of the ACh innervation in mouse hippocampus and cerebral cortex appeared as selective and extensive as in rat tissue, with strong immunostaining of a dense axonal network as well as a few intrinsic nerve cell bodies and dendrites.

The sampling windows from which the measurements were obtained were randomly located in relation to the layers and regions examined, and sufficiently large to ensure an extensive and reliable sampling of each layer across CA1, CA3 and the DG. Visual inspection of other hippocampal areas, in the same and other transverse sections, showed that the level examined was representative of the whole dorsal hippocampus, except for its rostral tip. The semi-computerized technique used for collecting the data ensured that all and only immunostained fibers were being measured across the full thickness of the sections. Although tedious, this procedure was the only way to obtain gray shade discrimination sufficient for tracing some of the more lightly stained axon segments between the darker varicosities. The mathematical correction for angulation, assuming a random orientation of the fibers in the sections, was a convenient way to convert these length measurements from a plane to a three-dimensional volume. The risk of an overestimation introduced by this correction was minimal, since none of the sampled areas displayed numerous fibers running preferentially within the plane of the section, except for the narrow band in CA1, at the border between radiatum and lacunosum moleculare (see below).

Axon varicosities were defined as dilations 0.5 µm or more in transverse diameter, on the basis of prior electron microscopic measurements (Umbriaco et al., 1995). These had also shown that the average diameter of intervaricose ACh segments is about 0.2 µm, allowing for a clearcut distinction between the varicosities and the axons. The fixed ratio of 4 ACh varicosities per 10 µm of axon, valid for mouse as well as rat hippocampus, allowed to directly infer the densities of varicosities from those of axon length. It also meant that both parameters were equally useful as indices of innervation density. Expressing length of axons and number of varicosities as densities (length or number per $mm^3$) facilitates correlations with other measurable parameters of cholinergic function and with cytometric data regarding this and other chemically defined systems.

**Topographical features of the ACh innervation**

The present study extended earlier observations on the distributional features of the hippocampal ACh innervation in adult mouse and rat made with AChE-histo- or immunocytochemistry (mouse: Slomianka and Geneser, 1991, 1993; rat: Storm-Mathisen and Blackstad, 1964), ChAT-immunocytochemistry (mouse: Kitt et al., 1994; rat: Lysakowski et al., 1989) and immunoctytochemistry of the vesicular transporter for ACh (rat: Arvidsson et al., 1997; Ichikawa et al., 1997; Schäfer et al., 1998). At variance with some early ChAT-immunocytochemical reports, however, we did not detect immunoreactive pyramidal cells in rat (Nishimura et al. 1988), nor numerous interneurons in either

species (Kitt et al., 1994; Matthews et al., 1987). According to an earlier description (Frotscher et al., 1986), it could be assumed that the morphology and distribution of ACh interneurons here observed in the dorsal hippocampus was representative of the whole region, at least for rat. Although in low number, hippocampal ACh interneurons appeared slightly more numerous in rat than mouse, perhaps due to the greater volume of this region in the rat. In both species, the predilection of these cells for both lips of the hippocampal fissure – lacunosum moleculare of CA1 and moleculare of DG – was suggestive of some preferential relationship with the perforant and temporo-ammonic pathways (Frotscher et al., 1986). The extent of the axonal arborization of these neurons, the nature of their putative coexistent transmitter(s) and the ultrastructural features of their terminals remain to be defined (Freund and Buzsaki, 1996).

In both species, there were particular aspects of the topographic distribution of the ACh innervation which were beyond the limits of resolution of the quantitative analysis, and yet of interest in terms of functional significance. For example, the three-layered pattern in the stratum pyramidale of CA1, with two denser bands of ACh innervation on either side of the thin and compact layer of pyramidal cell bodies, raised the question of a targeted versus non targeted innervation. This pattern could reflect some preferential relationships with the proximal dendrites of pyramidal neurons, and/or the GABA and glutamate synaptic inputs to these dendrites (Freund and Buzsaki, 1996). Yet, it was not observed in the equally densely innervated stratum pyramidale of CA3, in which

the more loosely grouped pyramidal cells form a thicker layer. Thus, this layering pattern could merely be the result of the particularly high packing density of pyramidal cell bodies in CA1. As for the dense narrow band of longitudinally oriented ACh fibers observed at the interface of the strata radiatum and lacunosum moleculare of CA1, it could represent a pathway for ACh axons entering the densely innervated stratum lacunosum moleculare of CA3 from the subiculum. Interestingly, this band coincides with the presence of interneurons which, upon activation by ACh, are known to be involved in the pacing of theta activity in CA1 pyramidal cells (Chapman and Lacaille, 1999).

In the DG, the granular layer also displayed a three-layered pattern of innervation, which was reminiscent of the pyramidal layer in CA1. The relatively thicker and darker rim, orthogonal to the apical dendrites of granular cells, seemed to relate more with the density of innervation of the adjacent neuropil (stratum moleculare). The discrete three-sublayer pattern in the molecular layer of the DG was more obvious in rat than mouse, but not as clear as initially described with AChE-histochemistry (Lysakowski et al., 1989). This pattern might be related to the particular distribution of some afferents to this layer, such as the innervation of its outer and middle thirds by the lateral and medial entorhinal cortex, respectively (Witter et al., 2000).

**Quantified distributional features of the ACh innervation**

The fixed ratio of 4 varicosities per 10 µm of ACh axon measured throughout mouse as well as rat hippocampus was the same as previously determined for the ACh innervation in the different layers of three neocortical areas (frontal, parietal, occipital) in adult rat (Mechawar et al., 2000). Such a constancy is suggestive of intrinsic determinants and conversely supports the view that the density of ACh innervation, which varies between layers and regions, must be regulated by local cues controlling the extent of axonal arborization (e.g. Super et al., 1998; Skutella and Nitsch, 2001).

Many distributional features of this ACh innervation, common to both species, were revealed by the quantitative analysis. A first was its ubiquity, with laminar densities (per $mm^3$) ranging from 10.4 to 20.2 meters of axons and 4.2 to 8.1 million axon varicosities in mouse, and from 6.4 to 20.4 meters of axons and 2.6 to 8.2 million axon varicosities in rat. These relatively high densities suggest that all hippocampal neurons in the rat and mouse might be within reach of ACh (see Descarries et al., 1997; Descarries and Mechawar 2000), in keeping with immunocytochemical observations that nearly all hippocampal interneurons and principal cells express cholinergic receptors (e.g., van der Zee and Luiten, 1999).

In accordance with earlier suggestions based on a quantification of AChE fibers in mouse (Schwegler et al., 1996) and rat (Matthews et al., 1987), the

present study also indicated that, in spite of similar patterns of laminar distribution, the average density of ACh innervation in CA3 was significantly higher than in CA1, and in fact closer to that of DG. The 16% (mouse) and 33% (rat) differences between the two sectors of Ammon's horn were largely accounted for by the 87% (mouse) and 194% (rat) higher densities of ACh innervation in the stratum lacunosum moleculare of CA3 compared to CA1. Anatomical studies in rat have shown that the stratum lacunosum moleculare of CA3 and CA1 are differentially innervated by layer II and III neurons of the entorhinal cortex (Amaral and Witter, 1995; Witter et al., 2000). The entorhinal cortex, which receives input from the perirhinal and postrhinal cortex (Burwell and Amaral, 1998; Burwell, 2000) has been implicated in both object recognition (Wan et al., 1999) and spatial memory (Aggleton et al., 2000; Vann et al., 2000a). Interestingly, the lacunosum moleculare of CA1 also receives afferents from the midline nucleus reuniens of thalamus (Amaral and Witter, 1995), another pathway implicated in spatial memory (Vann et al., 2000b). This nucleus has been shown to influence hippocampal transmission through activation of local inhibitory interneurons (Dolleman-Van der Weel et al., 1997, 2000), much as demonstrated for hippocampal ACh (Ji and Dani, 2000; McQuiston and Madison, 1999a). It may thus be speculated that the lower density of ACh innervation in the lacunosum moleculare of CA1 reflects a lesser role for ACh in the modulation of this type of information in this region. This would be consistent with computational models of CA1 predicting that, for effective associative

memory, cholinergic suppression of intrinsic synaptic transmission should be weaker in lacunosum moleculare than stratum radiatum, in order to favour the treatment of extrinsic inputs (Hasselmo and Bower, 1992, 1993; Hasselmo and Schnell, 1994).

Also characteristic of both species was the low density of ACh innervation in the stratum lucidum of CA3. In CA3, mossy fibers represent one of the main inputs to this layer, and direct modulation of their activity by exogenous ACh has been shown to be relatively weak (Vogt and Regehr, 2001). Taken together, these and the above data seem to relate the laminar density of innervation with the degree of influence exerted locally by ACh. Such a link would be in line with the largely asynaptic nature of this innervation (Umbriaco et al., 1995), and the potential importance of an ambient level of extracellular ACh in its functioning (Descarries et al., 1997). It will be for future studies to determine if and how the greater density of ACh innervation in mice versus rat strata radiatum (+ 25%) and lacunosum moleculare (+ 69%) of CA1, which is the major interspecies difference measured in the present study, might translate into species-specific physiological and behavioral traits.

**Other parameters of ACh function in hippocampus**

Previous autoradiographic and immunocytochemical descriptions of muscarinic receptor subtypes and nicotinic subunits in hippocampus have revealed similar widespread and complementary laminar distributions for mouse

and rat (Hill et al., 1993; Sargent, 1993; Séguéla et al., 1993; Dominguez del Toro et al., 1994; Hohmann et al., 1995; Levey et al., 1995; Aubert et al., 1996; Schwegler et al., 1996). In rat, m1, m3 and m4 subtypes have been shown to be expressed by principal cells, and m2 by interneurons (Freund and Buzsaki, 1996) and axon terminals (Levey et al., 1995). In both species, the most widely expressed $\alpha 7$ and $\beta 2$ nicotinic subunits (Sargent, 1993) were mainly found in the principal cell layers (Séguéla et al., 1993; Dominguez del Toro et al., 1994; Hill et al., 1993). The apparent match between the distribution of m2 receptors and the ACh innervation of CA1 and CA3 is consistent with the recent anatomical demonstration of a terminal autoreceptor as well as heteroreceptor location for hippocampal m2 (Rouse et al., 1999, 2000). Conversely, its relatively low expression in the DG (Levey et al., 1995), in which the ACh innervation is dense, suggests a lesser role as autoreceptor and its predominance as terminal heteroreceptor in this region.

The mean overall densities of 6.1 million ACh varicosities per $mm^3$ in mouse hippocampus, and 5.9 million in rat, represent the densest neuromodulatory innervations hitherto described in cerebral cortex. In rat, for example, the mean densities of the hippocampal serotonin and noradrenaline innervations have been respectively estimated at 2.7 and 2.1 million varicosities per $mm^3$ (Oleskevich and Descarries, 1990; Oleskevich et al., 1989). These numbers are also informative as regards the morphological characteristics of individual ACh neurons innervating mouse and rat hippocampus. Assuming that the density of

ACh innervation measured in the dorsal hippocampus is representative of the whole region, and based on hippocampal volumes of 21.3 $mm^3$ for mouse (West, 1990) and 56 $mm^3$ for rat (Coleman et al., 1987), the total length of ACh axons in one hippocampus may be estimated at 326 (mouse) and 823 meters (rat), and the corresponding numbers of varicosities at 130 and 329 millions. It is currently estimated that some 250 ACh nerve cell bodies in the septum and diagonal band of Broca project to mouse hippocampus (Schwegler et al., 1996), and 385 in the rat (McKinney et al., 1983). Thus, these ACh neurons should be endowed with an axonal arborization averaging 1.3 meter in length and bearing 520,000 axon varicosities in mouse, compared to 2.1 meters of axon and 840,000 varicosities in rat. The latter values are twice higher than previously extrapolated for nucleus basalis ACh neurons projecting to adult rat neocortex (Mechawar et al., 2000), which, in itself, provides compelling structural evidence for a crucial role of ACh in hippocampal function.

**Acknowledgments**

Supported by grant MT-3544 from the MRC of Canada. N.A. holds a PhD studentship from the Groupe de recherche sur le système nerveux central (FCAR) and N.M. a research studentship from the Medical Research Council of Canada. The authors are grateful to Jean-Claude Lacaille for fruitful discussions and a critical revision of the manuscript. They also thank Gaston Lambert for photographic work.

## References

Acquas E, Wilson C, Fibiger HC. 1996. Conditioned and unconditioned stimuli increase frontal cortical and hippocampal acetylcholine release: effects of novelty, habituation, and fear. J Neurosci 16:3089-3096.

Adler LE, Olincy A, Waldo M, Harris JG, Griffith J, Stevens K, Flach K, Nagamoto H, Bickford P, Leonard S, Freedman R. 1998. Schizophrenia, sensory gating, and nicotinic receptors. Schizophr Bull 24: 189-202.

Aggleton JP, Vann SD, Oswald CJ, Good M. 2000. Identifying cortical inputs to the rat hippocampus that subserve allocentric spatial processes: a simple problem with a complex answer. Hippocampus 10: 466-474.

Alkondon M, Pereira EF, Eisenberg HM, Albuquerque EX. 1999. Choline and selective agonists identify two subtypes of nicotinic acetylcholine receptors that modulate GABA release from CA1 interneurons in rat hippocampal slices. J Neurosci 19: 2693-2705.

Amaral DG and Kurz J. 1985. An analysis of the origins of the cholinergic and noncholinergic septal projections to the hippocampal formation of the rat. J Comp Neurol 240: 37-59.

Amaral DG and Witter MP. 1995. Hippocampal formation. In: Paxinos G, editor. The rat nervous system. San Diego : Academic Press. p 443-493

Arvidsson U, Riedl M, Elde R, Meister B. 1997. Vesicular acetylcholine transporter (VAChT) protein: a novel and unique marker for cholinergic neurons in the central and peripheral nervous systems. J Comp Neurol 378: 454-467.

Aubert I, Cecyre D, Gauthier S, Quirion R. 1996. Comparative ontogenic profile of cholinergic markers, including nicotinic and muscarinic receptors, in the rat brain. J Comp Neurol 369: 31-55.

Aznavour N, Mechawar N, Descarries L. 2000. Quantitative distribution of the cholinergic innervation in adult mouse hippocampus. Soc Neurosci Abstr 26: 2141.

Bartus RT, Dean RL, Beer B, Lippa AS. 1982. The cholinergic hypothesis of geriatric memory dysfunction. Science 217: 408-414.

Becker JT, Olton DS, Anderson CA, Breitinger ER. 1981. Cognitive mapping in rats: the role of the hippocampal and frontal system in retention and reversal. Behav Brain Res 3: 1-22.

Benson DM, Blitzer RD, Landau EM. 1988. An analysis of the depolarization produced in guinea-pig hippocampus by cholinergic receptor stimulation. J Physiol (Lond) 404: 479-496.

Berkovic SF and Steinlein OK. 1999. Genetics of partial epilepsies. Adv Neurol 79: 375-381.

Bertrand D and Changeux JP. 1999. Nicotinic receptor: a prototype of allosteric ligand-gated ion channels and its possible implications in epilepsy. Adv Neurol 79: 171-188.

Blaker SN, Armstrong DM and Gage FH. 1988. Cholinergic neurons within the rat hippocampus: response to fimbria-fornix transection. J Comp Neurol 272: 127-138.

Breese CR, Lee MJ, Adams CE, Sullivan B, Logel J, Gillen KM, Marks MJ, Collins AC, Leonard S. 2000. Abnormal regulation of high affinity nicotinic receptors in subjects with schizophrenia. Neuropsychopharmacology 23: 351-364.

Burwell RD. 2000. The parahippocampal region: corticocortical connectivity. Ann NY Acad Sci 911: 25-42.

Burwell RD and Amaral DG. 1998. Perirhinal and postrhinal cortices of the rat: interconnectivity and connections with the entorhinal cortex. J Comp Neurol 391: 293-321.

Butcher LL, Talbot K, Bilezikjian L. 1975. Acetylcholinesterase neurons in dopamine-containing regions of the brain. J Neural Transm 37: 127-153.

Chapman CA and Lacaille JC. 1999. Cholinergic induction of theta-frequency oscillations in hippocampal inhibitory interneurons and pacing of pyramidal cell firing. J Neurosci 19: 8637-8645.

Cobb SR, Bulters DO, Suchak S, Riedel G, Morris RG, Davies CH. 1999. Activation of nicotinic acetylcholine receptors patterns network activity in the rodent hippocampus. J Physiol (Lond) 518: 131-140.

Cole AE and Nicoll RA. 1984. The pharmacology of cholinergic excitatory responses in hippocampal pyramidal cells. Brain Res 305: 283-290.

Coleman PD, Flood DG, West MJ. 1987. Volumes of the components of the hippocampus in the aging F344 rat. J Comp Neurol 266: 300-306.

Cozzari C, Howard J, Hartman B. 1990. Analysis of epitopes of choline acetyltransferase (ChAT) using monoclonal antibodies (Mabs). Soc Neurosci Abstr 16:200.

Davies P and Maloney AJ. 1976. Selective loss of central cholinergic neurons in Alzheimer's disease (letter). Lancet 2: 1403.

Deller T, Katona I, Cozzari C, Frotscher M, Freund TF. 1999. Cholinergic innervation of mossy cells in the rat fascia dentata. Hippocampus 9: 314-320.

Descarries L. and Mechawar N. 2000. Ultrastructural evidence for diffuse transmission by monoamine and acetylcholine neurons of the central nervous system. Prog Brain Res 125: 27-47.

Descarries L, Gisiger V, Steriade M. 1997. Diffuse transmission by acetylcholine in the CNS. Prog Neurobiol 53: 603-625.

Dolleman-Van der Weel MJ and Witter MP. 2000. Nucleus reuniens thalami innervates gamma aminobutyric acid positive cells in hippocampal field CA1 of the rat. Neurosci Lett 278: 145-148.

Dolleman-Van der Weel, MJ, Lopes da Silva FH, Witter MP. 1997. Nucleus reuniens thalami modulates activity in hippocampal field CA1 through excitatory and inhibitory mechanisms. J Neurosci 17: 5640-5650.

Dominguez del Toro E, Juiz JM, Peng X, Lindstrom J, Criado M. 1994. Immunocytochemical localization of the alpha 7 subunit of the nicotinic

acetylcholine receptor in the rat central nervous system. J Comp Neurol 349: 325-342.

Franklin KBJ, and Paxinos G. 1997. The Mouse Brain in Stereotaxic Coordinates. San Diego: Academic Press.

Freedman R, LE Adler, Leonard S. 1999. Alternative phenotypes for the complex genetics of schizophrenia. Biol Psychiatry 45: 551-558.

Freedman R, Coon H, Myles-Worsley M, Orr-Urtreger A, Olincy A, Davis A, Polymeropoulos M, Holik J, Hopkins J, Hoff M, Rosenthal J, Waldo MC, Reimherr F, Wender P, Yaw J, Young DA, Breese CR, Adams C, Patterson D, Adler LE, Kruglyak L, Leonard S, Byerley W. 1997. Linkage of a neurophysiological deficit in schizophrenia to a chromosome 15 locus. Proc Natl Acad Sci USA 94: 587-592.

Freund TF and Buzsaki G 1996. Interneurons of the hippocampus. Hippocampus 6: 347-470.

Frotscher M 1988. Cholinergic neurons in the rat hippocampus do not compensate for the loss of septohippocampal cholinergic fibers. Neurosci Lett 87: 18-22.

Frotscher M, Schlander M, Leranth C. 1986. Cholinergic neurons in the hippocampus. A combined light- and electron-microscopic immunocytochemical study in the rat. Cell Tissue Res 246: 293-301.

Fujii S, Jia Y, Yang A, Sumikawa K. 2000. Nicotine reverses GABAergic inhibition of long-term potentiation induction in the hippocampal CA1 region. Brain Res 863: 259-265.

Gage FH, Bjorklund A, Stenevi U. 1983. Reinnervation of the partially deafferented hippocampus by compensatory collateral sprouting from spared cholinergic and noradrenergic afferents. Brain Res 268: 27-37.

Hasselmo ME and Bower JM. 1992. Cholinergic suppression specific to intrinsic not afferent fiber synapses in rat piriform (olfactory) cortex. J Neurophysiol 67: 1222-1229.

Hasselmo ME and Bower JM. 1993. Acetylcholine and memory. Trends Neurosci 16: 218-222.

Hasselmo ME and Schnell E. 1994. Laminar selectivity of the cholinergic suppression of synaptic transmission in rat hippocampal region CA1: computational modeling and brain slice physiology. J Neurosci 14: 3898-3914.

Henderson Z, Harrison PS, Jagger E, Beeby JH. 1998. Density of choline acetyltransferase-immunoreactive terminals in the rat dentate gyrus after entorhinal cortex lesions: a quantitative light microscope study. Exp Neurol 152: 50-63.

Hill JA, Zoli M, Bourgeois JP, Changeux JP. 1993. Immunocytochemical localization of a neuronal nicotinic receptor: the beta 2-subunit. J Neurosci 13: 1551-1568.

Hohmann CF, Potter ED, Levey AI. 1995. Development of muscarinic receptor subtypes in the forebrain of the mouse. J Comp Neurol 358: 88-101.

Houser CR, Crawford GD, Barber RP, Salvaterra PM, Vaughn JE. 1983. Organization and morphological characteristics of cholinergic neurons: an immunocytochemical study with a monoclonal antibody to choline acetyltransferase. Brain Res 266: 97-119.

Ichikawa T, Ajiki K, Matsuura J, Misawa H. 1997. Localization of two cholinergic markers, choline acetyltransferase and vesicular acetylcholine transporter in the central nervous system of the rat: in situ hybridization histochemistry and immunohistochemistry. J Chem Neuroanat 13: 23-39.

Ji D and Dani JA. 2000. Inhibition and disinhibition of pyramidal neurons by activation of nicotinic receptors on hippocampal interneurons. J Neurophysiol 83: 2682-2690.

Jones S and Yakel JL. 1997. Functional nicotinic ACh receptors on interneurones in the rat hippocampus. J Physiol (Lond) 504: 603-610.

Kim JS and Levin ED. 1996. Nicotinic, muscarinic and dopaminergic actions in the ventral hippocampus and the nucleus accumbens: effects on spatial working memory in rats. Brain Res 725: 231-240.

Kitt CA, Hohmann C, Coyle J T, Price DL. 1994. Cholinergic innervation of mouse forebrain structures. J Comp Neurol 341: 117-129.

Leonard S, Breese C, Adams C, Benhammou K, Gault J, Stevens K, Lee M, Adler L, Olincy A, Ross R, Freedman R. 2000. Smoking and schizophrenia: abnormal nicotinic receptor expression. Eur J Pharmacol 393: 237-242.

Levey AI, Edmunds SM, Koliatsos V, Wiley RG, Heilman CJ. 1995. Expression of m1-m4 muscarinic acetylcholine receptor proteins in rat hippocampus and regulation by cholinergic innervation. J Neurosci 15: 4077-4092.

Lindstrom J. 1997. Nicotinic acetylcholine receptors in health and disease. Mol Neurobiol 15: 193-222.

Lysakowski A, Wainer BH, Bruce G, Hersh LB. 1989. An atlas of the regional and laminar distribution of choline acetyltransferase immunoreactivity in rat cerebral cortex. Neuroscience 28: 291-336.

Madison DV, Lancaster B, Nicoll RA. 1987. Voltage clamp analysis of cholinergic action in the hippocampus. J Neurosci 7: 733-741.

Maeda, T, Kaneko S, Satoh M. 1994. Roles of endogenous cholinergic neurons in the induction of long-term potentiation at hippocampal mossy fiber synapses. Neurosci Res 20: 71-78.

Matthews DA, Salvaterra PM, Crawford GD, Houser CR, Vaughn JE. 1987. An immunocytochemical study of choline acetyltransferase-containing neurons and axon terminals in normal and partially deafferented hippocampal formation. Brain Res 402: 30-43.

McKinney M, Coyle JT, Hedreen JC. 1983. Topographic analysis of the innervation of the rat neocortex and hippocampus by the basal forebrain cholinergic system. J Comp Neurol 217: 103-121.

McQuiston AR and Madison DV. 1999a. Muscarinic receptor activity has multiple effects on the resting membrane potentials of CA1 hippocampal interneurons. J Neurosci 19: 5693-5702.

McQuiston AR and Madison DV. 1999b. Nicotinic receptor activation excites distinct subtypes of interneurons in the rat hippocampus. J Neurosci 19: 2887-2896.

Mechawar N and Descarries L. 2001. The cholinergic innervation develops early and rapidly in the rat cerebral cortex: A quantitative immunocytochemical study. J Neurosci, submitted.

Mechawar N, Cozzari C, Descarries L. 2000. Cholinergic innervation in adult rat cerebral cortex: A quantitative immunocytochemical description. J Comp Neurol 428: 305-318.

Mizuno T and Kimura F. 1996. Medial septal injection of naloxone elevates acetylcholine release in the hippocampus and induces behavioral seizures in rats. Brain Res 713: 1-7.

Nishimura Y, Natori M, Mato M. 1988. Choline acetyltransferase immunopositive pyramidal neurons in the rat frontal cortex. Brain Res 440: 144-148.

Nyakas C, Luiten PG, Spencer DG, Traber J. 1987. Detailed projection patterns of septal and diagonal band efferents to the hippocampus in the rat with

emphasis on innervation of CA1 and dentate gyrus. Brain Res Bull 18: 533-545.

Oleskevich S and Descarries L. 1990. Quantified distribution of the serotonin innervation in adult rat hippocampus. Neuroscience 34: 19-33.

Oleskevich S, Descarries L, Lacaille JC. 1989. Quantified distribution of the noradrenaline innervation in the hippocampus of adult rat. J Neurosci 9: 3803-3815.

Olton DS. 1977. Spatial memory. Sci Am 236: 82-98.

Radcliffe KA and Dani JA. 1998. Nicotinic stimulation produces multiple forms of increased glutamatergic synaptic transmission. J Neurosci 18: 7075-7083.

Radcliffe KA, Fisher JL, Gray R, Dani JA. 1999. Nicotinic modulation of glutamate and GABA synaptic transmission of hippocampal neurons. Ann NY Acad Sci 868: 591-610.

Robertson RT and Gorenstein C. 1987. 'Non-specific' cholinesterase-containing neurons of the dorsal thalamus project to medial limbic cortex. Brain Res 404: 282-292.

Roghani A, Shirzadi A, Kohan SA, Edwards RH, Butcher LL. 1996. Differential distribution of the putative vesicular transporter for acetylcholine in the rat central nervous system. Brain Res Mol Brain Res 43: 65-76.

Rouse ST, Edmunds SM, Yi H, Gilmor ML, Levey AI. 2000. Localization of M(2) muscarinic acetylcholine receptor protein in cholinergic and non-cholinergic terminals in rat hippocampus. Neurosci Lett 284: 182-186.

Rouse ST, Marino MJ, Potter LT, Conn PJ, Levey AI. 1999. Muscarinic receptor subtypes involved in hippocampal circuits. Life Sci 64: 501-509.

Rye DB, Wainer BH, Mesulam MM, Mufson EJ, Saper CB. 1984. Cortical projections arising from the basal forebrain: a study of cholinergic and noncholinergic components employing combined retrograde tracing and immunohistochemical localization of choline acetyltransferase. Neuroscience 13: 627-643.

Sargent PB 1993. The diversity of neuronal nicotinic acetylcholine receptors. Annu Rev Neurosci 16: 403-443.

Schäfer MK, Eiden LE, Weihe E. 1998. Cholinergic neurons and terminal fields revealed by immunohistochemistry for the vesicular acetylcholine transporter. I. Central nervous system. Neuroscience 84: 331-359.

Schwegler H, Boldyreva M, Linke R, Wu J, Zilles K, Crusio WE. 1996. Genetic variation in the morphology of the septo-hippocampal cholinergic and GABAergic systems in mice: II. Morpho-behavioral correlations. Hippocampus 6: 535-545.

Séguéla P, Wadiche J, Dineley-Miller K, Dani JA, Patrick JW. 1993. Molecular cloning, functional properties, and distribution of rat brain alpha 7: a nicotinic cation channel highly permeable to calcium. J Neurosci 13: 596-604.

Shi ZR, Itzkowitz SH, Kim YS. 1988. A comparison of three immunoperoxidase techniques for antigen detection in colorectal carcinoma tissues. J Histochem Cytochem 36: 317-322.

Shimono K, Brucher F, Granger R, Lynch G,. Taketani M. 2000. Origins and distribution of cholinergically induced beta rhythms in hippocampal slices. J Neurosci 20: 8462-8473.

Skutella T and Nitsch R. 2001. New molecules for hippocampal development. Trends Neurosci 24: 107-113.

Slomianka, L and Geneser FA. 1991. Distribution of acetylcholinesterase in the hippocampal region of the mouse: II. Subiculum and hippocampus. J Comp Neurol 312:525-36.

Slomianka, L and Geneser FA. 1993. Distribution of acetylcholinesterase in the hippocampal region of the mouse: III. The area dentata. J Comp Neurol 331: 225-235.

Soghomonian J-J, Doucet G, Descarries L. 1987. Serotonin innervation in adult rat neostriatum. I. Quantified regional distribution. Brain Res 425: 85-100.

Steinlein OK. 2000. Neuronal nicotinic receptors in human epilepsy. Eur J Pharmacol 393: 243-247.

Storm-Mathisen JS and Blackstad TW. 1964. Cholinesterase in the hippocampal region. Acta Anat 56: 216-253.

Super H, Martinez A, Del Rio JA, Soriano E. 1998. Involvement of distinct pioneer neurons in the formation of layer- specific connections in the hippocampus. J Neurosci 18: 4616-4626.

Swanson LW. 1992. Brain Maps: Structure of the Rat Brain. Amsterdam: Elsevier.

Umbriaco D, Watkins KC, Descarries L, Cozzari C, Hartman BK. 1994. Ultrastructural and morphometric features of the acetylcholine innervation in adult rat parietal cortex: an electron microscopic study in serial sections. J Comp Neurol 348: 351-373.

Umbriaco D, Garcia S, Beaulieu C, Descarries L. 1995. Relational features of acetylcholine, noradrenaline, serotonin and GABA axon terminals in the stratum radiatum of adult rat hippocampus (CA1). Hippocampus 5: 605-620.

van der Zee EA and Luiten PG. 1999. Muscarinic acetylcholine receptors in the hippocampus, neocortex and amygdala: a review of immunocytochemical localization in relation to learning and memory. Prog Neurobiol 58: 409-471.

Vann SD, Brown MW, Aggleton JP. 2000a. Fos expression in the rostral thalamic nuclei and associated cortical regions in response to different spatial memory tests. Neuroscience 101: 983-991.

Vann SD, Brown MW, Erichsen JT, Aggleton JP. 2000b. Fos imaging reveals differential patterns of hippocampal and parahippocampal subfield

activation in rats in response to different spatial memory tests. J Neurosci 20: 2711-2718.

Vogt KE and Regehr WG. 2001. Cholinergic Modulation of Excitatory Synaptic Transmission in the CA3 Area of the Hippocampus. J Neurosci 21: 75-83.

Wan H, Aggleton JP, Brown MW. 1999. Different contributions of the hippocampus and perirhinal cortex to recognition memory. J Neurosci 19: 1142-1148.

Weihe E, Tao-Cheng JH, Schafer MK, Erickson JD, Eiden LE. 1996. Visualization of the vesicular acetylcholine transporter in cholinergic nerve terminals and its targeting to a specific population of small synaptic vesicles. Proc Natl Acad Sci USA 93: 3547-3552.

West MJ. 1990. Stereological studies of the hippocampus: a comparison of the hippocampal subdivisions of diverse species including hedgehogs, laboratory rodents, wild mice and men. Prog Brain Res 83: 13-36.

Williams JH and Kauer JA. 1997. Properties of carbachol-induced oscillatory activity in rat hippocampus. J Neurophysiol 78: 2631-2640.

Witter MP, Naber PA, van Haeften T, Machielsen WC, Rombouts SA, Barkhof F, Scheltens P, Lopes da Silva FH. 2000. Cortico-hippocampal communication by way of parallel parahippocampal- subicular pathways. Hippocampus 10: 398-410.

Wong TP, Debeir T, Duff K, Cuello AC. 1999. Reorganization of cholinergic terminals in the cerebral cortex and hippocampus in transgenic mice

carrying mutated presenilin-1 and amyloid precursor protein transgenes. J Neurosci 19: 2706-2716.

Woolf NJ. 1991. Cholinergic systems in mammalian brain and spinal cord. Prog Neurobiol 37: 475-524.

Wyble BP, Linster C, Hasselmo ME. 2000. Size of CA1-evoked synaptic potentials is related to theta rhythm phase in rat hippocampus. J Neurophysiol 83: 2138-2144.

Yun SH, Cheong MY, Mook-Jung I, Huh K, Lee C, Jung MW. 2000. Cholinergic modulation of synaptic transmission and plasticity in entorhinal cortex and hippocampus of the rat. Neuroscience 97: 671-676.

## Figure legends

**Figure 1** Low and high power views from mouse (**A,B**) and rat (**C,D**) dorsal hippocampus. **A** and **C** illustrate the overall distribution of the ACh (ChAT-immunostained) innervation in the plane of section examined (interaural A 1.98 mm in mouse and bregma – 3.7 mm in rat). The three regions in which the ACh innervation was quantified are outlined: CA1, CA3 and DG. In each region, three rows of squares, disposed in the various layers, represent the sampling windows, 50 µm in side, from which length measurements of the ChAT-immunostained axon network were obtained, as described in Materials and Methods. See Results for a detailed description of the layered pattern of ACh innervation, and Table 1 for quantitative data on the density of ACh innervation in each layer and hippocampal region. The adjacent enlargements (**B** and **D**) are digitized light microscopic images of one of the sampling windows in the stratum radiatum of CA1. Note the greater density of ACh innervation in mouse than rat. Scale bars: for **A** and **C**, 0.5 mm in **C**; for **B** and **D**, 10 µm in **D**.

**Figure 2** Laminar distribution of the ACh innervation in the dorsal hippocampus of adult mouse: CA1 and DG (**A**), CA3 (**B**); (see Table 1 and Fig. 4 for quantitative data). The density of ACh innervation is obviously much less in CA1 than in DG or CA3. In CA1 (**A**), note the three layered pattern in the stratum pyramidale (pyr), and the presence of two interneurons (arrows) within the band of slightly denser innervation (asterisks) at the border of stratum radiatum (rad) and lacunosum

moleculare (lm). One of these two ACh interneurons is shown at higher magnification in **C**, among trajectories of fine varicose axons many of which appear to run medio-laterally. In the DG (**A**), the layered pattern formed by the alternation of strata moleculare (mol), granulare (gr) and polymorph (pm) is accentuated by the narrow bands of denser innervation on either side of the stratum granulare. CA3 (**B**) is rotated more than 90° for presentation. Note the dense innervation, but lack of stratification, in its widened pyramidal layer (pyr), contrasting with the low density in the underlying stratum lucidum (luc). The density in stratum radiatum (rad) is equivalent to that in CA1, whereas both oriens (or) and lacunosum moleculare (lm) are much more densely innervated in CA3 than CA1. Scale bars: for **A** and **B**, 100 µm in **B**; for **C**, 50 µm.

**Figure 3** Laminar distribution of the ACh innervation in the dorsal hippocampus of adult rat: CA1 and DG (**A**), CA3 (**B**); (see Table 1 and Fig. 5 for quantitative data). Same magnifications as in Fig. 2, for purposes of comparison. The contrast between the density of ACh innervation in CA1 versus DG or CA3 is greater than in mouse. In CA1 (**A**), the three layered pattern in the stratum pyramidale (pyr) resembles that in mouse, but the innervation of stratum radiatum (rad) and particularly of lacunosum moleculare (lm) is much less dense. Note the bipolar interneuron (arrow), and its thick proximal dendrites, near the border of lacunosum moleculare and radiatum (enlarged in **C**). In DG (**A**), the overall density of innervation is very similar to that in mouse, whereas the layering patterns on either side of the stratum granulare (gr) and within the

stratum moleculare (mol) are more prominent. In CA3 (**B**) the laminar distribution and density of innervation is almost identical to that in mouse. Note the axon with a string of relatively large varicosities running above the horizontal portion of the upper dendrite in **C**. luc, lucidum. Scale bars: for **A** and **B**, 100 μm in **B**; for **C**, 50 μm.

**Figure 4** Laminar and regional density of ACh axons and axon varicosities in the dorsal hippocampus of adult mouse (CA1, CA3 and DG). Data derived from the values in Table 1, as explained in Materials and Methods. Means ± s.e.m. in meter of axons or millions of axon varicosities per $mm^3$. The layers showing statistically significant differences are linked by hooks with asterisks in front of the differing layer(s). * ($p < 0.05$), ** ($p < 0.01$) and *** ($p < 0.001$) indicate significant differences between layers by Student t test.

**Figure 5** Laminar and regional density of ACh axons and axon varicosities in the dorsal hippocampus of adult rat (CA1, CA3 and DG). Data derived from the values in Table 1, as explained in Materials and Methods. Means ± s.e.m. in meter of axons or millions of axon varicosities per $mm^3$. The layers showing statistically significant differences are linked by hooks with asterisks in front of the differing layer(s). * ($p < 0.05$), ** ($p < 0.01$) and *** ($p < 0.001$) indicate significant differences between layers by Student t test.

Table 1. Laminar and regional density of ACh axons and varicosities in the dorsal hippocampus of adult mouse and rat

| | | MOUSE | | RAT | |
|---|---|---|---|---|---|
| | | Axons ($m/mm^3$) | Varicosities ($10^6/mm^3$) | Axons ($m/mm^3$) | Varicosities ($10^6/mm^3$) |
| CA1 | Oriens | 13.7 ± 0.9 | 5.5 ± 0.3 | 14.8 ± 1.1 | 5.9 ± 0.5 |
| | Pyramidale | 17.9 ± 1.0 | 7.2 ± 0.4 | 17.0 ± 1.8 | 6.8 ± 0.7 |
| | Radiatum | 13.3 ± 1.6 | 5.3 ± 0.6 | 10.6 ± 1.6 * | 4.2 ± 0.6 * |
| | L. Moleculare | 10.8 ± 1.3 | 4.3 ± 0.5 | 6.4 ± 1.2 *** | 2.6 ± 0.5 *** |
| | Mean | 13.9 ± 0.7 | 5.6 ± 0.3 | 12.2 ± 1.0 | 4.9 ± 0.4 |
| CA3 | Oriens | 16.7 ± 0.9 | 6.7 ± 0.3 | 17.8 ± 1.4 | 7.1 ± 0.6 |
| | Pyramidale | 19.6 ± 0.9 | 7.8 ± 0.4 | 20.4 ± 1.3 | 8.2 ± 0.5 |
| | Lucidum | 10.4 ± 1.2 | 4.2 ± 0.5 | 10.7 ± 1.6 | 4.3 ± 0.7 |
| | Radiatum | 13.7 ± 0.9 | 5.5 ± 0.3 | 13.2 ± 1.2 | 5.3 ± 0.5 |
| | L. Moleculare | 20.2 ± 1.0 | 8.1 ± 0.4 | 18.8 ± 1.4 | 7.5 ± 0.5 |
| | Mean | 16.1 ± 0.7 | 6.4 ± 0.3 | 16.2 ± 0.8 | 6.6 ± 0.3 |
| DG | Moleculare | 19.9 ± 1.2 | 8.0 ± 0.5 | 19.5 ± 1.2 | 7.8 ± 0.5 |
| | Granulare | 13.6 ± 1.6 | 5.4 ± 0.6 | 13.4 ± 1.7 | 5.4 ± 0.7 |
| | Polymorph | 13.9 ± 2.4 | 5.6 ± 1.0 | 13.8 ± 1.8 | 5.5 ± 0.7 |
| | Mean | 15.8 ± 1.2 | 6.2 ± 0.6 | 15.6 ± 1.2 | 6.2 ± 0.5 |
| HIPPOCAMPUS | | 15.3 ± 0.7 | 6.1 ± 0.7 | 14.7 ± 0.7 | 5.9 ± 0.3 |

Data from 6 mice and 6 rats. Means ± s.d. in meters of axon and millions of axon varicosities per $mm^3$. See Figs. 5 and 6 for statistical analysis of differences between layers in each species. * $p < 0.05$, *** $p < 0.001$ indicate interspecies differences by Student t test.

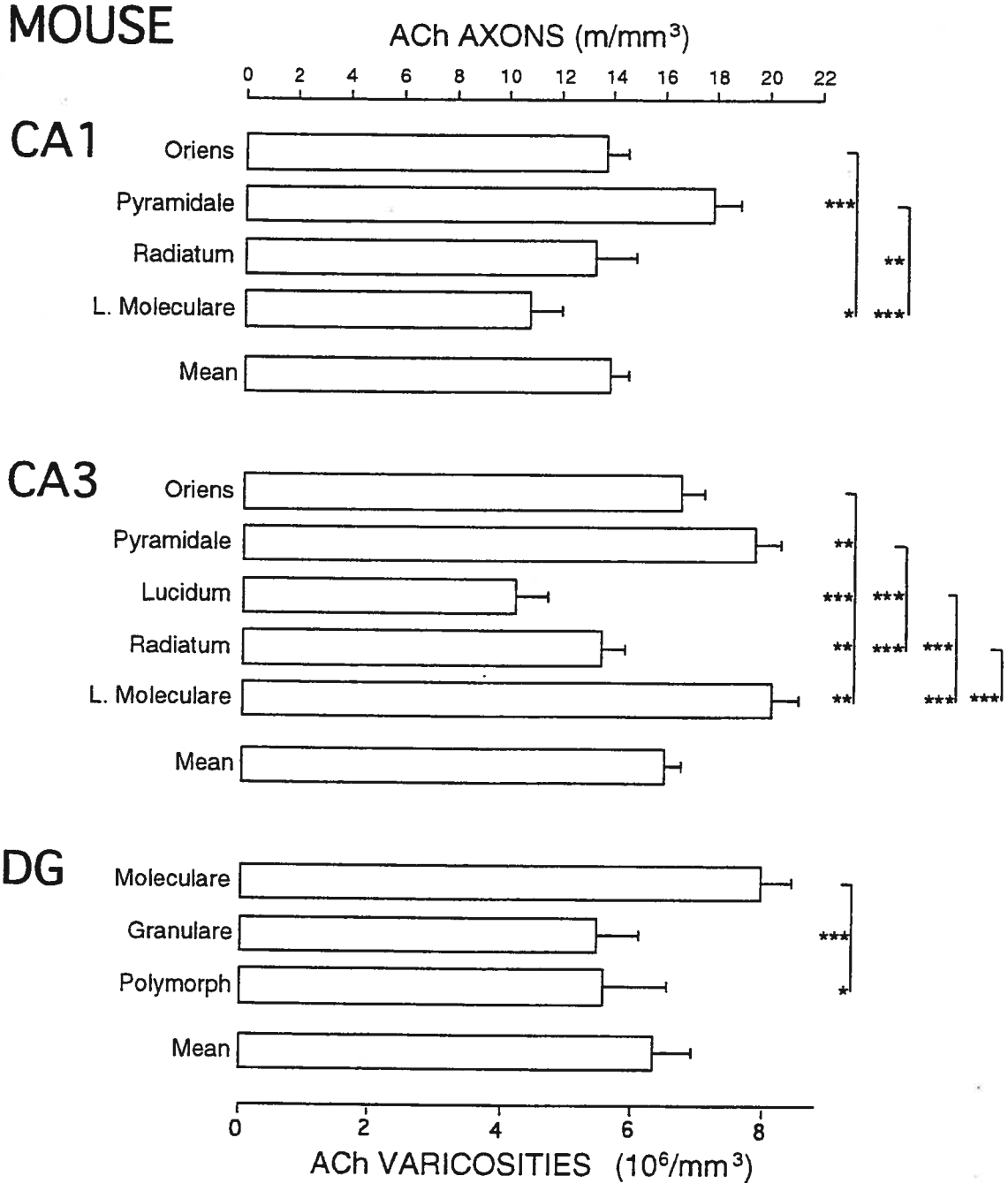
MOUSE
ACh AXONS (m/mm³)
0 2 4 6 8 10 12 14 16 18 20 22
CA1
Oriens
Pyramidale
Radiatum
L. Moleculare
Mean
***
**
*
***
CA3
Oriens
Pyramidale
Lucidum
Radiatum
L. Moleculare
Mean
**
***
***
**
***
***
**
***
***
DG
Moleculare
Granulare
Polymorph
Mean
***
*
0 2 4 6 8
ACh VARICOSITIES (10⁶/mm³)

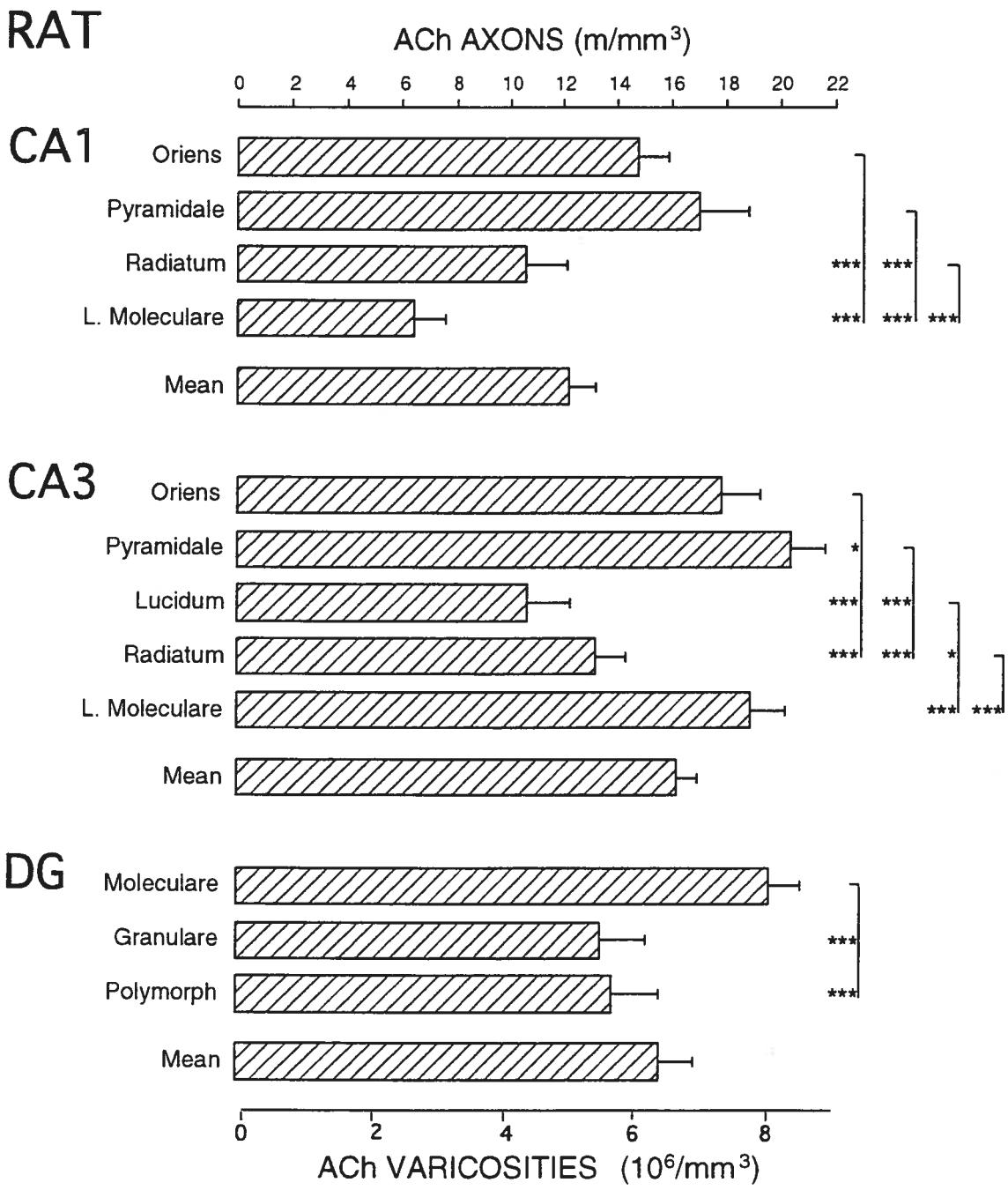
RAT
ACh AXONS (m/mm3)
0 2 4 6 8 10 12 14 16 18 20 22
CA1
Oriens
Pyramidale
Radiatum
L. Moleculare
Mean
***
***
***
***
***
CA3
Oriens
Pyramidale
Lucidum
Radiatum
L. Moleculare
Mean
*
***
***
***
***
*
***
***
DG
Moleculare
Granulare
Polymorph
Mean
***
***
0 2 4 6 8
ACh VARICOSITIES (10⁶/mm3)

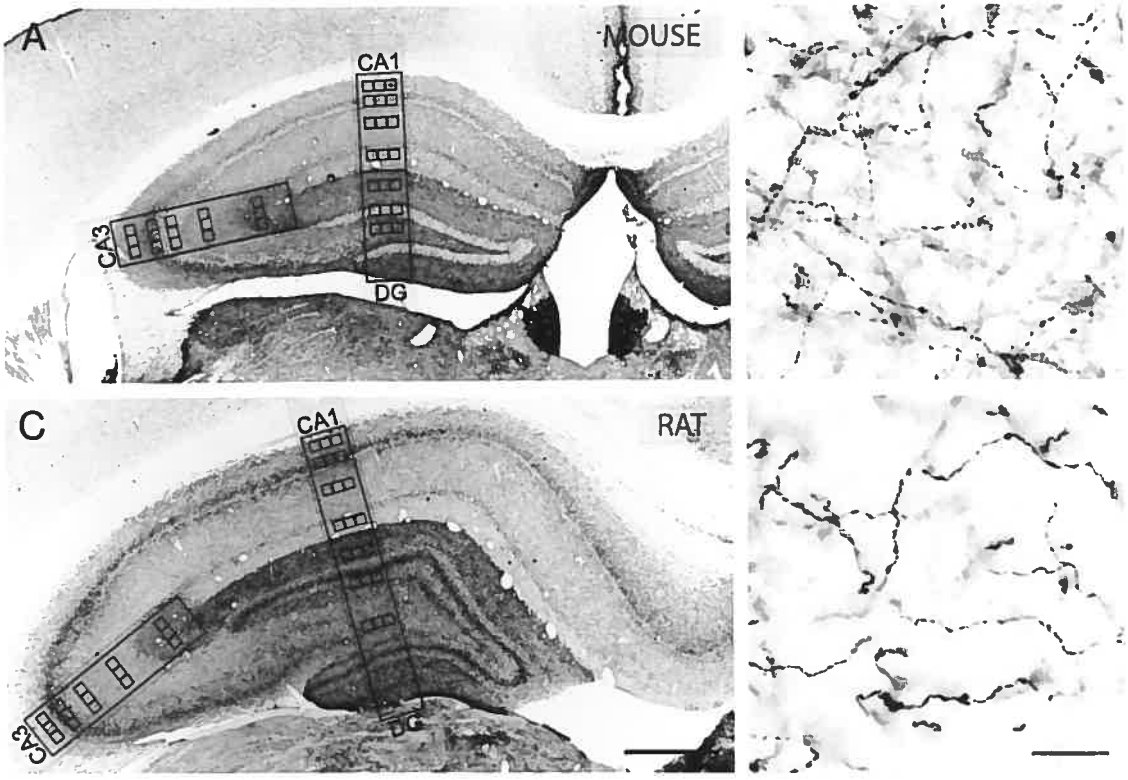
A
MOUSE
CA1
CA3
DG
C
RAT
CA1
CA3
DG

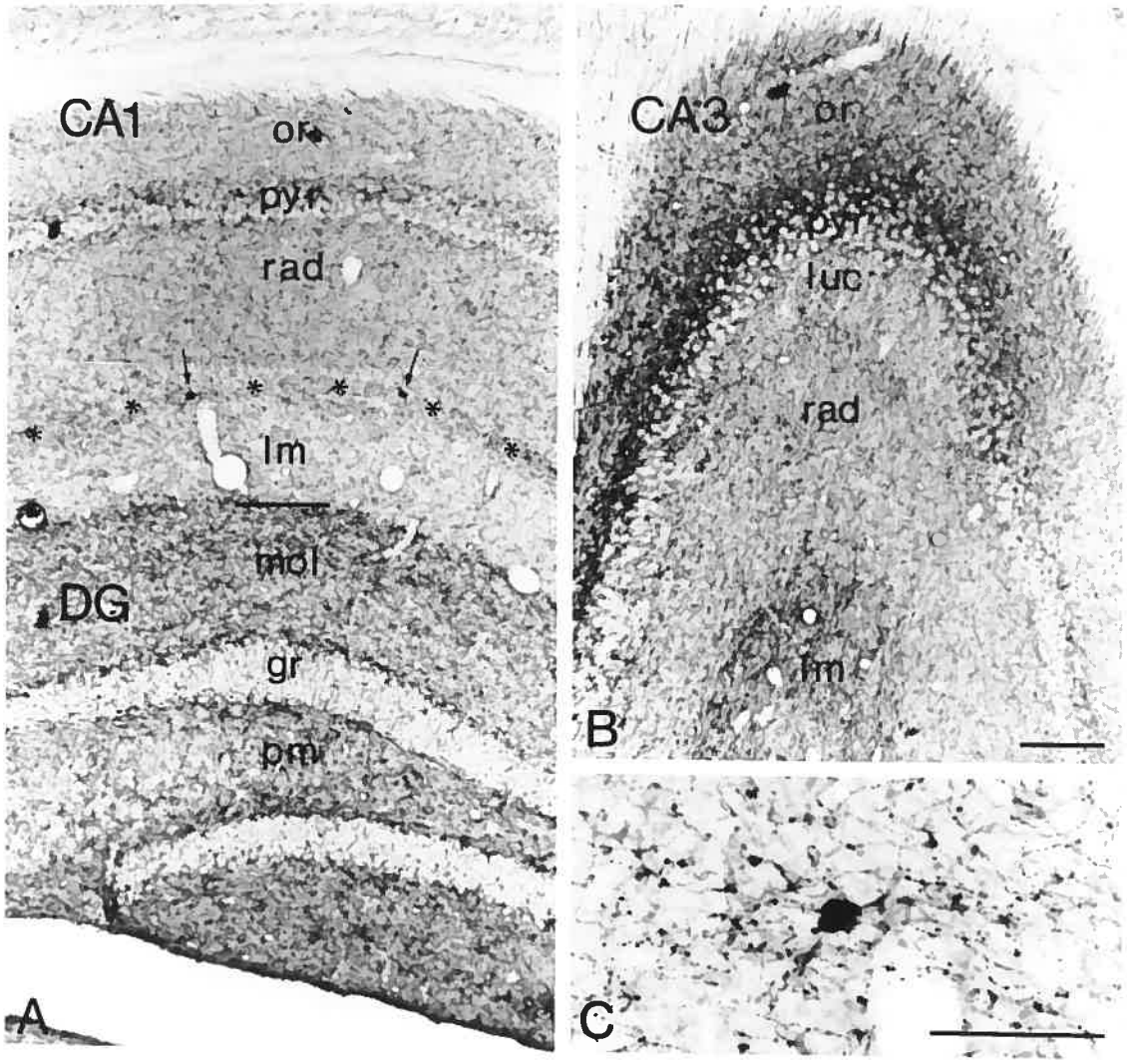
CA1
or
pyr
rad
lm
mol
DG
gr
pm
A
CA3
or
pyr
luc
rad
lm
B
C

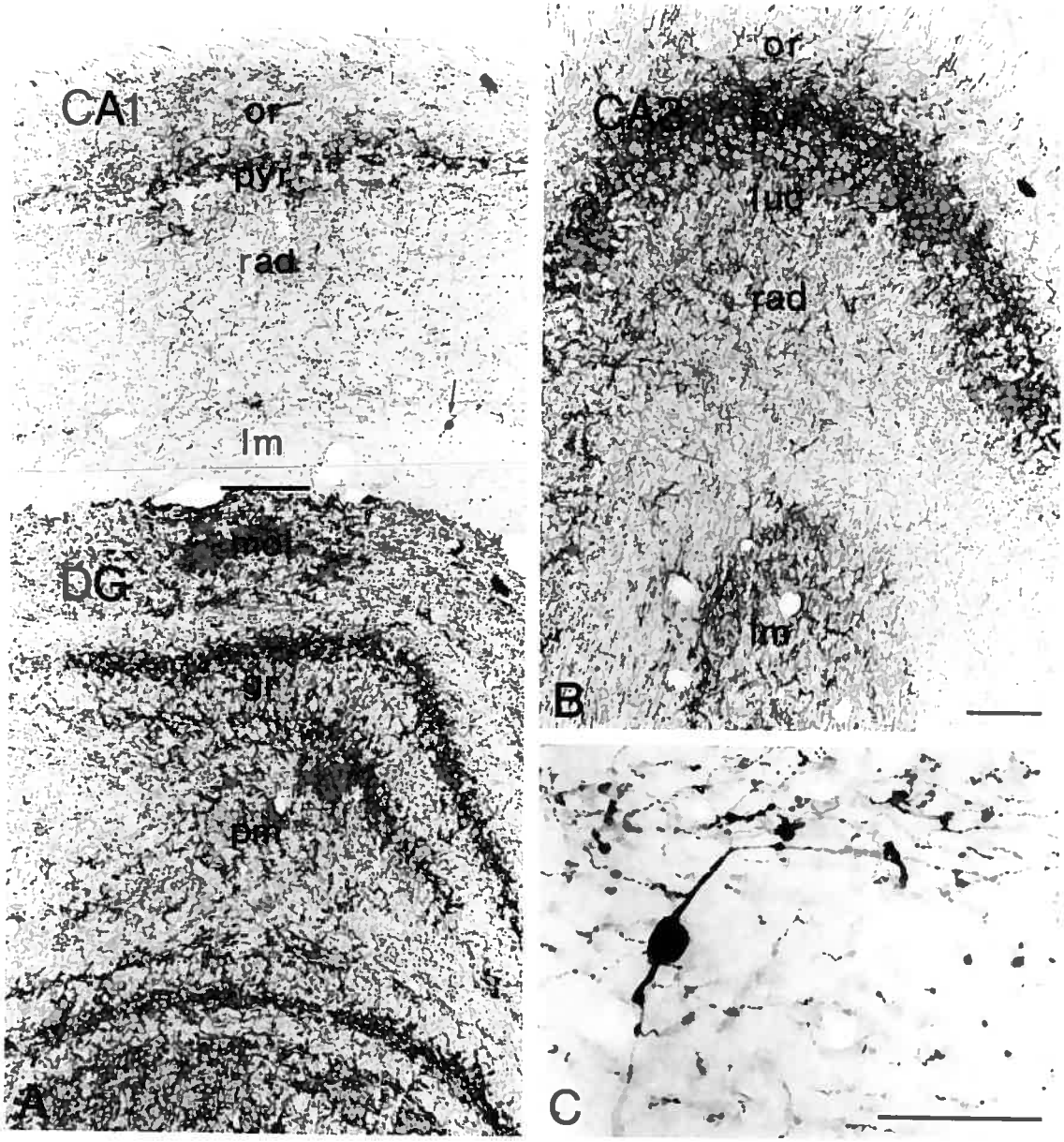
CA1
or
pyr
rad
lm
mol
DG
gr
pm
A
or
CA2
lud
rad
lm
B
C

Chapitre III

# POSTNATAL DEVELOPMENT OF THE CHOLINERGIC INNERVATION IN THE DORSAL HIPPOCAMPUS OF RAT: A QUANTITATIVE LIGHT AND ELECTRON MICROSCOPIC IMMUNOCYTOCHEMICAL STUDY

Sous presse dans *The Journal of Comparative Neurology*

(N AZNAVOUR, KC Watkins et L DESCARRIES)

# POSTNATAL DEVELOPMENT OF THE CHOLINERGIC INNERVATION IN THE DORSAL HIPPOCAMPUS OF RAT: A QUANTITATIVE LIGHT AND ELECTRON MICROSCOPIC IMMUNOCYTOCHEMICAL STUDY

Nicolas AZNAVOUR, Kenneth C. WATKINS and Laurent DESCARRIES

Départements de pathologie et biologie cellulaire et de physiologie, and

Centre de recherche en sciences neurologiques,

Faculté de médecine, Université de Montréal, Montréal, Québec,

Canada H3C 3J7

(44 text pages including figure legends, plus 3 tables and 7 figures)

Abbreviated title: **ACh innervation in the developing hippocampus**

KEYWORDS: acetylcholine – ACh – choline acetyltransferase – ChAT – axon – varicosities– distribution –immunocytochemistry – ontogeny

Correspondence: Laurent DESCARRIES m.d.
Département de pathologie et biologie cellulaire
Université de Montréal
CP 6128, Succursale Centre-ville
Montréal, QC, Canada H3C 3J7
tel. (514) 343-7070
fax (514) 343-5755
[redacted]

Grant sponsor: Canadian Institute of Health Research; Grant number: NRF 3544.

## ABSTRACT

Choline acetyltransferase (ChAT) immunocytochemistry was used to examine the distribution and ultrastructural features of the acetylcholine (ACh) innervation in the dorsal hippocampus of postnatal rat. The length of ChAT-immunostained axons was measured, and the number of ChAT-immunostained varicosities counted, in each layer of CA1, CA3 and the dentate gyrus, at postnatal ages P8, P16 and P32. At P8, an elaborate network of varicose ChAT-immunostained axons was already visible. At P16, the laminar distribution of this network resembled that in adult, but adult densities were reached only by P32. Between P8 and P32, the mean densities for the three regions increased from 8.4 to 14 meters of axons, and 2.3 to 5.7 million varicosities per $mm^3$ of tissue. At the three postnatal ages, the ultrastructural features of ChAT-immunostained axon varicosities from the strata pyramidale and radiatum of CA1 were similar between layers and comparable to those in adult, except for an increasing frequency of mitochondria (up to 41% at P32). The proportion of these profiles displaying a synaptic junction was similarly low at all ages, indicating an average synaptic incidence of 7% for whole varicosities, as already found in adult. The observed junctions were small, usually symmetrical and mostly made with dendritic branches. These results demonstrate the precocious and rapid maturation of the hippocampal cholinergic innervation and reveal its largely asynaptic nature as soon as it

is formed. They emphasize the remarkable growth capacities of individual ACh neurons and substantiate a role for diffuse transmission by ACh during hippocampal development.

## INTRODUCTION

There is considerable evidence implicating hippocampal acetylcholine (ACh) in cognitive processes, such as attention, learning and memory (reviewed in Hasselmo and McGaughy, 2004). Impairment of the ACh system in hippocampus has been reported at all stages of Alzheimer's disease (Davies and Maloney, 1976; Whitehouse et al., 1982; Geula and Mesulam, 1996; Beach, et al., 2000; Mufson et al., 2002; reviewed in Kar and Quirion, 2004), in certain forms of epilepsy (reviewed in Steinlein, 2004), and in schizophrenia (Freedman et al., 1997; Lindstrom, 1997; Adler et al., 1998; Freedman et al., 1999; Breese et al., 2000; Leonard et al., 2000).

In rat, the ACh innervation of hippocampus originates mainly from a population of 14 300 neuronal cell bodies in the medial septum and nucleus of the vertical limb of the diagonal band of Broca, named groups Ch1 and Ch2 (Mesulam et al., 1983; Rye et al., 1984; Amaral and Kurz, 1985; Nyakas et al., 1987; Woolf, 1991; Cadete-Leite et al., 2003). These cells are derived from the ganglionic eminence, a bulge on the ventricular wall, present during early stages of telencephalic development (Krnjevic and Silver, 1966, reviewed in Semba, 2004). They are born from E12 to E17, with a peak at E15 (Fine, 1987; Semba and Fibiger, 1988; Koh and Loy, 1989), and start to express choline acetyltranferase (ChAT) mRNA (Bender et al., 1996) when their first

projections reach the hippocampus (E19) (Linke and Frotscher, 1993). A lesser component of the hippocampal ACh innervation arises from bipolar interneurons, and accounts for 5-10% of the total choline acetyltransferase (ChAT) activity in this region (Gage et al. 1983).

ACh exerts its effects via muscarinic and nicotinic receptors, which are present and functional during the first postnatal days (Milburn and Prince, 1993; Goldbach et al., 1998; Avignone and Cherubini, 1999; Maggi et al., 2001; Leslie et al., 2002; Maggi et al., 2003). In rat hippocampus, it has been shown that the expression of the α7 and β4 nicotinic subunits, and protein levels of the α7 subunit, peak around the end of the first postnatal week, followed by a progressive decline to adult values around P30 (Shacka and Robinson, 1998; Adams et al., 2002). In contrast, muscarinic receptors only become noticeable during the first postnatal week in hippocampus, and then increase until adulthood (Miyoshi et al., 1987; Aubert et al., 1996; Tice et al., 1996). Prior studies have also shown that, in the adult and during development, ACh depolarizes a majority of pyramidal neurons in hippocampus (Cole and Nicoll, 1984; Madison et al., 1987; Benson et al., 1988; Reece and Schwartzkroin, 1991a) and modulates glutamate and/or GABA release (Reece and Schwartzkroin, 1991b; Radcliffe and Dani, 1998; Alkondon et al., 1999; Avignone and Cherubini 1999; McQuiston and Madison, 1999a,b; Radcliffe et al., 1999; Ji and Dani, 2000; Maggi et al., 2001, 2003). These widespread effects

presumably account for several types of large-scale, synchronous neuronal activities, such as the giant depolarizing potentials observed during the first postnatal week (Avignone and Cherubini 1999; Maggi et al., 2001), and for the θ rhythm, which appears during the first postnatal week (Jones and Yakel, 1997; Williams and Kauer, 1997; Chapman and Lacaille, 1999; Cobb et al., 1999; Shimono et al., 2000; Wyble et al., 2000; Karlsson and Blumberg, 2003).

In the present study, we took advantage of the availability of a highly sensitive monoclonal antibody against the whole molecule of rat ChAT (Cozzari et al., 1990) to describe qualitative and quantitative aspects of the growth, distribution and ultrastructural features of the cholinergic innervation in the developing hippocampus of postnatal rat. In particular, we sought to determine if this innervation develops as precociously and rapidly as the neocortical ACh innervation (Mechawar and Descarries, 2001), and if growing ACh axons in hippocampus are endowed with varicosities (terminals) that are morphologically mature. It was expected that such observations would allow for meaningful correlations with other parameters of cholinergic structure and function during hippocampal development.

# MATERIALS AND METHODS

## Tissue

All experiments abided by the policies and guidelines of the Canadian Council on Animal Care, and the regulations of the Animal Care Committee at the Université de Montréal. The study was carried out on 32 male Sprague-Dawley rats, purchased from Charles River Canada (St-Constant, Quebec, Canada).

For light microscopy, 4 rats per age (P0, P4, P8, P16, P32) were deeply anesthetized with sodium pentobarbital (80 mg/kg, i.p.), and perfused through the heart with ice-cold phosphate buffered saline (PBS; 50mM; pH 7.4; 25 ml), followed by 100-150 ml of 4% paraformaldehyde (PFA) in 0.1 M sodium phosphate buffer (PB; pH 7.4; 24°C) containing 0.1% glutaraldehyde, and last 250-300 ml PFA 4% in PB. The brain was then rapidly removed, postfixed overnight in PFA at 4°C, and cut with a Leica vibratome into 50 µm-thick (P0 and P4) or 20-µm-thick (P8-P32) transverse sections, at a transverse level corresponding to stereotaxic plane bregma – 3.7 mm in the adult (Swanson, 1992). The sections were then processed for ChAT-imunochemistry as described below, or stained with cresyl violet to delimit hippocampal regions and layers.

For electron microscopy, 4 rats per age (P8, P16, P32) were perfused with 25 ml PBS, followed by 300 ml PFA 4% in PB containing 0.25%

glutaraldehyde, and the brain postfixed for 90 minutes in the same solution before 50-µm sections were cut, as described above.

**ChAT-immunocytochemistry**

At room temperature, the free-floating sections were incubated 5 min in a 1% solution of sodium borohydride, rinsed with PBS (3 x 10 min), pre-incubated for 2 h in a blocking solution of PBS containing 2% normal horse serum (NHS; Vector, Burlingame, CA), 1% bovine serum albumin (BSA; Sigma, St. Louis, MO) and 0.2% Triton X-100, and incubated overnight in the same solution containing 2 µg/ml of monoclonal anti-ChAT antibody. Immunostaining was then performed, using the ABC method (Shi et al., 1988). After rinses in 0.1 M potassium phosphate buffer (KPB; pH 7,4; 3 x 10 min), sections were incubated for 2 h in biotinylated horse anti-mouse secondary antibody (Vector) diluted 1/200 in KPB containing 2% NHS and 1% BSA, followed by the avitidin-biotin complex procedure (ABC Kit, Vectastain Elite; Vector) for another 2 h. The labeling was then revealed for 2.25 min, in a 0.05% solution of 3,3'-diaminobenzidine (Sigma) containing 0.01% $CoCl_2$ and 0.01% $NiSO_4$, to which 0.005% $H_2O_2$ was added. Sections were rinsed in KPB (3 x 10 min), air-dried on gelatin-coated slides, dehydrated in ethanol, cleared in toluene, and mounted with DPX (Fluka; Sigma).

Sections intended for electron microscopy were processed similarly, except for the absence of Triton X-100 during incubations, and of $CoCl_2C/NiSO_4$ in the DAB solution. Following revelation in DAB, they were osmicated, dehydrated in ethanol and propylene oxide, and flat-embedded in Durcupan (Fluka; Sigma).

Control experiments included omission of the primary or secondary antibodies, which completely eliminated the immunostaining.

**Density of ChAT-immunostained axons and axon varicosities**

The density of the ChAT-immunostained axon network was measured at P8, P16 and P32, in three regions of dorsal hippocampus: CA1, CA3 and DG. In one section from 4 rats per age, digitized images of each region were obtained with an RT Color camera (Diagnostic Instruments, Inc., Sterling Heights, MI) mounted on a Leitz Diaplan microscope (25 X) and connected to a PC running SPOT RT Software (v3.1, Diagnostic Instruments). Using Photoshop (v7.0, Adobe Systems Inc., San Jose, CA), these images were assembled as a digital montage of the whole region, in which 3 square sampling windows, 50 µm in side, were positioned across each layer (e.g., Fig. 1). All ChAT-immunostained axons within the confines of these windows were then traced with an Intuos Graphics Tablet (Wacom, Vancouver, WA), for a total surface of 90 000 $\mu m^2$ per animal. Using the public domain program ImageJ (v1.3, NIH), the tracings

were reduced to a uniform width, all closed outlines were cut open by removal of 1 pixel, and the length of the network measured in micrometers, based on a prior calibration of the system with a microscopic scale. Assuming a random orientation of the axons in the section, the length values were converted to 1 $mm^3$ of tissue according to a simple stereological formula (Soghomonian et al. 1987), and the data expressed as average density of axons (meters per $mm^3$) in each layer, interlaminar mean for each region, and interregional mean for the entire dorsal hippocampus.

A further step was carried out to determine the density of ChAT-immunostained varicosities based on axon length values. In sections from 4 rats at each age (P8, P16 and P32), the average number of varicosities per unit length of immunostained axon was determined, with the aid of the image analysis system (40 X). The varicosities were defined as axon dilations > 0.5 µm in transverse diameter, since ChAT-immunostained axon dilations of that size have previously been shown to display all subcellular attributes of axon terminals in rat hippocampus (Umbriaco et al., 1995). Counts were obtained from 15 axon segments (at least 20 µm in length) per hippocampal layer in each region, for a total of 1850 counts. The resulting values at each age were then multiplied by the density of ChAT-immunostained axons to determine the laminar, regional and mean hippocampal densities of axon varicosities ($10^6$ per $mm^3$).

The densities of ChAT-immunostained axons and axon varicosities could thus be tabulated as means ± s.d. per $mm^3$ of tissue (n = 4). The P60 data, scored as end points, were from a previous publication (Aznavour et al., 2002).

**Electron microscopy**

Rectangular pieces from the center of CA1, spanning from the alveus to the hippocampal commissure, were removed from the flat-embedded ChAT-immunostained sections, glued to the tip of resin blocks, retrimmed to the size depicted in Fig. 1 (hatched area), and sectioned ultrathin (90-100 nm) with a Porter-Blum MT-2 Ultra Microtome. The sections were collected on Pioloform-coated, one-slot (2 x 0.6 mm) grids, stained with lead citrate, and examined with a Philips CM100 electron microscope. In each animal, 75-100 pictures of ChAT-immunostained varicosities from the stratum pyramidale, and the same number from the stratum radiatum, were taken at a working magnification of 13,500 X. As they were being examined in single thin sections, axon varicosities were defined as round or ovoid axonal profiles, greater than 0.25 µm in smallest diameter and containing aggregated small vesicles. On prints at 39 000 X, prepared under standard photographic and darkroom conditions, the first 50 sectional profiles of immunostained varicosities displaying a full contour and a distinct organelle content were kept for analysis.

With the aid of the public domain NIH Image program (1.61), these varicosity profiles were measured for area, long axis, short axis and diameter ((long axis + short axis) / 2), and classified as containing or not one or more mitochondria. The proportion engaged in synaptic junction was determined by categorizing the varicosity profiles as showing or not a junctional complex, i.e., a localized straightening of apposed plasma membranes with a slight widening of the intracellular space and/or a pre- or postsynaptic thickening. The synaptic frequency in single sections was converted to synaptic incidence for whole varicosities by means of the stereological formula of Beaudet and Sotelo (1981), which takes into account the average size of varicosity profiles, the length of their junctional complexes and the thickness of the sections. Measurement of the long axis rather than diameter was used in this formula, as proposed by Umbriaco et al. (1994). The junctions made by ChAT-immunostained profiles were further characterized as symmetrical or asymmetrical, and their synaptic targets identified, as dendritic branches or spines.

For purposes of comparison, we also examined the intrinsic and relational features of a population of unlabeled axon varicosities, selected at random in the electron micrographs from the stratum radiatum. For this purpose, a transparent overlay bearing a fixed mark in its upper left quadrant was used to identify the nearest fully visible unlabeled axon

varicosity profile in each print. Two hundred sectional profiles of unlabeled axon varicosities at each age were thus analyzed as above.

**Statistics**

The statistical comparisons between values at the different ages and the corresponding adult values were assessed by one-way analysis of variance, followed by Bonferroni's multiple comparison test. Differences were considered significant when $P < 0.05$. A one-way analysis of variance and a Student's t-test were used to determine if the dimensions (short axis, long axis, aspect ratio, diameter, area), synaptic incidence and synaptic targets of the ACh profiles differed significantly between the stratum pyramidale and the stratum radiatum at each age. Since no such differences were found, averages ± s.d. were calculated for all parameters, as presented in Tables 2 and 3. These results were then tested for age-related differences with Bonferroni's multiple comparison test, and differences considered significant when $P < 0.01$.

# RESULTS

## Laminar distribution of the ACh innervation in developing hippocampus

At P0, a few unbranched, ChAT-immunostained fibers, capped with growth cones, were already visible inside each region of the dorsal hippocampus (not illustrated, but see Fig. 2A). At P8, a network of fine varicose ChAT-immunostained axons already pervaded the whole hippocampus (Fig. 4), even if its distribution pattern did not yet match that of adult, notably in CA1 and in DG. Differences were particularly noticeable in CA1, where very few fibers were present at this age in the pyramidal layer, in sharp contrast with the adult (Fig. 4). Another difference was the presence, in the suprapyramidal blade of DG, of a remarkably dark band of ACh axons running in the inner-third of the molecular layer, adjacent to the outer border of the granular layer (Fig. 4). At P16, the laminar pattern of distribution of the ACh innervation resembled that in adult (Fig. 4). In CA1, the strata oriens, radiatum and lacunosum moleculare were homogeneously innervated, while a three layered pattern was noticeable in the stratum pyramidale, with dense bands of varicose axons on either side of the layer. A narrow band of innervation of lesser density was also visible at the border between the strata radiatum and lacunosum moleculare. In CA3, the stratum pyramidale already displayed a dark crescentic zone, riddled with the pale silhouettes of cell bodies outlined by varicose fibers on its inner face.

The stratum oriens showed an increasing density of ACh axons from its border with the alveus to that of the stratum pyramidale. In contrast the strata lucidum, radiatum, and the densely innervated lacunosum moleculare, were more homogeneously innervated. The DG also displayed a layered pattern, consisting of alternating bands of lesser and higher density of ACh innervation on either side of the stratum granulare.

**Quantitative data on the ACh innervation in developing hippocampus**

In all regions and layers of the hippocampus, the number of ACh varicosities per unit length of ACh axon increased rapidly during the first two postnatal weeks and slower thereafter, from 2.7 ± 0.11 ACh varicosities per 10 micrometers of axon at P8, to 3.6 ± 0.04 at P16, and 4.1 ± 0.13 (adult value; Aznavour et al., 2002) at P32 (Figs. 2 and 3).

As expressed in meters of ACh axon per $mm^3$, the growth of the ACh axon network was also maximal during the first two weeks (Table 1). On average, from P8 to P16, the length of the immunostained axon network increased by 56% in CA1, 57% in CA3 and 32% in DG. The combination of these two developmental parameters resulted in a strong augmentation of the density of ACh varicosities in the different layers and regions of hippocampus during the first postnatal weeks (Table 1, Figs. 4-5). Between P8 and P16, the density of ACh varicosities increased by 106% in CA1, 108% in CA3 and 74% in DG. A further maturation occurred from P16 to P32 with respective increases of 49%, 11% and 23% (average 28%) in the

three regions. At P32, all values were not significantly different from those previously measured in the adult (Aznavour et al., 2002).

**Ultrastructural features of ACh varicosities in the developing hippocampus**

Regardless of postnatal age, ACh axon varicosities shared similar ultrastructural characteristics in both the stratum pyramidale and radiatum of the dorsal hippocampus. As shown in Figs. 6 and 7, and quantified in Table 2, their sectional profiles arose from small diameter, unmyelinated axons, were generally elliptic, and contained numerous aggregated small clear vesicles, with or without a mitochondrion. The diaminobenzidine immunoprecipitate was of variable density, confined to the axoplasm, and often lined the the outer surface of organelles.

The various dimensions of ACh varicosities showed no statistically significant differences between P8, P16 and P32 (Table 2). Their average diameter across ages was $0.51 \pm 0.04$ μm, and their average sectional area $0.20 \pm 0.03$ $\mu m^2$. The proportion of ChAT-immunostained profiles containing one or more mitochondria increased significantly from 24.8% to 41%, between P16 and P32.

**Junctional relationships of ACh varicosities in the developing hippocampus**

Immunostained varicosity profiles endowed with a synaptic junction were observed at all ages in both stratum pyramidale and radiatum of

the dorsal hippocampus (e.g., Figs. 7C,F and I). The observed frequency of these synaptic profiles in single thin sections was consistently low, averaging 3% at P8 and 2% at P16 and P32 (Table 3). The mean length of the junctional complexes also appeared to be consistent, measuring 0.26 μm at P8, 0.24 μm at P16, and 0.28 μm at P32. The extrapolated synaptic incidence for whole varicosities, determined with the stereological formula of Beaudet and Sotelo (1981), amounted to 10% at P8, and 6% at P16 and P32. By comparison, the same extrapolation performed on randomly selected unlabeled profiles yielded considerably higher values, ranging from 84% at P8 to 147% (> one junction per varicosity) at P32.

As shown in Table 3 and Fig. 7, the relatively small synaptic junctions made by hippocampal ACh varicosities were always single, mostly symmetrical and more often made with dendritic branches than spines. In contrast, the synapses made by the unlabeled varicosities were in majority asymmetrical, irrespective of their localization on dendritic branches or spines. These unlabeled synapses were more frequent on dendritic branches than spines at P8, but became markedly different from those made by the ACh varicosities at P16 and P32, when they were mostly found on dendritic spines.

# DISCUSSION

This study provides a wealth of new data on the distribution and ultrastructural features of the ACh innervation in developing hippocampus. Earlier light microscopic descriptions of this innervation in posnatal rat had remained qualitative (Gould et al., 1991; Makuch et al., 2001), or semi-quantitative at best (Nyakas et al., 1994), and limited to particular hippocampal sectors. In addition, two of these studies had relied on histochemical staining for acetylcholinesterase. This enzyme is known to lack cholinergic specificity in adult (Butcher et al., 1975, Robertson and Gorenstein, 1987) and especially in developing rat brain (Kristt and Waldman, 1982; Kutscher, 1991).

## Methodological considerations

Previous studies have shown that the present experimental conditions allow for a specific and optimal immunocytochemical labeling of ChAT-immunoreactive axons in the rat CNS (e.g., Umbriaco et al., 1994; Mechawar et al., 2000; Mechawar and Descarries, 2001). As already demonstrated in adult mouse as well as rat hippocampus (Aznavour et al., 2002), nickel-cobalt enhancement of the ChAT-immunostaining revealed an intricate network of fine varicose axons against a light background (Figs. 2-4). Individual axons could thus be traced without

discontinuity across the full thickness of 20 µm-thick sections, attesting to complete penetration of immunoreagents in tissue.

The square windows from which the innervation density measurements were obtained were sufficiently large to ensure a reliable sampling of each layer across CA1, CA3 and DG of dorsal hippocampus. By visual inspection, the transverse level chosen for examination appeared representative of the whole dorsal hippocampus, except for its rostral tip. The semi-computerized technique used for collecting the data ensured that all and only immunostained fibers were being measured across the full thickness of the sections, including the more lightly stained axon segments between the darker varicosities. The mathematical correction for angulation, assuming a random orientation of the fibers in the sections, was a simple and convenient way to convert the two-dimensional measurements into three-dimensional values. However, in contrast with more sophisticated design-based counting techniques (e.g., Calhoun and Mouton, 2000; Calhoun et al., 2004), such an assumption-based calculation could introduce a bias. Indeed, ACh axons are not always randomly oriented in the z axis, as seen notably at the border between the strata radiatum and lacunosum moleculare. Moreover, the average densities calculated for each hippocampal region were means between layers, which did not take into account the relative volume of each layer in each region. Therefore, the present data on innervation

density had to be viewed as an approximation, to serve mainly as a basis for comparison between the three ages.

**Pattern of ACh innervation in the developing hippocampus**

Within the first week after birth, the ACh innervation in developing hippocampus evolved from scattered individual axons capped with growth cones into a relatively elaborate network of branching axons endowed with a considerable number of axon varicosities. Casual inspection of sections at other transverse levels revealed a similar pattern of growth throughout hippocampus. Thus, the hippocampal ACh innervation developed much sooner than previously suspected from the single earlier immunocytochemical study using antibodies against ChAT (Gould et al., 1991).

At P8, two distributional features characterized the ACh innervation pattern: sparse innervation of the pyramidal layer of CA1, to become very dense in the adult (Aznavour et al., 2002), and a prominent band of axons pervading the inner-third of the molecular layer. Because the differentiation of granule cells in the suprapyramidal blade of DG occurs early during the neonatal period (Altman and Das, 1965; Jones et al., 2003), and because these cells produce a variety of growth factors, including NGF, BDNF and NT3 (Lauterborn et al., 1994), it has been hypothesized that they can stimulate the proliferation of ACh axons in this specific area (Makuch et al., 2001). There is indeed strong *in vivo* as well

as *in vitro* evidence that neurotrophic factors can promote the maturation and survival of basal ACh forebrain neurons, and their release of ACh (Li et al., 1995; Ward and Hagg, 2000; Hartikka and Hefti, 1988; Alderson et al., 1990; Ha et al., 1996, 1999; Auld et al., 2001).

At P16, the hippocampus already displayed a mature pattern of ACh innervation. In CA1, the bands of denser ACh innervation present on either side of the stratum pyramidale were apparent, suggesting some preferential relationship with the proximal dendrites of the pyramidal neurons or with the synaptic input to these dendrites (Freund and Buzaki, 1996). As in the adult, a narrow band of denser innervation was also visible at the border between the strata radiatum and lacunosum moleculare, which coincides with the location of cholinoceptive neurons involved in the pacing of theta rhythmic activity in pyramidal cells (Chapman and Lacaille, 1999). In CA3, the pyramidal cell bodies were already enmeshed in a dense network of ACh fibers, as previously described in the adult (Aznavour et al., 2002).

**Growth of the ACh innervation**

Three parameters accounted for such early and rapid growth: an increase in the number of varicosities per unit length of axon, and the lengthening and branching of these varicose axons. The increase in number of axon varicosities per unit length of ACh axon, from 2.7 at P8 to 3.6 at P16 and 4 per 10 µm (the adult value) at P32, was comparable to

that previously measured in the developing cortex of postnatal rat (Mechawar and Decarries, 2001). As in the cerebral cortex, at all ages examined, this ratio did not vary between hippocampal layers or regions. It therefore seems to be an inherent feature of the developing basal forebrain cholinergic neurons projecting to hippocampus or cerebral cortex, independent of local factors, which could reflect the common germinal source of ACh neurons in the ventral telencephalon (Marin et al., 2000; Zhao et al., 2003).

As indicated by the quantification of axon length in the different layers and regions of dorsal hippocampus, the increase in number of ACh varicosities per length of axon was paralleled by a growth of ACh axons that was maximal during the first two weeks after birth, but continued at a slower pace to reach adult values at P32. The development of this ACh axon network was not homogeneous, however. Some layers, (e.g., the stratum moleculare of DG or the stratum lacunosum moleculare of CA3) seemed to be more precociously innervated than others (e.g., the stratum pyramidale of CA1). At variance with the number of varicosities per unit length of axon, such differences did suggest some control by local growth regulating factors.

The combination of these two developmental parameters resulted in a strong augmentation of the density of ACh varicosities in the different layers and regions of hippocampus, which mostly took place during the

first two postnatal weeks. The growth capacity of individual ACh neurons during this period could be roughly estimated, assuming that the density values in its dorsal part were representative of the whole hippocampus Based on the number of 7 150 ACh nerve cell bodies of origin (Cadete-Leite et al., 2003), and a calculated hippocampal volume of 25 $mm^3$ at P16 (64% of adult volume, as extrapolated from Miki et al., 2000 and West et al., 1990), it could be inferred that, within the two first postnatal weeks, the average Ch1-Ch2 ACh neuron produced 4.4 cm of axonal arborization bearing 16 000 varicosites. Thus, on average, these neurons should be capable of generating some 3 millimeters of axon and 1000 varicosities per day.

This rapid growth of the ACh innervation could account for other parameters of ACh function previously measured in developing hippocampus, such as the marked increases in ChAT and AChE activity during the first two postnatal weeks, reaching adult values between P21 and P27 (Nadler et al., 1974; Zahalka et al., 1993; Thal et al., 1992; but see ). It could also explain the presence as early as P4, and marked increase between P4 and P20, of eserine effects on the frequency of synchronous discharges recorded extracellularly during blockade of GABAergic inhibition in hippocampal slices (Gruslin et al., 1999). In contrast, radioligand binding to both the high-affinity choline transporter and the vesicular ACh transporter has been shown to be relatively high at birth,

and does not seem to increase very significantly during the first three postnatal weeks (Happe and Murrin 1992; Zahalka et al., 1993; Aubert al., 1996). Such a dissociation from innervation density may be viewed as an indication of transporter sites being expressed transiently by non cholinergic neurons during the first postnatal week, at a time when the blood brain barrier is still permeable (Loizou, 1970; Lossinsky et al., 1986).

**Ultrastructural features**

The morphometric features of ACh varicosities in developing hippocampus were not different from those already described in different regions of adult rat brain (e.g., Chédotal et al., 1994; Umbriaco et al., 1994; Vaucher and Hamel, 1995; Contant et al., 1996), including hippocampus (Umbriaco et al., 1995), and more recently, in the developing neocortex (Mechawar et al., 2002) and neostriatum (Aznavour et al., 2003). This supports the earlier suggestion that, as soon as they are formed, the varicosities of growing ACh axons are endowed with all necessary constituents to synthesize, store and release ACh.

As measured in single thin sections, the ACh varicosities in developing hippocampus were of comparable dimension from P8 to P32, and in the adult (Umbriaco et al., 1995). They were slightly smaller than the randomly selected, unlabeled varicosities, according to short axis, long axis, diameter and area, even if these differences did not reach statistical significance. The proportion of sectional profiles displaying mitochondria

was significantly higher for ACh than unlabeled varicosities, at all three postnatal ages, and increased significantly between P16 and P32 (from 24.8 to 41%), reaching a value comparable to that reported in the developing parietal cortex (44%; Mechawar et al., 2002). As noted earlier, this relatively high frequency of mitochondria could reflect the high metabolic demands placed on growing ACh axons and their increase in ACh synthesis, since these organelles produce the precursor acetyl-CoA.

As also observed in the developing cortex and neostriatum, the frequency with which the ACh varicosities in developing hippocampus made morphologically defined synaptic contacts was consistently low, irrespective of the postnatal age examined. When extrapolated to whole varicosities, it averaged 7%, the exact percentage previously found in adult (Umbriaco, et al., 1995). The largely asynaptic character of this innervation was further evidenced by the comparison of ACh and randomly selected, unlabeled varicosities, which displayed an eight (P8) to twenty-four times (P32) higher synaptic incidence. The 147% value for unlabeled varicosities at P32 presumably reflected the occurrence of hippocampal axon terminals bearing more than one junctional specialization, as frequently seen in the adult (Sorra and Harris, 1993).

At all postnatal ages examined, a majority of the few synaptic ACh varicosities made symmetrical contacts with dendritic branches, as also reported in prior ultrastructural studies of adult hippocampus (e.g.,

Heimrich and Frotscher, 1993; Frotscher and Leranth, 1985, 1986; Deller et al., 1999). Contacts with dendritic spines were rare. In both respects, the ACh varicosities differed significantly from the unlabeled ones, which mostly made synapses that were asymmetrical and which increased in frequency with age on dendritic spines as opposed to branches (see also Harris et al., 1992; Fiala et al., 1998). Recent studies have emphasized the presumptive role of dendrites in establishing synaptic contact with axon varicosities (Kim and Chiba, 2004; Niell et al., 2004) that are presumably equipped with the molecular machinery of active zones (Zhen and Jin, 2004). It will be of interest to determine if the exceedingly low frequency with which hippocampal ACh varicosities make morphologically differentiated synapses, particularly with dendritic spines, is related to a low expression or absence of some of these molecules in the varicosities of basal forebrain cholinergic neurons.

**Functional implications**

As originally postulated by Descarries et al. (1975), in their initial description of the serotonin innervation of cerebral cortex, it was recently demonstrated, in cultures of dissociated glutamatergic hippocampal neurons, that axon varicosities lacking synaptic specializations are subject to incessant movements of translocation and/or reshaping along their parent fibers, which constantly modify their position as release sites in relation to their microenvironment (Krueger et al., 2003). In view of the

rapid elongation and branching of the hippocampal ACh axons, and increase in their number of varicosities, this structural and functional plasticity might be even greater in the case of the ACh innervation in developing hippocampus.

Because most of the acetylcholinesterase present in CNS is of the tetrameric globular form (G4), a proposed regulator of extrasynaptic ACh levels at the motor endplate (Gisiger and Stephens, 1988), it has also been hypothesized that, at least in densely ACh-innervated brain regions, a low ambient level of ACh could be permanently maintained throughout the extracellular space (Descarries et al., 1997; Descarries, 1998). Consistent with this hypothesis, the basal levels of ACh measured by microdialysis in adult rat hipocampus are in the nanomolar affinity range of most nicotinic and muscarinic ACh receptors (Kurosaki et al., 1987; Quirion et al., 1989; Sharples and Wonnacott, 2001, Alkondon and Abuquerque, 2004). All cellular elements in developing hippocampus might thus be exposed to a low concentration of ACh, which could regulate the expression of homologous or heterologous receptors.

The presence of functional nicotinic and muscarinic receptors in the developing hippocampus within days after birth is indeed compatible with diffuse neurotransmission by ACh at this early stage. During the first postnatal week, muscarinic receptors have been shown to modulate evoked post-synaptic potentials (Milburn and Prince, 1993) and ACh

release (Goldbach et al., 1998), and nicotinic receptors to stimulate the release of norepinephrine (Leslie et al., 2002), and activate "silent synapses" by enhancing glutamate release (Maggi et al., 2003). Both receptor types have also been shown to increase the frequency of the "giant depolarizing potentials" present in hippocampus during this period of development (Avignone and Cherubini, 1999; Maggi et al., 2001). Such large-scale effects require a widespread distribution of receptors located on a variety of neuronal elements, also in keeping with the ubiquitous distribution and largely asynaptic character of the ACh innervation. As already proposed for the developing neocortex (Gu and Singer, 1993; Robertson et al., 1998; Zhu and Waite, 1998), they appear consistent with a permissive role of ACh during hippocampal development.

## AKNOWLEDGMENTS

This study was supported by grant NRF 3544 (now MOP 3544) to L.D., from the Canadian Institutes for Health Research. N.A. was recipient of a PhD studentship from the Groupe de recherche sur le système nerveux central (FCAR and FRSQ). The authors also thank Costantino Cozzari and Boyd K. Hartman for their generous gift of ChAT antibody, and Naguib Mechawar for a critical reading of the manuscript.

## REFERENCES

Adams CE, Broide RS, Chen Y, Winzer-Serhan UH, Henderson TA, Leslie FM, Freedman R. 2002. Development of the alpha7 nicotinic cholinergic receptor in rat hippocampal formation. Brain Res Dev Brain Res 139:175-187.

Adler LE, Olincy A, Waldo M, Harris JG, Griffith J, Stevens K, Flach K, Nagamoto H, Bickford P, Leonard S, Freedman R. 1998. Schizophrenia, sensory gating, and nicotinic receptors. Schizophr Bull 24:189-202.

Alderson RF, Alterman AL, Barde YA, Lindsay RM. 1990. Brain-derived neurotrophic factor increases survival and differentiated functions of rat septal cholinergic neurons in culture. Neuron 5:297-306.

Alkondon M, Pereira EF, Eisenberg HM, Albuquerque EX. 1999. Choline and selective antagonists identify two subtypes of nicotinic acetylcholine receptors that modulate GABA release from CA1 interneurons in rat hippocampal slices. J Neurosci 19: 2693-2705.

Alkondon M, Albuquerque EX. 2004. The nicotinic acetylcholine receptor subtypes and their function in the hippocampus and cerebral cortex. Prog Brain Res 145:109-20.

Altman J, Das GD. 1965. Autoradiographic and histological evidence of postnatal hippocampal neurogenesis in rats. J Comp Neurol 124:319-335.

Amaral DG, Kurz J. 1985. An analysis of the origins of the cholinergic and noncholinergic septal projections to the hippocampal formation of the rat. J Comp Neurol 240:37-59.

Aubert I, Cecyre D, Gauthier S, Quirion R. 1996. Comparative ontogenic profile of cholinergic markers, including nicotinic and muscarinic receptors, in the rat brain. J Comp Neurol 369:31-55.

Auld DS, Mennicken F, Day JC, Quirion R. 2001. Neurotrophins differentially enhance acetylcholine release, acetylcholine content and choline acetyltransferase activity in basal forebrain neurons. J Neurochem 77:253-262.

Auld DS, Kornecook TJ, Bastianetto S, Quirion R. 2002. Alzheimer's disease and the basal forebrain cholinergic system: relations to beta-amyloid peptides, cognition, and treatment strategies. Prog Neurobiol 68:209-245.

Avignone E, Cherubini E. 1999. Muscarinic receptor modulation of GABA-mediated giant depolarizing potentials in the neonatal rat hippocampus. J Physiol 518:97-107.

Aznavour N, Mechawar N, Descarries L. 2002. Comparative analysis of cholinergic innervation in the dorsal hippocampus of adult mouse and rat: A quantitative immunocytochemical study. Hippocampus 12:406-417.

Aznavour N, Mechawar N, Watkins KC, Descarries L. 2003. Fine structural features of the acetylcholine innervation in the developing neostriatum of rat. J Comp Neurol 460:280-291.

Balduini W, Cimino M, Reno F, Marini P, Princivalle A, Cattabeni F. 1993. Effects of postnatal or adult chronic acetylcholinesterase inhibition on muscarinic receptors, phosphoinositide turnover and m1 mRNA expression. Eur J Pharmacol 248:281-288.

Beach TG, Kuo YM, Spiegel K, Emmerling MR, Sue LI, Kokjohn K, Roher AE. 2000. The cholinergic deficit coincides with A□ deposition at the earliest histopathologic stages of Alzheimer disease. J Neuropathol Exp Neurol 59:308-313.

Beaudet A, Sotelo C. 1981. Synaptic remodeling of serotonin axon terminals in rat agranular cerebellum. Brain Res 206:305-329.

Bender R, Plaschke M, Naumann T, Wahle P, Frotscher M. 1996. Development of cholinergic and GABAergic neurons in the rat medial septum: different onset of choline acetyltransferase and glutamate decarboxylase mRNA expression. J Comp Neurol 372: 204-214.

Benson DM, Blitzer RD, Landau EM. 1988. An analysis of the depolarization produced in guinea-pig hippocampus by cholinergic receptor stimulation. J Physiol 404:479-496.

Bierer LM, Haroutunian V, Gabriel S, Knott PJ, Carlin LS, Purohit DP, Perl DP, Schmeidler J, Kanof P, Davis KL.1995. Neurochemical correlates of dementia severity in Alzheimer's disease: relative importance of the cholinergic deficits. J Neurochem 64:749-760.

Brakeman PR, Lanahan AA, O'Brien R, Roche K, Barnes CA, Huganir RL, Worley PF. 1997. Homer: a protein that selectively binds metabotropic glutamate receptors. Nature 386:284-288.

Breese CR, Lee MJ, Adams CE, Sullivan B, Logel J, Gillen KM, Marks MJ, Collins AC, Leonard S. 2000. Abnormal regulation of high affinity nicotinic receptors in subjects with schizophrenia. Neuropsychopharmacology 23:351-364.

Butcher LL, Talbot K, Bilezikjian L. 1975. Acetylcholinesterase neurons in dopamine-containing regions of the brain. J Neural Transm 37:127-153.

Cadete-Leite A, Pereira PA, Madeira MD, Paula-Barbosa MM. 2003. Nerve growth factor prevents cell death and induces hypertrophy of basal forebrain cholinergic neurons in rats withdrawn from prolonged ethanol intake. Neuroscience 119:1055-1069.

Calhoun ME, Mouton PR. 2000. Length measurement: new developments in neurostereology and 3D imagery. J Chem Neuroanat 20:61-69.

Calhoun ME, Mao Y, Roberts JE, Rapp PR. 2004. Reduction in hippocampal cholinergic innervation is unrelated to recognition

memory impairment in aged rhesus monkeys. J Comp Neurol 475:238-246.

Chédotal A, Umbriaco D, Descarries L, Hartman BK, Hamel E. 1994. Light and electron microscopic immunocytochemical analysis of the neurovascular relationships of choline acetyltransferase and vasoactive intestinal polypeptide nerve terminals in the rat cerebral cortex. J Comp Neurol. 343:57-71.

Chapman CA and Lacaille JC. 1999. Cholinergic induction of theta-frequency oscillations in hippocampal inhibitory interneurons and pacing of pyramidal cell firing. J Neurosci 19: 8637-8645.

Cobb SR, Bulters DO, Suchak S, Riedel G, Morris RG, Davies CH. 1999. Activation of nicotinic acetylcholine receptors patterns network activity in the rodent hippocampus. J Physiol (Lond) 518:131-140.

Cole AE and Nicoll RA. 1984. The pharmacology of cholinergic excitatory responses in hippocampal pyramidal cells. Brain Res 305:283-290.

Contant C, Umbriaco D, Garcia S, Watkins KC, Descarries L. 1996. Ultrastructural characterization of the acetylcholine innervation in adult rat neostriatum. Neuroscience 71:937-947.

Cozzari C, Howard J, Hartman B. 1990. Analysis of epitopes on choline acetyltransferase (ChAT) using monoclonal antibodies (Mabs). Soc Neurosci Abstr 16:200.

Davies P, Maloney AJ. 1976. Selective loss of central cholinergic neurons in Alzheimer's disease. Lancet 2:1403.

Deller T, Katona I, Cozzari C, Frotscher M, Freund TF. 1999. Cholinergic innervation of mossy cells in the rat fascia dentata. Hippocampus 9:314-320.

Descarries L. 1998. The hypothesis of an ambient level of acetylcholine in the central nervous system. J Physiol (Paris) 92:215-220.

Descarries L, Mechawar N. 2000. Ultrastructural evidence for diffuse transmission by monoamine and acetylcholine neurons of the central nervous system. Prog Brain Res 125: 27-47.

Descarries L, Beaudet A, Watkins KC. 1975. Serotonin nerve terminals in adult rat neocortex. Brain Res 100:563-588.

Descarries L, Gisiger V, Steriade M. 1997. Diffuse transmission by acetylcholine in the CNS. Prog Neurobiol 53:603-625

Descarries L, Mechawar N, Aznavour N, Watkins KC. 2004. Structural determinants of the roles of acetylcholine in cerebral cortex. Prog Brain Res 145:45-58.

Eckenstein F, Baughman RW. 1987. Cholinergic innervation in cerebral cortex. In: Jones EG, Peters A (eds). Cerebral Cortex. Further Aspects of Cortical Function, Including Hippocampus. Plenum Press, New York, Vol 6, pp 129-160.

Fiala JC, Feinberg M, Popov V, Harris KM. 1998. Synaptogenesis via dendritic filopodia in developing hippocampal area CA1. J Neurosci 18:8900-8911.

Fine A, Hoyle C, Maclean CJ, Levatte TL, Baker HF, Ridley RM. 1997. Learning impairments following injection of a selective cholinergic immunotoxin, ME20.4 IgG-saporin, into the basal nucleus of Meynert in monkeys. Neuroscience 81:331-343.

Freedman R, Coon H, Myles-Worsley M, Orr-Urtreger A, Olincy A, Davis A, Polymeropoulos M, Holik J, Hopkins J, Hoff M, Rosenthal J, Waldo MC, Reimherr F, Wender P, Yaw J, Young DA, Breese CR, Adams C, Patterson D, Adler LE, Kruglyak L, Leonard S, Byerley W. 1997. Linkage of a neurophysiological deficit in schizophrenia to a chromosome 15 locus. Proc Natl Acad Sci USA 94:587-592.

Freedman R, LE Adler, Leonard S. 1999. Alternative phenotypes for the complex genetics of schizophrenia. Biol Psychiatry 45:551-558.

Frotscher M, Leranth C. 1985. Cholinergic innervation of the rat hippocampus as revealed by choline acetyltransferase immunocytochemistry: a combined light and electron microscopic study. J Comp Neurol 239:237-246.

Frotscher M, Leranth C. The cholinergic innervation of the rat fascia dentata: identification of target structures on granule cells by

combining choline acetyltransferase immunocytochemistry and Golgi impregnation. J Comp Neurol 243:58-70.

Furrer MP, Kim S, Wolf B, Chiba A. 2003. Robo and Frazzled/DCC mediate dendritic guidance at the CNS midline. Nat Neurosci 6:223-230.

Gage FH, Björklund A, Stenevi U. 1983. Reinnervation of the partially deafferented hippocampus by compensatory collateral sprouting from spared cholinergic and noradrenergic afferents. Brain Res 268:27-37.

Geula C, Mesulam MM. 1996. Systematic regional variations in the loss of cortical cholinergic fibers in Alzheimer's disease. Cerebral Cortex 6:165-177.

Gisiger V, Stephens HR. 1988. Localization of the pool of G4 acetylcholinesterase characterizing fast muscles and its alteration in murine muscular dystrophy. J Neurosci Res 19:62-78.

Goldbach R, Allgaier C, Heimrich B, Jackisch R. 1998. Postnatal development of muscarinic autoreceptors modulating acetylcholine release in the septohippocampal cholinergic system. I. Axon terminal region: hippocampus. Brain Res Dev Brain Res 108:23-30.

Gorenstein C, Gallardo KA, Robertseon RT. 1991. Molecular forms of acetylcholinesterase in cerebral cortex and dorsal thalamus of developing rats. Brain Res Dev Brain Res 61:271-276.

Gould E, Woolf NJ, Butcher LL. 1991. Postnatal development of cholinergic neurons in the rat: I. Forebrain. Brain Res Bull 27:767-789.

Gruslin E, Descombes S, Psarropoulou C. 1999. Epileptiform activity generated by endogenous acetylcholine during blockade of GABAergic inhibition in immature and adult rat hippocampus. Brain Res 835:290-297.

Ha DH, Robertson RT, Ribak CE, Weiss JH. 1996. Cultured basal forebrain cholinergic neurons in contact with cortical cells display synapses, enhanced morphological features, and decreased dependence on nerve growth factor. J Comp Neurol 373:451-465.

Ha DH, Robertson RT, Roshanaei M, Weiss JH. 1999. Enhanced survival and morphological features of basal forebrain cholinergic neurons in vitro: role of neurotrophins and other potential cortically derived cholinergic trophic factors. J Comp Neurol 406:156-170.

Happe HK, Murrin LC. 1992. Development of high-affinity choline transport sites in rat forebrain: a quantitative autoradiography study with (3H)hemicholinium-3. J Comp Neurol 321:591-611.

Harris KM, Jensen FE, Tsao B. 1992. Three-dimensional structure of dendritic spines and synapses in rat hippocampus (CA1) at postnatal day 15 and adult ages: implications for the maturation of synaptic physiology and long-term potentiation. J Neurosci 2685-2705.

Hartikka J, Hefti F. 1988. Comparison of nerve growth factor's effects on development of septum, striatum, and nucleus basalis cholinergic neurons in vitro. J Neurosci Res 21:352-364.

Hasselmo ME, McGaughy J. 2004. High acetylcholine levels set circuit dynamics for attention and encoding and low acetylcholine levels set dynamics for consolidation. Prog Brain Res 145:207-231.

Heimrich B, Frotscher M. 1993. Formation of the septohippocampal projection in vitro: an electron microscopic immunocytochemical study of cholinergic synapses. Neuroscience 52:815-827.

Hernandez D, Sugaya K, Qu T, McGowann E, Duff K, McKinney M. 2001. Survival and plasticity of basal forebrain cholinergic systems in mice transgenic for presenilin-I and amyloid precursor protein mutant genes. Mol Neurosci 12:1377-1384.

Höhmann CF, Pert CC, Ebner FF. 1985. Development of cholinergic markers in mouse forebrain. II. Muscarinic receptor binding in cortex. Brain Res 355:243-253.

Ji D and Dani JA. 2000. Inhibition and disinhibition of pyramidal neurons by activation of nicotinic receptors on hippocampal interneurons. J Neurophysiol 83:2682-2690.

Jones S and Yakel JL. 1997. Functional nicotinic ACh receptors on interneurones in the rat hippocampus. J Physiol (Lond) 504:603-610.

Jones SP, Rahimi O, O'Boyle MP, Diaz DL, Claiborne BJ. 2003. Maturation of granule cell dendrites after mossy fiber arrival in hippocampal field CA3. Hippocampus 13:413-427.

Kar S, Quirion R. 2004. Amyloid beta peptides and central cholinergic neurons: functional interrelationship and relevance to Alzheimer's disease pathology. Prog Brain Res 145:261-274.

Karlsson KA, Blumberg MS. 2003. Hippocampal theta in the newborn rat is revealed under conditions that promote REM sleep. J Neurosci 23:1114-1118.

Kim S, Chiba A. 2004. Dendritic guidance. Trends Neurosci 27:194-202.

Koh S, Loy R. 1989. Localization and development of nerve growth factor-sensitive rat basal forebrain neurons and their afferent projections to hippocampus and neocortex. J Neurosci 9:2999-3018.

Kristt DA, Waldman JV. 1982. Developmental reorganization of acetylcholinesterase-rich inputs to somatosensory cortex of the mouse. Anat Embryol (Berl.) 164:331-342.

Krnjevic K, Silver A. 1966. Acetylcholinesterase in the developing forebrain. J Anat100:63-89.

Krueger SR, Kolar A, Fitzsimonds RM. 2003. The presynaptic release apparatus is functional in the absence of dendritic contact and highly mobile within isolated axons. Neuron 40:945-957.

Kurosaki T, Fukuda K, Konno T, Mori Y, Tanaka K, Mishina M, Numa S. 1987. Functional properties of nicotinic acetylcholine receptor subunits expressed in various combinations. FEBS Lett 214:253-258.

Kutscher CL. 1991. Development of transient acetylcholinesterase staining in cells and permanent staining in fibers in cortex of rat brain. Brain Res Bull 27:641-649.

Lauterborn JC, Isackson PJ, Gall CM. 1994. Cellular localization of NGF and NT-3 mRNAs in postnatal rat forebrain. Mol Cell Neurosci 5:46-62.

Leonard S, Breese C, Adams C, Benhammou K, Gault J, Stevens K, Lee M, Adler L, Olincy A, Ross R, Freedman R. 2000. Smoking and schizophrenia: abnormal nicotinic receptor expression. Eur J Pharmacol 393:237-242.

Leslie FM, Gallardo KA, Park MK. 2002. Nicotinic acetylcholine receptor-mediated release of ($^3$H)norepinephrine from developing and adult rat hippocampus: direct and indirect mechanisms. Neuropharmacology 42:653-661.

Li Y, Holtzman DM, Kromer LF, Kaplan DR, Chua-Couzens J, Clary DO, Knusel B, Mobley WC. 1995. Regulation of TrkA and ChAT expression in developing rat basal forebrain: evidence that both exogenous and endogenous NGF regulate differentiation of cholinergic neurons. J Neurosci 15:2888-2905.

Lindstrom J. 1997. Nicotinic acetylcholine receptors in health and disease. Mol Neurobiol 15:193-222.

Linke R, Frotscher M. 1993. Development of the rat septohippocampal projection: tracing with DiI and electron microscopy of identified growth cones. J Comp Neurol 332:69-88.

Loizou LA. 1970. Uptake of monoamines into central neurones and the blood-brain barrier in the infant rat. Br J Pharmacol 40:800-813.

Lossinsky AS, Vorbrodt AW, Wisniewski HM. 1986. Characterization of endothelial cell transport in the developing mouse blood-brain barrier. Dev Neurosci 8:61-75.

Madison DV, Lancaster B, Nicoll RA. 1987. Voltage clamp analysis of cholinergic action in the hippocampus. J Neurosci 7:733-741.

Maggi L, Sher E, Cherubini E. 2001. Regulation of GABA release by nicotinic acetylcholine receptors in the neonatal rat hippocampus. J Physiol 536:89-100.

Maggi L, Le Magueresse C, Changeux JP, Cherubini E. 2003. Nicotine activates immature "silent" connections in the developing hippocampus. Proc Natl Acad Sci USA 100:2059-2064.

Makuch R, Baratta J, Karaelias LD, Lauterborn JC, Gall CM, Yu J, Robertson RT. 2001. Arrival of afferents and the differentiation of target neurons: studies of developing cholinergic projections to the dentate gyrus. Neuroscience 104:81-91.

Marin O, Anderson SA, Rubenstein JL. Origin and molecular specification of striatal interneurons. J Neurosci 20:6063-6076.

McKinney M, Coyle JT, Hedreen JC. 1983. Topographic analysis of the innervation of the rat neocortex and hippocampus by the basal forebrain cholinergic system. J Comp Neurol 217:103-121.

McQuiston AR and Madison DV. 1999a. Muscarinic receptor activity has multiple effects on the resting membrane potentials of CA1 hippocampal interneurons. J Neurosci 19:5693-5702.

McQuiston AR and Madison DV. 1999b. Nicotinic receptor activation excites distinct subtypes of interneurons in the rat hippocampus. J Neurosci 19:2887-2896.

Mechawar N, Descarries L. 2001. The cholinergic innervation develops early and rapidly in the rat cerebral cortex: a quantitative immunocytochemical study. Neuroscience 108:555-567.

Mechawar N, Cozzari C, Descarries L. 2000. Cholinergic innervation in adult rat cerebral cortex: a quantitative immunocytochemical description. J Comp Neurol 428:305-318.

Mechawar N, Watkins KC, Descarries L. 2002. Ultrastructural features of the acetylcholine innervation in the developing parietal cortex of rat. J Comp Neurol 443:250-258.

Mesulam MM. 1998. Some cholinergic themes related to Alzheimer's disease: Synaptology of the nucleus basalis, location of m2 receptors,

interactions with amyloid metabolism, and perturbations of cortical plasticity. J Physiol (Paris) 92:293-298.

Mesulam MM, Mufson EJ, Wainer BH, Levey AI. 1983. Central cholinergic pathways in the rat: an overview based on an alternative nomenclature (Ch1-Ch6). Neuroscience 10:1185-1201.

Miki T, Harris SJ, Wilce P, Takeuchi Y, Bedi KS. 2000. Neurons in the hilus region of the rat hippocampus are depleted in number by exposure to alcohol during early postnatal life. Hippocampus 10:284-295.

Milburn CM, Prince DA. 1993. Postnatal development of cholinergic presynaptic inhibition in rat hippocampus. Brain Res Dev Brain Res 74:133-137.

Miyoshi R, Kito S, Shimizu M, Matsubayashi H. 1987. Ontogeny of muscarinic receptors in the rat brain with emphasis on the differentiation of M1- and M2-subtypes - semi-quantitative in vitro autoradiography. Brain Res 420:302-312.

Mufson EJ, Ma SY, Dills J, Cochran EJ, Leurgans S, Wuu J, Bennett DA, Jaffar S, Gilmor ML, Levey AI, Kordower JH. 2002. Loss of basal forebrain P75(NTR) immunoreactivity in subjects with mild cognitive impairment and Alzheimer's disease. J Comp Neurol 443: 136-153.

Nadler JV, Matthews DA, Cotman CW, Lynch GS. 1974. Development of cholinergic innervation in the hippocampal formation of the rat. II.

Quantitative changes in choline acetyltransferase and acetylcholinesterase activities. Dev Biol 36:142-154.

Niell CM, Meyer MP, Smith SJ. 2004. In vivo imaging of synapse formation on a growing dendritic arbor. Nat Neurosci 7:254-260.

Nyakas C, Luiten PG, Spencer DG, Traber J. 1987. Detailed projection patterns of septal and diagonal band efferents to the hippocampus in the rat with emphasis on innervation of CA1 and dentate gyrus. Brain Res Bull 18:533-545.

Plaschke M, Naumann T, Kasper E, Bender R, Frotscher M. 1997. Development of cholinergic and GABAergic neurons in the rat medial septum: effect of target removal in early postnatal development. J Comp Neurol 379:467-481.

Quirion R, Araujo D, Regenold W, Boksa P. 1989. Characterization and quantitative autoradiographic distribution of ($^3$H)acetylcholine muscarinic receptors in mammalian brain. Apparent labelling of an M2-like receptor sub-type. Neuroscience 29:271-289.

Radcliffe KA and Dani JA. 1998. Nicotinic stimulation produces multiple forms of increased glutamatergic synaptic transmission. J Neurosci 18:7075-7083.

Radcliffe KA, Fisher JL, Gray R, Dani JA. 1999. Nicotinic modulation of glutamate and GABA synaptic transmission of hippocampal neurons. Ann N Y Acad Sci 868:591-610.

Reece LJ, Schwartzkroin PA. 1991a. Effects of cholinergic agonists on immature rat hippocampal neurons. Brain Res Dev Brain Res 60:29-42.

Reece LJ, Schwartzkroin PA. 1991b. Effects of cholinergic agonists on two non-pyramidal cell types in rat hippocampal slices. Brain Res 1991 566:115-126.

Reinikainen KJ, Soininen H, Riekkinen PJ. 1990. Neurotransmitter changes in Alzheimer's disease: implications to diagnostics and therapy. J Neurosci Res 27:576-586.

Robertson RT, Gorenstein C. 1987. 'Non-specific' cholinesterase-containing neurons of the dorsal thalamus project to medial limbic cortex. Brain Res 404:282-292.

Rye DB, Wainer BH, Mesulam MM, Mufson EJ, Saper CB. 1984. Cortical projections arising from the basal forebrain: a study of cholinergic and noncholinergic components employing combined retrograde tracing and immunohistochemical localization of choline acetyltransferase. Neuroscience 13:627-643.

Semba K. 2004. Phylogenetic and ontogenetic aspects of the basal forebrain cholinergic neurons and their innervation of the cerebral cortex. Prog Brain Res 145:3-43.

Semba K, Fibiger HC. 1988. Time of origin of cholinergic neurons in the rat basal forebrain. J Comp Neurol 269:87-95.

Shacka JJ, Robinson SE. 1998. Postnatal developmental regulation of neuronal nicotinic receptor subunit alpha 7 and multiple alpha 4 and beta 2 mRNA species in the rat. Brain Res Dev Brain Res 109:67-75.

Sharples CG and Wonnacott S. 2001. Neuronal nicotinic receptors. TOCRIS Reviews No 19. Bristol: Tocris Cookson.

Shimono K, Brucher F, Granger R, Lynch G,. Taketani M. 2000. Origins and distribution of cholinergically induced beta rhythms in hippocampal slices. J Neurosci 20:8462-8473.

Shinotoh H, Namba H, Fukushi K, Nagatsuka S, Tanaka N, Aotsuka A, Ota T, Tanada S, Irie T. 2000. Progressive loss of cortical acetylcholinesterase activity in association with cognitive decline in Alzheimer's disease: a positron emission tomography study. Ann Neurol 48:194-200.

Soghomonian JJ, Doucet G, Descarries L. 1987. Serotonin innervation in adult rat neostriatum. I. Quantified regional distribution. Brain Res 425:85-100.

Sorra KE, Harris KM. 1993. Occurrence and three-dimensional structure of multiple synapses between individual radiatum axons and their target pyramidal cells in hippocampal area CA1. J Neurosci 13:3736-3748.

Steinlein OK. 2004. Nicotinic receptor mutations in human epilepsy. Prog Brain Res 145: 275-285.

Thal LJ, Gilbertson E, Armstrong DM, Gage FH. 1992. Development of the basal forebrain cholinergic system: phenotype expression prior to target innervation. Neurobiol Aging 13:67-72.

Tice MA, Hashemi T, Taylor LA, McQuade RD. 1996. Distribution of muscarinic receptor subtypes in rat brain from postnatal to old age. Brain Res Dev Brain Res 92:70-76.

Tong XK, Hamel E. 1999. Regional cholinergic denervation of cortical microvessels and nitric oxide synthase-containing neurons in Alzheimer's disease. Neuroscience 92:163-175.

Tribollet E, Bertrand D, Marguerat A, Raggenbass M. 2004. Comparative distribution of nicotinic receptor subtypes during development, adulthood and aging: an autoradiographic study in the rat brain. Neuroscience 124:405-420.

Umbriaco D, Garcia S, Beaulieu C, Descarries L. 1995. Relational features of acetylcholine, noradrenaline, serotonin and GABA axon terminals in the stratum radiatum of adult rat hippocampus (CA1). Hippocampus 5:605-620.

Umbriaco D, Watkins KC, Descarries L, Cozzari C, Hartman BK. 1994. Ultrastructural and morphometric features of the acetylcholine innervation in adult rat parietal cortex: an electron microscopic study in serial sections. J Comp Neurol 348:351-373.

van der Zee EA and Luiten PG. 1999. Muscarinic acetylcholine receptors in the hippocampus, neocortex and amygdala: a review of immunocytochemical localization in relation to learning and memory. Prog Neurobiol 58:409-471.

Vaucher E, Hamel E. 1995. Cholinergic basal forebrain neurons project to cortical microvessels in the rat: electron microscopic study with anterogradely transported Phaseolus vulgaris leucoagglutinin and choline acetyltransferase immunocytochemistry. J Neurosci 15:7427-7441.

Ward NL, Hagg T. 2000. BDNF is needed for postnatal maturation of basal forebrain and neostriatum cholinergic neurons in vivo. Exp Neurol 162:297-310.

West MJ. 1990. Stereological studies of the hippocampus: a comparison of the hippocampal subdivisions of diverse species including hedgehogs, laboratory rodents, wild mice and men. Prog Brain Res. 83:13-36.

Whitehouse PJ, Price DL, Struble RG, Clark AW, Coyle JT, Delon MR. 1982. Alzheimer's disease and senile dementia: loss of neurons in the basal forebrain. Science 215:1237-1239.

Williams JH and Kauer JA. 1997. Properties of carbachol-induced oscillatory activity in rat hippocampus. J Neurophysiol 78:2631-2640.

Woolf NJ. 1991. Cholinergic systems in mammalian brain and spinal cord. Progr Neurobiol 37:475-524.

Wyble BP, Linster C, Hasselmo ME. 2000. Size of CA1-evoked synaptic potentials is related to theta rhythm phase in rat hippocampus. J Neurophysiol 83:2138-2144.

Zahalka EA, Seidler FJ, Lappi SE, Yanai J, Slotkin TA. 1993. Differential development of cholinergic nerve terminal markers in rat brain regions: implications for nerve terminal density, impulse activity and specific gene expression. Brain Res 601:221-229.

Zhang X, Liu C, Miao H, Gong ZH, Nordberg A. 1998. Postnatal changes of nicotinic acetylcholine receptor alpha 2, alpha 3, alpha 4, alpha 7 and beta 2 subunits genes expression in rat brain. Int J Dev Neurosci 16:507-518.

Zhao Y, Marin O, Hermesz E, Powell A, Flames N, Palkovits M, Rubenstein JL, Westphal H. 2003. The LIM-homeobox gene Lhx8 is required for the development of many cholinergic neurons in the mouse forebrain. Proc Natl Acad Sci USA 100:9005-9010.

Zhen M, Jin Y. 2004. Presynaptic terminal differentiation: transport and assembly. Curr Opin Neurobiol 14:280-287.

## FIGURE LEGENDS

**Figure 1.** Schematic representation of the areas of dorsal hippocampus in which the density of ChAT-immunostained innervation was quantified (triplets of small square windows), and the electron microscopic features of the ChAT-immunostained varicosities characterized (larger hatched area), at postnatal ages P8, P16 and P32. Abbreviations for hippocampal strata: Gr, granulare; L Mol, lacunosum moleculare; Luc, lucidum; Mol, moleculare; Or, oriens; Pol, polymorph, Pyr, pyramidale, Rad, radiatum.

**Figure 2A-I.** High power digital micrographs of the ChAT-immunostained innervation in given layers of each hippocampal region (CA1(Rad); CA3 (Pyr); DG (Gr)), at the three postnatal ages indicated (P8, P16, P32). Every image corresponds to a full sampling window (50 x 50 μm), as depicted in Fig. 1. In all three layers represented, the density of the ACh axon network increases between P8 and P16, and shows a further increase, albeit smaller, between P16 and P32, in the stratum granulare of DG (see also Table 1 and Fig. 5). Between P8 and P16, an increase in the number of varicosities per unit length of immunostained axon is noticeable (which is also measurable between P16 and P32; see Fig. 3). Note the growth cone-tipped axon in the lower left quadrant of A, and the silhouettes of the pyramidal cell bodies in D-F. Contrast, brightness and sharpness of the

images were adjusted for esthetic purposes. Scale bar : 20 µm. Same abbreviations as in Fig. 1.

**Figure 3.** Average number of varicosities per µm of ChAT-immunostained axon in the dorsal hippocampus, at postnatal ages P8, P16 and P32, and in the adult (P60; data from Aznavour et al., 2002). Interlaminar means (± s.d.) from four rats per age. Note the sharp increase between P8 and P16, and the plateau at 4 varicosities per 10 µm of ACh axon after P32. ** $P < 0.01$, *** $P < 0.001$ compared to P32 or adult (P60).

**Figure 4.** Low power digital micrographs (scale bar: 100 µm) of the ChAT-immunostained innervation in CA1, CA3 and DG, and corresponding histograms of the laminar and regional (Mean) densities of ACh axon varicosities at the three postnatal ages examined (values from Table 1). CA3 was rotated 90° for presentation. Contrast, brightness and sharpness of the images were adjusted for esthetic purposes. See Results for detailed description of the laminar distribution in each region. Same abbreviations as in Fig. 1. * $P < 0.05$, ** $P < 0.01$, *** $P < 0.001$ compared to adult (P60; data from Aznavour et al., 2002).

**Figure 5.** Postnatal increase with age of the average density of ChAT-immunostained axon varicosities ($10^6$ per $mm^3$ of tissue) in CA1, CA3 and DG of dorsal hippocampus. In each region, note the marked increase during the first two weeks, and the further, albeit smaller, increase from

P16 to P32. As previously found in the adult (Aznavour et al., 2002), the average density was lower in CA1 than in CA3 and DG at all ages ($P < 0.05$ and $P < 0.01$ at P8 and P16, respectively).

**Figure 6AB.** Electron micrographs of ACh (ChAT-immunostained) axon varicosities from the stratum pyramidale (A) and radiatum (B) of CA1 at P32. The varicosities are identified as such by their content in aggregated synaptic vesicles, associated or not with a mitochondrion. Neither profile displays a synaptic junction. In A, the ACh varicosity is nested between a cell body (CB), two other axon varicosities (av), unlabeled, and an astrocytic leaflet (as). In B, another ACh varicosity is seen emerging from its parent, small unmyelinated axon. This one is in direct apposition with two dendritic branches (d), a large, unlabeled axon varicosity (av) and two astrocytic processes (as). Contrast, brightness and sharpness of the images were adjusted for esthetic purposes. Scale bar (in B): 0.5 µm.

**Figure 7A-I.** Examples of hippocampal ACh (ChAT-immunostained) axon varicosities from the stratum pyramidale (A, C, D, G) and the stratum radiatum (B, E, F, H, I) of CA1, at postnatal ages P8 (A-C), P16 (D-F) and P32 (G-I). The average size of these profiles does not significantly differ from P8 to P32. At each age, a synaptic junction is visible on one of the three immunoreactive varicosities presented (between small arrows in C, F and I). In C, the junction appears asymmetrical, and is made with a

large dendritic branch. In F, it looks rather symmetrical, on a dendritic spine. In I, it is clearly symmetrical, also on a dendritic spine, which also receives another synapse, asymmetrical, from an unlabeled varicosity. In all cases, a variety of elements are directly juxtaposed to the asynaptic or synaptic ACh profiles, including dendrites (d, in A-G), dendritic spines (sp, in D, F, H and I), unlabeled axon varicosities (av, in D, E, G and I) and astrocyte (as, in B and I). Contrast, brightness and sharpness of the images were adjusted for esthetic purposes. Scale bar (in I): 0.5 µm.

## Table 1- LAMINAR AND REGIONAL DENSITY OF ACh AXONS AND VARICOSITIES

| | P8 | | P16 | | P32 | | P60 | |
|---|---|---|---|---|---|---|---|---|
| | Axons ($m/mm^3$) | Varicosities ($10^6/mm^3$) | Axons ($m/mm^3$) | Varicosities ($10^6/mm^3$) | Axons ($m/mm^3$) | Varicosities ($10^6/mm^3$) | Axons ($m/mm^3$) | Varicosities ($10^6/mm^3$) |
| **CA1** | | | | | | | | |
| **Oriens** | 7.9 ± 0.9 *** | 2.2 ± 0.2 *** | 13.9 ± 1.7 | 5.0 ± 0.6 | 15.8 ± 2.7 | 6.4 ± 1.1 | 14.8 ± 1.1 | 5.9 ± 0.5 |
| **Pyramidale** | 4.1 ± 1.1 *** | 1.1 ± 0.3 *** | 8.4 ± 0.6 *** | 3.1 ± 0.2 *** | 15.4 ± 3.5 | 6.3 ± 1.4 | 17.0 ± 1.8 | 6.8 ± 0.7 |
| **Radiatum** | 7.1 ± 2.6 ** | 1.9 ± 0.7 ** | 8.5 ± 1.4 | 3.1 ± 0.5 | 11.5 ± 1.5 | 4.7 ± 0.6 | 10.6 ± 1.6 | 4.2 ± 0.6 |
| **L. moleculare** | 5.6 ± 1.0 | 1.5 ± 0.3 | 8.2 ± 1.6 | 3.0 ± 0.6 | 7.9 ± 1.4 | 3.2 ± 0.6 | 6.4 ± 1.2 | 2.6 ± 0.5 |
| ***Mean*** | 6.2 ± 1.0 *** | 1.7 ± 0.3 *** | 9.7 ± 1.2 * | 3.5 ± 0.4* | 12.7 ± 1.9 | 5.2 ± 0.8 | 12.2 ± 1.0 | 4.9 ± 0.4 |
| **CA3** | | | | | | | | |
| **Oriens** | 10.1 ± 2.5 *** | 2.8 ± 0.7 *** | 14.6 ± 0.9 ** | 5.3 ± 0.3 ** | 15.5 ± 1.4 | 6.3 ± 0.6 | 17.8 ± 1.4 | 7.1 ± 0.6 |
| **Pyramidale** | 7.9 ± 1.9 *** | 2.2 ± 0.5 *** | 19.4 ± 1.4 | 7.1 ± 0.5 | 17.9 ± 2.3 | 7.3 ± 0.9 | 20.1 ± 1.3 | 8.2 ± 0.5 |
| **Lucidum** | 7.9 ± 1.6 *** | 2.2 ± 0.4 *** | 9.9 ± 0.2 | 3.6 ± 0.1 | 8.3 ± 1.5 | 3.4 ± 0.6 | 10.7 ± 1.6 | 4.3 ± 0.7 |
| **Radiatum** | 7.2 ± 1.6 *** | 2.0 ± 0.4 *** | 11.7 ± 1.5 | 4.3 ± 0.6 | 12.1 ± 1.8 | 4.9 ± 0.8 | 13.2 ± 1.2 | 5.3 ± 0.5 |
| **L. moleculare** | 13.7 ± 2.0 *** | 3.8 ± 0.5 *** | 18.6 ± 1.3 | 6.8 ± 0.5 | 20.3 ± 1.6 | 8.3 ± 0.6 | 18.8 ± 1.4 | 7.5 ± 0.5 |
| ***Mean*** | 9.4 ± 1.9 *** | 2.6 ± 0.5 *** | 14.8 ± 0.7 * | 5.4 ± 0.3 * | 14.8 ± 1.1 | 6.0 ± 0.5 | 16.2 ± 0.8 | 6.6 ± 0.3 |
| **DG** | | | | | | | | |
| **Moleculare** | 15.7 ± 1.9 ** | 4.3 ± 0.5 ** | 17.6 ± 1.8 | 6.4 ± 0.6 | 19.9 ± 2.6 | 8.1 ± 1.1 | 19.5 ± 1.2 | 7.8 ± 0.5 |
| **Granulare** | 7.8 ± 1.0 *** | 2.1 ± 0.3 *** | 9.0 ± 0.8 *** | 3.3 ± 0.3 *** | 11.7 ± 0.5 | 4.8 ± 0.2 | 13.4 ± 1.7 | 5.4 ± 0.7 |
| **Polymorph** | 5.7 ± 2.2 *** | 1.6 ± 0.6 *** | 11.7 ± 1.5 | 4.3 ± 0.6 | 11.3 ± 2.1 | 4.6 ± 0.9 | 13.8 ± 1.8 | 5.5 ± 07 |
| ***Mean*** | 9.7 ± 1.7 *** | 2.7 ± 0.5 *** | 12.8 ± 0.8 ** | 4.7 ± 0.3 ** | 14.3 ± 1.7 | 5.8 ± 0.7 | 15.6 ± 1.2 | 6.2 ± 0.5 |
| **Hippocampus** | 8.4 ± 1.7 *** | 2.3 ± 0.8 *** | 12.6 ± 1.2 ** | 4.6 ± 0.4 ** | 14.0 ± 1.9 | 5.7 ± 0.5 | 14.7 ± 0.7 | 5.9 ± 0.3 |

(Caption of Table 1)

Laminar, regional and overall densities of ACh axons and axon varicosities in the developing dorsal hippocampus of rat (CA1, CA3 and DG), at three postnatal ages indicated and in the adult (P60, data from Aznavour et al., 2002). Means ± s.d., in meters of axon and millions of axon varicosities per $mm^3$, as explained in Materials and Methods. *P < 0.05, **P < 0.01, ***P < 0.001 denotes statistically significant differences from adult, as analysed by ANOVA followed by Bonferroni's multiple comparison test.

# Table 2 - MORPHOMETRIC FEATURES OF ACh (ChAT-IMMUNOSTAINED) VERSUS RANDOMLY SELECTED UNLABELED AXON VARICOSITIES

| | P8 | | P16 | | P32 | |
|---|---|---|---|---|---|---|
| | ACh | Unlabeled | ACh | Unlabeled | ACh | Unlabeled |
| **Dimensions** | | | | | | |
| **Short axis (μm)** | 0.37 ± 0.03 | 0.44 ± 0.01 | 0.34 ± 0.02 | 0.38 ± 0.05 | 0.34 ± 0.02 | 0.39 ± 0.03 |
| **Long axis (μm)** | 0.67 ± 0.11 | 0.69 ± 0.03 | 0.66 ± 0.04 | 0.67 ± 0.02 | 0.63 ± 0.04 | 0.68 ± 0.02 |
| **Aspect ratio** | 1.84 ± 0.20 | 1.58 ± 0.08 | 1.95 ± 0.12 | 1.76 ± 0.21 | 1.94 ± 0.09 | 1.75 ± 0.13 |
| **Diameter (μm)** | 0.52 ± 0.07 | 0.56 ± 0.02 | 0.51 ± 0.03 | 0.52 ± 0.03 | 0.49 ± 0.03 | 0.53 ± 0.02 |
| **Area ($\mu m^2$)** | 0.22 ± 0.05 | 0.26 ± 0.01 | 0.19 ± 0.02 | 0.21 ± 0.03 | 0.18 ± 0.02 | 0.22 ± 0.02 |
| **% with mitochondria** | 27.7 ± 2.2 ** | 16 ± 5 | 24.8 ± 6.6 ** | 16 ± 1 | 41 ± 2.9 | 20 ± 3 |

Data from 400 single sectional profiles of ChAT-immunostained (ACh) or 200 unlabeled varicosities at each postnatal age. The unlabeled profiles were selected at random from the same micrographs displaying the ACh varicosities, as explained in Materials and Methods. The proportion of ACh and unlabeled profiles displaying mitochondria is given as a percentage. Mean ± s.d. from 4 rats in each group. $^{**}P < 0.01$ indicate differences with P32, as analysed by ANOVA followed by Bonferroni's multiple comparison test.

## Table 3 - JUNCTIONAL FEATURES OF ACh (ChAT-IMMUNOSTAINED) VERSUS RANDOMLY SELECTED UNLABELED AXON VARICOSITIES

| | P8 | | P16 | | P32 | |
|---|---|---|---|---|---|---|
| | ACh | Unlabeled | ACh | Unlabeled | ACh | Unlabeled |
| **Synaptic incidence (%)** | | | | | | |
| **Single sections** | 3 ± 1 | 34 ± 4 ** | 2 ± 1 | 42 ± 8 | 2 ± 2 | 51 ± 5 |
| **Whole volume** | 10 ± 8 | 84 ± 7 *** | 6 ± 3 | 103 ± 19 ** | 6 ± 7 | 147 ± 17 |
| **Synaptic targets (%)** | | | | | | |
| **Dendritic branches** | 70 ± 28 | 60 ± 13 ** | 100 | 32 ± 14 | 70 ± 26 | 19 ± 10 |
| **Dendritic spines** | 22 ± 31 | 33 ± 20 ** | - | 54 ± 9 | 30 ± 26 | 79 ± 11 |
| **Undetermined** | 8 ± 17 | 7 ± 11 | - | 14 ± 4 | - | - |

Data (mean ± s.d.) from the same sectional profiles as in Table 2. The varicosity profiles were classified as showing or not a synaptic junction according to the criteria described in Materials and Methods. The synaptic incidence for the whole volume of varicosities was extrapolated by mean of the stereological formula of Beaudet and Sotelo (1981), using the long axis as diameter of the profiles (Umbriaco et al., 1994). Synaptic incidence and the relative frequency of the various synaptic targets of ACh and unlabeled varicosities are given as a percentage. ** $P < 0.01$ and *** $P < 0.001$ indicate differences with P32, as analysed by ANOVA followed by Bonferroni's multiple comparison test.

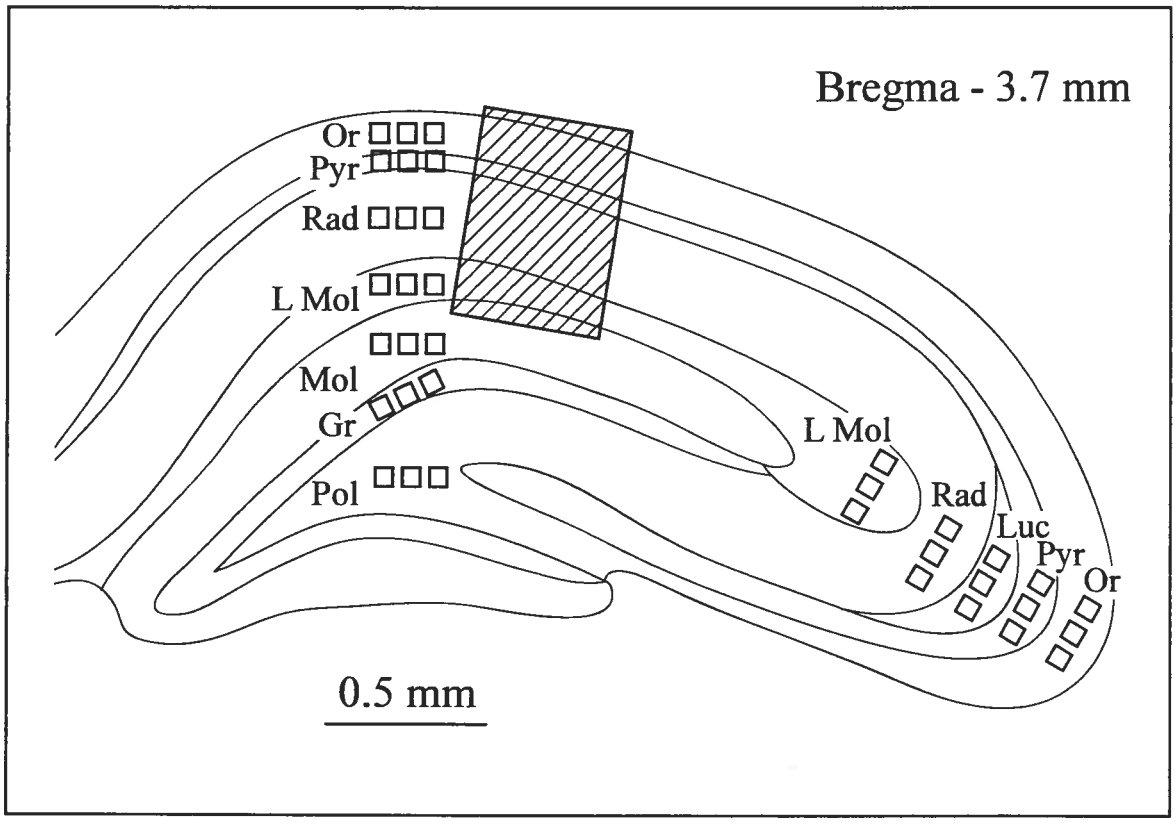
Bregma - 3.7 mm
Or
Pyr
Rad
L Mol
Mol
Gr
Pol
L Mol
Rad
Luc
Pyr
Or
0.5 mm

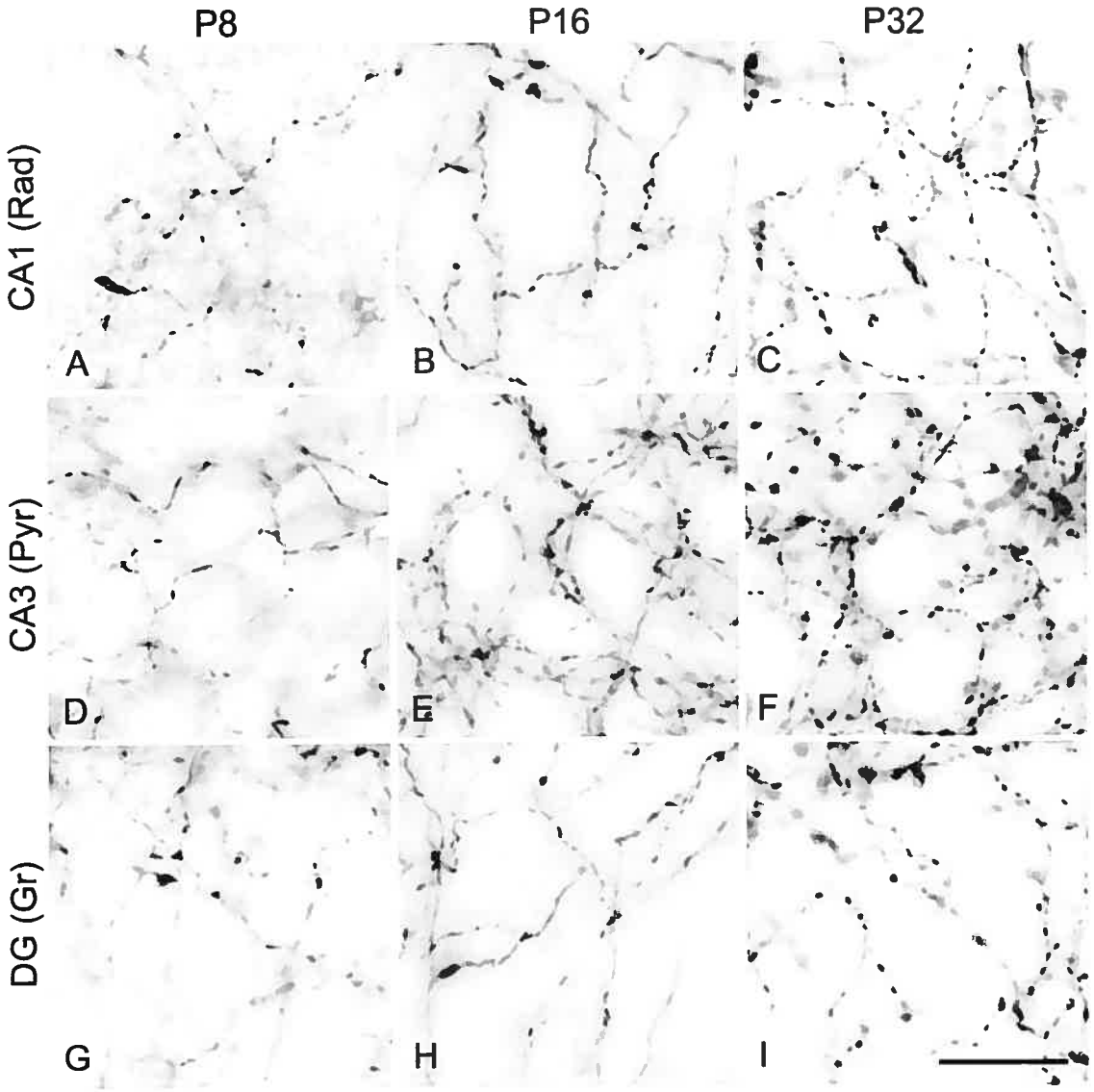
P8
P16
P32
CA1 (Rad)
CA3 (Pyr)
DG (Gr)
A
B
C
D
E
F
G
H
I

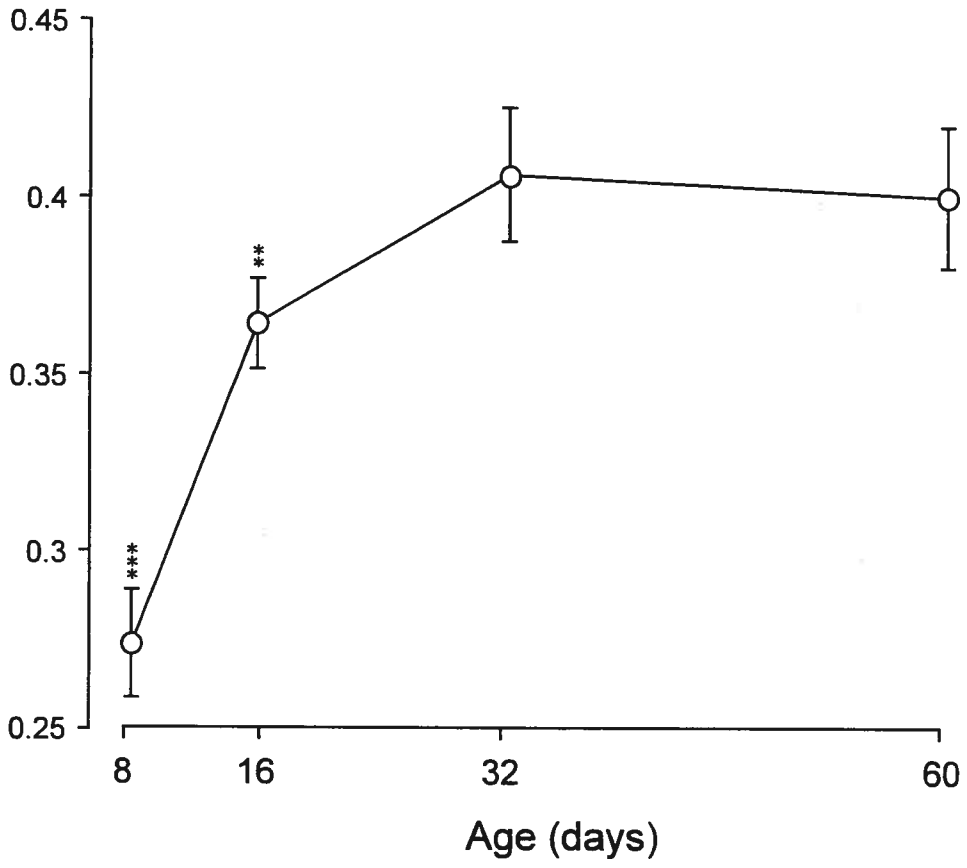
Number of varicosities per µm of ACh axon
0.45
0.4
0.35
0.3
0.25
***
**
8
16
32
60
Age (days)

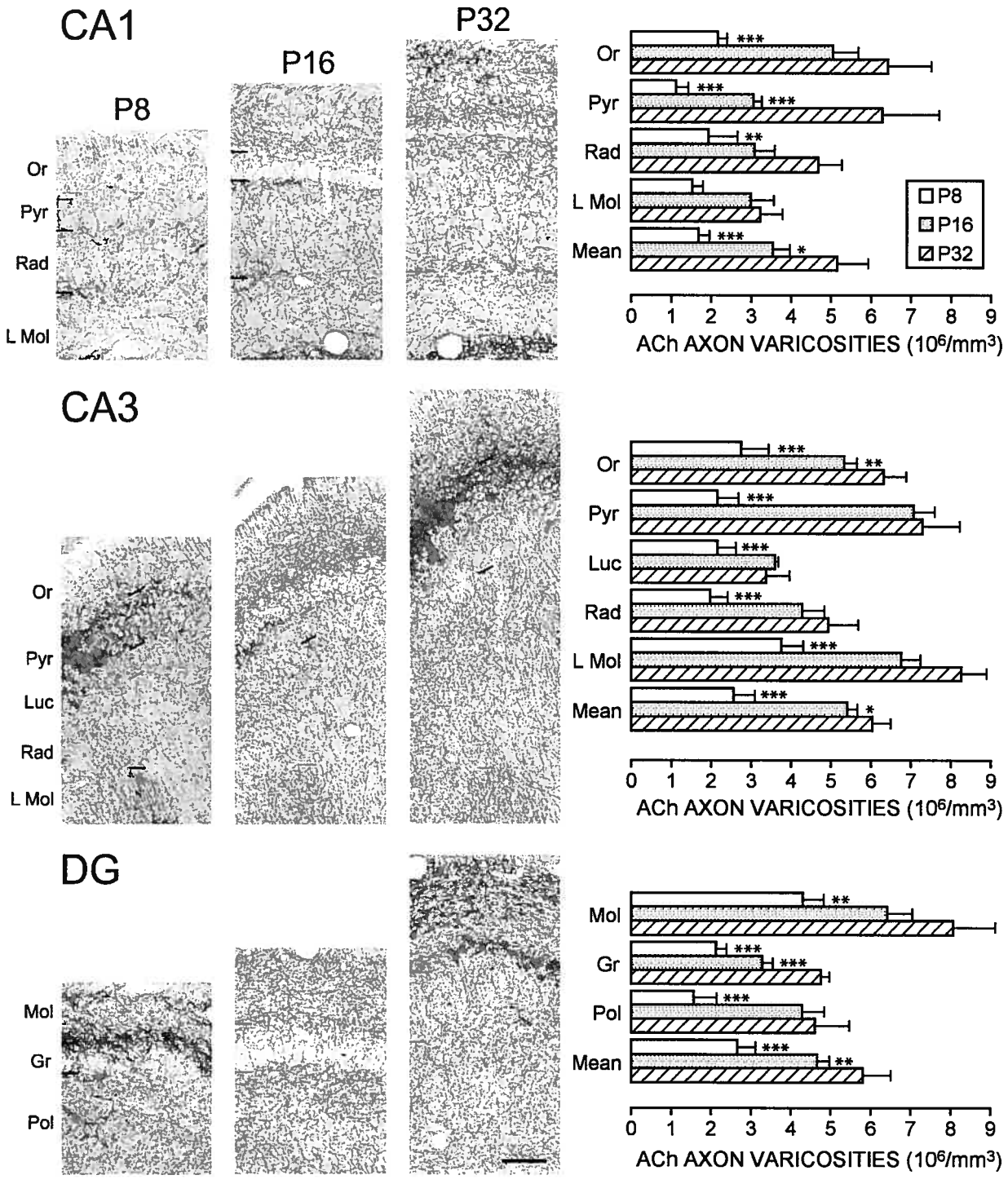
CA1
P8
P16
P32
Or
Pyr
Rad
L Mol
Mean
P8
P16
P32
0 1 2 3 4 5 6 7 8 9
ACh AXON VARICOSITIES (10⁶/mm³)
CA3
Or
Pyr
Luc
Rad
L Mol
Mean
0 1 2 3 4 5 6 7 8 9
ACh AXON VARICOSITIES (10⁶/mm³)
DG
Mol
Gr
Pol
Mean
0 1 2 3 4 5 6 7 8 9
ACh AXON VARICOSITIES (10⁶/mm³)

Density of ACh innervation in the developing hippocampus of rat

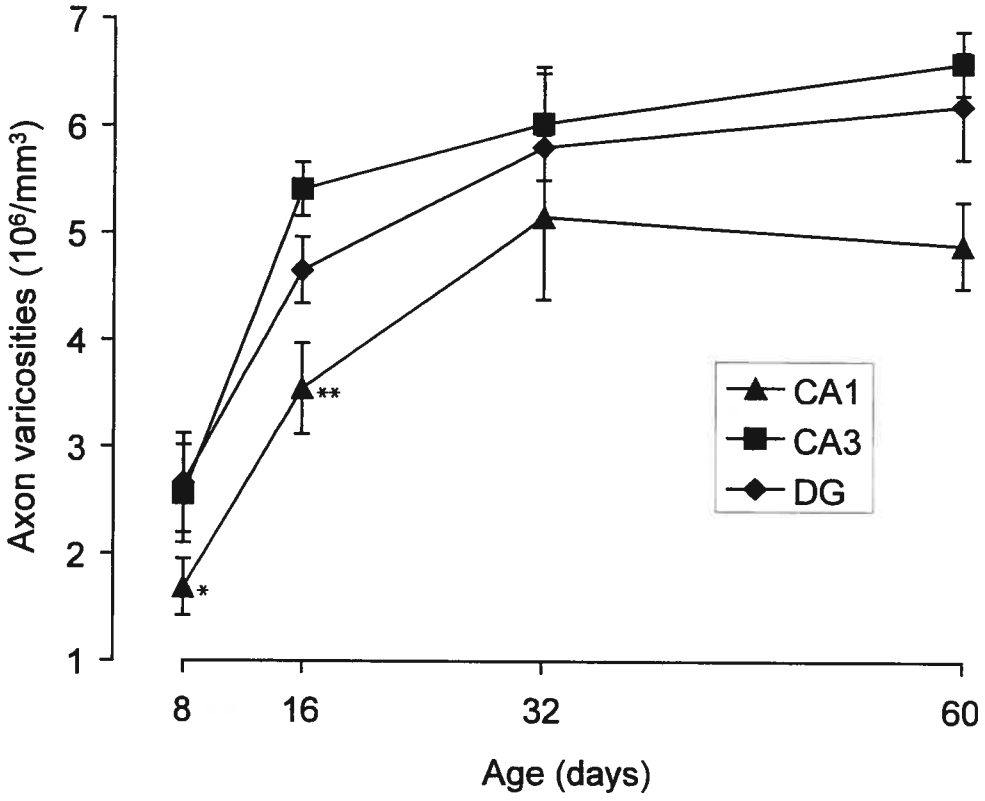

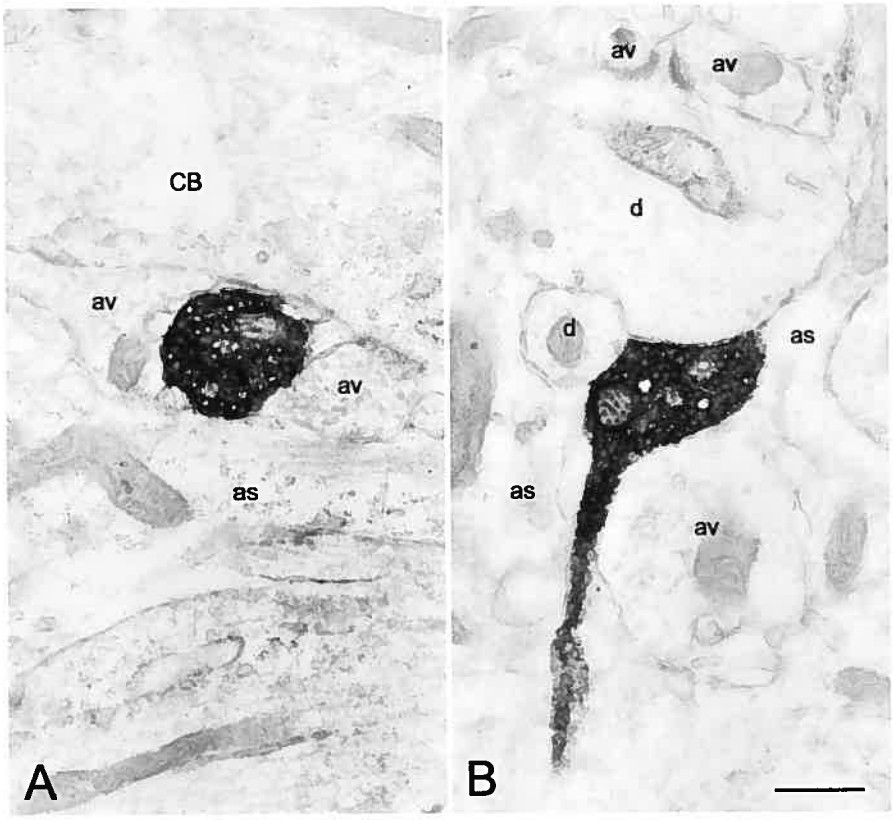
CB
av
av
as
A
av
av
d
d
as
as
av
B

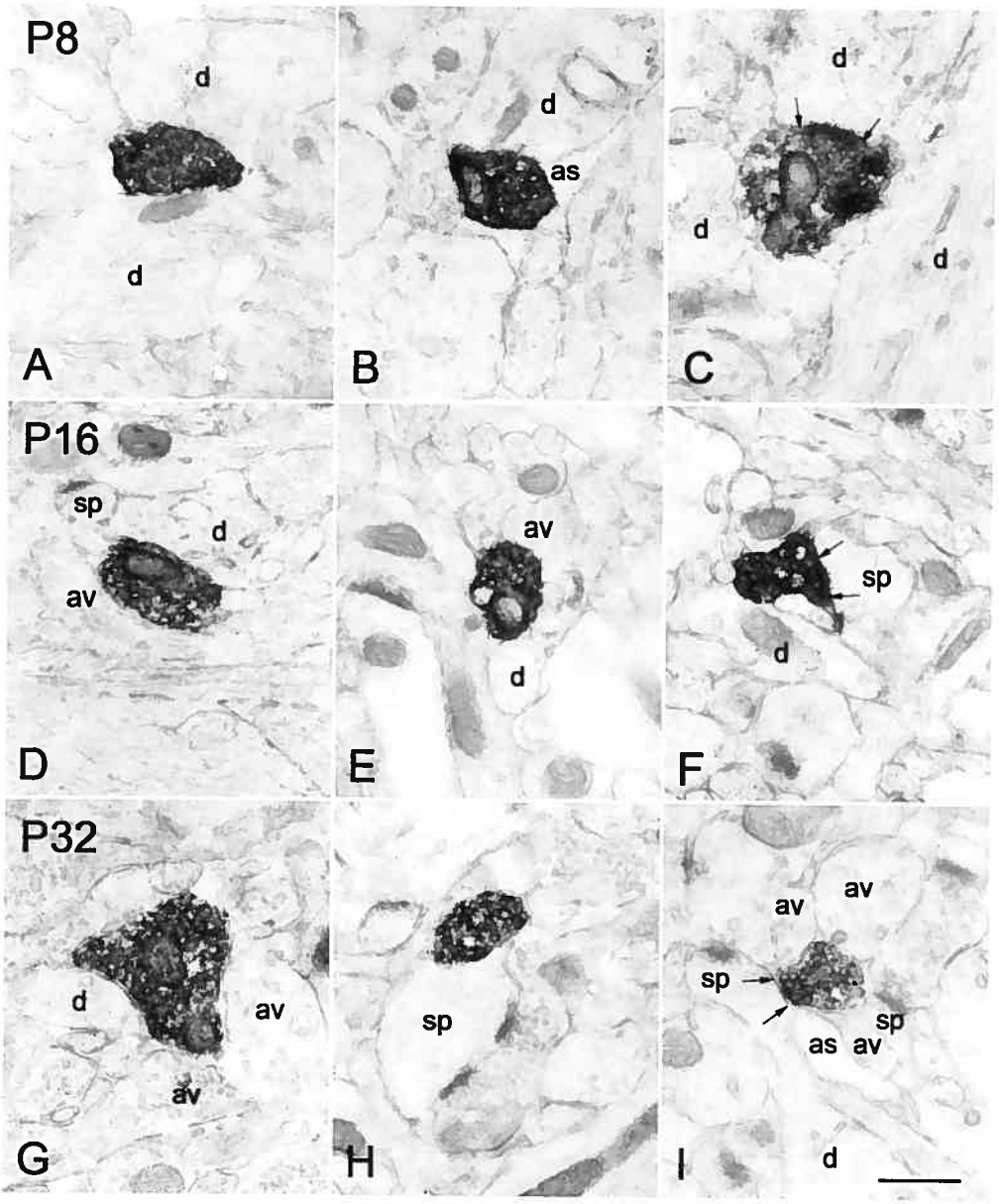
P8
d
d
A
d
as
B
d
d
d
C
P16
sp
d
av
D
av
d
E
sp
d
F
P32
d
av
av
G
sp
H
av
av
sp
sp
as
av
I
d

Chapitre IV

# FINE STRUCTURAL FEATURES OF THE ACETYLCHOLINE INNERVATION IN THE DEVELOPING NEOSTRIATUM OF THE RAT

Publié en 2003

*J Comp Neurol* 460:280-291

(N AZNAVOUR, KC WATKINS et L DESCARRIES)

# FINE STRUCTURAL FEATURES OF THE ACETYLCHOLINE INNERVATION IN THE DEVELOPING NEOSTRIATUM OF RAT

Nicolas AZNAVOUR [1], Naguib MECHAWAR [1], Kenneth C. WATKINS, and Laurent DESCARRIES *

Départements de pathologie et biologie cellulaire et de physiologie, and Centre de recherche en sciences neurologiques, Faculté de médecine, Université de Montréal, Montréal, Québec, Canada H3C 3J7

[1] These two authors have contributed equally to this work

(36 text pages including figure legends; 3 tables and 5 figures)

Abbreviated title: **ACh innervation in developing neostriatum**

Associate editor: Dr. Oswald STEWARD

KEYWORDS ChAT, striatum, immunocytochemistry, electron microscopy, varicosities, axons

* Correspondance: Laurent DESCARRIES m.d.
Département de pathologie et biologie cellulaire
Université de Montréal
CP 6128, Succursale Centre-ville
Montréal, QC, Canada H3C 3J7

tel. (514) 343-7070
fax (515) 343-5755
[redacted]

Grant sponsor: Grant NRF 3544 to L.D., from the Canadian Institutes for Health Research (CIHR).

## ABSTRACT

The acetylcholine (ACh) innervation in the developing neostriatum of rat was examined by means of light and electron microscopic immunocytochemistry with a highly sensitive antibody against choline acetyltransferase (ChAT). ChAT-immunoreactive cell bodies and their emerging processes, located at birth in the lateral part of neostriatum, progressively pervaded the whole region, to give rise to an extremely dense axonal network. As visualized and measured in single thin sections at postnatal ages P8, P16 and P32, the intrinsic and relational features of ChAT-immunostained profiles of axon varicosities in the lateral and medial parts of neostriatum were similar to those previously described in the adult. At the three postnatal ages, the immunoreactive profiles were comparable in shape, size and vesicular content, and displayed one or more mitochondria with increasing frequency (from 10% at P8 to 29% at P32). The proportion which showed a synaptic junction was low at the three ages (8% to 16%), indicating an average synaptic incidence of 22% for whole varicosities, after stereological extrapolation. The observed junctions were relatively small, mostly symmetrical, and made with dendritic spines or branches. The frequency of synapses on spines versus branches increased with age, from 20% at P8 to almost 60% at P32. Thus, the relational features of the neostriatal ACh innervation were similar to adult as soon as it appeared, as previously observed to be the case in the developing cerebral cortex. The diffuse mode of transmission may therefore be characteristic of both ACh interneurons (neostriatum)

and projection neurons (cerebral cortex) in the CNS, and could be determining their functional properties during development as well as at maturity.

## INTRODUCTION

It has long been known that, together with its dopamine counterpart, the acetylcholine (ACh) innervation of the caudate-putamen (neostriatum) is one of the densest transmitter-defined innervations in mammalian brain (e.g., Phelps et al., 1985; DiFiglia, 1987; Contant et al., 1996; see also Saper, 1990). Accordingly, high concentrations and/or activities of all known cholinergic markers have been measured in the neostriatum of the rat: ACh itself, choline acetyltransferase (ChAT), acetylcholinesterase (AChE), choline uptake, choline transporter, vesicular ACh transporter, muscarinic receptors (mAChRs), and nicotinic receptors (nAChRs) (Sorimachi et al., 1974; Hoover et al., 1978; Weiner et al., 1990; Pascual et al., 1991; Hersch et al.,1994; Hersch and Levey, 1995; Aubert et al., 1996). The neostriatal ACh innervation arises almost exclusively from aspiny interneurons that represent less than 2% of the total neuron population of neostriatum in rat (Woolf and Butcher, 1981; Phelps et al., 1985). A minor cholinergic projection from the pedunculopontine tegmental area has also been described (Woolf and Butcher, 1981, 1986).

ACh is among the first neurotransmitter/modulator to appear in neostriatum, in keeping with the fact that ACh interneurons are born during early neurogenesis (Semba et al., 1988; Phelps et al., 1989; Olsson et al., 1998). They arise from a population of germinal cells which migrates tangentially to the striatum from the medial ganglionic eminence and adjacent preoptic/anterior entopeduncular areas (Marin et al., 2000). Born in rat between embryonic days 11 and 18 (E11-18), they

develop along a caudo-rostral and a latero-medial axis (Semba et al., 1988; Phelps et al., 1989), and display a distinctive spatiotemporal pattern of distribution in the patch and matrix compartments (van Vulpen and van der Kooy, 1996, 1999). In rat neostriatum, ChAT is detected as early as E13.5 days (Kessler, 1986), and is thus presumably expressed by the first generated neurons of the patch compartment (van Vulpen and van der Kooy, 1998). Levels of ChAT as well as other cholinergic markers remain relatively low until the end of the first postnatal week (Guyenet et al., 1975; Coyle and Campochiaro, 1976; Coyle and Yamamura, 1976; Hiley, 1976; Happe and Murrin, 1992; Aubert et al., 1996; Zhang et al., 1998), and then rise steadily to reach adult levels around the fourth postnatal week.

Although there is increasing evidence that ACh influences various growth and maturation processes in the CNS (Bear and Singer, 1986; Mattson, 1988; Gu and Singer, 1993; Broide et al., 1996; Role and Berg, 1996; Zhu and Waite, 1998; Broide and Leslie, 1999; Ma et al., 2000; Peinado, 2000), little is known about its roles in the developing neostriatum. An implication in neuronal plasticity, as evidenced in the neocortex, appears likely. In the absence of functional data, knowledge of the ultrastructural features of the developing neostriatal ACh innervation might prove meaningful as regards underlying mechanisms.

In adult rat neocortex, which receives most of its ACh input from projection neurons, it has been demonstrated by electron microscopy in serial as well as single thin sections that only a small proportion of ChAT-immunoreactive axon terminals (varicosities) engage in morphologically defined synaptic junctions (Umbriaco et al., 1994). A low frequency of synapses has also been described for the ACh innervation

in adult rat hippocampus (Umbriaco et al., 1995) and neostriatum (Contant et al., 1996). Such a morphological feature has been taken as an indication that ACh could act primarily via diffuse (volume) transmission in addition to synaptic transmission (for review, see Descarries et al., 1997). Recently, this characteristic of ACh innervation has also been observed in the immature neocortex (Mechawar et al., 2002). In this context, it was of particular interest to examine the distribution of the ACh innervation in the developing neostriatum, and to determine its relational features during development.

## MATERIAL AND METHODS

### Tissue processing

All experiments abided by the policies and guidelines of the Canadian Council on Animal Care and the regulations of the Animal Care Committee at the Université de Montréal. The study was carried out on 14 male Sprague-Dawley rats (Charles River, St-Constant, Québec, Canada), purchased at known ages and kept with their lactating mother, or born in the laboratory (P0).

For light microscopy, 1 rat per age (PO, P4, P8, P16, P32) was deeply anaesthetized with sodium pentobarbital (65 mg/kg, i.p.), and perfused through the heart with ice-cold phosphate-buffered saline (PBS; 50 mM; pH 7.4; 25-50 ml) followed by 100-150 ml of 4% paraformaldehyde (PFA) in 0.1 M sodium phosphate buffer (pH 7.4; 24°C). Immediately after, the brain was dissected out, postfixed overnight in 4% PFA, and cut into consecutive 50 μm-thick transverse sections with a vibratome (Leica). Sections at levels equivalent to stereotaxic plane A-7.23 mm in the Swanson's

stereotaxic atlas of the adult rat brain (1992) were selected with the aid of an atlas of the developing rat brain (Paxinos et al., 1991), and processed for ChAT-immunocytochemistry as described below.

For electron microscopy, tissue from 3 rats per age (P8, P16 and P32) was similarly processed, except for the use of a different protocol for perfusion fixation: PBS 50 mM followed in sequence by 4% PFA (100-150 ml), 4% PFA + 1% glutaraldehyde (100-150 ml) and finally 4% PFA (150-200 ml).

**ChAT-immunocytochemistry**

The following protocol, allowing for an optimal detection of ChAT-immunostained axons in rat brain sections has also been previously described in detail (Mechawar and Descarries, 2001; Mechawar et al, 2002). In brief, the sections were sequentially incubated at room temperature in: 1) a blocking solution of PBS containing 2% normal horse serum (NHS; Vector, Burlingame, CA), 1% bovine serum albumin (BSA; Sigma, St-Louis, MO) and 0.2% Tx-100, for 2h; 2) the same solution containing 2 µg/ml of mouse monoclonal antibody against purified rat brain ChAT (Cozzari et al., 1990), overnight, and 3) a 1/200 dilution of biotinylated horse anti-mouse antibody (Vector), in KPB containing 2% NHS, 1% BSA and 0.2% Tx-100, for 2h. This was followed by the avidin-biotin complex procedure (ABC Kit, Vectastain Elite; Vector) (2h), and a 2 min revelation in a 0.05% solution of 3,3'-diaminobenzidine (DAB; Sigma), prepared in Tris buffer (pH 7.4), to which 0.005% $H_2O_2$ was added. Sections intended for electron microscopy were processed similarly, except for an initial incubation in a 1% solution of sodium borohydride and the absence of Tx-100 in all

solutions. After revelation in DAB, they were osmicated, dehydrated in ethanol and propylene oxide, and flat-embedded in Durcupan (Fluka; Sigma). Control experiments included omission of the primary or secondary antibodies, which completely abolished the immunostaining.

**Electron microscopy**

Two regions at a middle transverse level (decussation of the anterior commissure) across neostriatum were examined: one lateral bordered by the radiations of corpus callosum, the other medial, bordered by the ependymal lining of the lateral ventricle (see Fig. 1). At mid-height vertically, rectangular pieces of these regions were removed from the flat embedded ChAT-immunostained vibratome sections, glued to the tip of resin blocks, and sectioned ultrathin (90-100 nm) with a Porter-Blum MT-2 Ultra-Microtome. The sections were collected on bare 150-mesh grids, stained with lead citrate, and examined with a Philips CM100 electron microscope. From each of the two neostriatal regions in each animal, 75-100 pictures of ChAT-immunostained varicosities were taken at a working magnification of 15 500 X. The varicosities were defined as round or ovoid axon dilations greater than 0.25 □m in small diameter and containing aggregated small vesicles. On prints at 39 000 X, prepared under standard photographic and darkroom conditions, the first 50 sectional profiles of varicosities with a full contour and distinct content were kept for analysis.

With the aid of the public domain NIH Image program (1.61), these varicosity profiles were then measured for area, long axis, short axis and diameter ((long axis + short axis) / 2) and classified as containing or not one or more mitochondria. The

proportion engaged in synaptic junction was tallied by categorizing the varicosity profiles as showing or not a junctional complex, i.e., a localized straightening of apposed plasma membranes with a slight widening of the intracellular space and/or a pre- or postsynaptic thickening. The length of the junctions was measured, and the observed synaptic frequency converted to synaptic incidence for whole varicosities by means of the stereological formula of Beaudet and Sotelo (1981), using the long axis as diameter of the profiles (Umbriaco et al., 1994). This formula takes into account the average size of varicosity profiles, the length of their junctional complexes and the thickness of the sections, to predict the probability of seeing a synapse if there is one on every varicosity. The synaptic incidence is then inferred by comparison with this predicted value. The reliability of this procedure has been validated experimentally by Umbriaco et al. (1994), who found almost identical values of synaptic incidence for a large population of ChAT-immunostained cortical varicosities examined in serial sections across the entire volume and which were also treated as a randomized single section sample.

The junctions made by ChAT-immunostained profiles were further characterized as symmetrical or asymmetrical, their synaptic targets identified, and the composition of their immediate microenvironment scrutinized for the presence of one or more juxtaposed axon varicosity or dendritic spine.

The intrinsic and relational features of the ChAT-immunostained varicosities were also compared to those of a population of unlabeled axon varicosities selected at random from the same electron micrographs. For this purpose, we used a transparent overlay bearing a fixed mark in its upper left quadrant, to select the

nearest fully visible unlabeled axon varicosity profile in each print. Thus, 300 unlabeled profiles were also analyzed at each age, as described above.

**Statistical analysis**

A Kruskal-Wallis test, followed by a Student's *t*-test was used to determine if the dimensions (area, long axis, diameter) and junctional features of ACh or unlabeled varicosities differed significantly between the medial and lateral parts of neostriatum at each age. Since no such variations were found, averages ± s.d. were calculated for all parameters, as presented in Tables 1-3. These results were then tested for age-related differences with the Kruskal-Wallis test. In view of the relatively small number of animals examined, differences were considered statistically significant at $p < 0.01$.

# RESULTS

## Light microscopic distribution of ChAT-immunostaining

In addition to the relatively large immunoreactive neuronal cell bodies and ramified dendrites described in earlier studies (Bolam et al., 1984; DiFiglia 1987; Izzo and Bolam 1988; Phelps et al., 1985; Pickel and Chan 1990; Houser 1990), the present anti-ChAT antibody revealed the existence of a network of fine, beaded ChAT positive axons which spread from the lateral to the medial part of neostriatum and became increasingly dense from P0 to P32 (Figs. 1 - 3).

In keeping with previous descriptions, the immunoreactive cell bodies were intensely labelled and had a spindle-like, oval, triangular or multipolar shape, with long, essentially smooth and sparsely branched dendrites, typical of neostriatal ACh interneurons (Figs. 1 - 3). At P0, these cell bodies were small and mostly bipolar, but their size increased dramatically between P4 and P16 and then, to a lesser extent even until P32. At P0, they were distributed along a steep decreasing lateromedial gradient, which attenuated at P8 and was no longer visible at P16 (Figs. 1 and 2). However, their number appeared to be constant, amounting to approximately two hundred per section of neostriatum at all ages.

Both the distribution and density of ChAT positive axons showed marked changes with age (Figs. 1 - 3). At P0, some were already present in the lateral region of neostriatum. Between P4 and P8, they expanded into a heterogeneous network toward the medial part of neostriatum, in a pattern of discrete patches of lighter and denser innervation. At P16, this network was much denser, spreading across the

entire neostriatum among the scattered ACh cell bodies, except in a narrow zone of lighter innervation along the lateral ventricle. At P32, it had almost reached its adult density, and a subtle decreasing lateromedial gradient of axons was still noticeable.

**Ultrastructural features of neostriatal ChAT positive axon varicosities**

Regardless of postnatal age, ChAT-immunostained axon varicosities shared similar ultrastructural characteristics in both the lateral and medial parts of neostriatum. As shown in Figs. 4 and 5 and quantified in Table 1, their sectional profiles arose from small diameter, unmyelinated axons, were generally elliptic, and contained numerous aggregated small clear vesicles, with or without a mitochondrion. The diaminobenzidine immunoprecipitate was of variable density, confined to the axoplasm, and often lined the plasma membrane and the outer surface of organelles.

The dimensions of ChAT positive varicosities showed a slight, non significant reduction between P8 and P32 (Table 1). Their average diameter across ages was 0.48 μm, and their average sectional area 0.17 $\mu m^2$. Slightly higher values were measured for the population of randomly selected unlabeled varicosities (0.53 μm and 0.22 $\mu m^2$). The proportion of ChAT positive varicosity profiles containing one or more mitochondria increased significantly with age, from 13.7% (P8), to 27.0% (P16) and 28.7% (P32). At each age, this percentage was higher than for unlabeled varicosities.

**Junctional relationships**

ChAT positive varicosity profiles endowed with a synaptic junction were observed at all ages in both the lateral and medial neostriatum. The frequency of these synaptic profiles was consistently low and relatively stable, averaging 16%, 8% and 10% at P8, P16 and P32, respectively (Table 2). The mean length of the junctional complexes also appeared to be stable, measuring 0.27 μm at P8, 0.25 μm at P16 and 0.22 μm at P32. The extrapolated synaptic incidence for whole varicosities, determined with the stereological formula from Beaudet and Sotelo (1981), amounted to 30% at P8, 16% at P16 and 22% at P32, without any statistically significant difference between ages. By comparison, the same extrapolation performed on randomly selected unlabeled profiles yielded considerably higher values, ranging from 76% at P8 to 81% at P32.

As shown in Table 2 and Fig. 5, the synaptic junctions made by neostriatal ChAT-immunostained varicosities were always single, more often symmetrical than asymmetrical, and mostly made with dendritic branches or spines. A small proportion only was found on cell bodies (e.g. Fig. 4). At P8 and P16, the synapses made by the ChAT positive varicosities were more frequent on dendritic branches than spines, but this was no longer the case at P32. At all ages, these synapses were more often symmetrical than asymmetrical. Most of those made with dendritic branches were symmetrical, whereas those made with spines were almost equally divided between symmetrical and asymmetrical. The vast majority of synapses made by the unlabeled varicosities were asymmetrical, irrespective of their localization on dendritic branches or spines. As synapses made by ChAT positive varicosities, the

unlabeled synapses were more frequent on dendritic branches than spines at P8, but became markedly different at P16 and P32, when they were mostly found on dendritic spines.

**Structural microenvironment**

The frequency with which ChAT positive and randomly selected unlabeled varicosities, whether synaptic or not, were juxtaposed to axon terminals and dendritic spines is given in Table 3. At P8, axon varicosities were more frequent than spines around both categories of profiles. From P8 to P32, the number of axon varicosities and dendritic spines increased around the two categories of profiles, but the increase in number of spines appeared to be greater around unlabeled than around ChAT positive varicosities.

## DISCUSSION

In addition to describing its ultrastructural features, this study provides new information on the distributional characteristics of the ACh innervation in developing neostriatum. At birth, ACh axons were already visible in the lateral part of neostriatum, in keeping with observations indicating that this is the first region of neostriatum to be reached by migrating ACh neurons (Marin et al., 2000). At P4, ACh axons had grown into a larger lateral zone, to which they remained confined, whereas the cell bodies were already found across the entire neostriatum. At P8, when they began to fill the entire region, ACh axons in the lateral neostriatum formed discrete patches of lighter and denser innervation. At later postnatal ages (P16 and P32), this pattern was no longer apparent, as the network of ACh axons was extremely dense throughout, even if a slight lateromedial gradient of density was still visible. A transient patchy distribution has already been reported for other cholinergic markers in the developing neostriatum of several mammalian species, including rat (Graybiel, 1984; Natsuk and Graybiel, 1989). It could be related to other aspects of the cytoarchitectural compartmentation in immature neostriatum, and particularly to the early presence of dopamine and mu opiate receptor rich islands (Graybiel et al., 1981; Moon Edley and Herkenham, 1984; Natsuk and Graybiel, 1985). This might in turn account for some interactions between these systems, as suggested by the observation that ACh regulates DA release as early as P3 in rat brain slices (Nomura et al., 1981).

The presence of a neostriatal ACh axon network endowed with a considerable number of axon varicosities as soon as a week after birth was in line with numerous findings previously made in this brain region during its postnatal development. ChAT protein and activity, concentration of ACh, ACh release from slices, choline uptake and binding to high affinity choline transport sites have all been measured during the first postnatal week in rat neostriatum, and shown to rise markedly afterward (Guyenet et al., 1975; Coyle and Campochiaro, 1976; Coyle and Yamamura, 1976; De Vries et al., 1992; Happe and Murrin 1992). The density of both muscarinic and nicotinic receptors also increases significantly during the first postnatal week, as demonstrated by ligand binding autoradiography (Naeff et al., 1992; Wall et al., 1992a; Aubert et al., 1996; Zhang et al., 1998). As mentioned above, distinct actions of ACh in neostriatum have been detected as early as a few days after birth. By the end of the first postnatal week, these include the inhibition of ACh release by muscarinic autoreceptors and the coupling of inhibitory muscarinic receptors to dopamine sensitive adenylate cyclase (De Vries et al., 1992). Modulation of ACh release by other transmitters, such as dopamine, opoids and tachykinins, has also been reported (Perez-Navarro et al., 1993). Given that the number of neostriatal ACh interneurons appears to remain stable between birth and adulthood, and that the size of their somata increases only two-fold from P8 onward (Gould et al., 1991; Schlösser et al., 1999), it is likely that most of the above properties depend on the proliferation of ACh axons.

The morphometric and relational features of ACh varicosities observed in the developing neostriatum were comparable to those already described for adult ACh

innervations in different regions of the adult rat brain (e.g. Chedotal et al., 1994; Umbriaco et al., 1994, 1995; Vaucher and Hamel, 1995) and notably the neostriatum (Contant et al., 1996). Similar features were also reported recently for ACh varicosities in the developing neocortex (Mechawar et al., 2002). As in neocortex, the present observations suggest that varicosities borne by ACh axons proliferating in the neostriatum have the capacity to release ACh as soon as they are formed.

As measured in single sections, the dimensions of ACh varicosities in the developing neostriatum were the same from P8 to P32, and slightly superior to those in adult rat (Contant et al., 1996). For example, their area and mean diameter averaged 0.17 $\mu m^2$ and 0.48 $\mu m$ between P8 and P32, compared to 0.12 $\mu m^2$ and 0.43 $\mu m$ in the adult. Such small differences could in fact result from variations in tissue processing in addition to limited sampling. As already observed in the adult (Contant et al., 1996), ACh varicosities were consistently smaller than randomly selected, unlabeled ones, according to short axis, long axis, diameter and area, even if these differences appeared to be statisticaly significant only for area, at P32. The proportion of sectional profiles displaying mitochondria was higher for ACh than unlabeled varicosities at the three postnatal ages examined, a difference particularly noticeable at P16. Even if this proportion increased twofold between P8 and P32 (from 13.7% to 28.7%), it remained lower than that reported in the adult (66%) (Contant et al., 1996). The steep increase in frequency of mitochondria in the ACh varicosities between P8 and P16 could reflect the high metabolic demands placed on these growing ACh interneurons, but also their increase in ACh synthesis, since these organelles produce the precursor acetyl-CoA.

As previously demonstrated in different regions of the adult and developing rat brain (Chédotal et al., 1994; Umbriaco et al., 1994, 1995; Vaucher and Hamel, 1995; Contant et al., 1996; Mechawar et al., 2002; but see Turrini et al., 2001), the frequency with which neostriatal ACh varicosities made morphologically defined synaptic junctions was low, irrespective of the postnatal age examined. When extrapolated to whole varicosities, it averaged 22%, a higher percentage than previously measured in the adult (8.8%; Contant et al., 1996), perhaps because of the limited number of observations available for analysis. The mostly asynaptic character of this innervation contrasted sharply with that of the randomly selected, unlabeled varicosities, which displayed a three to five times higher synaptic incidence.

At all postnatal ages examined, a majority of the junctions formed by the neostriatal synaptic ACh varicosities were symmetrical, as observed in earlier ultrastructural studies of this region in adult rat (Wainer et al., 1994; Phelps et al., 1985; Izzo and Bolam, 1988; Pickel and Chan, 1995). In this regard, ACh varicosities differed significantly from the unlabeled ones, which mostly made asymmetrical synapses. Although ACh synapses on dendritic branches appeared to be more frequent at P8 and P16, this trend was no longer found at P32, when synapses on spines had increased in both the ACh and unlabeled populations. This presumably reflected the maturation of medium spiny neurons, a process known to span the entire first postnatal month (Sharpe and Tepper 1998; Tepper et al., 1998). It is interesting to speculate that the predominance of ACh synapses onto dendritic branches before P32 could translate into an input of greater synaptic weight than in adult, owing to

the absence of attenuation of current flow by spine necks (Wilson, 1984; Tepper et al., 1998).

The finding that this ACh innervation was largely asynaptic as soon as it developed suggests that this relational feature is a fundamental characteristic of the ACh phenotype, common to both ACh interneurons (neostriatum) and projection neurons (neocortex and hippocampus). It could also indicate that the development and maintenance of this feature is intrinsically governed, rather than dependent on factors produced in the territory of innervation, in keeping with the common progenitor origin of all basal forebrain ACh neurons (Marin et al., 2000). Interestingly, a low frequency of synaptic axon varicosities maintained throughout development and adulthood has also been recently reported for the noradrenaline innervation in rat visual and motor cortex (Latsari et al., 2002).

In adult neostriatum, neocortex and hippocampus, the largely asynaptic nature of ACh varicosities has been viewed as an indication that the effects of ACh are largely exerted through a diffuse mode of transmission, on a wide variety of cellular targets and a relatively large tissue volume. This mode of transmission appears consistent with the fact that nicotinic and muscarinic receptors are expressed by diverse cellular elements in the neostriatum, including medium spiny neurons, GABA interneurons, neuropeptide Y-containing neurons, dopaminergic afferents and cortical afferents (Giorguieff et al., 1977; Vuillet et al., 1992; Calabresi et al., 2000; Zhou et al., 2001; Koos and Tepper, 2002). It might also explain the widespread subcellular distribution of these receptors at extrasynaptic sites and non

cholinergic synapses, at least in the adult neostriatum (Jones et al., 2001; Hersch et al., 1994; Hersch and Levey, 1995).

Because most of the acetylcholinesterase present in the developing as well as adult CNS is of the tetrameric globular form (G4) (Gorenstein et al., 1991), the one that regulates extrasynaptic ACh levels at the motor endplate (Gisiger and Stephens, 1988), it has been hypothesized that a low ambient level of ACh might be permanently maintained throughout the extracellular space, at least in densely ACh-innervated brain regions such as the neostriatum (Descarries et al., 1997, 1998). The high acetylcholinesterase content in this region would primarily serve to keep the ambient level of ACh within physiological limits, rather than totally eliminate it from the extracellular space. The basal levels of ACh measured by microdialysis in adult rat striatum are consistent with this hypothesis, being in the order of 10 nM (Ajima and Kato, 1987; Damsma et al., 1988; deBoer et al., 1990; Messamore et al., 1993; Taber and Fibiger, 1994; Vinson and Justice, 1997). This is in the range of sensitivity measured for many of the nicotinic or muscarinic ACh receptors (Kurosaki et al., 1987; Quirion et al., 1989; Sharples and Wonnacott, 2001). A variety of cellular elements in neostriatum might thus be exposed to this low concentration of ACh, which might regulate the expression of homologous or heterologous receptors (Descarries, 1998). There are clear indications that ACh may control the expression and distribution of some of its receptors in the adult neostriatum (Fung and Lau, 1988; Wall et al., 1992b; Bernard et al., 1998, 1999). There is also evidence that activation of ACh receptors during development may transiently or permanently alter muscarinic or nicotinic ACh receptor levels in neostriatum (Fung, 1989; Fung and Lau, 1989; Ibarra et al., 1995;

Shacka and Robinson 1998; Zhu et al., 1998; Miao et al., 1998), and/or affect locomotor activity (Denson et al., 1975; Peters et al., 1979; Fung, 1988; Shacka et al., 1997; Newman et al., 1999). Thus, the mechanisms involved in the regulation of ACh receptor expression are already functional during development and could be activated by ACh liberated from proliferating axons. It remains to be determined whether distinct or complementary functions are then being subserved by the synaptic versus asynaptic component of the ACh innervation, but clearly, diffuse transmission by ACh might be operational in the developing as well as in the adult neostriatum.

## ACKNOWLEDGMENTS

N.A. is recipient of a PhD studentship from the Groupe de recherche sur le système nerveux central (FCAR), and N.M. held a research studentship from the Medical Research Council of Canada. The authors are grateful to Costantino Cozzari and Boyd K. Hartman for their generous gift of ChAT antibody. They also thank Gaston Lambert and Jean Léveillé for photographic work.

## REFERENCES

Ajima A, Kato T. 1987. Brain dialysis: detection of acetylcholine in the striatum of unrestrained and unanesthetized rats. Neurosci Lett. 81:129-132.

Aubert I, Cecyre D, Gauthier S, Quirion R. 1996. Comparative ontogenic profile of cholinergic markers, including nicotinic and muscarinic receptors, in the rat brain. J Comp Neurol. 369:31-55.

Bear MF, Singer W. 1986. Modulation of visual cortical plasticity by acetylcholine and noradrenaline. Nature. 320:172-176.

Beaudet A, Sotelo C. 1981. Synaptic remodeling of serotonin axon terminals in rat agranular cerebellum. Brain Res. 206:305-329.

Bernard V, Levey AI, Bloch B. 1999. Regulation of the subcellular distribution of m4 muscarinic acetylcholine receptors in striatal neurons in vivo by the cholinergic environment: evidence for regulation of cell surface receptors by endogenous and exogenous stimulation. J Neurosci. 19:10237-10249.

Bernard V, Laribi O, Levey AI, Bloch B. 1998. Subcellular redistribution of m2 muscarinic acetylcholine receptors in striatal interneurons in vivo after acute cholinergic stimulation. J Neurosci. 18:10207-10218.

Bolam JP. 1984. Synapses of identified neurons in the neostriatum. Ciba Found Symp. 107:30-47.

Broide RS, Leslie FM. 1999. The alpha7 nicotinic acetylcholine receptor in neuronal plasticity. Mol Neurobiol. 20:1-16.

Broide RS, Robertson RT, Leslie FM. 1996. Regulation of alpha7 nicotinic acetylcholine receptors in the developing rat somatosensory cortex by thalamocortical afferents. J Neurosci. 16:2956-2971.

Calabresi P, Centonze D, Gubellini P, Pisani A, Bernardi G. 2000. Acetylcholine-mediated modulation of striatal function. Trends Neurosci. 23:120-126.

Chedotal A, Umbriaco D, Descarries L, Hartman BK, Hamel E. 1994. Light and electron microscopic immunocytochemical analysis of the neurovascular relationships of choline acetyltransferase and vasoactive intestinal polypeptide nerve terminals in the rat cerebral cortex. J Comp Neurol. 343:57-71.

Contant C, Umbriaco D, Garcia S, Watkins KC, Descarries L. 1996. Ultrastructural characterization of the acetylcholine innervation in adult rat neostriatum. Neuroscience. 71:937-947.

Coyle JT, Campochiaro P. 1976. Ontogenesis of dopaminergic-cholinergic interactions in the rat striatum: a neurochemical study. J Neurochem. 27:673-678.

Coyle JT, Yamamura HI. 1976. Neurochemical aspects of the ontogenesis of cholinergic neurons in the rat brain. Brain Res. 118:429-440.

Cozzari C, Howard J, Hartman B. 1990. Analysis of epitopes on choline acetyltranferse (ChAT) using monoclonal antibodies (Mabs). Soc Neurosci Abstr. 16:200.

Damsma G, Westerink BH, de Boer P, de Vries JB, Horn AS. 1988. Basal acetylcholine release in freely moving rats detected by on-line trans-striatal dialysis: pharmacological aspects. Life Sci. 43:1161-1168.

De Vries TJ, Mulder AH, Schoffelmeer AN. 1992. Differential ontogeny of functional dopamine and muscarinic receptors mediating presynaptic inhibition of

neurotransmitter release and postsynaptic regulation of adenylate cyclase activity in rat striatum. Brain Res Dev Brain Res. 66:91-96.

deBoer P, Abercrombie ED, Heeringa M, Westerink BH. 1993. Differential effect of systemic administration of bromocriptine and L-dopa on the release of acetylcholine from striatum of intact and 6-OHDA-treated rats. Brain Res. 608:198-203.

Denson R, Nanson JL, McWatters MA. 1997. Hyperkinesis and maternal smoking. Can Psychiatr Assoc J. 20:183-187.

Descarries L. 1998. The hypothesis of an ambient level of acetylcholine in the central nervous system. J Physiol (Paris). 92:215-220.

Descarries L, Gisiger V, Steriade M. 1997. Diffuse transmission by acetylcholine in the CNS. Prog Neurobiol. 53:603-625.

Descarries L, Mechawar N. 2001. Ultrastructural evidence for diffuse transmission by monoamine and acetylcholine neurons of the central nervous system. Prog Brain Res. 125:27-47.

DiFiglia M. 1987. Synaptic organization of cholinergic neurons in the monkey neostriatum. J Comp Neurol. 255:245-258.

Fung YK. 1988. Postnatal behavioural effects of maternal nicotine exposure in rats. J Pharm Pharmacol. 40:870-872.

Fung YK. 1989. Postnatal effects of maternal nicotine exposure on the striatal dopaminergic system in rats. J Pharm Pharmacol. 41:576-578.

Fung YK, Lau YS. 1988. Receptor mechanisms of nicotine-induced locomotor hyperactivity in chronic nicotine-treated rats. Eur J Pharmacol. 152:263-271.

Fung YK, Lau YS. 1989. Effects of prenatal nicotine exposure on rat striatal dopaminergic and nicotinic systems. Pharmacol Biochem Behav. 33:1-6.

Giorguieff MF, Le Floc'h ML, Glowinski J, Besson MJ. 1977. Involvement of cholinergic presynaptic receptors of nicotinic and muscarinic types in the control of the spontaneous release of dopamine from striatal dopaminergic terminals in the rat. J Pharmacol Exp Ther. 200:535-544.

Gisiger V, Stephens HR. 1988. Localization of the pool of G4 acetylcholinesterase characterizing fast muscles and its alteration in murine muscular dystrophy. J Neurosci Res. 19:62-78.

Gorenstein C, Gallardo KA, Robertson RT. 1991. Molecular forms of acetylcholinesterase in cerebral cortex and dorsal thalamus of developing rats. Brain Res Dev Brain Res. 61:271-276.

Gould E, Woolf NJ, Butcher LL. 1991. Postnatal development of cholinergic neurons in the rat: I. Forebrain. Brain Res Bull. 27:767-789.

Graybiel AM. 1984. Correspondence between the dopamine islands and striosomes of the mammalian striatum. Neuroscience. 13:1157-1187.

Graybiel AM, Pickel VM, Joh TH, Reis DJ, Ragsdale CW Jr. 1981. Direct demonstration of a correspondence between the dopamine islands and acetylcholinesterase patches in the developing striatum. Proc Natl Acad Sci USA. 78:5871-5875.

Gu Q, Singer W. 1989. The role of muscarinic acetylcholine receptors in ocular dominance plasticity. EXS. 57:305-314.

Guyenet PG, Beaujouan JC, Glowinski J. 1975. Ontogenesis of neostriatal cholinergic neurones in the rat and development of their sensitivity to neuroleptic drugs. Naunyn Schmiedebergs Arch Pharmacol. 288:329-334

Happe HK, Murrin LC. 1992. Development of high-affinity choline transport sites in rat forebrain: a quantitative autoradiography study with ($^3$H)hemicholinium-3. J Comp Neurol. 321:591-611.

Hersch SM, Gutekunst CA, Rees HD, Heilman CJ, Levey AI. 1994. Distribution of m1-m4 muscarinic receptor proteins in the rat striatum: light and electron microscopic immunocytochemistry using subtype-specific antibodies. J Neurosci. 14:3351-3363.

Hersch SM, Levey AI. 1995. Diverse pre- and post-synaptic expression of m1-m4 muscarinic receptor proteins in neurons and afferents in the rat neostriatum. Life Sci. 56:931-938.

Hiley CR. 1976. Ontogenesis of muscarinic receptor sites in rat brain. Br J Pharmacol. 58:427-28.

Hoover DB, Muth EA, Jacobowitz DM. 1978. A mapping of the distribution of acetycholine, choline acetyltransferase and acetylcholinesterase in discrete areas of rat brain. Brain Res. 153:295-306.

Houser CR. 1990. Cholinergic synapses in the central nervous system: studies of the immunocytochemical localization of choline acetyltransferase. J Electron Microsc Tech. 15:2-19.

Ibarra GR, Rodriguez JA, Paratcha GC, Azcurra JM. 1995. Permanent alteration of muscarinic acetylcholine receptor binding in rat striatum after circling training during development. Brain Res. 705:39-44.

Izzo PN, Bolam JP. 1988. Cholinergic synaptic input to different parts of spiny striatonigral neurons in the rat. J Comp Neurol. 269:219-234.

Jones IW, Bolam JP, Wonnacott S. 2001. Presynaptic localisation of the nicotinic acetylcholine receptor beta2 subunit immunoreactivity in rat nigrostriatal dopaminergic neurones. J Comp Neurol. 439:235-247.

Kessler JA. 1986. Differential regulation of cholinergic and peptidergic development in the rat striatum in culture. Dev Biol. 113:77-89.

Koos T, Tepper JM. 2002. Dual cholinergic control of fast-spiking interneurons in the neostriatum. J Neurosci. 22:529-535.

Kurosaki T, Fukuda K, Konno T, Mori Y, Tanaka K, Mishina M, Numa S. 1987. Functional properties of nicotinic acetylcholine receptor subunits expressed in various combinations. FEBS Lett. 214:253-258.

Latsari M, Dori I, Antonopoulos J, Chiotelli M, Dinopoulos A. 2002. The noradrenergic innervation of the developing and mature visual and motor cortex of the rat brain: a light and electron microscopic immunocytochemical analysis. J Comp Neurol. 445:145-158.

Ma W, Maric D, Li BS, Hu Q, Andreadis JD, Grant GM, Liu QY, Shaffer KM, Chang YH, Zhang L, Pancrazio JJ, Pant HC, Stenger DA, Barker JL. 2000. Acetylcholine stimulates cortical precursor cell proliferation in vitro via muscarinic receptor activation and MAP kinase phosphorylation. Eur J Neurosci. 12:1227-1240.

Marin O, Anderson SA, Rubenstein JL. 2000. Origin and molecular specification of striatal interneurons. J Neurosci. 20:6063-6076.

Mattson MP. 1988. Neurotransmitters in the regulation of neuronal cytoarchitecture. Brain Res. 472:179-212.

Mechawar N, Descarries L. 2001. The cholinergic innervation develops early and rapidly in the rat cerebral cortex: A quantitative immunocytochemical study. Neuroscience. 108:555-567.

Mechawar N, Watkins KC, Descarries L. 2002. Ultrastructural features of the acetylcholine innervation in the developing parietal cortex of rat. Neuroscience. 111:83-94.

Messamore E, Ogane N, Giacobini E. 1993. Cholinesterase inhibitor effects on extracellular acetylcholine in rat striatum. Neuropharmacology. 32:291-296.

Miao H, Liu C, Bishop K, Gong ZH, Nordberg A, Zhang X. 1998. Nicotine exposure during a critical period of development leads to persistent changes in nicotinic acetylcholine receptors of adult rat brain. J Neurochem. 70:752-762.

Moon Edley S, Herkenham M. 1984. Comparative development of striatal opiate receptors and dopamine revealed by autoradiography and histofluorescence. Brain Res. 305:27-42.

Naeff B, Schlumpf M, Lichtensteiger W. 1992. Pre- and postnatal development of high-affinity ($^{3}$H)nicotine binding sites in rat brain regions: an autoradiographic study. Brain Res Dev Brain Res. 68:163-174.

Nastuk MA, Graybiel AM. 1985. Patterns of muscarinic cholinergic binding in the striatum and their relation to dopamine islands and striosomes. J Comp Neurol. 237:176-194.

Nastuk MA, Graybiel AM. 1989. Ontogeny of M1 and M2 muscarinic binding sites in the striatum of the cat: relationships to one another and to striatal compartmentalization. Neuroscience. 33:125-147.

Navarro HA, Seidler FJ, Eylers JP, Baker FE, Dobbins SS, Lappi SE, Slotkin TA. 1989. Effects of prenatal nicotine exposure on development of central and peripheral cholinergic neurotransmitter systems. Evidence for cholinergic trophic influences in developing brain. J Pharmacol Exp Ther. 251:894-900.

Newman MB, Shytle RD, Sanberg PR. 1999. Locomotor behavioral effects of prenatal and postnatal nicotine exposure in rat offspring. Behav Pharmacol. 10:699-706.

Nomura Y, Yotsumoto I, Segawa T. 1981. Ontogenetic development of high potassium- and acetylcholine-induced release of dopamine from striatal slices of the rat. Brain Res. 227:171-177.

Olsson M, Bjorklund A, Campbell K. 1998. Early specification of striatal projection neurons and interneuronal subtypes in the lateral and medial ganglionic eminence. Neuroscience. 84:867-876.

Pascual J, Gonzalez AM, Pazos A. 1991. Further studies on the biochemical characterization and autoradiographic distribution of ($^3$H)hemicholinium-3 binding sites in rat brain: a presynaptic cholinergic marker. Pharmacol Res. 24:345-355.

Paxinos G, Törk I, Tecott LH, Valentino KL. 1991. Atlas of the developing Rat Brain. Academic Press, San Diego, CA.

Peinado A. 2000. Traveling slow waves of activity: a novel form of network activity in developing neocortex. J Neurosci. 20:RC54 (1-6).

Perez-Navarro E, Alberch J, Marsal J. 1993. Postnatal development of functional dopamine, opioid and tachykinin receptors that regulate acetylcholine release from rat neostriatal slices. Effect of 6-hydroxydopamine lesion. Int J Dev Neurosci. 11:701-708.

Peters A, Palay SL, Webster HdeF. 1991. The Fine Structure of the Nervous System. Neurons and Their Supporting Cells. New York, Oxford, Oxford University Press.

Peters DA, Taub H, Tang S. 1979. Postnatal effects of maternal nicotine exposure. Neurobehav Toxicol. 1:221-225.

Phelps PE, Houser CR, Vaughn JE. 1985. Immunocytochemical localization of choline acetyltransferase within the rat neostriatum: a correlated light and electron microscopic study of cholinergic neurons and synapses. J Comp Neurol. 238:286-307.

Phelps PE, Brady DR, Vaughn JE. 1989. The generation and differentiation of cholinergic neurons in rat caudate-putamen. Brain Res Dev Brain Res. 46:47-60.

Pickel VM, Chan J. 1990. Spiny neurons lacking choline acetyltransferase immunoreactivity are major targets of cholinergic and catecholaminergic terminals in rat striatum. J Neurosci Res. 25:263-280.

Quirion R, Araujo D, Regenold W, Boksa P. 1989. Characterization and quantitative autoradiographic distribution of ($^3$H)acetylcholine muscarinic receptors in mammalian brain. Apparent labelling of an M2-like receptor sub-type. Neuroscience. 29:271-289.

Role LW, Berg DK. 1996. Nicotinic receptors in the development and modulation of CNS synapses. Neuron. 16:1077-1085.

Saper CB. 1990. Cholinergic system. In: Paxinos G, editor: The Human Nervous System. San Diego: Academic Press. p 1095-1113.

Schlösser B, Klausa G, Prime G, Ten Bruggencate G. 1999. Postnatal development of calretinin- and parvalbumin-positive interneurons in the rat neostriatum: an immunohistochemical study. J Comp Neurol. 405:185-198.

Semba K, Vincent SR, Fibiger HC. 1988. Different times of origin of choline acetyltransferase and somatostatin-immunoreactive neurons in the rat striatum. J Neurosci. 8:3937-3944.

Shacka JJ, Fennell OB, Robinson SE. 1997. Prenatal nicotine sex-dependently alters agonist-induced locomotion and stereotypy. Neurotoxicol Teratol. 19:467-476.

Shacka JJ, Robinson SE. 1998. Exposure to prenatal nicotine transiently increases neuronal nicotinic receptor subunit alpha7, alpha4 and beta2 messenger RNAs in the postnatal rat brain.Neuroscience. 84:1151-1161.

Sharpe NA, Tepper JM. 1998. Postnatal development of excitatory synaptic input to the rat neostriatum: an electron microscopic study. Neuroscience. 84:1163-1175.

Sharples CG and Wonnacott S. 2001. Neuronal nicotinic receptors. TOCRIS Reviews No 19. Bristol: Tocris Cookson.

Sorimachi M, Miyamoto K, Kataoka K. 1974. Postnatal development of choline uptake by cholinergic terminals in rat brain. Brain Res. 79:343-346.

Swanson LW. 1992. Brain Maps: Structure of the Rat Brain. Amsterdam: Elsevier.

Taber MT, Fibiger HC. 1994. Cortical regulation of acetylcholine release in rat striatum. Brain Res. 639:354-356.

Tepper JM, Sharpe NA, Koos TZ, Trent F. 1998. Postnatal development of the rat neostriatum: electrophysiological, light- and electron-microscopic studies. Dev Neurosci. 20:125-145.

Tizabi Y, Russell LT, Nespor SM, Perry DC, Grunberg NE. 2000. Prenatal nicotine exposure: effects on locomotor activity and central ($^{125}$I)alpha-BT binding in rats. Pharmacol Biochem Behav. 66:495-500.

Turrini P, Casu MA, Wong TP, De Koninck Y, Ribeiro-da-Sylva A, Cuello C. (2001) Cholinergic nerve terminals establish classical synapses in the rat cerebral cortex: synaptic pattern and age-related atrophy. Neuroscience. 105:277-285.

Umbriaco D, Garcia S, Beaulieu C, Descarries L. 1995. Relational features of acetylcholine, noradrenaline, serotonin and GABA axon terminals in the stratum radiatum of adult rat hippocampus (CA1). Hippocampus 5:605-620.

Umbriaco D, Watkins KC, Descarries L, Cozzari C, Hartman BK. 1994. Ultrastructural and morphometric features of the acetylcholine innervation in adult rat parietal cortex: an electron microscopic study in serial sections. J Comp Neurol. 348:351-373.

van Vulpen EH, van Der Kooy D. 1996. Differential maturation of cholinergic interneurons in the striatal patch versus matrix compartments. J Comp Neurol. 365:683-691.

van Vulpen EH, van der Kooy D. 1998. Striatal cholinergic interneurons: birthdates predict compartmental localization. Brain Res Dev Brain Res. 109:51-58.

van Vulpen EH, Van Der Kooy D. 1999. NGF facilitates the developmental maturation of the previously committed cholinergic interneurons in the striatal matrix. J Comp Neurol. 41:187-196.

Vaucher E, Hamel E. 1995. Cholinergic basal forebrain neurons project to cortical microvessels in the rat: electron microscopic study with anterogradely transported Phaseolus vulgaris leucoagglutinin and choline acetyltransferase immunocytochemistry. J Neurosci. 15:7427-7441.

Vinson PN, Justice JB Jr. 1997. Effect of neostigmine on concentration and extraction fraction of acetylcholine using quantitative microdialysis. J Neurosci Methods. 73:61-67.

Vuillet J, Dimova R, Nieoullon A, Goff LK. 1992. Ultrastructural relationships between choline acetyltransferase and neuropeptide y-containing neurons in the rat striatum. Neuroscience. 46:351-360.

Wall SJ, Yasuda RP, Li M, Ciesla W, Wolfe BB. 1992a. The ontogeny of m1-m5 muscarinic receptor subtypes in rat forebrain. Brain Res Dev Brain Res. 66:181-185.

Wall SJ, Yasuda RP, Li M, Ciesla W, Wolfe BB. 1992b. Differential regulation of subtypes m1-m5 of muscarinic receptors in forebrain by chronic atropine administration. J Pharmacol Exp Ther. 262:584-588.

Wainer BH, Bolam JP, Freund TF, Henderson Z, Totterdell S, Smith AD. 1984. Cholinergic synapses in the rat brain: a correlated light and electron microscopic immunohistochemical study employing a monoclonal antibody against choline acetyltransferase. Brain Res. 308:69-76.

Weiner DM, Levey AI, Brann MR. 1990. Expression of muscarinic acetylcholine and dopamine receptor mRNAs in rat basal ganglia. Proc Natl Acad Sci USA. 87:7050-7054.

Wilson CJ. 1984. Passive cable properties of dendritic spines and spiny neurons. J Neurosci. 4:281-297.

Woolf NJ, Butcher LL. 1981. Cholinergic neurons in the caudate-putamen complex proper are intrinsically organized: a combined Evans blue and acetylcholinesterase analysis. Brain Res Bull. 7:487-507.

Woolf NJ, Butcher LL. 1986. Cholinergic systems in the rat brain: III. Projections from the pontomesencephalic tegmentum to the thalamus, tectum, basal ganglia, and basal forebrain. Brain Res Bull. 16:603-637.

Zhang X, Liu C, Miao H, Gong ZH, Nordberg A. 1998. Postnatal changes of nicotinic acetylcholine receptor alpha 2, alpha 3, alpha 4, alpha 7 and beta 2 subunits genes expression in rat brain. Int J Dev Neurosci. 16:507-518.

Zhou FM, Liang Y, Dani JA. 2001. Endogenous nicotinic cholinergic activity regulates dopamine release in the striatum. Nat Neurosci. 4:1224-1229.

Zhu J, Taniguchi T, Konishi Y, Mayumi M, Muramatsu I. 1998. Nicotine administration decreases the number of binding sites and mRNA of M1 and M2 muscarinic receptors in specific brain regions of rat neonates. Life Sci. 62:1089-1098.

Zhu XO, Waite PM. 1998. Cholinergic depletion reduces plasticity of barrel field cortex. Cereb Cortex. 8:63-72.

## FIGURE LEGENDS

**Figure 1.** Low power photomicrographs illustrating the growth of the cholinergic (ChAT-immunostained) innervation in rat neostriatum, from birth (P0) to postnatal day 32 (P32). All sections were taken in a transverse plane across the genu of corpus callosum. Note the striking increase in brain size from P0 to P16. See text (Results) and Fig. 2 for details on the distribution of the immunoreactive cell bodies and axons at the different ages. Scale bar: 1 mm.

**Figure 2.** Photomicrographs from the same sections as in Fig. 1 and a section from adult (>P60) rat brain. The field of view is at mid-height across the lateral neostriatum. All pictures are shown at the same magnification. At PO, the small ChAT-immunoreactive nerve cell bodies, endowed with short dendrites, appear much more numerous than at later stages, because they are confined to the outer half of the neostriatum. Scattered thin varicose axons and punctate varicosities are visible among them. At P4, the cell bodies are less numerous within the same area, having migrated to the entire neostriatum. An increase in their average size is also noticeable. At P8, the major change is the increased density of the network of fine varicose axons pervading the neuropil. At P16, the immunoreactive cell bodies have reached adult size and it is obvious that their dendrites are much thicker and longer. The ChAT immunoreactive axon network has become denser. At P32, the density of ACh innervation is almost as great as in the adult. Scale bar (in adult): 100 □m.

**Figure 3.** High power photomicrographs from the same sections as in the previous figures, demonstrating the presence of fine, varicose ChAT immunoreactive axons in the neuropil of the lateral neostriatum at P8, P16 and P32. Note the progressive increase in the density of this axonal network from P8 to P32. The size of the immunoreactive varicosities and their intensity of immunostaining is comparable at the three ages. Scale bar (in P32): 10 μm.

**Figure 4AB.** Electron micrographs of ACh (ChAT-immunostained) axon varicosities from the lateral neostriatum (P32). In A, at least five varicosities (arrows) are visible along the same thin unmyelinated axon. The varicosities are identified as such by their content in aggregated synaptic vesicles, associated or not with a mitochondrion. None of these varicosity profiles displays a synaptic junction. In B, two immunoreactive varicosities are visible, one of which forms an unusual, incurvated and asymmetrical synaptic junction (between small arrows) onto a cell body (N in nucleus), presumably belonging to a medium-sized spiny neuron Scale bars : 0.5 μm.

**Figure 5A-I.** Examples of neostriatal ACh axon varicosities at postnatal ages P8 (A-C), P16 (D-F) and P32 (G-I). The average size of these profiles does not significantly differ from P8 to P32. Of the three at P8 (A-C), from the medial (A and C) and the lateral neostriatum (B), only the one in B displays a small zone of apposition to a dendritic branch (d), suggestive of a symmetrical synaptic junction (between small arrows). The immunoreactive varicosity in A is juxtaposed to two dendritic branches (d) and two other axon varicosities (v), unlabeled. The one in B is seen in continuity with the

thin unmyelinated axon from which it emerges (between asterisks). In C, the immunoreactive varicosity is juxtaposed to a nerve cell body (N in nucleus). Of the varicosities at P16 (D-F), all from the medial neostriatum, only the one in F displays a synaptic junction (between small arrows), which is clearly symmetrical and made with a dendritic branch (d). In D, the two relatively large ACh varicosity profiles seemingly belong to the same axon, even if a portion of the thinner intervaricose segment is hidden by a dendrite (d). In E, the varicosity is surrounded by neurites, two of which can be positively identified as axons (a). The varicosities at P32 are from the lateral neostriatum. Both varicosities in G presumably belong to the same axon and are juxtaposed to the same dendritic branch (d). In H, the microenvironment of the ACh varicosity comprises a dendritic branch (d) bearing a spine (s), two unlabeled axon varicosities (v), one of which contacts the spine (asterisk), and small unidentifiable neurites. The immunoreactive varicosity in I makes an asymmetrical synaptic contact (between small arrows) with a dendritic spine (s1) and is juxtaposed to another spine (s2) and an unlabeled varicosity (v). Scale bar (in I): 0.5 μm.

## TABLE 1. MORPHOMETRIC FEATURES OF ACh (ChAT-IMMUNOSTAINED)VERSUS RANDOMLY SELECTED UNLABELED AXON VARICOSITIES

| Postnatal age | P8 | | P16 | | P32 | |
|---|---|---|---|---|---|---|
| | ACh | Unlabeled | ACh | Unlabeled | ACh | Unlabeled |
| **Dimensions** | | | | | | |
| **Short axis (μm)** | 0.34 ± 0.03 | 0.37 ± 0.03 | 0.31 ± 0.02 | 0.33 ± 0.04 | 0.29 ± 0.03 | 0.36 ± 0.05 |
| **Long axis (μm)** | 0.66 ± 0.04 | 0.71 ± 0.06 | 0.67 ± 0.03 | 0.67 ± 0.07 | 0.63 ± 0.07 | 0.71 ± 0.06 |
| **Aspect ratio (μm)** | 2.04 ± 0.27 | 2.04 ± 0.12 | 2.25 ± 0.20 | 2.24 ± 0.16 | 2.31 ± 0.25 | 2.06 ± 0.26 |
| **Diameter (μm)** | 0.50 ± 0.02 | 0.54 ± 0.04 | 0.49 ± 0.02 | 0.50 ± 0.05 | 0.46 ± 0.05 | 0.54 ± 0.05 |
| **Area ($\mu m^2$)** | 0.19 ± 0.02 | 0.23 ± 0.04 | 0.18 ± 0.01 | 0.19 ± 0.04 | 0.15 ± 0.03 | 0.23 ± 0.05 |
| **% with mitochondria** | 13.7 ± 3.7** | 10.3 ± 4.7 | 27.0 ± 4.1** | 10.0 ± 4.7 | 28.7 ± 9.4** | 22.7 ± 6.7 |

Data from 300 single sectional profiles of ChAT-immunostained (ACh) or unlabeled varicosities at each postnatal age. The unlabeled profiles were selected at random from the same micrographs displaying the ACh varicosities, as explained in Materials and Methods. The proportion of ACh and unlabeled profiles displaying mitochondria is given as a percentage. Mean ± s.d. from 3 rats in each group. **$P < 0.01$ for age related differences, as analysed by Kruskal-Wallis test.

## TABLE 2. JUNCTIONAL FEATURES OF ACh (ChAT-IMMUNOSTAINED) VERSUS RANDOMLY SELECTED UNLABELED AXON VARICOSITIES

| Postnatal age | P8 | | P16 | | P32 | |
|---|---|---|---|---|---|---|
| | ACh | Unlabeled | ACh | Unlabeled | ACh | Unlabeled |
| **Synaptic incidence (%)** | | | | | | |
| **Single sections** | 16 ± 5 | 35 ± 9 | 8 ± 4 | 35 ± 8 | 10 ± 8 | 38 ± 7 |
| **Whole volume** | 30 ± 12 | 76 ± 24 | 16 ± 9 | 75 ± 21 | 22 ± 17 | 81 ± 14 |
| **Synaptic targets (%)** | | | | | | |
| **Dendritic branches** | 74 ± 20 | 69 ± 16** | 66 ± 29 | 28 ± 8** | 41 ± 35 | 11 ± 10** |
| **Dendritic spines** | 19 ± 21 | 31 ± 16** | 23 ± 21 | 72 ± 8** | 58 ± 34 | 89 ± 10** |
| **Cell bodies** | 7 ± 13 | | 11 ± 14 | | 1 ± 3 | |
| **Junctions (%)** | | | | | | |
| **Symmetrical** | 67 ± 4 | 18 ± 7 | 67 ± 5 | 24 ± 13 | 58 ± 8 | 6 ± 1 |
| **Asymmetrical** | 33 ± 4 | 82 ± 11 | 33 ± 13 | 76 ± 11 | 42 ± 3 | 94 ± 3 |

Data (mean ± s.d.) from the same sectional profiles as in Table 1. The varicosity profiles were classified as showing or not a synaptic junction according to the criteria described in Materials and Methods. The synaptic incidence for the whole volume of varicosities was extrapolated by mean of the stereological formula of Beaudet and Sotelo (1981), using the long axis as diameter of the profiles (Umbriaco et al., 1994). Synaptic incidence and the relative frequency of the various synaptic targets of ACh and unlabeled varicosities are given as a percentage. **$P < 0.01$ for age related differences, as analysed by Kruskal-Wallis test.

## TABLE 3. NUMBER OF AXON VARICOSITIES AND DENDRITIC SPINES AROUND ACh (ChAT-IMMUNOSTAINED) VERSUS RANDOMLY SELECTED UNLABELED AXON VARICOSITIES

| Postnatal age | P8 | | P16 | | P32 | |
|---|---|---|---|---|---|---|
| | ACh | Unlabeled | ACh | Unlabeled | ACh | Unlabeled |
| **Axon varicosities** | 49.3 ± 11.1** | 52.0 ± 21.0 | 70.0 ± 9.9** | 66.3 ± 17.8 | 93.0 ± 19.3** | 82.0 ± 11.1 |
| **Dendritic spines** | 25.7 ± 12.1** | 24.7 ± 11.5*** | 39.0 ± 13.8** | 53.0 ± 8.4*** | 57.3 ± 11.5** | 57.3 ± 15.2*** |

Data from the same sectional profiles as in Table 1, normalized to 100 varicosities in each group (means ± s.d. from 3 rats per postnatal age). **P < 0.01 and ***P < 0.001 for age related differences, as analysed by Kruskal-Wallis test.

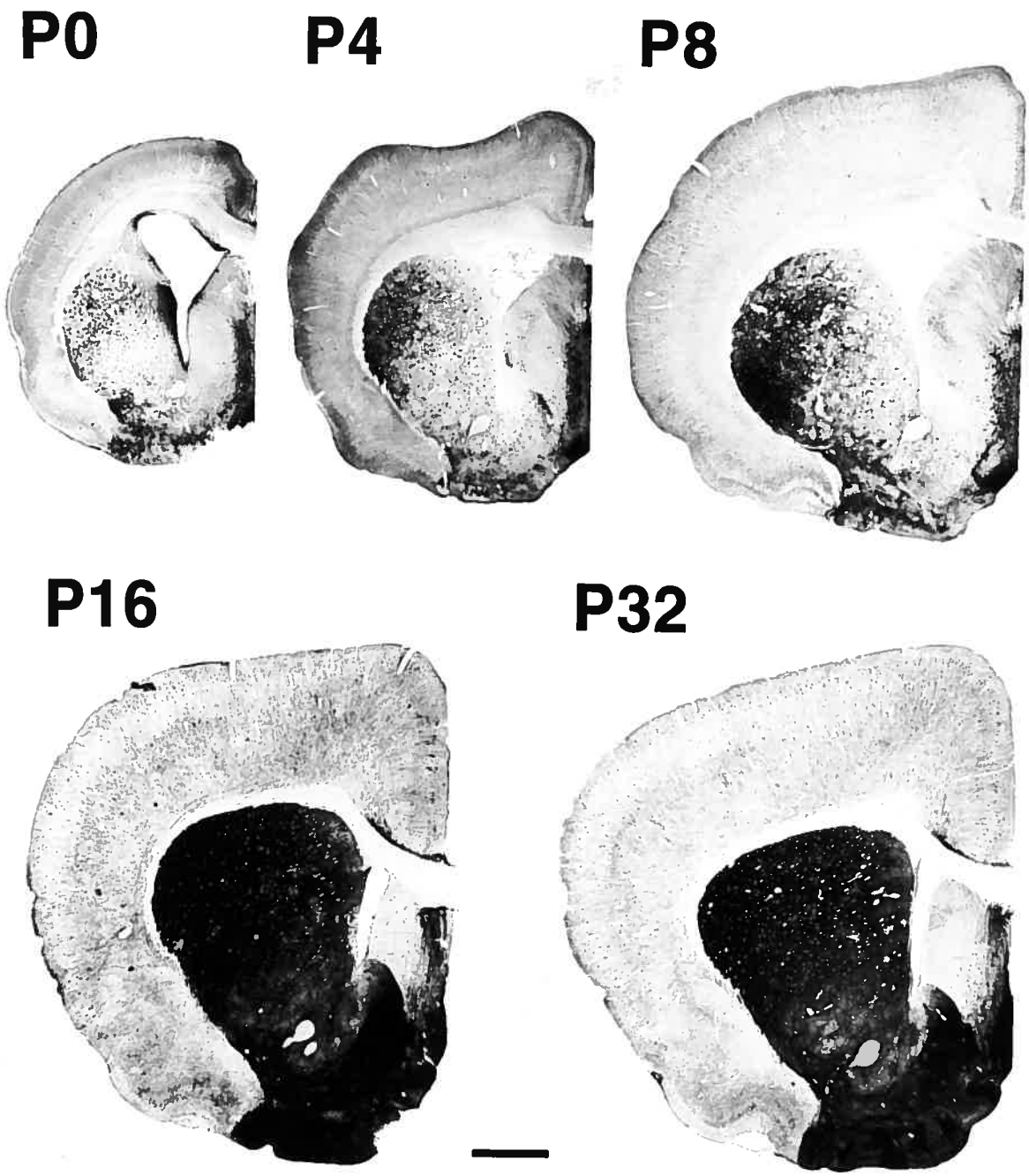
P0
P4
P8
P16
P32

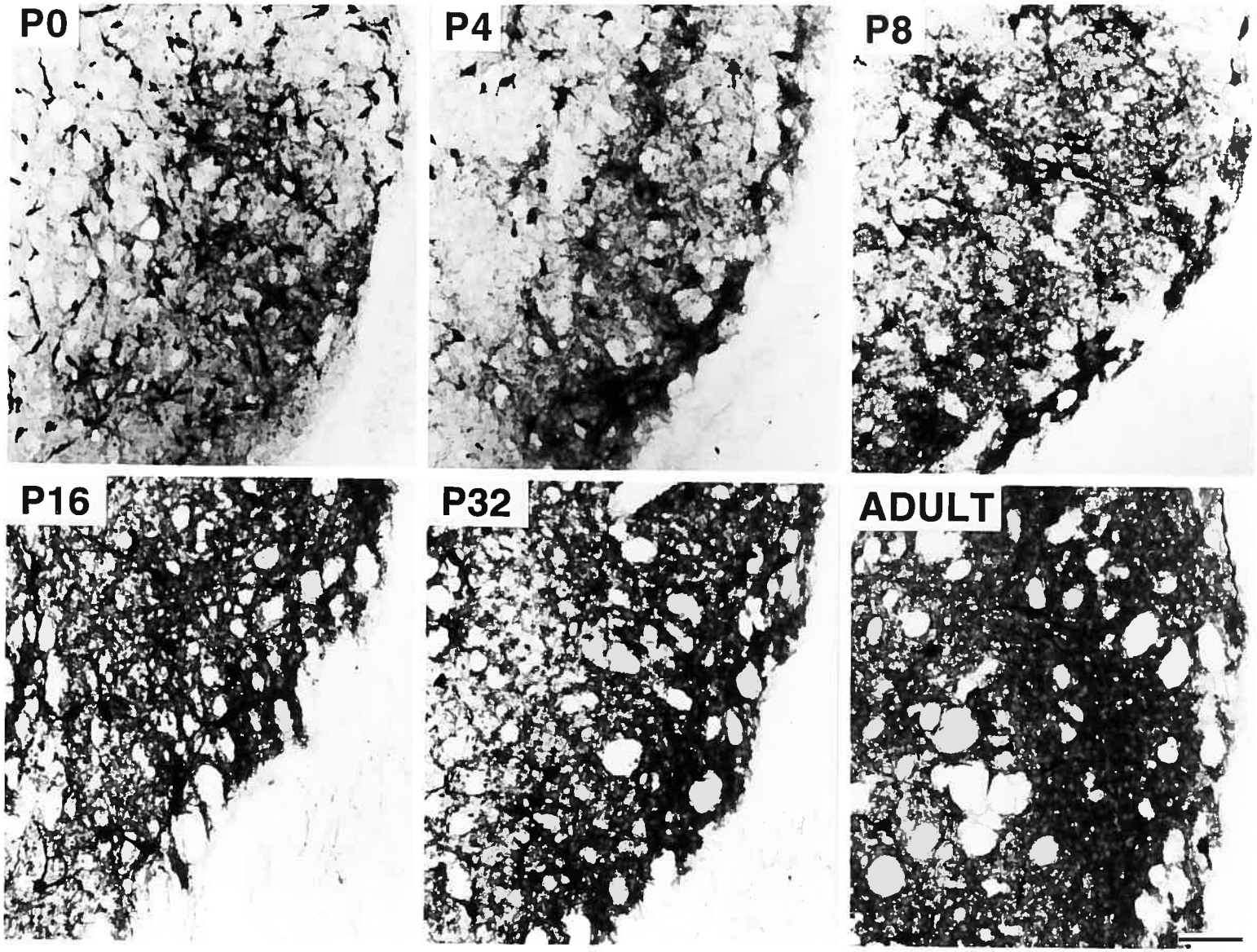
P0
P4
P8
P16
P32
ADULT

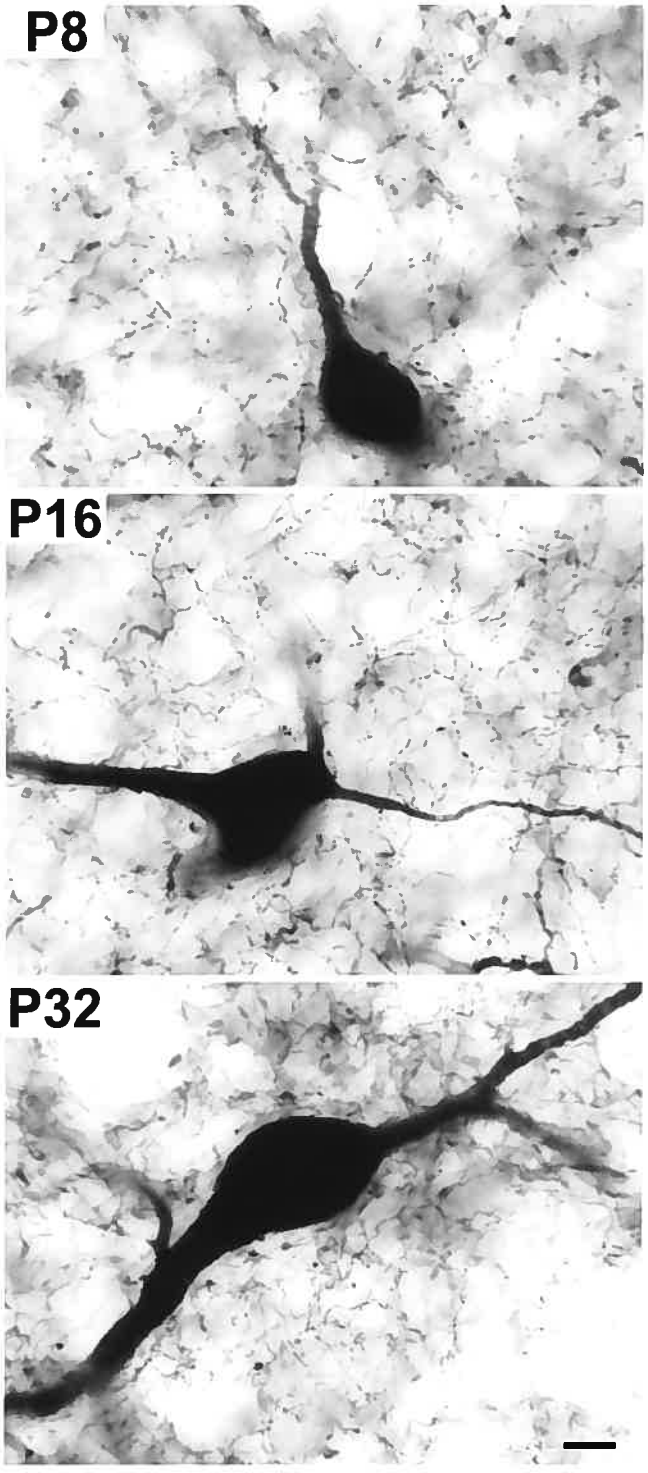
P8
P16
P32

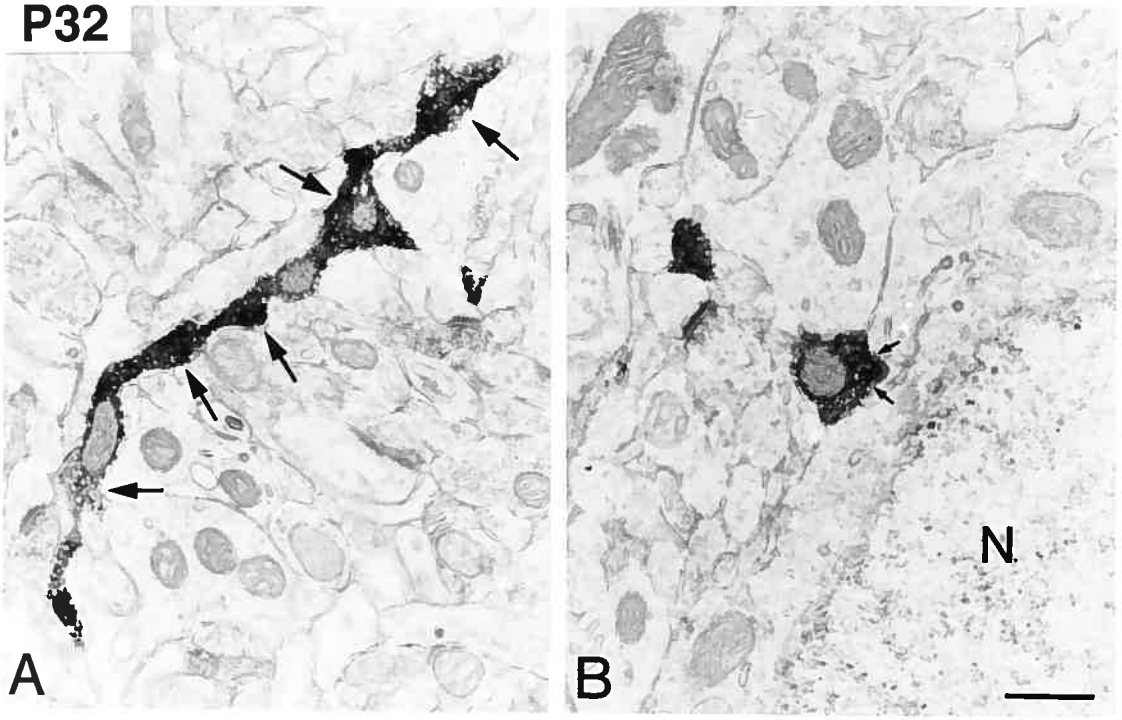
P32
A
B
N

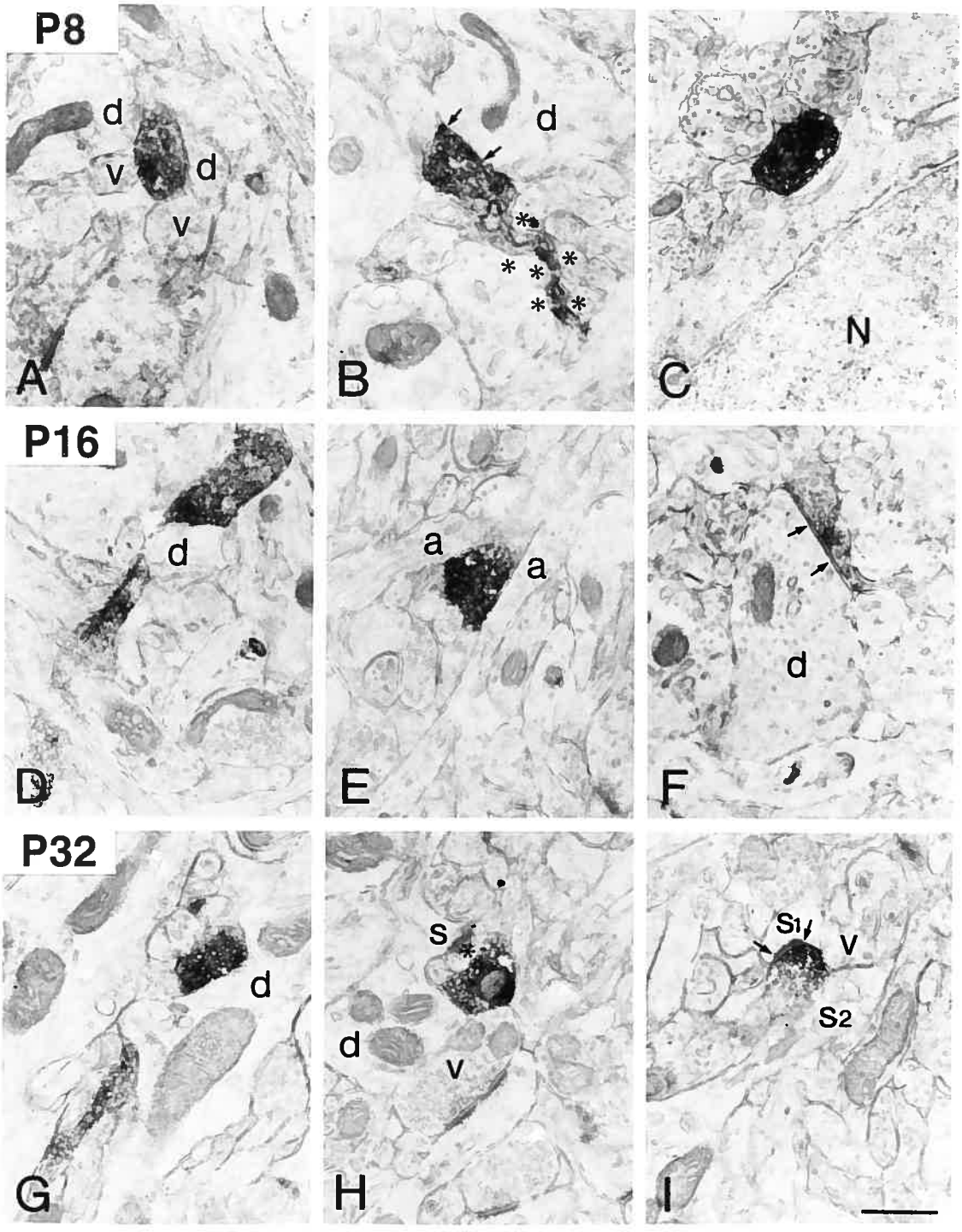
P8
d
v
d
v
A
d
B
N
C
P16
d
D
a
a
E
d
F
P32
d
G
s
d
v
H
S1
v
S2
I

# Chapitre V

# DISCUSSION GÉNÉRALE

## V.1 CONSIDÉRATIONS MÉTHODOLOGIQUES

### V.1.1 L'anticorps

La disponibilité d'un anticorps à très haut affinité dirigé contre la molécule entière de choline acétyltransférase (ChAT) isolée à partir du cerveau du rat a été déterminante pour la réalisation de toutes les études constituant cet ouvrage. La caractérisation et la spécificité immunologiques de cet anticorps ont déjà fait l'objet d'un résumé publié (Cozzari et al., 1990) et de deux manuscrits encore en préparation (Cozzari and Hartman). Sa spécificité immunocytochimique s'est avérée parfaite dans un grand nombre d'études neuroanatomiques (Cossette et al., 1993; Chédotal et al., 1994a,b; Umbriaco et al., 1994, 1995; Contant et al., 1996; Jaarsma et al., 1996; Bayraktar et al., 1997; Molnar et al., 1998; Deller et al., 1999; Oakman et al., 1999; Mechawar et al., 2000; Mechawar and Descarries, 2001; Mechawar et al., 2002 ), qui ont illustré son extrême sensibilité pour la ChAT, permettant une visualisation intégrale du réseau axonal ACh.

### V.1.2 Marquage de l'innervation cholinergique en microscopie optique

Lors de leur étude antérieure, Mechawar et al. (2000) ont utilisé des concentrations croissantes d'anticorps et une vaste gamme de temps de révélation pour démontrer que les conditions utilisées pour nos propres

expériences, incluant les modalités de fixation du tissu, autorisaient une visualisation complète du réseau axonal ACh (ChAT-immunoréactif), à travers toute l'épaisseur de coupes du cerveau de rat examinées en microscopie photonique

Jusqu'à maintenant, l'anticorps a ainsi permis la démonstration et la quantification de l'innervation cholinergique dans le cortex cérébral (frontal, pariétal et occipital) du rat adulte (Mechawar et al., 2000), le cortex pariétal de la souris adulte (Annexe 2 et 4), trois secteurs de l'hippocampe (CA1,CA3 et GD) chez le rat et chez la souris adultes (Chapitre II), et dans le cortex cérébral (Mechawar et al., 2001), l'hippocampe (Chapitre III) et le néostriatum du rat postnatal (Chapitre IV). Dans ces trois régions, c'était la première fois que des fibres ACh (ChAT-immunoréactives) pouvaient être visualisées au cours de la première semaine post-natale.

### V.1.3 La méthode de quantification

L'ensemble des données quantitatives que nous avons recueillies a tiré profit de certaines avancées méthodologiques par rapport à la méthode semi-informatisée initialement mise au point au laboratoire. Tel qu'originellement élaborée (Mechawar et al. , 2001), cette méthode s'appliquait à des coupes histologiques de 50 µm d'épaisseur, qu'il fallait examiner dans trois plans focaux pour visualiser le réseau axonal dans

toute l'épaisseur des coupes au grossissement nécessaire à la réalisation de tracés manuels. En poursuivant cette étude au cours du développement, Mechawar et Descarries (2001) ont constaté que les mesures obtenues de l'un ou l'autre des trois plans focaux étaient une fraction identique, donc représentative, des valeurs obtenues pour toute l'épaisseur. C'est ainsi que nous avons pu nous contenter de mesurer la longueur d'axone ACh dans un seul plan focal de coupes de 50 µm d'épaisseur, lors d'une étude de la région CA3 de l'hippocampe chez un rat modèle d'épilepsie (Annexe 1). Dans cette étude, en effet, il suffisait de comparer les valeurs par unité de surface de coupe obtenues chez les rats traités à celles de témoins. Au cours de cette même étude, nous avons cependant constaté que, du fait de la très forte densité d'innervation ACh dans certaines couches de l'hippocampe et de la superposition de nombreuses fibres dans les coupes de 50 µm d'épaisseur, les mesures de longueur axonale obtenues d'un seul des trois plans focaux n'étaient pas toujours représentatives de l'innervation totale. Nous avons donc opté par la suite pour l'utilisation de coupes histologiques de 20 µm d'épaisseur, où l'ensemble du réseau axonal ACh pouvait être visualisé dans un seul plan focal, éliminant tout risque d'une sous-estimation des mesures lié à la superposition de nombreuses fibres sur les tracés. Cette modification de la méthode a grandement facilité la collecte de données. Il est aujourd'hui évident que la méthode ainsi

améliorée peut s'appliquer à différentes régions du cerveau, quelle que soit l'espèce animale étudiée, ainsi qu'à divers systèmes immunocytochimiquement définis. Elle pourra servir dans l'avenir à la quantification rigoureuse de nombreux systèmes neuronaux chimiquement définis, dans différentes conditions expérimentales.

Connaissant la longueur du réseau axonal ACh dans un volume tissulaire donné, nous avons voulu obtenir des données sur la densité d'innervation en nombre de varicosités axonales, puisque celles-ci représentent le site présumé de libération du transmetteur. Pour ce faire, il nous a fallu mesurer le nombre de varicosités par longueur d'axone immunoréactif, de manière à pouvoir convertir les longueurs de réseau axonal en nombre de varicosités. Ces mesures effectuées directement au microscope ont montré un ratio moyen de 4 varicosités par 10 µm, identique dans toutes les couches du néocortex (frontal, pariétal et occipital) chez le rat adulte (Mechawar et al., 2001), toutes les couches de trois secteurs (CA1, CA3 et DG) de l'hippocampe chez le rat et la souris adultes (Chapitre I), et les différentes couches du cortex pariétal chez la souris adulte (Annexe 2 et 4).

À partir de ces données, nous avons pu déterminer la densité des varicosités axonales ACh et l'exprimer en millions par millimètre cube de tissu dans les différentes couches et régions précédemment mentionnées. Par contre, lors de l'étude de l'hippocampe en développement

(Chapitre III), nous avons constaté que le ratio du nombre de varicosités par unité de longueur d'axone augmentait avec l'âge postnatal, tel que précédemment observé dans le néocortex en développement (Mechawar et al., 2001). Ce paramètre a donc été mesuré à chacun des âges postnataux (P8, P16 et P32) et pris en compte pour déterminer le nombre de varicosités par unité de volume dans l'hippocampe en développement. Grâce à l'obtention de ces valeurs absolues, la corrélation avec d'autres paramètres neurocytologiques ou neurochimiques chiffrés devenait possible et signifiante.

### V.1.4 Visualisation des varicosités cholinergiques en microscopie électronique

Après avoir quantifié l'innervation ACh dans l'hippocampe du rat chez l'adulte et au cours du développement, nous nous sommes intéressé à ses propriétés ultrastructurales au cours du développement, lesquelles n'avaient jamais été décrites. Un des objectifs de cette étude était de déterminer si l'innervation ACh était de nature largement asynaptique au cours de sa croissance tout comme chez l'adulte (Umbriaco et al., 1995). Encore ici, c'est grâce à l'anticorps de Cozzari et Hartman que nous avons pu mener cette investigation à bien, parce que sa détection immunocytochimique tolérait l'ajout de glutaraldéhyde à la solution de

fixation, en concentration suffisante pour assurer une préservation convenable des ultrastructures.

Nous avons du tenir compte de deux paramètres dans le choix des âges des rats examinés en microscopie électronique. Étant donné qu'antérieurement à P8, les densités d'innervation ACh dans l'hippocampe et le neostriatum sont relativement faibles, et considérant le fait que la préparation des tissus pour la microscopie électronique induit une perte de marquage, il devenait impossible d'échantillonner un nombre suffisant de varicosités ACh avant P8. Un second paramètre limitant le choix des âges examinés, est la très grande fragilité des tissus durant la première semaine postnatale qui ne permet pas d'obtenir une préservation suffisante des ultrastructures pour la microscopie électronique.

Les caractéristiques ultrastructurales des varicosités ACh de l'hippocampe en développement ont été examinées dans le stratum pyramidale et le stratum radiatum de CA1, à trois âges postnataux: P8, P16 et P32. L'extrapolation de l'incidence synaptique observée en coupes fines isolées au volume entier des varicosités a pu être réalisée grâce à la formule stéréologique de Beaudet et Sotelo (1981), qui prend en compte le diamètre des profils, la longueur de leurs complexe de jonction et l'épaisseur des coupes fines. Cette formule a été utilisée telle que modifiée par Umbriaco et al. (1994), qui ont démontré sa validité sur

un échantillon étudié en coupes fines sériées, pour autant que la plus grande largeur soit utilisée comme diamètre des varicosités. Au cours de notre travail, nous nous sommes également intéressés aux caractéristiques intrinsèques des varicosités ACh : soit leurs diverses dimensions, leur contenu et la fréquence avec laquelle elles sont dotées d'une ou plusieurs mitochondries.

Ayant ainsi décrit l'innervation ACh de l'hippocampe en développement, dont on sait qu'elle est issue de neurones de projection des groupes neuronaux Ch1-2, il devenait intéressant de déterminer si l'innervation ACh du néostriatum en développement, essentiellement issue d'interneurones locaux, présentait les mêmes caractéristiques. Puisque l'ultrastructure de cette innervation à l'état adulte avait été précédemment examinées au laboratoire (Contant el al., 1996), nous disposions d'un point de référence pour savoir si ses caractéristiques relationnelles et intrinsèques présentaient des changements importants au cours du développement.

## V.2 DISTRIBUTION RÉGIONALE ET LAMINAIRE DE L'INERVATION CHOLINERGIQUE DE L'HIPPOCAMPE CHEZ LE RAT ET LA SOURIS ADULTES

### V.2.1 Rappel des principaux résultats

Dans le but d'obtenir des données quantitatives sur la distribution de l'innervation ACh dans l'hippocampe dorsal du rat (Sprague Dawley) et de la souris (C57/B6) adultes, nous avons employé une méthode semi-informatisée permettant de mesurer la densité des axones et des varicosités cholinergiques, préalablement marqués à l'aide d'un anticorps à haute affinité dirigé contre l'enzyme de synthèse de l'acétylcholine (ACh), la choline acétyltransférase (ChAT). La densité du réseau axonal ACh, telle qu'exprimé en mètres d'axones par $mm^3$, a été mesurée dans les différents couches des trois régions formant l'hippocampe (CA1, CA3 et le gyrus dentelé). Le nombre de varicosités ACh par unité de longueur d'axone s'est avéré constant (4 varicosités par 10 µm) dans toutes les couches des trois régions et chez la souris et le rat. La densité d'innervation ACh de l'hippocampe de la souris a pu ainsi être estimée à 13.9, 16.1 et 15.8 mètres d'axones, correspondant à 5.6, 6.4 et 6.3 millions de varicosités par $mm^3$ de tissu, dans CA1, CA3 et le gyrus dentelé, respectivement. Des valeurs comparables ont été mesurées chez le rat, à l'exception de la région CA1, où les densités d'innervation du stratum lacunosum moleculare et du stratum radiatum se sont avérées plus faibles, de 40% et 20%, respectivement. Les patrons laminaires

d'innervation sont apparus semblables dans les deux espèces. Les plus fortes densités laminaires étaient celles du stratum moleculare de CA3 (18.8 à 20.2 mètres d'axones ACh par $mm^3$ et 7.5 à 8.1 millions de varicosités ACh par $mm^3$), du stratum pyramidale de CA1 (17.0 à 17.9 mètres d'axones ACh par $mm^3$ et 6.8 à 7.2 millions de varicosités ACh par $mm^3$) et de CA3 (19.6 à 20.4 mètres d'axones ACh par $mm^3$ et 7.8 à 8.2 millions de varicosités ACh par $mm^3$), et du stratum moleculare du GD (19.5 à 19.9 mètres d'axones ACh par $mm^3$ et 7.8 à 8.0 millions de varicosités ACh par $mm^3$).

### V.2.2 Implications fonctionnelles

Les densités moyennes de 6.1 millions de varicosités par $mm^3$ chez la souris, et de 5.9 millions chez le rat, indiquent que l'innervation ACh de l'hippocampe adulte constitue l'entrée neuromodulatrice la plus dense ayant décrite à ce jour dans cette région, dépassant largement les innervations à noradrénaline (Oleskevich et al., 1989) ou à sérotonine (Oleskevich and Descarries, 1990). Si ces densités mesurées dans l'hippocampe dorsal sont extrapolées à l'ensemble de cette région anatomique, la longueur totale d'axones ACh peut être estimée à 326 mètres de chaque côté du cerveau chez la souris et 823 mètres chez le rat, correspondant respectivement à des nombres de 130 et 329 millions de varicosités ACh. Compte tenu de la distribution ubiquitaire de cette

innervation, une aussi forte densité de varicosités suggère que tous les éléments neuronaux de l'hippocampe puissent être influencés par l'ACh et constituent un premier indice structurel de l'importance de ce système dans l'hippocampe.

Ces données quantitatives apportent également des renseignements sur les caractéristiques morphologiques des neurones ACh du prosencéphale basal. Le nombre de neurones ACh dans la région Ch1-2 a été évalué à 250 chez la souris (Schwegler et al., 1996) et à 385 chez le rat (McKinney et al., 1983). Ces comptages permettent d'estimer que chacun de ces neurones innerve l'hippocampe avec une arborisation axonale mesurant 1.3 mètres et dénombrant 520 000 varicosités chez la souris, comparativement à 2.1 mètres d'axones et 840 000 varicosités chez le rat. Chez le rat, ces valeurs représentent le double de celles extrapolées pour les neurones ACh du noyau *basalis* qui se projettent au néocortex (Mechawar et al., 2000). Par ailleurs il semble exister une relation de cohérence entre la distribution ubiquitaire et divergente de l'innervation ACh de l'hippocampe (et du néocortex) issue d'un nombre restreint de corps cellulaires neuronaux ACh du prosencéphale basal et la neuromodulation que l'ACh exercerait sur l'ensemble des neurones de cette région incluant ses cellules principales (Cole and Nicoll, 1984; Madison et al., 1987; Benson et al., 1988) et ses interneurones (Radcliffe and Dani, 1998; McQuiston and Madison,

1999a,b; Radcliffe et al., 1999; Alkondon et al., 1999; Ji and Dani, 2000). Cette relation, s'appliquant également à la sérotonine, à la noradrénaline et à l'histamine dans le cortex, marque une dichotomie avec les autres systèmes essentiellement synaptiques, où les neurones établissent des projections précises et des connexions peut-être plus stables avec des sous-ensembles neuronaux bien caractérisés. Elle justifie la distinction entre systèmes de neuromodulation et systèmes de neurotransmission (au sens strict) dans le cortex, pour ces systèmes divergents et largement distribués dont on sait maintenant qu'ils font principalement appel à un mode de communication diffus plutôt que ponctuel, du moins dans toutes les régions corticales jusqu'à maintenant étudiées et aussi plusieurs autres régions du cerveau (voir annexe 3 et 5).

## V.3 DISTRIBUTION ET ULTRASTRUCTURE DE L'INNERVATION CHOLINERGIQUE DE L'HIPPOCAMPE EN DÉVELOPPEMENT CHEZ LE RAT

### V.3.1 Rappel des principaux résultats

À la suite de notre étude portant sur l'innervation cholinergique (ACh) de l'hippocampe dorsal chez la souris et le rat adultes, nous avons décidé de nous pencher sur sa distribution et ses caractéristiques ultrastructurales au cours du développement. Nous avons utilisé le même anticorps à haute affinité dirigé contre la choline acétyltransférase (ChAT) afin de marquer l'innervation ACh de l'hippocampe dorsal du rat à trois âges postnataux : P8, P16 et P32.

Dans un premier temps, nous avons quantifié la distribution de cette innervation en mesurant les densités laminaires des axones ACh, exprimées en mètres par $mm^3$ de tissu. Nous avons pu ensuite déterminer les densités laminaires et régionales des varicosités ACh, exprimées en millions par $mm^3$ de tissu, après avoir mesuré le nombre de varicosités par longueur d'axone dans toutes les couches et régions examinées. À P8, l'innervation ACh formait déjà un réseau axonal élaboré, avec un nombre considérable de varicosités; à P16, son patron de distribution était semblable à celui de l'adulte; à P32, les densités d'innervation laminaires adultes étaient déjà atteintes. Les valeurs moyennes pour toutes les couches de l'hippocampe dorsal ont montré une augmentation rapide de 8.4 à 14 mètres d'axone ACh par $mm^3$, et de 2.3 à 5.7 millions de

varicosités axonales ACh par $mm^3$, entre P8 et P32. Cette augmentation de la densité des varicosités ACh traduit d'une part l'élongation et à l'arborisation des axones ACh, et d'autre part l'augmentation du nombre de varicosités par unité de longueur d'axone, qui passe de 2.7 à P8 à 4.1 varicosités par 10 µm à P32.

Dans un deuxième temps, nous avons employé la microscopie électronique dans le but d'examiner les propriétés ultrastructurales de ces varicosités au cours du développement. Aux trois âges postnataux, P8, P16 et P32, les caractéristiques ultrastructurales intrinsèques et relationnelles des varicosités ACh sont apparues semblables à celles antérieurement décrites chez l'adulte (Umbriaco et al., 1995). La fréquence avec laquelle ces profils présentaient une mitochondrie a montré une augmentation avec l'âge, de 28% à P8 jusqu'à 41% à P32. La proportion des varicosités ACh présentant une spécialisation membranaire synaptique était très faible comparativement à celle de varicosités non marquées choisies au hasard dans les mêmes photomicrographies, avec une incidence jonctionnelle extrapolée à 7% pour le volume entier des varicosités. Quel que soit l'âge, ces rares jonctions étaient pour la plupart petites, symétriques, et le plus souvent formées avec des branches et non des épines dendritiques.

### V.3.2 Implications fonctionnelles

Au cours des deux premières semaines postnatales, l'innervation ACh de l'hippocampe croît avec une célérité maximale. Durant cette période, chaque neurone ACh de Ch1-2 produit quotidiennement plus de 3 mm d'axone arborant 1 000 varicosités. Ces données soulignent la grande capacité de croissance de ces neurones.

Trois paramètres contribuent à cette croissance : l'élongation et l'arborisation des axones ACh, et l'augmentation du nombre de varicosités ACh par longueur d'axone. Les couches préférentiellement innervées à P8 ne correspondent pas à des voies empruntées par les fibres ACh qui pénètrent dans l'hippocampe, ce qui suggère une croissance axonale guidée par des facteurs trophiques locaux. À l'inverse, l'augmentation du nombre de varicosités ACh par longueur d'axone apparaît similaire dans les différentes couches et secteurs de l'hippocampe en développement, et comparable à celle précédemment observée dans le néocortex en développement (Mechawar et al., 2001). Il semble donc que l'évolution de ce ratio au cours de la période postnatale tant pour les neurones de Ch1-2 que du noyau *basalis* (Ch4) soit une propriété intrinsèque, qui pourrait refléter l'origine ontogénique commune des neurones ACh du prosencéphale basal.

Dès la première semaine postnatale, les varicosités ACh possèdent toutes les caractéristiques intrinsèques et relationnelles observées chez le rat adulte. La nature essentiellement asynaptique de cette innervation, à tous les âges examinés, prédit que les effets de l'ACh au cours du développement seront, comme chez l'adulte, tributaires d'une transmission diffuse. Ce type de neurotransmission semble naturellement s'accorder avec les effets de l'ACh qui ont été décrits dans l'hippocampe en développement, tant au niveau de la neuromodulation (Goldbach et al., 1998 ; Milburn and Prince, 1993 ; Leslie et al., 2002), de la maturation des connexions synaptiques (Maggi et al., 2003)que de la synchronisation de l'activité neuronale (Avignone and Cherubini, 1999; Maggi et al., 2001). La grande diversité des éléments neuronaux influencés par l'ACh et l'échelle relativement vaste à laquelle ces effets s'exercent, semble encore une fois en accord avec la distribution ubiquitaire et divergente de l'innervation ACh, telle que mise en évidence dans l'hippocampe en développement.

L'ensemble de ces données sur la distribution et l'ultrastructure de l'innervation cholinergique et l'hippocampe suggère que l'ACh pourrait jouer un rôle important au cours du développement de cette région du cerveau, tel que déjà démontré par diverses données expérimentales dans le néocortex en développement (Gu and Singer, 1993; Robertson et al., 1998; Zhu and Waite, 1998).

## V.4 ULTRASTRUCTURE DE L'INNERVATION CHOLINERGIQUE DU NÉOSTRIATUM EN DÉVELOPPEMENT CHEZ LE RAT

### V.4.1 Rappel des principaux résultats

Nous avons examiné l'innervation cholinergique du néostriatum du rat au cours du développement en microscopie optique et électronique avec le même anticorps à haute affinité dirigé contre la choline acétyltransférase (ChAT). Les corps cellulaires des interneurones cholinergiques et leurs projections émergentes étaient présents dès la naissance dans la partie latérale du néostriatum avant d'envahir progressivement toute la région néostriatale pour former un réseau extrêmement dense. L'utilisation de la microscopie électronique a permis de démontrer que, dès la première semaine postnatale, ces varicosités possèdent toutes les caractéristiques intrinsèques et relationnelles décrites chez l'adulte. Aux trois âges postnataux (P8, P16 et P32), les profiles immunoréactifs étaient comparable en terme de dimension, de forme et de contenu vésiculaire. La fréquence avec laquelle ces profils présentaient au moins une mitochondrie augmentait avec l'âge, passant de 10% à P8 jusqu'à 29% à P32. Comme chez l'adulte, la grande majorité des ces profils était dépourvue de spécialisation synaptique avec une incidence synaptique moyenne de 11% en coupes isolées, représentant une incidence de 22% pour les varicosités entières après extrapolation stéréologique. Ces jonctions étaient généralement petites,

majoritairement symétriques, et formées sur des épines ou des branches dendritiques. La fréquence des synapses ACh trouvées sur les épines dendritiques montrait une augmentation significative entre P8 (20%) et P32 (60%), au détriment de celles trouvées sur les branches dendritiques.

### V.4.2 Implications fonctionnelles

L'apparition dans le néostriatum d'une innervation ACh possédant toutes les caractéristiques ultrastructurales précédemment décrites chez l'adulte, dès la première semaine postnatale, permet de supposer que l'ACh joue un rôle important dans cette région au cours du développement. Ces données indiquent que la nature principalement asynaptique des varicosités axonales ACh est une caractéristique qui ne se limite pas seulement aux neurones ACh de projection du prosencéphale basal, mais s'étend également aux interneurones ACh du néostriatum. Encore une fois ce trait partagé, pourrait être relié à l'origine ontogénique commune de tous les neurones ACh du prosencéphale basal.

## V.5 PERSPECTIVES D'AVENIR

L'étude que nous avons menée sur l'hippocampe du rat et de la souris adultes a fourni une pléthore de données qualitatives et quantitatives nouvelles, sur la distribution régionale et laminaire de cette innervation cholinergique chez les deux espèces (Chapitre II). Les progrès méthodologiques accomplis et les résultats normatifs de cette étude ont également servi de base à une investigation du sort des innervations ACh et sérotoninergique de l'hippocampe et du néocortex chez une souris transgénique modèle de la maladie d'Alzheimer (Annexe 2 et 4). Nous poursuivons actuellement cet axe de recherche au laboratoire, en examinant les déficits ACh chez une souris transgénique exprimant une forme mutée de la protéine TGF-β1 et qui présente une dégénérescence périvasculaire analogue à celle observée dans la maladie d'Alzheimer. L'obtention de tels résultats dans divers modèles de maladies neurodégénératives devrait pouvoir servir de base à l'évaluation thérapeutique d'agents pharmacologiques, neuroprotecteurs ou autres (ex. activateurs cognitifs).

Grâce à l'application de cette méthodologie chez la souris, il devrait être aussi possible d'étudier les effets potentiels de l'invalidation de plusieurs gènes (souris knock-out) sur l'innervation ACh de diverses régions du cerveau. De même, la disponibilité de données chiffrées portant sur

des régions importantes du cerveau du rat ou de la souris devrait permettre de valider expérimentalement des méthodes de visualisation quantitative des densités d'innervation cholinergique régionales par imagerie cérébrale, notamment avec l'avènement de radioligands des transporteurs vésiculaires de l'ACh et de la tomographie par émission de positions pour petits animaux.

Les données que nous avons obtenues sur la distribution et l'ultrastructure de l'innervation ACh dans l'hippocampe en développement sont de précieux indices de l'importance fonctionnelle de cette innervation durant la période postnatale. En l'absence de données morphologiques antérieures, elles permettent d'envisager comment l'ACh peut exercer des effets aussi généraux que ceux qui ont été jusqu'à maintenant décrits durant cette période cruciale du développement cérébral. La distribution ubiquitaire et la nature principalement asynaptique de cette innervation en croissance, qui laissent supposer une neurotransmission-modulation diffuse par l'ACh, peuvent rendre compte de ces effets et d'actions potentiellement exercées sur de vastes ensembles neuronaux et une variété d'éléments cellulaires. De telles données devraient aussi pouvoir faire l'objet de corrélations intéressantes avec d'autres paramètres de fonction cholinergique comme la distribution cellulaire et subcellulaire des

récepteurs nicotiniques et muscariniques, afin de mieux comprendre les rôles de l'ACh dans le développement de cette région cérébrale.

## BIBLIOGRAPHIE GÉNÉRALE

Acquas E, Wilson C, Fibiger HC. 1996. Conditioned and unconditioned stimuli increase frontal cortical and hippocampal acetylcholine release: effects of novelty, habituation, and fear. J Neurosci 16:3089-3096.

Alkondon M, Albuquerque EX. 2004. The nicotinic acetylcholine receptor subtypes and their function in the hippocampus and cerebral cortex. Prog Brain Res 145:109-120.

Alkondon M, Pereira EF, Eisenberg HM, Albuquerque EX. 1999. Choline and selective agonists identify two subtypes of nicotinic acetylcholine receptors that modulate GABA release from CA1 interneurons in rat hippocampal slices. J Neurosci 19: 2693-2705.

Aloisi AM, Casamenti F, Scali C, Pepeu G, Carli G. 1997. Effects of novelty, pain and stress on hippocampal extracellular acetylcholine levels in male rats. Brain Res 748:219-26.

Amaral DG, Kurz J. 1985. An analysis of the origins of the cholinergic and noncholinergic septal projections to the hippocampal formation of the rat. J Comp Neurol 240:37-59.

Armstrong DM, Bruce G, Hersh LB, Gage FH. 1987. Development of cholinergic neurons in the septal/diagonal band complex of the rat. Brain Res 433:249-256.

Atri A, Sherman S, Norman KA, Kirchhoff BA, Nicolas MM, Greicius MD, Cramer SC, Breiter HC, Hasselmo ME, Stern CE. 2004. Blockade of central cholinergic receptors impairs new learning and increases proactive interference in a word paired-associate memory task. Behav Neurosci 118:223-236.

Aubert I, Cecyre D, Gauthier S, Quirion R. 1996. Comparative ontogenic profile of cholinergic markers, including nicotinic and muscarinic receptors, in the rat brain. J Comp Neurol 369:31-55.

Auerbach JM, Segal M. 1996. Muscarinic receptors mediating depression and long-term potentiation in rat hippocampus. J Physiol 492:479-493.

Avignone E, Cherubini E. 1999. Muscarinic receptor modulation of GABA-mediated giant depolarizing potentials in the neonatal rat hippocampus. J Physiol 518: 97-107.

Balduini W, Cimino M, Reno F, Marini P, Princivalle A, Cattabeni F. 1993. Effects of postnatal or adult chronic acetylcholinesterase inhibition on muscarinic receptors, phosphoinositide turnover and m1 mRNA expression. Eur J Pharmacol 248:281-288.

Banerjee C, Nyengaard JR, Wevers A, de Vos RA, Jansen Steur EN, Lindstrom J, Pilz K, Nowacki S, Bloch W, Schroder H. Related 2000. Cellular expression of alpha7 nicotinic acetylcholine receptor protein in the temporal cortex in Alzheimer's and Parkinson's disease--a stereological approach. Neurobiol Dis 7:666-672.

Barger G, Dale HH. 1910-1911. Chemical structure and sympathomimetic action of amines. J Physiol 41:19-59.

Bartus RT, Dean RL 3rd, Beer B, Lippa AS. 1982. The cholinergic hypothesis of geriatric memory dysfunction. Science 217:408-414.

Bartus RT. 2000. On neurodegenerative diseases, models, and treatment strategies: lessons learned and lessons forgotten a generation following the cholinergic hypothesis. Exp Neurol 163:495-529.

Bayraktar T, Staiger JF, Acsady L, Cozzari C, Freund TF, Zilles K. 1997. Co-localization of vasoactive intestinal polypeptide, gamma-aminobutyric acid and choline acetyltransferase in neocortical interneurons of the adult rat. Brain Res 757:209-217.

Beach TG, Kuo YM, Spiegel K, Emmerling MR, Sue LI, Kokjohn K, Roher AE. 2000. The cholinergic deficit coincides with Abeta deposition at the earliest histopathologic stages of Alzheimer disease. J Neuropathol Exp Neurol 59:308-313.

Beaudet A, Sotelo C. 1981. Synaptic remodeling of serotonin axon terminals in rat agranular cerebellum. Brain Res 206:305 329.

Behrends JC, ten Bruggencate G. 1993. Cholinergic modulation of synaptic inhibition in the guinea pig hippocampus in vitro: excitation of GABAergic interneurons and inhibition of GABA-release. J Neurophysiol 69:626-629.

Ben-Ari Y, Cherubini E, Corradetti R, Gaiarsa JL. 1989. Giant synaptic potentials in immature rat CA3 hippocampal neurones. J Physiol 416:303-325.

Bender R, Plaschke M, Naumann T, Wahle P, Frotscher M. 1996. Development of cholinergic and GABAergic neurons in the rat medial septum: different onset of choline acetyltransferase and glutamate decarboxylase mRNA expression. J Comp Neurol 372:204-214.

Bennett BD, Wilson CJ. 1999. Spontaneous activity of neostriatal cholinergic interneurons in vitro. J Neurosci 19:5586-5596.

Bennett BD, Callaway JC, Wilson CJ. 2001. Intrinsic membrane properties underlying spontaneous tonic firing in neostriatal cholinergic interneurons. J Neurosci 20:8493-8503.

Benson DM, Blitzer RD, Landau EM. 1988. An analysis of the depolarization produced in guinea-pig hippocampus by cholinergic receptor stimulation. J Physiol (Lond) 404: 479-496.

Bianchi L, Ballini C, Colivicchi MA, Della Corte L, Giovannini MG, Pepeu G. 2003. Investigation on acetylcholine, aspartate, glutamate and GABA extracellular levels from ventral hippocampus during repeated exploratory activity in the rat. Neurochem Res 28:565-573.

Blaker SN, Armstrong DM, Gage FH. 1988. Cholinergic neurons within the rat hippocampus: response to fimbria-fornix transection. J Comp Neurol 272:127-138.

Blitzer RD, Gil O, Landau EM. Related 1990. Cholinergic stimulation enhances long-term potentiation in the CA1 region of rat hippocampus. Neurosci Lett 119:207-210.

Bonner TI, Buckley NJ, Young AC, Brann MR. 1987. Identification of a family of muscarinic acetylcholine receptor genes. Science 237:527-532.

Bowen DM, Smith CB, White P, Davison AN. 1976. Neurotransmitter-related enzymes and indices of hypoxia in senile dementia and other abiotrophies. Brain 99:459-496.

Buckley NJ, Bonner TI, Brann MR. 1988. Localization of a family of muscarinic receptor mRNAs in rat brain. J Neurosci 8:4646-4652.

Buresova O, Bolhuis JJ, Bures J. 1986. Differential effects of cholinergic blockade on performance of rats in the water tank navigation task and in a radial water maze. Behav Neurosci 100:476-482.

Burgard EC, Sarvey JM. 1990. Muscarinic receptor activation facilitates the induction of long-term potentiation (LTP) in the rat dentate gyrus. Neurosci Lett 116:34-39.

Butcher LL, Talbot K, Bilezikjian L. 1975. Acetylcholinesterase neurons in dopamine-containing regions of the brain. J Neural Transm 37:127-153.

Bymaster FP, Heath I, Hendrix JC, Shannon HE. 1993. Comparative behavioral and neurochemical activities of cholinergic antagonists in rats. J Pharmacol Exp Ther 267:16-24.

Caldwell JA Jr, Stephens RL, Carter DJ, Jones HD. 1992. Effects of 2 mg and 4 mg atropine sulfate on the performance of U.S. Army helicopter pilots. Aviat Space Environ Med 63:857-864.

Canales JJ, Graybiel AM. 2000. A measure of striatal function predicts motor stereotypy. Nat Neurosci 3:377-383.

Centonze D, Gubellini P, Bernardi G, Calabresi P. 1999. Permissive role of interneurons in corticostriatal synaptic plasticity. Brain Res Brain Res Rev 31:1-5.

Chang HC, Gaddum JH. 1933. Choline esters in tissue extracts. J Physiol 79:255-285.

Chedotal A, Cozzari C, Faure MP, Hartman BK, Hamel E. 1994a. Distinct choline acetyltransferase (ChAT) and vasoactive intestinal polypeptide (VIP) bipolar neurons project to local blood vessels in the rat cerebral cortex. Brain Res 646:181-193.

Chédotal A, Umbriaco D, Descarries L, Hartman BK, Hamel E. 1994b. Light and electron microscopic immunocytochemical analysis of the neurovascular relationships of choline acetyltransferase and vasoactive intestinal polypeptide nerve terminals in the rat cerebral cortex. J Comp Neurol 343:57-71.

Cherubini E, Gaiarsa JL, Ben-Ari Y. 1991. GABA: an excitatory transmitter in early postnatal life. Trends Neurosci 14:515-519.

Cole AE, Nicoll RA1984. Characterization of a slow cholinergic post-synaptic potential recorded in vitro from rat hippocampal pyramidal cells. J Physiol 352:173-188.

Contant C, Umbriaco D, Garcia S, Watkins KC, Descarries L. 1996. Ultrastructural characterization of the acetylcholine innervation in adult rat neostriatum. Neuroscience 71:937-947.

Cossette P, Umbriaco D, Zamar N, Hamel E, Descarries L. 1993. Recovery of choline acetyltransferase activity without sprouting of the residual acetylcholine innervation in adult rat cerebral cortex after lesion of the nucleus basalis. Brain Res 630:195-206.

Court JA, Lloyd S, Johnson M, Griffiths M, Birdsall NJ, Piggott MA, Oakley AE, Ince PG, Perry EK, Perry RH. 1997. Nicotinic and muscarinic cholinergic receptor binding in the human hippocampal formation during development and aging. Brain Res Dev Brain Res 101:93-105.

Cowburn RF, Wiehager B, Ravid R, Winblad B. 1996. Acetylcholine muscarinic M2 receptor stimulated (35S)GTP gamma S binding shows regional selective changes in Alzheimer's disease postmortem brain. Neurodegeneration 5:19-26.

Coyle JT, Campochiaro P. 1976. Ontogenesis of dopaminergic-cholinergic interactions in the rat striatum: a neurochemical study. J Neurochem 27:673-678.

Cozzari C, Howard J, Hartman B. 1990. Analysis of epitopes on choline acetyltransferase (ChAT) using monoclonal antibodies (Mabs). Soc Neurosci Abstr 16: 200.

Dale HH. 1914a. The action of certain esters and ethers of choline, and their relation to muscarine. J Pharamacol Exp Ther 6:147-190.

Dale HH, 1914b. The occurrence in ergot and action of acetyl-choline. J of Physiol 48:iii-iv.

Dale HH, 1936. Sir Henry Dale – Nobel Lecture. From Nobel Lectures, Physiology or Medicine 1922-1941, Elsevier Publishing Company, Amsterdam.

Davies P, Maloney AJ. 1976. Selective loss of central cholinergic neurons in Alzheimer's disease. Lancet 2:1403.

Deller T, Katona I, Cozzari C, Frotscher M, Freund TF. 1999. Cholinergic innervation of mossy cells in the rat fascia dentata. Hippocampus 9:314-320.

Descarries L, Gisiger V, Steriade M. 1997. Diffuse transmission by acetylcholine in the CNS. Prog Neurobiol 53:603-625.

Descarries L. 1998. The hypothesis of an ambient level of acetylcholine in the central nervous system. J Physiol Paris 92:215-220.

Descarries L, Mechawar N. 2000. Ultrastructural evidence for diffuse transmission by monoamine and acetylcholine neurons of the central nervous system. Prog Brain Res 125:27-47.

De Vries TJ, Mulder AH, Schoffelmeer AN. 1992. Differential ontogeny of functional dopamine and muscarinic receptors mediating presynaptic inhibition of neurotransmitter release and postsynaptic regulation of adenylate cyclase activity in rat striatum. Brain Res Dev Brain Res 66:91-96.

Dominguez del Toro E, Juiz JM, Peng X, Lindstrom J, Criado M. 1994. Immunocytochemical localization of the alpha 7 subunit of the nicotinic acetylcholine receptor in the rat central nervous system. J Comp Neurol 349:325-342.

Ewins AJ. 1914. Biochem J 8:44.

Fellous JM, Sejnowski TJ. 2000. Cholinergic induction of oscillations in the hippocampal slice in the slow (0.5-2 Hz), theta (5-12 Hz), and gamma (35-70 Hz) bands. Hippocampus 10:187-197.

Ferrari-DiLeo G, Mash DC, Flynn DD. 1995. Attenuation of muscarinic receptor-G-protein interaction in Alzheimer disease. Mol Chem Neuropathol 1995. 24:69-91.

Fisahn A, Pike FG, Buhl EH, Paulsen O. 1998. Cholinergic induction of network oscillations at 40 Hz in the hippocampus in vitro. Nature 394:186-189.

Flynn DD, Ferrari-DiLeo G, Mash DC, Levey AI. 1995. Differential regulation of molecular subtypes of muscarinic receptors in Alzheimer's disease. J Neurochem 64:1888-1891.

Frotscher M, Schlander M, Leranth C. 1986. Cholinergic neurons in the hippocampus. A combined light- and electron-microscopic immunocytochemical study in the rat. Cell Tissue Res 246:293-301.

Fujii S, Sumikawa K. 2001. Nicotine accelerates reversal of long-term potentiation and enhances long-term depression in the rat hippocampal CA1 region. Brain Res 894:340-346.

Fujii S, Ji Z, Morita N, Sumikawa K. 1999. Acute and chronic nicotine exposure differentially facilitate the induction of LTP. Brain Res 846:137-143.

Giovannini MG, Rakovska A, Benton RS, Pazzagli M, Bianchi L, Pepeu G. 2001. Effects of novelty and habituation on acetylcholine, GABA, and glutamate release from the frontal cortex and hippocampus of freely moving rats. Neuroscience 106:43-53.

Givens BS, Olton DS. 1990. Cholinergic and GABAergic modulation of medial septal area: effect on working memory. Behav Neurosci 104:849-855.

Goldbach R, Allgaier C, Heimrich B, Jackisch R. 1998. Postnatal development of muscarinic autoreceptors modulating acetylcholine

release in the septohippocampal cholinergic system. I. Axon terminal region: hippocampus. Brain Res Dev Brain Res 108:23-30.

Gould E, Woolf NJ, Butcher LL. 1991. Postnatal development of cholinergic neurons in the rat: I. Forebrain. Brain Res Bull 27:767-789.

Graybiel AM, Aosaki T, Flaherty AW, Kimura M. 1994. The basal ganglia and adaptive motor control. Science 265:1826-1831.

Gu Q, Singer W. 1989. The role of muscarinic acetylcholine receptors in ocular dominance plasticity. EXS 57:305-314.

Guan ZZ, Zhang X, Ravid R, Nordberg A. 2000. Decreased protein levels of nicotinic receptor subunits in the hippocampus and temporal cortex of patients with Alzheimer's disease. J Neurochem 74:237-243.

Guyenet PG, Javoy F, Agid Y, Beaujouan JC, Glowinski J. 1975. Dopamine receptors and cholinergic neurons in the rat neostriatum. Adv Neurol 9:43-51.

Halliwell JV, Adams PR. 1982. Voltage-clamp analysis of muscarinic excitation in hippocampal neurons. Brain Res 250:71-92.

Happe HK, Murrin LC. 1992. Development of high-affinity choline transport sites in rat forebrain: a quantitative autoradiography study with ($^3$H)hemicholinium-3. J Comp Neurol 321:591-611.

Hasselmo ME. 1999. Neuromodulation: acetylcholine and memory consolidation. Trends Cogn Sci 3:351-359.

Hasselmo ME, Schnell E. 1994. Laminar selectivity of the cholinergic suppression of synaptic transmission in rat hippocampal region CA1: computational modeling and brain slice physiology. J Neurosci 14:3898-3914.

Hasselmo ME, McGaughy J. 2004. High acetylcholine levels set circuit dynamics for attention and encoding and low acetylcholine levels set dynamics for consolidation. Prog Brain Res 145:207-231.

Hellstrom-Lindahl E, Court JA. 2000. Nicotinic acetylcholine receptors during prenatal development and brain pathology in human aging. Behav Brain Res 113:159-168.

Henderson Z. 1991. Early development of the nucleus basalis-cortical projection but late expression of its cholinergic function. Neuroscience 44:311-324.

Henke H, Lang W. 1983. Cholinergic enzymes in neocortex, hippocampus and basal forebrain of non-neurological and senile dementia of Alzheimer-type patients. Brain Res 267:281-291.

Hepler DJ, Olton DS, Wenk GL, Coyle JT. 1985. Lesions in nucleus basalis magnocellularis and medial septal area of rats produce qualitatively similar memory impairments. J Neurosci 5:866-73.

Higgins ST, Lamb RJ, Henningfield JE. 1989. Dose-dependent effects of atropine on behavioral and physiologic responses in humans. Pharmacol Biochem Behav 34:303-311.

Hill JA Jr, Zoli M, Bourgeois JP, Changeux JP. 1993. Immunocytochemical localization of a neuronal nicotinic receptor: the beta 2-subunit. J Neurosci 13:1551-1568.

Hirotsu I, Hori N, Katsuda N, Ishihara T. 1989. Effect of anticholinergic drug on long-term potentiation in rat hippocampal slices. Brain Res 482:194-197.

Houser CR, Crawford GD, Barber RP, Salvaterra PM, Vaughn JE. 1983. Organization and morphological characteristics of cholinergic neurons: an immunocytochemical study with a monoclonal antibody to choline acetyltransferase. Brain Res 266:97-119.

Hunt R, Taveau M. 1906. On the physiological action of certain esters and ethers of choline and their relation to muscarine. Brit Med J 2:1788-1791.

Hyman JM, Wyble BP, Goyal V, Rossi CA, Hasselmo ME. 2003. Stimulation in hippocampal region CA1 in behaving rats yields long-term potentiation when delivered to the peak of theta and long-term depression when delivered to the trough. J Neurosci 23:11725-11731.

Ikonen S, McMahan R, Gallagher M, Eichenbaum H, Tanila H. 2002. Cholinergic system regulation of spatial representation by the hippocampus. Hippocampus 12:386-397.

Ito T, Miura Y, Kadokawa T. 1988. Effects of physostigmine and scopolamine on long-term potentiation of hippocampal population spikes in rats. Can J Physiol Pharmacol 66:1010-1016.

Izzo PN, Bolam JP. 1988. Cholinergic synaptic input to different parts of spiny striatonigral neurons in the rat. J Comp Neurol 269:219-234.

Jaarsma D, Dino MR, Cozzari C, Mugnaini E. 1996. Cerebellar choline acetyltransferase positive mossy fibres and their granule and unipolar brush cell targets: a model for central cholinergic nicotinic neurotransmission. J Neurocytol 25:829-842.

Ji D and Dani JA. 2000. Inhibition and disinhibition of pyramidal neurons by activation of nicotinic receptors on hippocampal interneurons. J Neurophysiol 83: 2682-2690.

Johnson DA, Zambon NJ, Gibbs RB. 2002. Selective lesion of cholinergic neurons in the medial septum by 192 IgG-saporin impairs learning in a delayed matching to position T-maze paradigm. Brain Res 943:132-141.

Jones GM, Sahakian BJ, Levy R, Warburton DM, Gray JA. 1992. Effects of acute subcutaneous nicotine on attention, information processing and short-term memory in Alzheimer's disease. Psychopharmacology 108:485-494.

Jope RS, Song L, Powers RE. 1997. Cholinergic activation of phosphoinositide signaling is impaired in Alzheimer's disease brain. Neurobiol Aging 18:111-120.

Katsuki H, Saito H, Satoh M. 1992. The involvement of muscarinic, beta-adrenergic and metabotropic glutamate receptors in long-term potentiation in the fimbria-CA3 pathway of the hippocampus. Neurosci Lett 142:249-252.

Kessler JA. 1986. Differential regulation of cholinergic and peptidergic development in the rat striatum in culture. Dev Biol 113:77-89.

Koh S, Loy R. Localization and development of nerve growth factor-sensitive rat basal forebrain neurons and their afferent projections to hippocampus and neocortex. J Neurosci 9:2999-3318.

Krnjević K. 2004. Synaptic mechanisms modulated by acetylcholine in cerebral cortex. Prog Brain Res 145:81-93.

Kubo T, Fukuda K, Mikami A, Maeda A, Takahashi H, Mishina M, Haga T, Haga K, Ichiyama A, Kangawa K, et al. 1986. Cloning, sequencing and expression of complementary DNA encoding the muscarinic acetylcholine receptor. Nature 323:411-416.

Kumari V, Gray JA, ffytche DH, Mitterschiffthaler MT, Das M, Zachariah E, Vythelingum GN, Williams SC, Simmons A, Sharma T. 2003. Cognitive effects of nicotine in humans: an fMRI study. Neuroimage 19:1002-1013.

Ladner CJ, Celesia GG, Magnuson DJ, Lee JM. 1995. Regional alterations in M1 muscarinic receptor-G protein coupling in Alzheimer's disease. J Neuropathol Exp Neurol 54:783-789.

Lamprea MR, Cardenas FP, Silveira R, Walsh TJ, Morato S. 2003. Effects of septal cholinergic lesion on rat exploratory behavior in an open-field. Braz J Med Biol Res 36:233-238.

Leanza G, Muir J, Nilsson OG, Wiley RG, Dunnett SB, Bjorklund A. Selective immunolesioning of the basal forebrain cholinergic system disrupts short-term memory in rats. Eur J Neurosci 8:1535-1544.

Lehmann O, Grottick AJ, Cassel JC, Higgins GA. 2003. A double dissociation between serial reaction time and radial maze performance in rats subjected to 192 IgG-saporin lesions of the nucleus basalis and/or the septal region. Eur J Neurosci 18:651-666.

Leslie FM, Gallardo KA, Park MK. 2002. Nicotinic acetylcholine receptor-mediated release of (3H)norepinephrine from developing and adult rat hippocampus: direct and indirect mechanisms. Neuropharmacology 42:653-661.

Leung LS, Shen B, Rajakumar N, Ma J. 2003. Cholinergic activity enhances hippocampal long-term potentiation in CA1 during walking in rats. J Neurosci 23:9297-9304.

Levey AI, Kitt CA, Simonds WF, Price DL, Brann MR. 1991. Identification and localization of muscarinic acetylcholine receptor proteins in brain with subtype-specific antibodies. J Neurosci 11:3218-3226.

Levey AI, Edmunds SM, Koliatsos V, Wiley RG, Heilman CJ. 1995a. Expression of m1-m4 muscarinic acetylcholine receptor proteins in rat hippocampus and regulation by cholinergic innervation. J Neurosci 15:4077-4092.

Levey AI, Edmunds SM, Hersch SM, Wiley RG, Heilman CJ. 1995b. Light and electron microscopic study of m2 muscarinic acetylcholine receptor in the basal forebrain of the rat. J Comp Neurol 351:339-356.

Levin ED, Conners CK, Silva D, Hinton SC, Meck WH, March J, Rose JE. 1998. Transdermal nicotine effects on attention. Psychopharmacology 140:135-141.

Linke R, Frotscher M. 1993. Development of the rat septohippocampal projection: tracing with DiI and electron microscopy of identified growth cones. J Comp Neurol 332:69-88.

Lips KS, Pfeil U, Kummer W. 2002. Coexpression of alpha 9 and alpha 10 nicotinic acetylcholine receptors in rat dorsal root ganglion neurons. Neuroscience 115:1-5.

Loewi O. 1921. Über humorale Übertaragung der Erregung von einem Neuron auf das andere. Pflugers Arch Gesamte Physiol Menschen Tiere 232:432-443.

Loewi O, Navratil. 1926. Uber humorale Ubertragbarkeit der Herznervenwirkung. X. Mitteilung: Uber das Schicksal des Vagusstoffs. Pflugers Arch Gesamte Physiol Menschen Tiere 214:689-696.

Macintosh FC, Oborin PE. 1953. Release of acetylcholine from intact cerebral cortex. Abstr XIX Int Physiol Congr Montreal: The Congress, pp. 580-581.

Madison DV, Nicoll RA. 1984. Control of the repetitive discharge of rat CA1 pyramidal neurones in vitro. J Physiol 354:319-331.

Madison DV, Lancaster B, Nicoll RA. Related 1987. Voltage clamp analysis of cholinergic action in the hippocampus. J Neurosci 7:733-741.

Maeda T, Kaneko S, Satoh M. 1994. Roles of endogenous cholinergic neurons in the induction of long-term potentiation at hippocampal mossy fiber synapses. Neurosci Res 20:71-78.

Maggi L, Sher E, Cherubini E. 2001. Regulation of GABA release by nicotinic acetylcholine receptors in the neonatal rat hippocampus. J Physiol 536:89-100.

Maggi L, Le Magueresse C, Changeux JP, Cherubini E. 2003. Nicotine activates immature "silent" connections in the developing hippocampus. Proc Natl Acad Sci U S A 100:2059-2064.

Marin O, Anderson SA, Rubenstein JL. 2000. Origin and molecular specification of striatal interneurons. J Neurosci 20:6063-6076.

McGehee DS. 1999. Molecular diversity of neuronal nicotinic acetylcholine receptors. Ann N Y Acad Sci 868:565-577.

McKinney M, Coyle JT, Hedreen JC. 1983. Topographic analysis of the innervation of the rat neocortex and hippocampus by the basal forebrain cholinergic system. J Comp Neurol 217:103-121.

McQuiston AR and Madison DV. 1999a. Muscarinic receptor activity has multiple effects on the resting membrane potentials of CA1 hippocampal interneurons. J Neurosci 19: 5693-5702.

McQuiston AR and Madison DV. 1999b. Nicotinic receptor activation excites distinct subtypes of interneurons in the rat hippocampus. J Neurosci 19: 2887-2896.

Mechawar N, Descarries L. 2001. The cholinergic innervation develops early and rapidly in the rat cerebral cortex: A quantitative immunocytochemical study. Neuroscience. 108:555-67.

Mechawar N, Cozzari C, Descarries L. 2000. Cholinergic innervation in adult rat cerebral cortex: a quantitative immunocytochemical description. J Comp Neurol 428: 305 318.

Mechawar N, Watkins KC, Descarries L. 2002. Ultrastructural features of the acetylcholine innervation in the developing parietal cortex of rat. J Comp Neurol 443: 250-258.

Meck WH, Church RM, Wenk GL, Olton DS. 1987. Nucleus basalis magnocellularis and medial septal area lesions differentially impair temporal memory. J Neurosci 7:3505-3511.

Miao H, Liu C, Bishop K, Gong ZH, Nordberg A, Zhang X. 1998. Nicotine exposure during a critical period of development leads to persistent changes in nicotinic acetylcholine receptors of adult rat brain. J Neurochem 70:752-762.

Milburn CM, Prince DA. 1993. Postnatal development of cholinergic presynaptic inhibition in rat hippocampus. Brain Res Dev Brain Res 74:133-7.

Milner TA, Loy R, Amaral DG. 1983. An anatomical study of the development of the septo-hippocampal projection in the rat. Brain Res 284:343-371.

Miyoshi R, Kito S, Shimizu M, Matsubayashi H. 1987. Ontogeny of muscarinic receptors in the rat brain with emphasis on the differentiation of M1- and M2-subtypes--semi-quantitative in vitro autoradiography. Brain Res 420:302-312.

Molnar M, Tongiorgi E, Avignone E, Gonfloni S, Ruberti F, Domenici L, Cattaneo A. 1998. The effects of anti-nerve growth factor monoclonal antibodies on developing basal forebrain neurons are transient and reversible. Eur J Neurosci 10:3127-3140.

Monmaur P, Breton P. 1991. Elicitation of hippocampal theta by intraseptal carbachol injection in freely moving rats. Brain Res 544:150-155.

Nachmansohn D, Machado AL. 1943. The formation of acetylcholine. A new enzyme 'choline acetylase'. J Neurophysiol 6:397-403.

Nyakas C, Luiten PG, Spencer DG, Traber J. 1987. Detailed projection patterns of septal and diagonal band efferents to the hippocampus in the rat with emphasis on innervation of CA1 and dentate gyrus. Brain Res Bull 18:533-545.

Nyakas C, Buwalda B, Kramers RJ, Traber J, Luiten PG. 1994. Postnatal development of hippocampal and neocortical cholinergic and serotonergic innervation in rat: effects of nitrite-induced prenatal hypoxia and nimodipine treatment. Neuroscience 59:541-559.

Oakman SA, Faris PL, Cozzari C, Hartman BK. 1999. Characterization of the extent of pontomesencephalic cholinergic neurons' projections to the thalamus: comparison with projections to midbrain dopaminergic groups. Neuroscience 94:529-547.

Oleskevich S and Descarries L. 1990. Quantified distribution of the serotonin innervation in adult rat hippocampus. Neuroscience 34: 19-33.

Oleskevich S, Descarries L, Lacaille JC. 1989. Quantified distribution of the noradrenaline innervation in the hippocampus of adult rat. J Neurosci 9: 3803-3815.

Orr G, Rao G, Houston FP, McNaughton BL, Barnes CA. 2001. Hippocampal synaptic plasticity is modulated by theta rhythm in the fascia dentata of adult and aged freely behaving rats. Hippocampus 11:647-54.

Pavlides C, Greenstein YJ, Grudman M, Winson J. 1988. Long-term potentiation in the dentate gyrus is induced preferentially on the positive phase of theta-rhythm. Brain Res 439:383-387.

Perez-Navarro E, Alberch J, Marsal J. 1993. Postnatal development of functional dopamine, opioid and tachykinin receptors that regulate acetylcholine release from rat neostriatal slices. Effect of 6-hydroxydopamine lesion. Int J Dev Neurosci 11:701-708.

Perry EK, Perry RH, Blessed G, Tomlinson BE. 1977. Necropsy evidence of central cholinergic deficits in senile dementia. Lancet 1:189.

Phelps PE, Houser CR, Vaughn JE. 1985. Immunocytochemical localization of choline acetyltransferase within the rat neostriatum: a correlated light and electron microscopic study of cholinergic neurons and synapses. J Comp Neurol 238:286-307.

Phelps PE, Brady DR, Vaughn JE. 1989. The generation and differentiation of cholinergic neurons in rat caudate-putamen. Brain Res Dev Brain Res 46:47-60.

Pickel VM, Chan J. 1990. Spiny neurons lacking choline acetyltransferase immunoreactivity are major targets of cholinergic and catecholaminergic terminals in rat striatum. J Neurosci Res 25:263-280.

Pisani A, Bonsi P, Picconi B, Tolu M, Giacomini P, Scarnati E. 2001. Role of tonically-active neurons in the control of striatal function: cellular mechanisms and behavioral correlates. Prog Neuropsychopharmacol Biol Psychiatry 25:211-230.

Pitler TA, Alger BE. 1992. Cholinergic excitation of GABAergic interneurons in the rat hippocampal slice. J Physiol 450:127-142.

Quastel JH, Tennenbaum M, Wheatley AHM. 1936. Choline ester formation in, and choline esterase activities of, tissues *in vitro*. Biochem J 30:1668-1681.

Quirion R, Wilson A, Rowe W, Aubert I, Richard J, Doods H, Parent A, White N, Meaney MJ. 1995. Facilitation of acetylcholine release and cognitive performance by an M(2)-muscarinic receptor antagonist in aged memory-impaired. J Neurosci 15:1455-62.

Radcliffe KA, Dani JA. 1998. Nicotinic stimulation produces multiple forms of increased glutamatergic synaptic transmission. J Neurosci 18:7075-7083.

Radcliffe KA, Fisher JL, Gray R, Dani JA. 1999. Nicotinic modulation of glutamate and GABA synaptic transmission of hippocampal neurons. Ann N Y Acad Sci 868:591-610.

Richter JA, Perry EK, Tomlinson BE. Related 1980. Acetylcholine and choline levels in post-mortem human brain tissue: preliminary observations in Alzheimer's disease. Life Sci 26:1683-1689.

Riekkinen P Jr, Sirvio J, Riekkinen P. 1990. Similar memory impairments found in medial septal-vertical diagonal band of Broca and nucleus basalis lesioned rats: are memory defects induced by nucleus basalis lesions related to the degree of non-specific subcortical cell loss? Behav Brain Res 37:81-88.

Robertson RT, Gorenstein C. 1987. 'Non-specific' cholinesterase-containing neurons of the dorsal thalamus project to medial limbic cortex. Brain Res 404:282-292.

Robertson RT, Poon HK, Mirrafati SJ, Yu J. 1989. Transient patterns of acetylcholinesterase activity in developing thalamus: a comparative study in rodents. Brain Res Dev Brain Res 48:309-315.

Robertson RT, Gallardo KA, Claytor KJ, Ha DH, Ku KH, Yu BP, Lauterborn JC, Wiley RG, Yu J, Gall CM, Leslie FM. 1998. Neonatal treatment with 192 IgG-saporin produces long-term forebrain cholinergic deficits and reduces dendritic branching and spine density of neocortical pyramidal neurons. Cereb Cortex 8:142-55.

Rodriguez-Puertas R, Pascual J, Vilaro T, Pazos A. Related 1997. Autoradiographic distribution of M1, M2, M3, and M4 muscarinic receptor subtypes in Alzheimer's disease. Synapse 26:341-350.

Rossor MN, Garrett NJ, Johnson AL, Mountjoy CQ, Roth M, Iversen LL. 1982. A post-mortem study of the cholinergic and GABA systems in senile dementia. Brain 105:313-330.

Rouse ST, Edmunds SM, Yi H, Gilmor ML, Levey AI. 2000. Localization of M(2) muscarinic acetylcholine receptor protein in cholinergic and non-cholinergic terminals in rat hippocampus. Neurosci Lett 284:182-186.

Rouse ST, Levey AI. 1997. Muscarinic acetylcholine receptor immunoreactivity after hippocampal commissural/associational pathway lesions: evidence for multiple presynaptic receptor subtypes. J Comp Neurol 380:382-394.

Rouse ST, Marino MJ, Potter LT, Conn PJ, Levey AI. 1999. Muscarinic receptor subtypes involved in hippocampal circuits. Life Sci 64:501-509.

Rye DB, Wainer BH, Mesulam MM, Mufson EJ, Saper CB. 1984. Cortical projections arising from the basal forebrain: a study of cholinergic and noncholinergic components employing combined retrograde tracing and immunohistochemical localization of choline acetyltransferase. Neuroscience 13:627-643.

Scheindlin S. 2001. A brief history of pharmacology. Modern Drug Discovery 4:87-88.

Schlaggar BL, De Carlos JA, O'Leary DD. 1993. Acetylcholinesterase as an early marker of the differentiation of dorsal thalamus in embryonic rats. Brain Res Dev Brain Res 75:19-30.

Schwaber JS, Rogers WT, Satoh K, Fibiger HC. 1987. Distribution and organization of cholinergic neurons in the rat forebrain demonstrated by computer-aided data acquisition and three-dimensional reconstruction. J Comp Neurol 263:309-325.

Schwegler H, Boldyreva M, Pyrlik-Gohlmann M, Linke R, Wu J, Zilles K. 1996. Genetic variation in the morphology of the septo-hippocampal cholinergic and GABAergic system in mice. I. Cholinergic and GABAergic markers. Hippocampus 6:136-148.

Seguela P, Wadiche J, Dineley-Miller K, Dani JA, Patrick JW. 1993. Molecular cloning, functional properties, and distribution of rat brain alpha 7: a nicotinic cation channel highly permeable to calcium. J Neurosci 13:596-604.

Semba K. 2004. Phylogenetic and ontogenetic aspects of the basal forebrain cholinergic neurons and their innervation of the cerebral cortex. Prog Brain Res 145:3-43.

Semba K, Fibiger HC. 1988. Time of origin of cholinergic neurons in the rat basal forebrain. J Comp Neurol 269:87-95.

Semba K, Vincent SR, Fibiger HC. 1988. Different times of origin of choline acetyltransferase- and somatostatin-immunoreactive neurons in the rat striatum. J Neurosci 8:3937-3944.

Shacka JJ, Robinson SE. 1998. Postnatal developmental regulation of neuronal nicotinic receptor subunit alpha 7 and multiple alpha 4 and beta 2 mRNA species in the rat. Brain Res Dev Brain Res 109:67-75.

Shatz CJ. 1990. Impulse activity and the patterning of connections during CNS development. Neuron 5:745-756.

Shelton DL, Nadler JV, Cotman CW. 1979. Development of high affinity choline uptake and associated acetylcholine synthesis in the rat fascia dentata. Brain Res 163:263-275.

Shimono K, Brucher F, Granger R, Lynch G, Taketani M. 2000. Origins and distribution of cholinergically induced beta rhythms in hippocampal slices. J Neurosci 20:8462-8473.

Sokolov MV, Kleschevnikov AM. 1995. Atropine suppresses associative LTP in the CA1 region of rat hippocampal slices. Brain Res 672:281-284.

Sudweeks SN, Yakel JL. Related 2000. Functional and molecular characterization of neuronal nicotinic ACh receptors in rat CA1 hippocampal neurons. J Physiol 3:515-528.

Tanaka Y, Sakurai M, Hayashi S. 1989. Effect of scopolamine and HP 029, a cholinesterase inhibitor, on long-term potentiation in hippocampal slices of the guinea pig. Neurosci Lett 98:179-183.

Thal LJ, Gilbertson E, Armstrong DM, Gage FH. 1992. Development of the basal forebrain cholinergic system: phenotype expression prior to target innervation. Neurobiol Aging 13:67-72.

Thiel CM, Huston JP, Schwarting RK. 1998. Hippocampal acetylcholine and habituation learning. Neuroscience 85:1253-1262.

Tice MA, Hashemi T, Taylor LA, McQuade RD. 1996. Distribution of muscarinic receptor subtypes in rat brain from postnatal to old age. Brain Res Dev Brain Res 92:70-76.

Tiesinga PH, Fellous JM, Jose JV, Sejnowski TJ. 2001. Computational model of carbachol-induced delta, theta, and gamma oscillations in the hippocampus. Hippocampus 11:251-274.

Tribollet E, Bertrand D, Marguerat A, Raggenbass M. 2004. Comparative distribution of nicotinic receptor subtypes during development, adulthood and aging: an autoradiographic study in the rat brain. Neuroscience 124:405-420.

Umbriaco D, Garcia S, Beaulieu C, Descarries L. 1995. Relational features of acetylcholine, noradrenaline, serotonin and GABA axon terminals in the stratum radiatum of adult rat hippocampus (CA1). Hippocampus 5:605-620.

Umbriaco D, Watkins KC, Descarries L, Cozzari C, Hartman BK. 1994. Ultrastructural and morphometric features of the acetylcholine

innervation in adult rat parietal cortex: an electron microscopic study in serial sections. J Comp Neurol 348: 351 373.

Van Vulpen EH, Van Der Kooy D. 1996. Differential maturation of cholinergic interneurons in the striatal patch versus matrix compartments. J Comp Neurol 365:683-691.

van Vulpen EH, van der Kooy D. 1998. Striatal cholinergic interneurons: birthdates predict compartmental localization. Brain Res Dev Brain Res 109:51-58.

Vesey R, Birrell JM, Bolton C, Chipperfield RS, Blackwell AD, Dening TR, Sahakian BJ. 2002. Cholinergic nicotinic systems in Alzheimer's disease: prospects for pharmacological intervention. CNS Drugs 16:485-500.

Vogel JR, Hughes RA, Carlton PL. 1967. Scopolamine, atropine and conditioned fear. Psychopharmacologia 10:409-416.

Voronin LL, Cherubini E. 2003. "Presynaptic silence" may be golden. Neuropharmacology 45:439-449.

Wainer BH, Bolam JP, Freund TF, Henderson Z, Totterdell S, Smith AD. 1984. Cholinergic synapses in the rat brain: a correlated light and electron microscopic immunohistochemical study employing a monoclonal antibody against choline acetyltransferase. Brain Res 308:69-76.

Wallenstein GV, Vago DR. 2001. Intrahippocampal scopolamine impairs both acquisition and consolidation of contextual fear conditioning. Neurobiol Learn Mem 75:245-252.

Watabe AM, Zaki PA, O'Dell TJ. 2000. Coactivation of beta-adrenergic and cholinergic receptors enhances the induction of long-term potentiation and synergistically activates mitogen-activated protein kinase in the hippocampal CA1 region. J Neurosci 20:5924-5931.

Wetzel W, Ott T, AMtthies H. Related 1977. Post-training hippocampal rhythmic slow activity ("theta") elicited by septal stimulation improves memory consolidation in rats. Behav Biol 21:32-40.

Williams S, Johnston D. 1988. Muscarinic depression of long-term potentiation in CA3 hippocampal neurons. Science 242:84-87.

Winson J. 1978. Loss of hippocampal theta rhythm results in spatial memory deficit in the rat. Science 201:160-163.

Woolf NJ. 1991. Cholinergic systems in mammalian brain and spinal cord. Prog Neurobiol 37:475-524.

Woolf NJ, Butcher LL. 1981. Cholinergic neurons in the caudate-putamen complex proper are intrinsically organized: a combined Evans blue and acetylcholinesterase analysis. Brain Res Bull 7:487-507.

Woolf NJ, Butcher LL. 1986. Cholinergic systems in the rat brain: III. Projections from the pontomesencephalic tegmentum to the

thalamus, tectum, basal ganglia, and basal forebrain. Brain Res Bull 16:603-637.

Yun SH, Cheong MY, Mook-Jung I, Huh K, Lee C, Jung MW. 2000. Cholinergic modulation of synaptic transmission and plasticity in entorhinal cortex and hippocampus of the rat. Neuroscience 97:671-676.

Zahalka EA, Seidler FJ, Lappi SE, Yanai J, Slotkin TA. 1993. Differential development of cholinergic nerve terminal markers in rat brain regions: implications for nerve terminal density, impulse activity and specific gene expression. Brain Res 601:221-229.

Zhang X, Liu C, Miao H, Gong ZH, Nordberg A. 1998. Postnatal changes of nicotinic acetylcholine receptor alpha 2, alpha 3, alpha 4, alpha 7 and beta 2 subunits genes expression in rat brain. Int J Dev Neurosci 16:507-518.

Zhu XO, Waite PM. 1998. Cholinergic depletion reduces plasticity of barrel field cortex. Cereb Cortex 8:63-72.

# LISTE DES PUBLICATIONS

## Chapitres de livre

Descarries L., **Aznavour N**. (2003) Diffuse (volume) transmission. Dans: The Encyclopedia of Neuroscience. Adelman G and Smith BH, eds. Amsterdam: Elsevier Science.

Descarries L, Mechawar N, **Aznavour N**, Watkins KC. (2004). Structural determinants of the roles of acetylcholine in the cerebral cortex. Prog Brain Res 145:45-58.

## Articles publiés

**Aznavour N**, Mechawar N, Descarries L. (2002). Comparative analysis of the cholinergic innervation in the dorsal hippocampus of adult mouse and rat: A quantitative immunocytochemical study. *Hippocampus* 12:206-217.

**Aznavour N**, Mechawar N, KC Watkins, Descarries L (2003). Fine structural features of the acetylcholine innervation in the developing neostriatum of rat. *J Comp Neurol* 460:280-291.

Meilleur S, **Aznavour N**, Descarries L, Carmant L, Orval A, Psarropoulou C. (2003). Pentylenetetrazol-induced Seizures in Immature Rats Provoke Long-term Changes in Adult Hippocampal Cholinergic Excitability. *Epilepsia* 44:507-517.

L Descarries, **N Aznavour**, E Hamel. (2004). The acetylcholine innervation of cerebral cortex: New data on its normal development and its fate in the $hAPP_{SW,IND}$ mouse model of Alzheimer's disease. *J Neural Transmission* 112:149-162.

## Articles sous presse

**Aznavour N**, Watkins KC, Descarries L. (2004). Postnatal development of the cholinergic innervation in the dorsal hippocampus of rat: a quantitative light and electron microcopic immunocytochemical study. *J Comp Neurol.*

JS Aucoin, P Jiang, **Aznavour N**, XK Tong, M Buttini, Descarries L, Hamel E. (2004). Selective cholinergic denervation, independent from oxidative stress, in a mouse model of Alzheimer's disease. *Neuroscience.*

## Abrégés publiés

**Aznavour N**, KC Watkins, Descarries L. (2004). Early and rapid postnatal development of the cholinergic innervation in the dorsal hippocampus of rat. *Abstract Viewer/Itinerary Planner.* Washington, DC: Society for Neuroscience, 2004. Online.

**Aznavour N**, Tong XK, Aucoin J-S, Descarries L, Hamel E. (2003). Neurotoxicity of β-amyloid and selective, age-dependant loss of cholinergic fibers in the hippocampus and cerebral cortex of the PDAPP mouse. Program No. 842.7. *Abstract Viewer/Itinerary Planner.* Washington, DC: Society for Neuroscience, 2003. Online.

**Aznavour N.**, Mechawar N, Watkins KC, Descarries L (2003). Innervation cholinergique (ACh) du néostriatum en développement : caractérisation ultrastructurale. *Congrès de l'AEGSFM,* Montréal Méd Sci, Suppl 2, 19:4.

Descarries L, **Aznavour N**, Aucoin J-S, M Buttini, L.Mucke, Hamel E. (2003). Loss of cholinergic innervation in the cerebral cortex and hippocampus of transgenic mice overexpressing V717F β-amyloid precursor protein. *Journée scientifique 2003, Département de pathologie et biologie cellulaire.*

**Aznavour N**, Mechawar N, KC Watkins, Descarries L (2002). Ultrastructural features in the developing neostriatum of rat. Program No. 129.7. 2002 Abstract Viewer/Itinerary Planner. Washington, DC : Society for Neuroscience, 2002. Online.

**Aznavour N**, Mechawar N, Watkins KC, Descarries L. (2002). Caractéristiques ultrastructurales de l'innervation cholinergique (ACh) du néostriatum en développement. *Journée scientifique 2002, Département de pathologie et biologie cellulaire.*

Descarries L, **Aznavour N,** Aucoin J-S, M Buttini, L Mucke, Hamel E. (2002). Loss of cholinergic innervation in the cerebral cortex and hippocampus of transgenic mice overexpressing V717F β-amyloid precursor protein. Program No. 295.17. Abstract Viewer/Itinerary Planner. Washington, DC: Society for Neuroscience, 2002. Online.

**Aznavour N.**, Mechawar N, Descarries L. (2002). Données quantitatives sur l'innervation cholinergique de l'hippocampe chez la souris et le rat adultes. *Congrès de l'AEGSFM,* Montréal.

**Aznavour N**, Mechawar N, Watkins KC, Descarries L. (2002). Caractéristiques ultrastructurales de l'innervation cholinergique (ACh) du néostriatum en développement. *Journée scientifique 2002, Département de pathologie et biologie cellulaire.*

**Aznavour N**, Mechawar N, Descarries L. (2001). Cholinergic innervation of the dorsal hippocampus in adult mouse and rat: A comparative immunocytochemical study. *Soc Neurosci Abstr* 27:1566.

**Aznavour N**, Mechawar N, Descarries L. (2001). Données quantitatives sur l'innervation cholinergique de l'hippocampe chez la souris et le rat adultes. *Congrès de l'AEGSFM,* Montréal.

**Aznavour N**, Mechawar N, Descarries L. (2001). Description quantitative de l'innervation cholinergique (ACh) de l'hippocampe chez la souris

adulte. *Journée scientifique 2001, Département de pathologie et biologie cellulaire.*

**Aznavour N**, Mechawar N, Dubuc R, Descarries L. (2000). Quantitative data on the cholinergic innervation in adult hippocampus. *Soc Neurosci Abstr* 26:2141.

**Aznavour N**, Mechawar N, Descarries L. (2000). Données quantitatives sur l'innervation cholinergique de l'hippocampe chez la souris. *Congrès de l'AEGSFM*, Montréal.

**Aznavour N**, Mechawar N, Descarries L. (2000). Données quantitatives sur l'innervation cholinergique de l'hippocampe chez la souris. *Journée scientifique 2000, Département de pathologie et biologie cellulaire.*

Meilleur S, **Aznavour N**, Mechawar N, Descarries L, Psarropoulou C. (2000). Pentylenetetrazol-induced convulsions in immature and adult rats have different long-term effects on cholinergic transmission in the hippocampal CA3 area. *Soc. Neurosci. Abstr.* 26:1053

Meilleur S, **Aznavour N**, Mechawar N, Descarries L, Psarropoulou C. (2000). Pentylenetetrazol-induced convulsions in immature and adult rats have different long-term effects on cholinergic transmission in the hippocampal CA3 area. *American Epilepsy Society.* Epilepsia 41:S7, p. 52.

# ANNEXES

## Annexe 1

# PENTYLENETETRAZOL-INDUCED SEIZURES IN IMMATURE RATS PROVOKE LONG-TERM CHANGES IN ADULT HIPPOCAMPAL CHOLINERGIC EXCITABILITY

Publié en 2003

*Epilepsia* 44:507-517

(S MEILLEUR, N AZNAVOUR, L DESCARRIES, L CARMANT, A ORVAL, C PSARROPOULOU)

*Epilepsia*, 44(4):507–517, 2003
Blackwell Publishing, Inc.


# Pentylenetetrazol-induced Seizures in Immature Rats Provoke Long-term Changes in Adult Hippocampal Cholinergic Excitability

*Sébastien Meilleur, †Nicolas Aznavour, †Laurent Descarries, *Lionel Carmant, ‡Orval A. Mamer, and *Caterina Psarropoulou

**Department of Pediatrics, Ste-Justine Hospital Research Center, †Department of Pathology and Cellular Biology, and CRSN, Faculty of Medicine, Université de Montréal; and ‡Mass Spectrometry Unit, Faculty of Medicine, McGill University, Montreal, Quebec, Canada*

**Summary:** *Purpose:* We previously demonstrated that the anticholinesterase eserine provokes interictal-like discharges in the CA3 area of hippocampal slices from rats in which generalized seizures had been induced by pentylenetetrazol (PTZ) when immature. In this study, we investigated several factors as the possible mechanism for this effect, including age at convulsions.

*Methods:* Rats were injected with PTZ on postnatal day (P) 18–20 or >P60, and neuronal activity was recorded intra- and extracellularly from CA3 5–10 or >40 days later. In additional experiments, convulsions were triggered by kainate or were blocked by pentobarbital. Hippocampal (a) acetylcholine (ACh) innervation density was measured by immunocytochemistry, and ACh and γ-aminobutyric acid (GABA) contents were determined by high-performance liquid chromatography (HPLC)-electrospray ionization.

*Results:* The excitatory effect of eserine was the most consistent in slices from rats PTZ-treated when immature and after the long interval, whereas the reverse was true in rats treated as adults. This effect was dependent on the occurrence of a seizure and was less prevalent when the seizure had been provoked by kainate. Adult animals PTZ-treated at P20 did not differ from control in (a) poly- or monosynaptic $GABA_A$ and $GABA_B$ CA3 inhibitory postsynaptic potentials (IPSPs); (b) density of ACh innervation; or (c) tissue content of ACh and GABA.

*Conclusions:* A PTZ-induced generalized seizure in immature rat provokes endogenous ACh-induced interictal-like discharges in adult hippocampal CA3. This effect is only transiently observed if the seizure was induced in adult. It does not appear to be related to a change in GABAergic inhibition, in density of ACh innervation, or in ACh or GABA content.
**Key Words:** Acetylcholine—Eserine—Evoked potentials—Neuronal synchronization—Spontaneous discharges—$GABA_A$ IPSPs—$GABA_B$ IPSPs.

Most epileptic syndromes are first manifested in infancy or childhood (1). The use of experimental models has indicated that paroxysmal discharges occurring during convulsions may leave their imprint in brain physiology depending on their cellular mechanism, duration, and age at onset (2–5). Our previous work showed that the anticholinesterase (AChE) eserine could provoke the generation of interictal-like discharges, a precursor to the ictal state (seizure) (6,7), in the in vitro CA3 hippocampal area of adult animals that had been subjected to pentylenetetrazol (PTZ)-induced seizures at postnatal days 10 or 20 (8). Brain acetylcholine (ACh) levels increase in various behavioral states (9,10) or pathological conditions (11–13). Taken together, this information suggests that an increase in brain ACh levels may have a proconvulsive effect in animals with a history of seizures during brain maturation.

In the present study, we first compared the dependence of the eserine effect (8) on the drug injection versus the ensuing seizure [pretreatment with pentobarbital (PTB)], the agent used to induce the seizure (kainate vs. PTZ), and the age of the animals (immature vs. adult) at the time of the seizure. We then investigated three putative cellular mechanisms that might have facilitated the generation of eserine-induced interictal-like discharges in the PTZ-treated animals: (a) a decrease in $GABA_A$-mediated synaptic inhibition (indirect effect); (b) an increase in density of cholinergic innervation, and/or (c) an increase in the ambient ACh (direct effects).

Accepted November 3, 2002.
Address correspondence and reprint requests to Dr. C. Psarropoulou at Ste-Justine Hospital Research Center, 3175 Côte Ste-Catherine, Montréal, QC, Canada H3T 1W5. [redacted]

## METHODS

### Animals

Sprague–Dawley rat pups and adult rats (Charles River, St-Constant, QC, Canada) were used in all experiments. Animal care and use conformed to institutional policy and guidelines (Ste-Justine Research Center, Université de Montréal).

*Pentylenetetrazol-induced seizures*

Forty P18–P20 rat pups of either sex and 25 adult (P60, 150–200 g) male rats were injected intraperitoneally (i.p.) with the $GABA_A$ antagonist PTZ (90 mg/kg, dissolved in 0.9% NaCl), after which the occurrence of generalized convulsions was monitored visually for 2 h before the animals were returned to their home cage. Ten to thirty percent mortality was associated with this part of the experiment (pups, adults). Fourteen additional P20 rat pups were sedated with 30 mg/kg PTB 10 min before the PTZ injection to prevent convulsions.

*Kainate-induced seizures*

Six P20 rat pups were injected i.p. with kainic acid (8 mg/kg, dissolved in 0.9% NaCl), instead of PTZ, and six littermates were injected with an identical volume of saline to be used as controls.

### Preparation of hippocampal slices

Hippocampal slices were prepared from PTZ-injected animals 7–12 days (short interval) or 40–50 days (long interval) after treatment, and 40 days after the kainate-induced seizure. Only rats with confirmed behavioral seizures (PTZ, kainate) were considered "epileptic" for the electrophysiologic recordings. Animals were decapitated under halothane anesthesia (by inhalation), and both hippocampi were dissected out and kept in cold (0–4°C) artificial cerebrospinal fluid (aCSF). Transverse hippocampal slices 450–500 μm thick were cut with a vibratome. Slices from the middle third of hippocampus were selected and placed in two independent submersion chambers, perfused with heated (32 ± 1°C) oxygenated (95% $O_2$/5% $CO_2$) aCSF and allowed to equilibrate for ≥1 h before recording. The volume of each submersion channel was 0.28 ml, and the perfusion rate was ~0.6 ml/min. The composition of standard aCSF was as follows (in m*M*): NaCl, 124; KCl, 2; $KH_2PO_4$, 1.25; $CaCl_2$, 2; $MgSO_4$, 2; $NaHCO_3$, 26; glucose, 10; at pH 7.4. (All reagents from BDH Inc., Toronto, Ontario, Canada)

### Electrophysiologic recordings in vitro and data analysis

All recordings were carried out in the pyramidal layer of the CA3 hippocampal area. Recording electrodes were glass pipettes with filament (WPI) filled with 4 *M* K-acetate (resistance, 30–50 MΩ, intracellular recordings) or with 4 *M* NaCl (resistance, 10–20 MΩ, extracellular recordings). Bipolar stimulating electrodes, made from Teflon-coated wire, were placed in the mossy fiber pathway, and orthodromic synaptic stimuli were delivered at frequencies ranging from 0.025–0.040 Hz (one stimulus every 25–40 s). Intracellular signals were fed to a high-impedance amplifier with bridge circuit that allowed current to pass through the intracellular electrode (Axoprobe 1A). The bridge was monitored throughout the experiments and adjusted as necessary. Signals were displayed on a storage oscilloscope and a chart recorder and were also stored on computer (Axotape 2.0.2) for further analysis.

*Extracellularly* recorded evoked responses were displayed in a storage oscilloscope, where four to eight successive responses were averaged and printed. The maximal amplitude of field excitatory postsynaptic potentials (fEPSPs, in mV) was measured as the difference between the positive peak of the signal minus the prestimulus baseline. fEPSP duration (in ms) was measured from the artifact of stimulation to the intercept of the trace with the prestimulus baseline. The amplitude of the population spikes (PSs) was measured from their negative peak to the half-distance of their positive peaks (in mV); the optical detection limit of a PS was ~0.2 mV.

*Intracellularly* recorded evoked responses: EPSP amplitude (mV) was measured from the prestimulus baseline to its peak; the reciprocal period (ms) was the "time to EPSP peak." EPSP duration was measured from the stimulation artifact to the time when the trace became negative to the prestimulus baseline. The early (fast) IPSP and the late (slow) IPSP maximal amplitude (mV) were determined as the difference between their negative peaks and the prestimulus baseline. All measurements were taken from averaged traces (four traces/average).

### Chemicals

PTZ and kainic acid were purchased from Research Biochemicals (RBI); eserine, PTB, and the $GABA_A$-receptor antagonist bicuculline methiodide (BMI) from Sigma, and the respective antagonists of *N*-methyl-D-aspartate (NMDA) and non-NMDA glutamate receptors, D(−)-2-amino-5-phosphonopentanoic (APV) and 6-cyano-7-nitroquinoxaline-2,3-dione (CNQX) from Tocris. All bath-applied drugs were tested at a concentration of 10 μ*M*.

### Measurements of ACh innervation density

These experiments were carried out on the dorsal hippocampus of two pairs of adult rats (P60) injected at P20, one with PTZ and the other with saline. The tissue from each pair was simultaneously processed for light microscopic, choline acetyltransferase (ChAT) immunocytochemistry, according to a procedure previously described in detail (14–16). The length of ChAT-immunostained axons was determined in single 50-μm-thick transverse sections across the mid-portion of the dorsal hippocampus, with the aid of an image-analysis system consisting of a light microscope (Leitz Ortho-

plan; ×25 PlanApo objective lens) connected to a microcomputer (Macintosh Quadra 950; NIH Image software 1.61) via a video camera (Panasonic WV-BD400; 768 × 493 pixels for 1.7 $cm^2$). In CA1, CA3 and the dentate gyrus (DG), at a transverse level equivalent to stereotaxic plane A-6.2 mm in the atlas of Paxinos and Watson (17), a 240–μm-wide strip, perpendicular to the hippocampal surface, was captured and printed on paper at a magnification of ×645. Within every layer of each sector, three square sampling windows, 32.25 mm in side at this magnification, were delineated on the prints, and the axonal network in each window was traced by hand on transparent film. These tracings were in turn digitized with the image-analysis system, and their total length was measured after opening all closed surfaces by 1 pixel and reducing the thickness of lines to 1 pixel with the "skeletonize" function of the software. A total surface of 0.0825 $mm^2$ per rat was thus examined. The values for each hippocampal layer were expressed as average length of ACh axons (μm) per sampling window (2,500 $\mu m^2$).

**Measurement of endogenous ACh and GABA**

ACh and GABA were determined by high-performance liquid chromatography (HPLC) electrospray ionization mass spectrometry (18), with a method modified from (19).

*Sample preparation*

The hippocampi from the brain of P60 animals treated with PTZ at P20–21 or their saline-injected littermates (controls) were extracted and immersed in 1 ml of methanol (Fisher Scientific, HPLC grade), homogenized in a polytron (Virtis Handspear, 4 times 20 s), and sonicated (Branson Sonifier 450, 6 times 10 s). Immediately after the tissue extraction, 1 μ*M* eserine and 1 μ*M* vigabatrin (VGB) were added to each 1 ml solution to prevent the catabolism of ACh and GABA, respectively. The homogenate was centrifuged at 110,000 rpm for 2 h at 4°C, and the supernatant was recovered and frozen at −80°C until the analysis day. The samples were dissolved in a 50% acetonitrile solution containing 4 m*M* ammonium acetate before the test. In each analysis, six samples (six hippocampi) from three PTZ-treated and six samples from three control animals were processed simultaneously.

*Mass spectrometry analysis*

A Quattro II triple quadrupole (Micromass, Manchester, U.K.) was configured for direct infusion positive-product ion analysis and used with the cone voltage set to 25 V; source temperature, 80°C; sample infusion rate, 2 μl/min; nitrogen bath gas flow rate, 150 L/h; capillary voltage, 3.15 kV; and collision cell energy, 21 eV; with argon pressure $1 \times 10^{-3}$ mbar. The spectrometer was programmed to scan from 102 to 115 Da in multichannel acquisition mode (MCA) for neutral loss of 17 Da from GABA-d0 (d, deuterium labeled) and GABA-d6 and from m/z 140–160 for the parent of a molecule of 87 m/z produced by ACh-d0 and ACh-d9 (CDN Isotopes). All solvents were of analytic grade (Fisher Scientific).

Solutions of increasing concentration of ACh or GABA were prepared, to which a standard concentration of labeled ACh or GABA was added. The labeled/unlabeled ratios were measured in the mass spectrometer, and calibrating curves were obtained by plotting the measured ratios against the known concentrations of unlabeled GABA and ACh. Tissue extract samples were prepared to which the same quantities of labeled ACh or GABA internal standards were added. The lower limit of quantitation was conservatively placed at the lowest concentrations of both GABA and ACh in the samples (0.25 n*M*) prepared for calibration over the useful range. Ultimate sensitivities were not determined, as <0.25 n*M*, both calibrations began to depart from linearity. The endogenous hippocampal ACh or GABA concentrations were calculated from the measured ratios and the standard curves.

## RESULTS

**Pentylenetetrazol- and kainate-induced seizures**

Convulsions started 1–8 min after i.p. PTZ injection, with a similar pattern in immature and adult animals. The first signs of epileptic activity were myoclonic jerks, followed by wild running, and then clonic seizures with a preservation of the righting reflex. A tonic phase ensued, followed by clonic seizures with loss of the righting reflex, and culminated to a generalized tonic–clonic seizure. Generalized PTZ-induced convulsions lasted >15 min in most animals, and they appeared to be longer in immature compared with adult animals (36.33 ± 5.68 min, n = 12, vs. 15.73 ± 2.73 min, n = 19; two-tailed unpaired Student's *t* test, p = 0.001). In some immature or adult animals, brief and repetitive episodes of generalized seizures were observed; the total duration of these was similar to that given earlier. These animals were not included in the calculation of mean seizure duration, but were used for electrophysiologic recordings. Seizures were absent in all P20 rat pups pretreated with PTB.

Kainate-induced seizures started 10–15 min after i.p. injection of the convulsant. Their manifestations included staring, wet-dog shakes, myoclonic jerks, and clonus evolving to rearing and falling (generalized seizures). However, unlike the PTZ-induced convulsions, generalized kainate-induced convulsions were very brief, lasting 1–2 min, amid milder epileptic manifestations lasting for a total of 26–105 min, during which time animals never regained normal behavior.

**Effects of eserine on spontaneous field potentials** .

Before the assessment of spontaneous activity, the viability of all slices was ensured by eliciting a CA3 synaptic response, after which stimulation was turned off. Bath application of eserine (10 $\mu M$) provoked spontaneous synchronous interictal-like discharges, with a rate of occurrence of 0.18 ± 0.02 Hz (n = 27), in the CA3 region of hippocampal slices from PTZ-treated animals but not in slices from saline-injected or naive age-matched animals (Table 1). These discharges were blocked reversibly by atropine (Fig. 1) [see also (8)]. An animal was considered "eserine responsive" in Table 1 if interictal discharges were induced in at least one slice of a sample of usually five to six slices, during a recording session lasting ≤30 min after the onset of eserine perfusion (a slice was considered "eserine negative" if, after this time, spontaneous discharges were not observed).

To investigate short- and long-term changes in hippocampal physiology (8), two survival periods were chosen, 7–12 and 40–50 days, respectively. A comparison of hippocampal slices prepared after a short or a long survival time after a PTZ-induced convulsion at P18–P20 revealed that the excitatory effects of eserine were expressed in consistently more animals or slices per total tested, after the long survival time (Table 1). Eserine-induced synchronous CA3 interictal-like discharges could be recorded as late as 7 months postnatally in

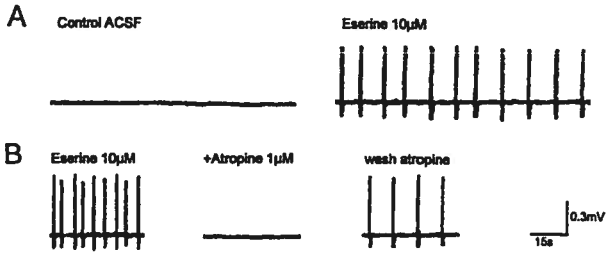


**FIG. 1.** Excitatory effect of eserine in a P67 hippocampal slice taken from an animal injected with pentylenetetrazol (PTZ) at P20. **A:** Bath application of 10 $\mu M$ eserine provoked spontaneous interictal-like discharges recorded extracellularly from the CA3 pyramidal layer. **B:** In a different slice (PTZ injection at P20, recording at P71), the muscarinic antagonist atropine reversed the excitatory effects of eserine; the effect of atropine was partially reversed after 10-min washout.

slices (five of 11) from two rats treated with PTZ at P20, suggesting a permanent effect. In 14 pups injected with PTZ at P20 after pretreatment with PTB, which prevented all behavioral epileptic manifestations in the 2 h of observation after PTZ injection, eserine induced spontaneous discharges in only two slices (each from a different animal) out of 67, a statistically significant difference compared with the non-sedated age-matched groups (Table 1). As also shown in Table 1, the incidence of eserine-induced interictal discharges in slices from six adult rats, in which seizures had been induced by kainate at P18, was significantly lower compared with

**TABLE 1.** *Number of rats or of hippocampal slices per total tested, in which the anticholinesterase eserine (10 µM) induced spontaneous CA3 interictal discharges*

| Drug injected (age of rat) | Postinjection interval | Eserine-responsive rats | Eserine-responsive hippocampal slices |
|---|---|---|---|
| Immature (P18–P20) | | | |
| PTZ | Short | 4/11, 36% (1) | 11/39, 28% (2) |
| PTZ | Long | 8/8, 100% (3)<br>(1) vs. (3), p = 0.013 | 16/40, 40% (4)<br>(2) vs. (4), NS |
| Pentobarbital + PTZ | Short | 2/7, 29% (5)<br>(1) vs. (5) NS | 2/32, 6% (6)<br>(2) vs. (6) p = 0.028 |
| Pentobarbital + PTZ | Long | 2/7, 29% (7)<br>(3) vs. (7), p = 0.007 | 2/35, 6% (8)<br>(4) vs. (8), p = 0.0008 |
| Kainic acid | Long | 2/6, 33% (9)<br>(3) vs. (9), p = 0.015 | 2/21, 9% (10)<br>(4) vs. (10), p = 0.017 |
| Saline injection/naive | Short | 0/9 | 0/46 |
| Saline injection/naive | Long | 0/7 | 0/36 |
| Adult (P60) | | | |
| PTZ | Short | 8/10, 80% (11)<br>(1) vs. (11), NS | 15/58, 26% (12)<br>(2) vs. (12), NS |
| PTZ | Long | 2/9, 22% (13)<br>(3) vs. (13), p = 0.002<br>(11) vs. (13), p = 0.02 | 2/40, 5% (14)<br>(4) vs. (14), p = 0.0003<br>(12) vs. (14), p = 0.007 |
| Saline injection/naive | Long | 0/6 | 0/31 |

The variables tested were age of the animal, type of convulsant (PTZ vs. kainate), and interval between seizure and in vitro recording (short, 7–12 days; or long, 40–50 days). Saline-injected or naive age-matched animals were used as controls.

(1)–(14), statistical significance of differences between the number of eserine-sensitive animals or slices per total was assessed by Fisher's exact test ($\chi^2$ for two pairs of numbers).

PTZ, pentylenetetrazol; NS, not significant.

that in rats treated at the same age with PTZ. Eserine had no excitatory effect in any slice (0 of 46, 0 of 36) from 16 age-matched controls (Table 1).

In slices from 19 rats injected with PTZ as adults (P60), interictal-like discharges occurred at a rate of 0.22 ± 0.02 Hz on exposure to eserine (n = 14; three slices were not included in this measurement because the discharges were sporadic). Such discharges were observed mostly after short-term and had practically disappeared after long-term survival (Table 1). No excitatory effect of eserine was seen in any slice (0 of 31) from six age-matched controls (Table 1).

We also tested whether the presence of an excitatory effect of eserine correlated with the duration of the PTZ convulsion by computing the mean seizure duration in animals that later responded to eserine with spontaneous activity *in vitro* versus those that did not, in both groups (adult, immature). As shown in Fig. 2A, the seizure duration was similar for eserine-responsive versus nonresponsive animals, in line with the observation that spontaneous discharges could be observed in slices from animals with the shortest duration of generalized convulsion (2–3 min), and absent in slices from other animals having convulsed >30 min. Slices from all adult (three) and immature (four) rats having had 1- to 5-min brief PTZ-induced convulsions (Fig. 2A) exhibited eserine-induced spontaneous discharges after a short (one adult) or a long (two adult, four immature) survival period.

No correlation was noted between the number of eserine-responsive slices per animal versus the seizure duration in the immature and adult groups (Fig. 2B). In both graphs in Fig. 2, short and long survival times were pooled for this analysis, as only two animals yielded eserine-responsive slices in the long term [Table 1, (11)–(14)]. Moreover, in the immature group, eserine-responsive slices were found at both survival periods, with statistically significant differences in the number of animals [(1) vs. (3) in Table 1] but not of slices [(2) vs. (4) in Table 1].

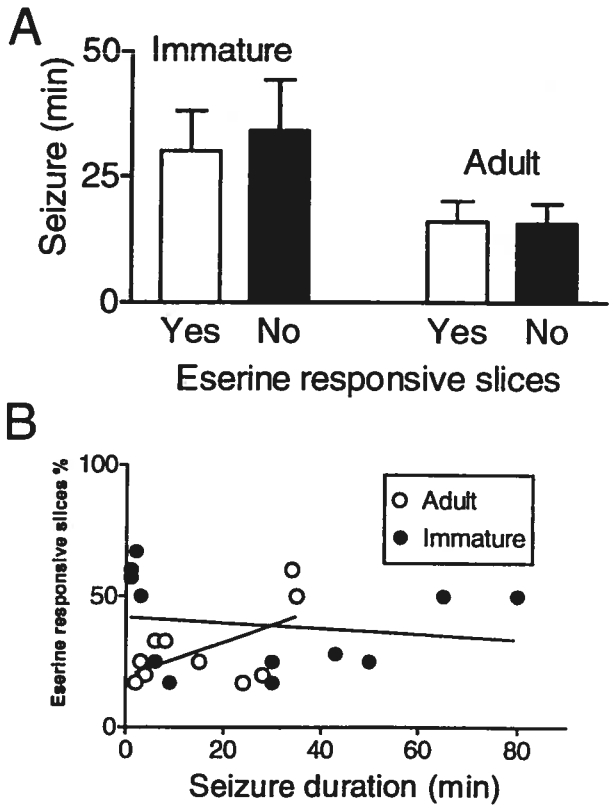


**FIG. 2.** Relation between the duration of the pentylenetetrazol (PTZ)-induced generalized seizure and the incidence of eserine-induced spontaneous CA3 field potentials in hippocampal slices from the same animal. **A:** The duration of seizures was plotted depending on whether eserine induced (Yes) or not (No) spontaneous activity in at least one hippocampal slice per animal. The left and right sets of bars represent data from immature and adult animals, respectively, at the time of PTZ injection. Data for this graph were obtained from immature, n = 15 (Y), n = 5 (N) and adult n = 10 (Y), n = 9 (N) animals. Data from three immature eserine-responsive rats injected at P21–P22 were included in this figure, but not in Table 1. Conversely, data from two immature eserine-nonresponsive rats with brief repetitive generalized seizures were included in Table 1, but not in this figure. Short and long survival times were pooled. **B:** The percentage of eserine-responsive slices per animal is plotted as a function of the duration of the PTZ-induced generalized seizure in the same animal. Only data from animals in which at least one hippocampal slice was eserine responsive were used in this graph (immature, n = 12; adult, n = 10). The slope of the best-fit line (linear regression analysis) passing through the data points of either group was not significantly different from zero, thus indicating absence of correlation between the two parameters.

### Evoked field potentials after pentylenetetrazol-induced convulsions at P18–P20

CA3 responses evoked by mossy fiber stimulation were recorded in six slices from five rats examined at short survival time after PTZ injection at P18–P20, and five age-matched controls. The amplitude and number of population spikes (PSs) and the amplitude and duration of the field EPSP (fEPSP) of control and PTZ slices were very similar in both standard aCSF and after the addition of 10 $\mu M$ of the $GABA_A$ antagonist BMI (Fig. 3A, upper and middle traces). Eserine (10 $\mu M$) in the presence of BMI depressed evoked responses in line with previous findings (20–22). The depressant effects of eserine, expressed as percentage depression of the BMI responses in the two populations of slices, appeared slightly smaller than control in the slices from PTZ-treated animals, but this trend did not reach statistical significance (Fig. 3B).

In the same set of slices, no spontaneous activity was recorded in standard aCSF, whereas BMI induced spontaneous discharges in slices from three of five controls and three of six of the PTZ-treated rats, with similar rates of occurrence. Addition of eserine increased the frequency and/or induced spontaneous discharges in all slices, and this potentiation appeared to be greater in PTZ compared with control slices, a trend that did not reach statistical significance (Fig. 3C).

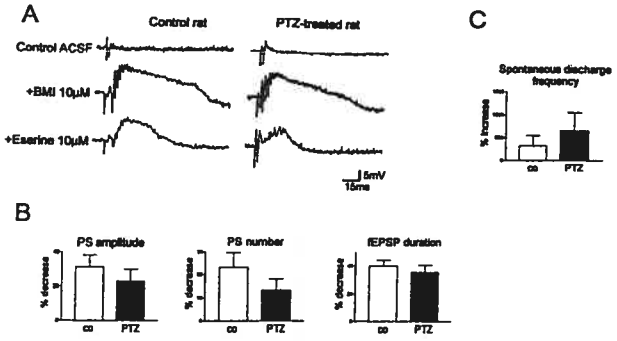


**FIG. 3.** Field potentials recorded in the CA3 pyramidal layer of hippocampal slices after mossy fiber–pathway stimulation and graphs summarizing the effects of eserine on evoked and spontaneous potentials in six slices from five pentylenetetrazol (PTZ)-injected animals and five slices from five age-matched controls. **A:** Averaged traces from a P25 control animal (left) and a P26 animal PTZ-treated at P19 (right). Synaptic responses recorded in standard artificial CSF were very similar (upper traces). Bath application of the γ-aminobutyric acid type A–receptor antagonist bicuculline methiodide (BMI; middle traces) increased the amplitude and duration of the field excitatory postsynaptic potential (fEPSP) as well as the amplitude of the first population spike (PS) and the number of PSs similarly in both groups of slices. Addition of the anticholinesterase eserine-depressed synaptic potentials (lower traces). **B:** The depressant effects of eserine were expressed as percentage decrease of the BMI responses (controls). Eserine had a more pronounced, although not significantly, depressant effect on the amplitude of the first PS, the number of PSs, and the fEPSP duration from PTZ slices. **C:** In the same slices, eserine increased the frequency of spontaneous interictal-like epileptiform discharges in the presence of BMI. This effect was more pronounced in PTZ slices, although this trend did not reach statistical significance.

### Intracellularly recorded synaptic potentials after pentylenetetrazol-induced convulsions at P20

CA3 synaptic potentials evoked after stimulation of the mossy fiber pathway were recorded from nine neurons from six adult animals (P60) treated with PTZ at P20 (PTZ neurons) and 11 neurons from 10 age-matched controls (control neurons). The resting membrane potential (RMP) and the membrane input resistance ($R_{in}$) were similar in all impaled cells (Table 2).

Just-subthreshold synaptic potentials, elicited in standard aCSF (Fig. 4A) were used to determine the following parameters, as described in Experimental procedures: EPSP amplitude, time to peak and duration, the early or fast $GABA_A$-dependent IPSP and the late or slow $GABA_B$-dependent IPSP. All had similar mean values in the two groups, with the exception of the fast IPSP, which appeared to be larger in PTZ neurons (Table 2). Furthermore, the falling (hyperpolarizing) and rising (repolarizing) slopes of the fast IPSP proved to be significantly larger in PTZ neurons (Table 2). The reversal potential of the $GABA_A$ IPSP was calculated by recording synaptic responses at four to five different membrane potentials, as shown in Fig. 4B, and by plotting the 30-ms poststimulus $GABA_A$ IPSP amplitude versus membrane potential. Linear regression analysis was used to establish the best fit through these data points, and from this line, the membrane potential corresponding to 0mV amplitude as the apparent reversal potential of the $GABA_A$ IPSP. Data obtained in this way from three PTZ and two control neurons were similar (not shown).

Monosynaptic $GABA_A$ IPSPs were recorded from the same neurons in the presence of the glutamate receptor antagonists APV (10 µ*M*) and CNQX (10 µ*M*), and monosynaptic $GABA_B$ IPSPs were recorded after the addition of the $GABA_A$-receptor antagonist BMI (10 µ*M*). No differences were found in mean values for any of these parameters between PTZ and control neurons (Table 2).

### Density of acetylcholine innervation in adult hippocampus after pentylenetetrazol-induced convulsions at P20

In adult PTZ-injected rats (at P20) and their controls, the pattern of distribution of ChAT-immunostained axons in the dorsal hippocampus was identical on both sides of the brain and similar to that previously described and quantified in normal Sprague–Dawley rat (14). As illustrated here for CA3 (Fig. 5A–D), no hint of a difference was seen in the number of varicosities per unit length of ChAT-immunostained axon, or in the size of immunoreactive varicosities, between control and treated rat. Nor was there any significant difference in the average length of ACh axons per 2,500 $\mu m^2$ section in the three hippocampal sectors examined (CA1, CA3, DG) and their various layers (Fig. 5E).

### Endogenous acetylcholine and γ-aminobutyric acid in adult hippocampus after pentylenetetrazol-induced convulsions at P20

One assay was conducted to determine the hippocampal content of ACh, and two assays, to determine that of GABA. The results obtained are shown in Table 3. No apparent difference was found in the hippocampal content of either neurotransmitter between adult rats in which convulsions had been induced at P20 and age-matched controls.

## DISCUSSION

This study confirms that PTZ-induced convulsions in the immature rat provoke a long-term change in cholinergic–muscarinic neurotransmission in the CA3 hippocampal area, whereas similar seizures in adult animals produce such an effect only transiently. This change is neither the indirect result of a decrease in IPSPs or in endogenous GABA levels, nor that of an increase in density of hippocampal ACh innervation or in endogenous ACh. It is therefore likely the result of a permanent increase in the expression of muscarinic receptors, and/or their coupling to G proteins, which remains to be determined.

**TABLE 2.** *Intrinsic properties and characteristics recorded from hippocampal CA3 pyramidal neurons of control and PTZ-injected (at P20) adult rats*

| | Control neurons (n = 11) | PTZ neurons (n = 9) |
|---|---|---|
| RMP (mV) | −64 ± 2 | −62 ± 3 |
| $R_{in}$ (MΩ) | 32 ± 3 | 25 ± 4 |
| EPSP amplitude (mV) | 4.3 ± 1.4 | 5.0 ± 1.3 |
| Time to EPSP peak (ms) | 6.8 ± 1.1 | 7.8 ± 0.6 |
| EPSP duration (ms) | 12.2 ± 2.8 | 13.4 ± 1.8 |
| IPSPs in standard aCSF | | |
| Fast ($GAGA_A$) (mV) | 3.1 ± 0.7 | 4.1 ± 1.0 |
| Fast IPSP falling slope (mV/ms) | −2.22 ± 0.12 | −3.56 ± 0.12 ($p < 0.0001$) |
| Fast IPSP rising slope (mV/ms) | 0.52 ± 0.12 | 1.11 ± 0.16 ($p = 0.0075$) |
| Slow ($GABA_B$) (mV) | 6.9 ± 1.5 | 5.5 ± 1.3 |
| IPSPs in APV and CNQX | | |
| Fast ($GABA_A$) (mV) | 4.3 ± 1.0 | 4.4 ± 0.7 |
| Slow ($GABA_B$) (mV) | 5.7 ± 1.0 | 6.1 ± 1.5 |
| IPSPs in APV, CNQX, and BMI | | |
| Slow ($GABA_B$) (mV) | 5.0 ± 0.8 | 5.2 ± 1.4 |

Amplitude (mV), in standard aCSF (di- or polysynaptic IPSPs), in the presence of the glutamate-receptor antagonists APV and CNQX (monosynaptic IPSPs), and after the addition of the $GABA_A$-receptor antagonist BMI (monosynaptic $GABA_B$ IPSP). Differences from control were analyzed with the two-tailed *t* test for unpaired samples.

RMP, resting membrane potential; EPSP, excitatory postsynaptic potential; IPSP, inhibitory postsynaptic potential; aCSF, artificial cerebrospinal fluid; GABA, γ-aminobutyric acid; BMI, bicuculline methiodide; APV, D(−)-2-amino-5-phosphonopeutanoic acid; CNQX, 6-cyano-7-nitroquinoxaline-2,3-dione.

### Convulsant effects of pentylenetetrazol

The $GABA_A$ channel blocker PTZ was chosen as convulsant agent because it is rapidly absorbed and completely bioavailable in immature and adult CNS, without any significant age-related trends in its systemic kinetics (23); it has a short half-life [2.5–3.8 h (24, 25)] in rodent brain, and its effects disappear from the EEG after 24 h (26); it generates reliably major seizures throughout maturation (27–29), and its $CD_{50}$ (dose required to induce seizures in 50% of the animals tested) or the threshold brain concentration to provoke a seizure is similar in P20 and adult rats (23,30).

PTZ-induced epileptic manifestations culminated rapidly into generalized seizures, the duration of which varied between individuals, but tended to be longer in immature compared with adult animals, as in other experimental models [e.g., kainate-induced status epilepticus (31), tetanus toxin convulsions (32)]. As PTZ seizures were defined behaviorally and not electrographically, it could not be excluded that their actual duration was longer than measured.

### Eserine effects in vitro

The interictal-like epileptiform discharges observed in eserine-exposed hippocampal slices from rats in which a PTZ seizure had been induced, but not in age-matched controls, suggested an enhancement of cholinergic neurotransmission. As previously shown (8), these discharges were blocked by the muscarinic antagonist atropine, indicating that they depended on endogenous ACh acting on muscarinic receptors. During $GABA_A$ inhibition block, eserine depressed the evoked and increased the incidence or frequency of spontaneous excitatory potentials (Fig. 3B and C), in line with earlier findings (20,22). This depressant effect was slightly weaker and the excitatory slightly stronger in PTZ slices compared with controls, a trend that did not reach sta-

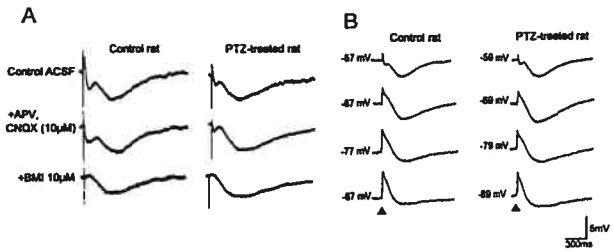


**FIG. 4.** Synaptic responses recorded intracellularly from the CA3 pyramidal layer after mossy fiber pathway stimulation. **A:** Recordings were made in a P64 control neuron [resting membrane potential (RMP), −63 mV, left] and a P69 PTZ neuron (RMP, −59 mV, right) of a PTZ treated animal at P20. Stimulation intensity was adjusted to induce the maximal amplitude excitatory postsynaptic potential (EPSP) and inhibitory PSP (IPSP) in the absence of an action potential (just subthreshold). First, synaptic responses were recorded in standard artificial CSF (upper traces). Monosynaptic IPSPs were recorded after the addition of glutamate receptor antagonists APV acid and CNQX, which blocked excitatory transmission (middle traces; notice the disappearance of the fast positive deflection after the artifact of stimulation, EPSP). Monosynaptic γ-aminobutyric acid $(GABA)_B$ IPSPs were recorded in isolation after the addition of the $GABA_A$ antagonist BMI to the aCSF (lower traces; notice the disappearance of the fast negative deflection after the artifact of stimulation, $GABA_A$ IPSP). **B:** Amplitude of $GABA_A$-mediated IPSP recorded in a P74 control (RMP, −57 mV, left) and a P81 PTZ neuron (RMP, −59 mV, right; from an animal PTZ-treated at P20) in standard aCSF at four different membrane potentials. $GABA_A$ IPSP amplitude was measured at 30 ms after stimulus and was plotted as a function of membrane potential to determine its apparent reversal potential (not shown).

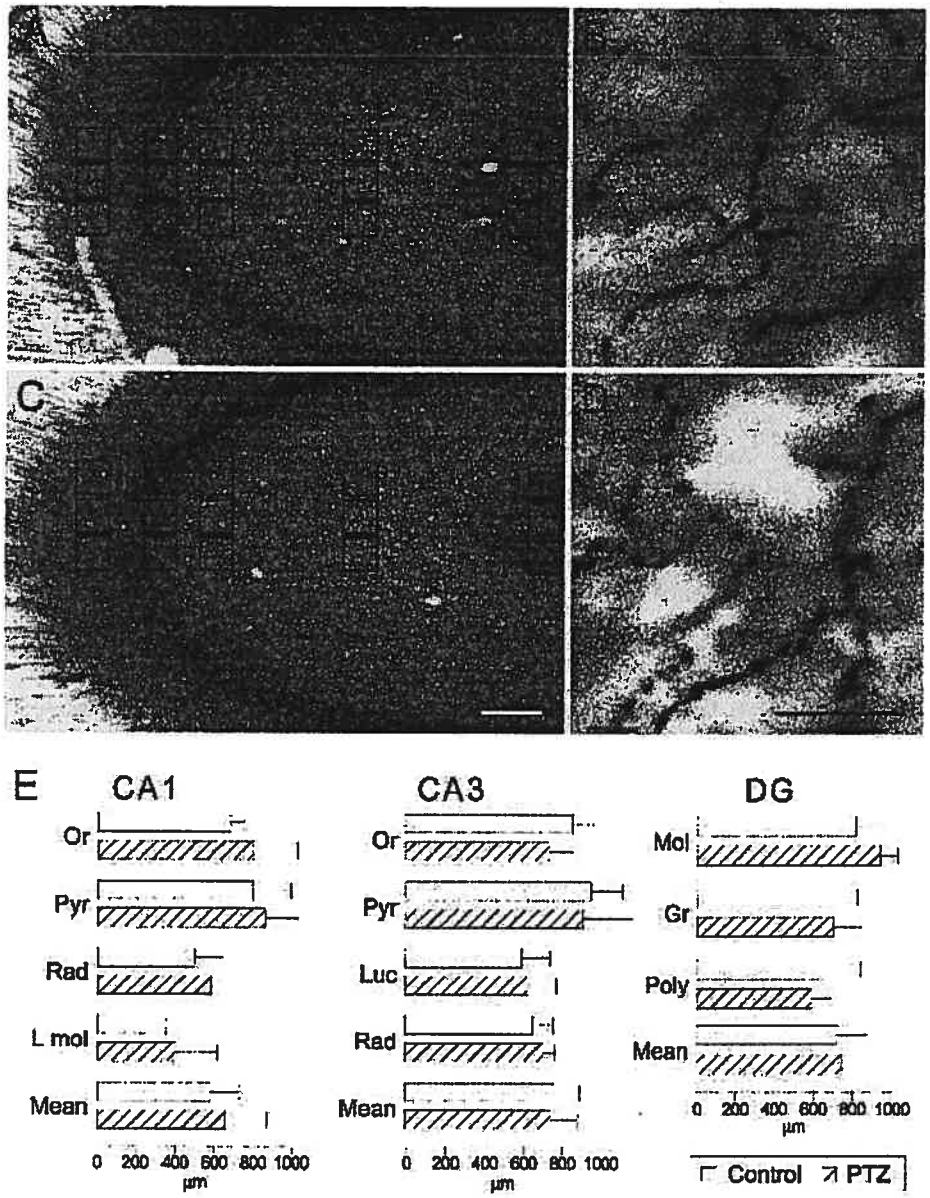


**FIG. 5.** Distribution and density of acetylcholine innervation [choline acetyltransferase (ChAT)-immunostained axons] in the dorsal hippocampus of control and pentylenetetrazol (PTZ)-injected (at P20) adult rats. **A–D:** Digitized light-microscopic images of the whole CA3 sector **(A, C)** and of one sampling window in the stratum radiatum **(B, D)** from a control **(A, B)** and a PTZ-injected animal **(C, D).** The rows in squares in **A** and **C** represent the sampling windows, 50 µm in side, from which length measurements of the ChAT-immunostained axons were obtained for the different hippocampal layers. In **B** and **D,** note the similar appearance of the ChAT-immunostained varicose axons in the control and the experimental condition. The histograms at bottom **(E)** are means ± SEM for length of ChAT-immunostained axons per sampling window in CA1, CA3, and dentate gyrus of control and PTZ-treated rats, as explained in Experimental procedures. Or, oriens; Pyr, pyramidale; Rad, radiatum; L mol, lacunosum moleculare; Luc, lucidum; Mol, moleculare; Gr, granulare; Poly, polymorph. Scale bars for **A** and **C,** 100 µm in **C;** for **B** and **D,** 10 µm in **D.**

tistical significance. It remains to be determined which of the different subtypes of muscarinic receptors present in hippocampus (33) might mediate such depressant and excitatory actions of ACh [see also discussion in (21)].

**TABLE 3.** *Endogenous ACh and GABA concentrations in the hippocampi of control and PTZ-injected (at P20) adult rats*

| | Control (n = 6) | PTZ (n = 6)[a] | Ratio |
|---|---|---|---|
| ACh (n*M*) | 1.42 ± 0.09 | 1.29 ± 0.05 | 91% |
| GABA (n*M*) | 3.61 ± 0.27 | 4.21 ± 0.11 | 117% |
| | 5.42 ± 0.76 | 4.18 ± 0.28 | 77% |

[a] Number of hippocampi.

ACh, acetylcholine; GABA, γ-aminobutyric acid; PTZ, pentylenetetrazol.

## Eserine effects as the result of pentylenetetrazol seizures

It has been shown that PTZ seizures in immature rats do not result in neuronal damage (27). Prevention of the PTZ seizures by pretreatment with PTB reduced significantly the incidence of the excitatory effect of eserine in both the short and the long term (Table 1), indicating a change that resulted from the PTZ seizure and not the PTZ administration per se. Eserine, however, induced interictal discharges in a small number of slices (four of 67) from PTB-sedated animals (Table 1). This finding could be explained by the somewhat longer half-life of PTZ (28,34) compared with DTB sedation (~2 h), which may have permitted PTZ to induce a convulsion after recovery from sedation. In addition, the PTB-treated ani-

mals may have experienced electrographic, behaviorally undetectable, PTZ seizures.

The incidence of eserine-provoked spontaneous field potentials was significantly lower in hippocampal slices from animals in which seizures had been provoked by kainate instead of PTZ (Table 1). Although both convulsants did provoke long-lasting epileptic manifestations, the episodes of generalized seizures after kainate were very brief compared with those after PTZ. This suggested that the resulting change, at least in the long term, also was dependent on the type of seizure and/or the mechanism of its generation.

Not all hippocampal slices from "eserine-responsive" animals showed epileptiform activity in the presence of eserine. This could reflect differences in preparative technique, but also reported differences in excitability along the dorsoventral axis of hippocampus (35,36).

**The permanence of eserine effects after immature versus adult seizures**

Whereas the proconvulsant effect of eserine was detectable in slices from both immature and adult rats after a PTZ seizure, its incidence increased markedly with survival time in the animals having convulsed as immature, and the reverse was true in those having convulsed as adults (Table 1). This suggested that the state of brain maturation was a major determinant of the increase in cholinergic responsiveness, and hence the plasticity of cholinergic transmission after seizures.

The duration of PTZ-induced generalized seizures was not correlated with the subsequent occurrence of eserine-induced interictal-like discharges in either the immature or adult group (Fig. 2A and B). It could not be excluded that the longer seizures in immature versus adult animals may have contributed to the high incidence of long-term eserine effect in the immature group. However, in the short term, eserine-induced discharges were observed in slices from nearly all adult animals having had short generalized seizures, but only one third of slices from immature animals having had longer generalized seizures (Table 1).

PTZ seizures in immature animals induced during the third postnatal week led to a higher incidence of eserine proconvulsant effect in the long term, compared with PTZ seizures in the second postnatal week (8). This, together with the reported enhanced susceptibility to pilocarpine-induced seizures during the third postnatal week (37), suggests a particular vulnerability at this time of the mechanism responsible for the long-term enhancement of cholinergic transmission.

**Cellular mechanisms underlying the excitatory effects of eserine**

*Synaptic excitation*

Independent of the duration of survival, spontaneous discharges were not recorded from PTZ slices bathed in standard aCSF, ruling out a general increase in excitation or breakdown of inhibition in this model. This was at variance with the findings of Lee et al. (38), who recorded interictal spikes in the CA3 area of aCSF-bathed hippocampal slices from adult animals subjected to tetanus toxin seizures when immature. Such a discrepancy emphasizes eventual model-dependent differences in the long-term outcome of early life seizures. The fact that field excitatory potentials recorded after $GABA_A$-receptor block by BMI, as well as intracellular subthreshold excitatory potentials recorded in standard aCSF, were similar in PTZ and control slices further argues against any generalized increase in excitation (e.g., glutamatergic).

*Synaptic inhibition and endogenous γ-aminobutyric acid*

Earlier evidence for decreases in GABAergic inhibition after PTZ seizures (39) or on changes in ACh release (40,41) prompted us to examine IPSPs in CA3 neurons from PTZ-treated animals. We compared poly- or monosynaptic $GABA_A$ and $GABA_B$ IPSPs, because earlier reports had suggested differential long-term effects of seizures on these responses [poly- vs. monosynaptic IPSPs (38); $GABA_A$ vs. $GABA_B$ IPSPs (42)]. Our experiments revealed no differences in either $GABA_A$ (monosynaptic) or $GABA_B$ (di- or monosynaptic) IPSPs between CA3 neurons from PTZ-treated and control rats. In addition, we found a marginally larger amplitude and increased slope of (rate of rise) $GABA_A$ IPSP in PTZ neurons (Table 2), which suggested a possible increase in feedforward and/or recurrent $GABA_A$-mediated inhibition. Together with the unchanged endogenous hippocampal GABA levels measured by HPLC/electrospray ionization, these findings rule out an impairment of GABAergic inhibition in the CA3 area from PTZ-treated animals, at least *in vitro*. Similar results (i.e., a lack of changes in adult synaptic inhibition after seizures during maturation) were previously reported in this same model (43) (PTZ seizure at P21) and after flurothyl seizures induced neonatally (2,44).

*Density of acetylcholine innervation and endogenous acetylcholine*

In spite of the earlier report of a seizure-induced sprouting of cholinergic axons in adult rat hippocampus (45), the detailed quantitative assessment of ACh innervation density in the dorsal hippocampus of adult rats PTZ treated at P20 did not demonstrate any significant difference from control, ruling out such a change as the eventual cause of the observed eserine effects. The lack of increase in hippocampal ACh content, as measured by HPLC/electrospray ionization, was in keeping with this negative finding. The lack of change in ACh content and density of ACh innervation does not preclude a possible increase in spontaneous or evoked ACh release if accompanied by an increase in catabolism (46). This could

underlie the eserine-induced epileptiform activity, especially if combined with glutamatergic axon sprouting (30) [review in (47)]. In this line of thinking, it is noteworthy that hippocampal ACh release has been reported to increase right before seizures (48), suggesting a cholinergic amplification of glutamatergic excitation as the underlying mechanism. Stress-induced changes in AChE activities also have been described (46). A presumed increase in the postseizure activity of AChE would limit ACh effects, which would then appear larger in the presence of an AChE inhibitor. However, such a mechanism would tend to amplify all ACh effects, contrary to our observations suggesting a muscarinic effect [see also (20,22)].

*Other avenues*

In this context, it appears more likely that the *in vitro* excitatory effect of eserine represents a change in expression and/or second-messenger cascade of muscarinic-receptor subtypes in hippocampus. Postseizure increases in the expression of hippocampal muscarinic receptors have already been reported (49), and might be demonstrable in the present model by in situ hybridization. A possible increase in the coupling of muscarinic receptors also could be investigated by using the [$^{25}$S]guanosine triphosphate (GTP)γS autoradiographic technique after activation with a muscarinic-receptor agonist.

**Relevance for epileptogenesis**

The occurrence of eserine-induced interictal-like discharges in rats previously subjected to PTZ seizures raises the possibility of epileptogenic effects of endogenous ACh in this model. Although no current proof exists that such an effect is linked to increased incidence of seizures *in vivo,* several lines of evidence link a potentiation of hippocampal cholinergic neurotransmission to epilepsy. Repeated carbachol injections into amygdala cause chemical kindling (50); elevation of hippocampal ACh levels potentiates PTZ-induced convulsions (51); and intrahippocampal grafts of ACh-rich fetal basal forebrain are epileptogenic (52). Moreover, microinjection of cholinergic agents into the inferior colliculus, the initiation site for audiogenic seizures, provokes convulsions (53), whereas on the contrary, the development of (amygdalar) kindling is retarded by the muscarinic antagonist atropine (54).

The eserine effect also could signify an abnormal cholinergic response affecting other ACh-related functions or behavior. For example, impaired development of spatial memory was recently reported in rat pups subjected to repeated PTZ seizures, in a protocol similar to ours, but in the apparent absence of changes in seizure threshold (55). Given the pivotal role of ACh in brain function, the present model may eventually help to establish a much needed link between early life seizures and cognitive development.

**Acknowledgment:** This project was funded by NSERC and Savoy Foundation for Epilepsy (C.P.), CIHR grant MT-3544 (L.D.), and Ste-Justine Hospital Research Centre (studentship to S.M.). Our thanks to Ms. C. Garofalo (Dr. E. Levy) for her assistance with the tissue sample preparation for the assessment of ACh and GABA and Ms. Danielle Dennie (Dr. O. Mamer) for the actual test.

## REFERENCES

1. McNamara J. Emerging insights into the genesis of epilepsy. *Nature* 1999;399:A15–22.
2. Huang L, Cilio MR, Silveira CD, et al. Long-term effects of neonatal seizures: a behavioral, electrophysiological, and histological study. *Dev Brain Res* 1999;118:99–107.
3. Mathern GW, Pretorius JK, Babb TL. Influence of the type of initial precipitating injury and at what age it occurs on course and outcome in patients with temporal lobe seizures. *J Neurosurg* 1995;82:220–7.
4. Schmid R, Tandon P, Stafstrom C, et al. Effects of neonatal seizures on subsequent seizure-induced brain injury. *Neurology* 1999; 53:1754–61.
5. Vernadakis A, Woodbury DM. The developing animal as a model. *Epilepsia* 1969;10:163–78.
6. Traynelis SF, Dingledine R. Potassium-induced spontaneous electrographic seizures in the rat hippocampal slice. *J Neurophysiol* 1988;59:259–76.
7. Wada JA, Sato M, Corcoran ME. Persistent seizure susceptibility and recurrent spontaneous seizures in kindled cats. *Epilepsia* 1974; 15:465–78.
8. Meilleur SL, Carmant L, Psarropoulou C. Immature rat convulsions and long term effects on hippocampal cholinergic neurotransmission. *Neuroreport* 2000;11:521–4.
9. Acquas E, Wilson C, Fibiger H. Conditioned and unconditioned stimuli increase frontal cortical and hippocampal acetylcholine release: effects of novelty, habituation and fear. *J Neurosci* 1996;16: 3089–96.
10. Moor E, Schirm E, Jacso J, et al. Involvement of medial septal glutamate and $GABA_A$ receptors in behaviour-induced acetylcholine release in the hippocampus: a dual probe microdialysis study. *Brain Res* 1998;789:1–8.
11. Gardner C, Webster R. Convulsant-anticonvulsant interactions on seizure activity and cortical acetylcholine release. *Eur J Pharmacol* 1977;42:247–56.
12. Imperato A, Dazzi L, Carta G, et al. Rapid increase in basal acetylcholine release in the hippocampus of freely moving rats induced by withdrawal from long-term ethanol intoxication. *Brain Res* 1998;784:347–50.
13. Lapchak P, Araujo D, Quirion R, et al. Chronic estradiol treatment alters central cholinergic function in the female rat: effect on choline acetyltransferase activity, acetylcholine content, and nicotinic autoreceptor function. *Brain Res* 1990;525:249–55.
14. Aznavour N, Mechawar N, Descarries L. Comparative analysis of cholinergic innervation in the dorsal hippocampus of adult mouse and rat: a quantitative immunocytochemical study. *Hipppocampus* 2002;12:206–17.
15. Mechawar N, Cozzari C, Descarries L. Cholinergic innervation in adult rat cerebral cortex: a quantitative immunocytochemical description. *J Comp Neurol* 2000;428:305–18.
16. Umbriaco D, Watkins KC, Descarries L, et al. Ultrastructural and morphometric features of the acetylcholine innervation in adult rat parietal cortex: an electron microscopic study in serial sections. *J Comp Neurol* 1994;348:351–73.
17. Paxinos G, Watson C. The rat brain in stereotaxic coordinates. 2nd ed. Orlando, Fla.: 1986.
18. Gaskell S. Electrospray: principles and practice. *J Mass Spectrom* 1997;32:677–88.
19. Acevedo LY, Xu X, Zhang R, et al. Quantification of acetylcholine in cell culture systems by semi-micro high-performance liquid chromatography and electrospray ionization mass spectrometry. *J Mass Spectrom* 1996;31:1399–402.
20. Gruslin E, Descombes S, Psarropoulou C. Epileptiform activity generated by endogenous acetylcholine during blockade of

GABAergic inhibition in immature and adult rat hippocampus. *Brain Res* 1999;835:290–7.
21. Psarropoulou C, Beaucher J, Harnois C. Comparison of the effects of MI and M2 muscarinic receptor activation in the absence of GABAergic inhibition in immature rat hippocampal CA3 area. *Dev Brain Res* 1998;107:285–90.
22. Psarropoulou C, Dallaire F. Activation of muscarinic receptors during blockade of $GABA_A$-mediated inhibition induces synchronous epileptiform activity in immature rat hippocampus. *Neuroscience* 1998;82:1067–77.
23. Haberer L, Pollack G. Central nervous system uptake kinetics of pentylenetetrazol in the developing rat. *Biopharm Drug Dispos* 1991;12:59–71.
24. Esplin D, Woodbury D. The fate and excretion of $^{14}C$-labelled pentylenetetrazol in the rat with comments on analytical methods. *J Pharmacol Exp Ther* 1957;118:129.
25. Vohland H, Koransky W. Effect of hexachlorocyclohexane on metabolism and excretion of pentazol (Metrazol) in the rat. *Naunyn Schmiedebergs Arch Pharmacol* 1972;273:99–108.
26. Halonen T, Pitkanen A, Partanen J, et al. Amino acid levels in cerebrospinal fluid of rats after administration of pentylenetetrazol. *Comp Biochem Physiol* 1992;101C:21–5.
27. Nehlig A, Pereira de Vasconcelos A. The model of pentylenetetrazol-induced status epilepticus in the immature rat: short- and long-term effects. *Epilepsy Res* 1996;26:93–103.
28. Velisek L, Kubova H, Pohl M, et al. Pentylenetetrazol-induced seizures in rats: an ontogenetic study. *Naunyn Schmiedebergs Arch Pharmacol* 1992;346:588–91.
29. Weller A, Mostofsky DI. Ontogenetic development and pentylenetetrazol seizure thresholds in rats. *Physiol Behav* 1995;57:629–31.
30. Holmes GL, Sarkisian M, Ben-Ari Y, et al. Mossy fiber sprouting after recurrent seizures during early development in rats. *J Comp Neurol* 1999;404:537–53.
31. Carmant L, Liu Z, Werner S, et al. Effect of kainic-acid induced status epilepticus on inositol-triphosphate and seizure-induced brain damage in mature and immature animals. *Dev Brain Res* 1995;89:67–72.
32. Anderson A, Hrachovy R, Swann J. Increased susceptibility to tetanus toxin-induced seizures in immature rats. *Epilepsy Res* 1997;26:433–42.
33. Rouse ST, Marino MJ, Potter LT, et al. Muscarinic receptor subtypes involved in hippocampal circuits. *Life Sci* 1999;64:501–9.
34. Lal H, Mann PA Jr, Shearman GT, et al. Effect of acute and chronic pentylenetetrazol treatment on benzodiazepine and cholinergic receptor binding in rat brain. *Eur J Pharmacol* 1981; 75:115–9.
35. Lothman EW, Bertram EH III, Stringer JL. Functional anatomy of hippocampal seizures. *Prog Neurobiol* 1991;37:1–82.
36. Papatheodoropoulos C, Kostopoulos G. Spontaneous GABA(A)-dependent synchronous periodic activity in adult rat ventral hippocampal slices. *Neurosci Lett* 2002;319:17–20.
37. Turski L, Ikonomidou C, Turski WA, et al. Review: cholinergic mechanisms and epileptogenesis: the seizures induced by pilocarpine: a novel experimental model of intractable epilepsy. *Synapse* 1989;3:154–71.
38. Lee C, Hrachovy R, Smith K, et al. Tetanus toxin-induced seizures in infant rats and their effects on hippocamapal excitability in adulthood. *Brain Res* 1995;677:97–109.
39. Psarropoulou C, Matsokis N, Angelatou F, et al. Pentylenetetrazol-induced seizures decrease GABA-mediated recurrent inhibition and enhance adenosine-mediated depression. *Epilepsia* 1994;35: 12–9.
40. Imperato A, Dazzi L, Obinu MC, et al. Inhibition of hippocampal acetylcholine release by benzodiazepines: antagonism by flumazenil. *Eur J Pharmacol* 1993;238:135–7.
41. Roussinov K, Lazarova M. On some relationships between gamma-aminobutyric acid (GABA) and the cholinergic mechanisms in pentylenetetrazol convulsions. *Acta Physiol Pharmacol Bulg* 1977;3:28–36.
42. Mangan P, Rempe D, Lothman E. Changes in inhibitory neurotransmission in the CA1 region and dentate gyrus in a chronic model of temporal lobe epilepsy. *J Neurophysiol* 1995;74:829–40.
43. Zhao D, Leung LS, Boon F, et al. Persistent physiological effects caused by a single pentylenetetrazol induced seizure in neonatal rats. *Dev Brain Res* 1994;80:190–8.
44. Holmes GL, Gairsa JL, Chevassus-Au-Louis N, et al. Consequences of neonatal seizures in the rat: morphological and behavioral effects. *Ann Neurol* 1998;44:845–57.
45. Holtzman DM, Lowenstein DH. Selective inhibition of axon outgrowth by antibodies to NGF in a model of temporal lobe epilepsy. *J Neurosci* 1995;15:7062–70.
46. Somani SM, Babu SR, Arneric SP, et al. Effect of cholinesterase inhibitor and exercise on choline acetyltransferase and acetylcholinesterase activities in rat brain regions. *Pharmacol Biochem Behav* 1991;39:337–43.
47. Parent JM, Lowenstein DH. Mossy fiber reorganization in the epileptic hippocampus. *Curr Opin Neurol* 1997;10:103–9.
48. Lallement G, Carpentier P, Collet A, et al. Extracellular acetylcholine changes in rat limbic structures during soman-induced seizures. *Neurotoxicology* 1992;13:557–67.
49. Mingo NS, Cottrell GA, Mendonca A, et al. Amygdala-kindled and electroconvulsive seizures alter hippocampal expression of the M1 and M3 muscarinic cholinergic receptor genes. *Brain Res* 1998; 810:9–15.
50. Vosu H, Wise RA. Cholinergic seizure kindling in the rat: comparison of caudate, amygdala and hippocampus. *Behav Biol* 1975; 13:491–5.
51. Kawasaki K, Eigyo M, Ikeda M, et al. A novel benzodiazepine inverse agonist, S-8510, as a cognitive enhancer. *Prog Neuropsychopharmacol Biol Psychiatry* 1996;20:1413–25.
52. Cassel JC, Kelche C, Will BE. Susceptibility to pentylenetetrazol-induced and audiogenic seizures in rats with selective fimbria-fornix lesions and intrahippocampal septal grafts. *Exp Neurol* 1987;97:564–76.
53. Bagri A, Di Scala G, Sandner G. Myoclonic and tonic seizures elicited by microinjection of cholinergic drugs into the inferior colliculus. *Therapie* 1999;54:589–94.
54. Cain DP, Desborough KA, McKitrick DJ. Retardation of amygdala kindling by antagonism of NMD-aspartate and muscarinic cholinergic receptors: evidence for the summation of excitatory mechanisms in kindling. *Exp Neurol* 1988;100:179–87.
55. Huang LT, Yang SN, Liou CW, et al. Pentylenetetrazol-induced recurrent seizures in rat pups: time course on spatial learning and long-term effects. *Epilepsia* 2002;43:567–73.

## Annexe 2

# THE ACETYLCHOLINE INNERVATION OF CEREBRAL CORTEX: NEW DATA ON ITS NORMAL DEVELOPMENT AND ITS FATE IN THE HAPP$_{SW,IND}$ MOUSE MODEL OF ALZHEIMER'S DISEASE

Publié en ligne 2005

*J Neural Transmission* 112:149-162.

(L Descarries, N Aznavour, E Hamel)

DOI 10.1007/s00702-004-0186-z
J Neural Transm (2004)

Journal of Neural Transmission
Printed in Austria

# The acetylcholine innervation of cerebral cortex: new data on its normal development and its fate in the $hAPP_{SW,IND}$ mouse model of Alzheimer's disease

**L. Descarries[1], N. Aznavour[1], and E. Hamel[2]**

[1] Départements de pathologie et biologie cellulaire et de physiologie, and Centre de recherche en sciences neurologiques, Faculté de médecine, Université de Montréal, and
[2] Complex Neural Systems, Department of Neurology and Neurosurgery, Montreal Neurological Institute, McGill University, Montréal, QC, Canada

Received January 28, 2004; accepted June 3, 2004
Published online July 20, 2004; 

**Summary.** To follow on prior studies of the cerebral cortex, we examined the acetylcholine innervation in the developing hippocampus of rat, by means of light and electron microscopic immunocytochemistry with a highly sensitive antibody against choline acetyltransferease. As in neocortex, the growth of this innervation mostly occurred within the first two weeks after birth. A preliminary ultrastructural survey indicated that a vast majority of these ChAT-immunostained axon varicosities were asynaptic during development as in the adult. In parallel, we quantified the cholinergic innervations of cerebral cortex and hippocampus in transgenic mice overexpressing human β-amyloid peptide ($hAPP_{SW,IND}$). A selective, widespread, plaque independent cholinergic denervation was thus demonstrated, first in hippocampus and then neocortex, in addition to a non-selective, plaque-dependent, local neurotoxic effect of aggregated β-amyloid on ACh and 5-HT axons.

**Keywords:** Cerebral cortex, hippocampus, amyloid, senile plaques, neurodegeneration, denervation.

## Introduction

There is considerable evidence implicating acetylcholine (ACh) in higher brain functions such as attention, learning and memory (Hasselmo and McGaughy, 2004). As suggested in a recent review of phylogenetic and ontogenetic aspects of the ACh neurons innervating the cerebral cortex (Semba, 2004), the basal forebrain ACh system becomes larger and more complex as higher functions are acquired during evolution and during ontogenesis. Immunocytochemical studies

have provided a wealth of information on the distribution and ultrastructural features of the ACh projection in developing and mature rat neocortex (Umbriaco et al., 1994; Mechawar et al., 2000, 2002). The largely asynaptic nature of this innervation has thus been demonstrated, not only in the adult but also during development, emphasizing the importance of diffuse or volume transmission at all stages of its functioning. Similar data have been recently obtained on the ACh innervation of hippocampus, which will be briefly reported in the first part of this paper.

A second part will summarize recent data on the fate of the hippocampal and neocortical ACh innervations in a transgenic mouse model of Alzheimer's disease (AD). ACh neurons of the basal forebrain are known to be precociously and severely affected in AD (Davies and Maloney, 1976; Whitehouse et al., 1982; Geula and Mesulam, 1996; Beach et al., 2000; Mufson et al., 2002), and the resulting ACh defects have been shown to correlate with memory and cognitive impairments (Reinikainen et al., 1990; Bierer et al., 1995; Mesulam, 1998; Auld et al., 2002; Shinotoh et al., 2000). In transgenic mice overexpressing mutated forms of human β-amyloid (Aβ), ACh dysfunctions of varying severity have been described, depending on mouse type and age (Wong et al., 1999; Bronfman et al., 2000; Diez et al., 2000; Jaffar et al., 2001; Hernandez et al., 2001; Boncristiano et al., 2002; Buttini et al., 2002; German et al., 2003; Klingner et al., 2003; Luth et al., 2003). As reported elsewhere (Aznavour et al., 2003; Aucoin et al., 2004), we have recently used quantitative immunocytochemistry to examine the selectivity and extent of an eventual ACh denervation in the hippocampus and cerebral cortex of $hAPP_{SW,IND}$ transgenic mice (line J20 from Mucke et al., 2000), and its temporal relationship with the Aβ pathology. Further insights were thus gained into the pathophysiology of AD.

## Method

The study on developing hippocampus was carried out according to technical protocols previously described in detail (Aznavour et al., 2002, 2003). A total of 24 male Sprague-Dawley rats (Charles River, St-Constant, Québec, Canada), purchased at known ages and kept with their lactating mother under a 12 hr/12 hr light/dark cycle, were used.

For light microscopy, two rats at PO and four rats at P8, P16 and P32 were deeply anesthetized with sodium pentobarbital and perfused through the heart with ice-cold phosphate-buffered saline followed by 4% paraformaldehyde in sodium phosphate buffer. The brain was removed, postfixed overnight in the same solution, and 20-μm thick transverse sections including the dorsal hippocampus were cut with a vibratome and processed for light microscopic immunocytochemistry with a high affinity mouse monoclonal antibody against purified rat brain choline acetyltransferase (ChAT; Cozzari et al., 1990).

In P8, P16 and P32 rats, ChAT-immunostained axon length was measured, and the number of axon varicosities per unit length of immunostained axon counted, at a transverse level corresponding to bregma −3.7 mm in the adult (Swanson, 1992). This was done within vertical strips (240 μm wide) across CA1, CA3 and the dentate gyrus (DG) of dorsal hippocampus, in three square sampling windows (50 μm in side) positioned in each hippocampal layer. Axon length was corrected for angulation of the fibers in the sections (Soghomonian et al., 1987), and expressed in meters per cubic millimeter of tissue (density of axons). Density of axon varicosities (in $10^6$ per cubic millimeter) was calculated by multiplying the density of axons by the number of axon varicosities per unit length of axon.

For electron microscopy, the immunocytochemical protocol was the same as above, except for the addition of 0.25% glutaraldehyde in the fixative solution, initial incubation of the vibratome

sections in a 1% solution of sodium borohydride, and omission of Triton X-100 from all solutions. The immunostained vibratome sections were osmicated, dehydrated in ethanol and propylene oxide, and flat-embedded in Durcupan. Thin sections were obtained from the strata pyramidale and radiatum of CA1, in 4 rats per age (P8, P16, and P32). A large number of ChAT-immunostained axon varicosities (>100) were examined in each rat, at a final magnification of 40 000 X.

The transgenic mice under study carried the $670/671_{KM\rightarrow NL}$ (SW) double mutation and the $717_{V\rightarrow F}$ mutation (IND) ($hAPP_{SW,IND}$, line J20), as originally described by Mucke et al. (2000). Two methods were used to examine and quantify their cholinergic (ChAT-immunostained) and serotonin (5-HT-immunostained) innervations. Initially, frozen sections from 12–14 month-old wild-type (WT) or transgenic mice fixed as above were cut at a transverse level between stereotaxic planes interaural A 1.5 and 1.98 mm (Franklin and Paxinos, 1997), immunostained with anti ChAT (Chemicon) or anti 5-HT antibodies (ImmunoStar), embedded in resin, and processed as 2 µm-thick transverse sections as previously described in detail (Tong and Hamel, 1999). Immunostained axon varicosities were then counted across layers III–V of the parietal cortex and the strata pyramidale (ChAT) or radiatum (5-HT) of CA3 (hippocampus), in photomicrographs printed at X 400.

In 6 and 18 month-old WT and $hAPP_{SW,IND}$ mice, more extensive and detailed quantitative data were sought on material prepared for ChAT immunocytochemistry as in developing rat. In 4 wild-type and 4 transgenic mice at both ages, measurements of ChAT-immunostained axons, as well as counts of axon varicosities per unit length of immunostained axon, were obtained from all layers of CA1, CA3 and DG of hippocampus and from the primary somatosensory area (Par1) of parietal cortex, at a transverse level equivalent to A 1.98 mm (Franklin and Paxinos, 1997). Sections from the same 18 month-old mice were also processed for 5-HT immunostaining (ImmunoStar antibodies) after antigen retrieval (Shi et al., 1991).

In addition, frozen sections from mice at the three ages were stained for amyloid with thioflavin-S (green), and Aβ plaques counted in the hippocampus and cortex by confocal microscopy. Lastly, the relationships between plaques and ACh or 5-HT axon terminals were examined by combined thioflavin-S staining and ChAT or 5-HT immunofluorescence (Chemicon and Immunostar antibodies) detected with Cy3-labeled secondary antibodies (Sigma).

## Results and discussion

### *Cholinergic innervation of the developing hippocampus*

Previous studies have indicated that in rat brain, or in human for that matter, the acetylcholine (ACh) innervation of the hippocampus originates mainly from a small population of cell bodies in the medial septum and nucleus of the vertical limb of the diagonal band of Broca, named groups Ch1 and Ch2 by Mesulam (McKinney et al., 1983; Mesulam et al., 1983; Rye et al., 1984; Amaral and Kurz, 1985; Nyakas et al., 1987; Woolf, 1991). These cells have been estimated to number 385 on each side of the rat brain (McKinney et al., 1983). A few ACh interneurons are also present in the hippocampus of rodents, which might account for 5–10% of its total ACh innervation in rat (Gage et al., 1983; Eckenstein and Baughman, 1987). As reviewed by Semba (2004), the cells of origin of the hippocampal ACh projection are derived from the ganglionic eminence, a bulge on the ventricular wall present during early stages of telencephalic development (Krnjević and Silver, 1966). By combining thymidine autoradiography with ChAT or AChE-immunocytochemistry, it has also been demonstrated that the ACh neurons destined to the medial septum and nucleus of the vertical limb of the diagonal band are born from E12 to E17 in rat, with a peak at E15 (Fine, 1987; Semba and Fibiger, 1988). p75-NGF receptor immunoreactivity (Koh and Loy, 1989) has also been detected as early as E15 in the dorsomedial wall of the embryonic striatal ventricular zone.

According to some of the above studies, septo-hipppocampal fibers reach the hippocampus around E20. In the present study, a few unbranched, ChAT-immunostained fibers, capped with growth cones, were already visible inside

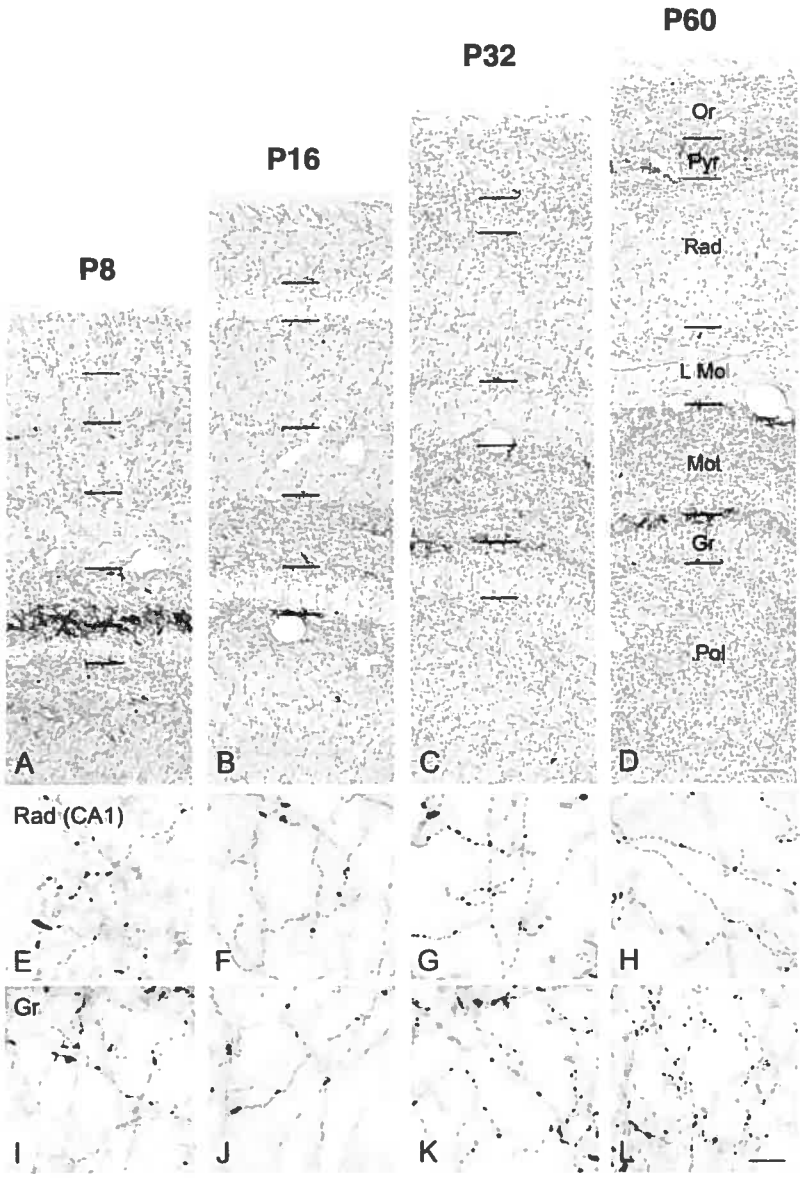


**Fig. 1.** Low- (**A–D**) and higher-power (**E–L**) photomicrographs illustrating the distribution of the ACh innervation in CA1 and the underlying dentate gyrus of dorsal hippocampus at the postnatal ages indicated. The P60 panels, included for comparative purposes, are from adult material previously described in Aznavour et al. (2002). All lower panels, **E–H** and **I–L**, are from the stratum radiatum (Rad) of CA1 and the stratum granulare (Gr) of the dentate gyrus (DG), respectively. Scale bars: 100 µm (**A–D**) and 10 µm (**E–L**). *Or* oriens; *Pyr* pyramidale; *Rad* radiatum, *L Mol* lacunosum moleculare; *Mol* moleculare, *Gr* granulare, *Pol* polymorph

hippocampus at birth (E21 or PO) (not illustrated). During the postnatal period, the ACh innervation was found to grow rapidly, as illustrated in Fig. 1.

At P8, the network of fine varicose ChAT-immunostained axons already extended throughout hippocampus (Fig. 1), but its pattern of laminar distribution did not exactly match that of adult. In the dentate gyrus (DG), notably, the inner third of the molecular layer appeared very densely innervated, perhaps due to growth promoting effects of neurotrophins produced by granule cells (Makuch et al., 2001). Around P16, the ACh innervation was already distributed according to the adult pattern (Aznavour et al., 2002), even if the laminar densities had not yet reached adult values (see below).

In addition to the lengthening and branching of axons, a third parameter characterized the growth of this innervation. As previously demonstrated in the developing cerebral cortex, in hippocampus, the number of axon varicosities per unit length of ACh axon increased steadily from 2.7 per 10 µm at P8 to 4 at P32, a value which then remained constant throughout adulthood. This parameter had to be taken into account when quantifying the density of innervation in actual number of axon varicosities per cubic mm of tissue.

Figure 2 illustrates the actual density of ACh innervation in CA1, CA3 and DG of the dorsal hippocampus from P8 to P60 and in different areas of the neocortex from P4 to P60. Clearly, in hippocampus as well as neocortex, the most rapid growth took place within the first two weeks, and further maturation occurred from P16 to P32, at least in CA1 and the dentate gyrus. As in neocortex, adult densities were reached throughout hippocampus by P32.

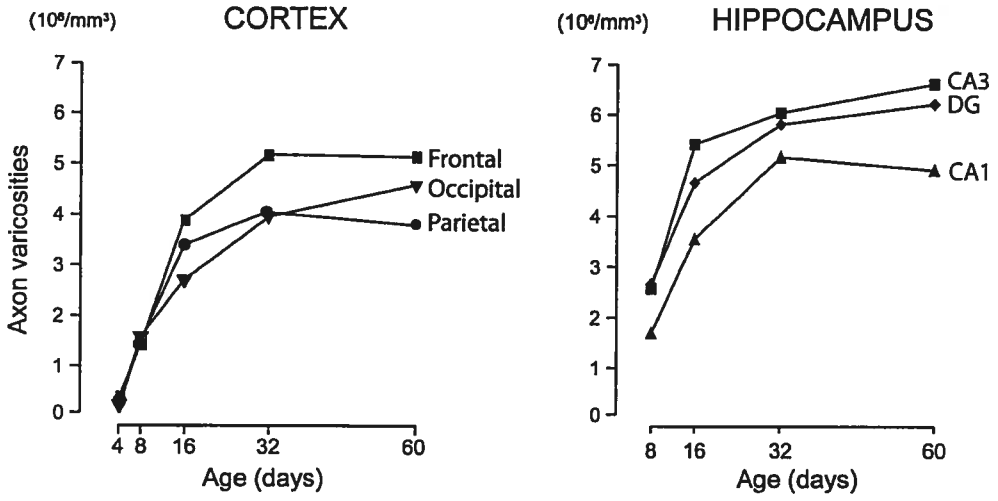


**Fig. 2.** Postnatal increase with age of the average density of ChAT-immunostained axon varicosities ($10^6$ per $mm^3$ of tissue) in the CA1, CA3 and DG regions of dorsal hippocampus (right) compared to three areas of the neocortex (left). The hippocampal values at P60 are from Aznavour et al. (2002). The data for cortex is derived from Mechawar and Descarries (2001). Note the rapid increase in density of ACh innervation during the first two weeks in both hippocampus and cerebral cortex, and the further increase from P16 to P32 in all regions. Except in the occipital cortex, adult density of ACh innervation is reached by P32

These quantitative data confirm our earlier finding of a lower density of ACh innervation in CA1 compared to CA3 and DG of adult rat (Aznavour et al., 2002), as well as the higher average density of ACh innervation in rat hippocampus compared with cerebral cortex at all ages examined. But more importantly, they substantiate the truly phenomenal growth capacities of developing ACh neurons. Based on an estimated hippocampal volume of 36 $mm^3$ at P16 (Coleman et al., 1987; Miki et al., 2002), it may be inferred that, within the first two postnatal weeks, the average Ch1–Ch2 ACh neuron of rat must be producing some 120 cm of axonal arborization bearing 430 000 terminals or varicosities. Thus, on average, these neurons must be capable of generating almost 7.5 centimeters of axon and 27 000 varicosities per day, i.e. more than 3 mm of axon and 1125 varicosities per hour. Such growth rates are even higher than those previously calculated for basalocortical ACh neurons innervating the developing cerebral cortex (Mechawar and Descarries, 2001).

*Ultrastructural features of the hippocampal cholinergic innervation*

We are currently pursuing the ultrastructural examination of the ChAT-immunostained innervation in developing hippocampus. Irrespective of the postnatal age examined, the vast majority of these axon varicosities appear to be asynaptic. In 1995, we have reported a synaptic frequency of 7% for adult rat hippocampal ACh varicosities (Umbriaco et al., 1995), a value extrapolated stereologically from a relatively small sample of single sections from the stratum radiatum of CA1. Our current examination, albeit preliminary, of a much greater number of ChAT-immunostained varicosities in both the strata pyramidale and radiatum of CA1 confirms this exceedingly low synaptic incidence. Whether synaptic or not, the ACh terminals in developing hippocampus are about the same size as in the adult. Their rare synaptic junctions are small and mostly symmetrical, and usually found on dendritic branches rather than spines.

We have already proposed two hypotheses on the basis of the low synaptic incidence of ACh varicosities in different regions of the adult rat brain (Descarries et al., 1997, 2004; Descarries, 1998; Descarries and Mechawar, 2000). The first is that ACh released from non synaptic varicosities might diffuse in the extracellular space to reach distant receptors, located on various elements, neuronal, glial or microvascular, within a sphere of influence around ACh terminals. A complement to this hypothesis is that, in areas densely innervated by ACh terminals, a low ambient level of ACh might be permanently maintained in the extracellular space, which could regulate the expression or sensitivity of ACh or other receptors. Indeed, in the adult as during development, the major molecular form of acetylcholinesterase (AChE) present in the CNS is the tetrameric G4 globular form (Gorenstein et al., 1991). At motor endplates, this molecular form of AChE is thought to regulate levels of ACh spilling over from synaptic junctions (Gisiger and Stephens, 1988), at variance with the T12 form, inserted in the membrane, and which presumably eliminates ACh from synaptic clefts (see Descarries et al., 1997).

For the time being, these studies allow two general conclusions. The first is that, much as its counterpart in cerebral cortex, the ACh innervation of hippocampus develops sooner and more rapidly than was previously suspected.

The second is that diffuse transmission, presumably associated with an ambient level of ACh, may account for much of the influences exerted by ACh on the neurobiological and physiological processes that shape the developing hippocampus.

### *The $hAPP_{SW,IND}$ mouse model*

The $hAPP_{SW,IND}$ mouse line J20, produced by Mucke et al. (2000), carries familial AD-linked, double-swedish and indiana mutations. Mice carrying only the Indiana mutation have already been shown to develop neuritic plaques, reactive gliosis, loss of synaptophysin immunoreactivity, degeneration of nerve fibers and terminals, as well as cognitive deficits (Games et al., 1995; Diez et al., 2000; Dodart et al., 2000; Masliah et al., 2001). In addition, the $hAPP_{SW,IND}$ model has been shown to express even higher levels of beta Aβ protein (Mucke et al., 2000), which affects calcium-dependent pathways in the dentate gyrus and might perhaps explain the cognitive decline observed in this mouse (Palop, 2003).

After staining with thioflavin-S, both the hippocampus and cerebral cortex of transgenic mice in the three age groups displayed Aβ plaques (Fig. 3). These increased in number and size with age, almost 7 fold between 6 and 12–14 months, and more than twenty fold at 18 months. As also shown in Fig. 3

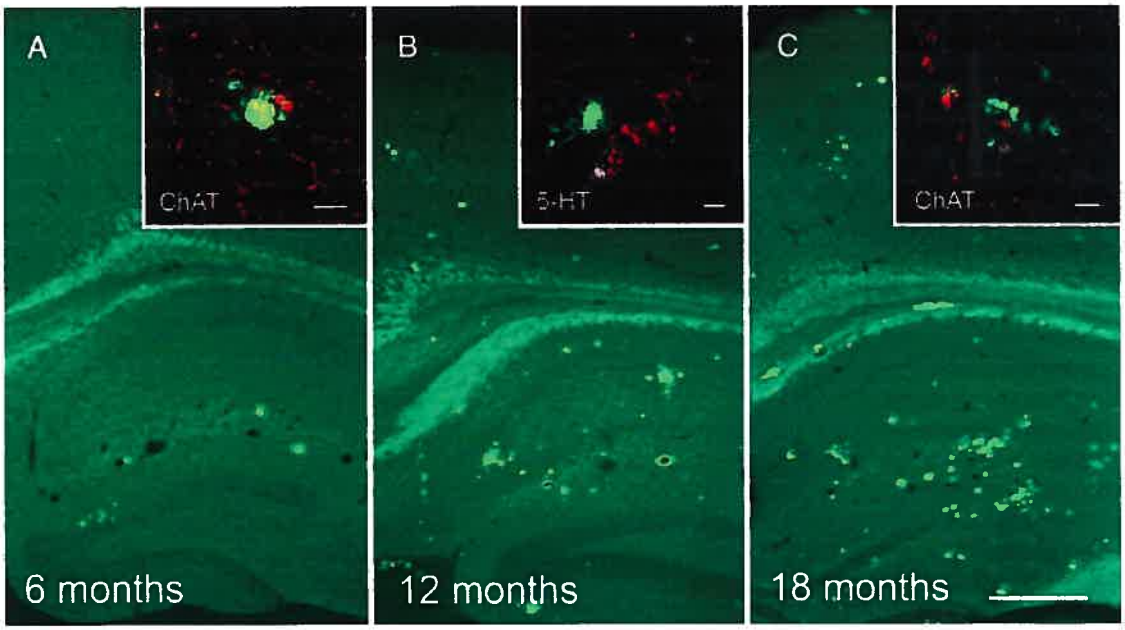


**Fig. 3.** Thioflavin-positive neuritic plaques in the hippocampus and cerebral cortex of 6, 12/14 and 18 month-old $hAPP_{SW,IND}$ mice. Note the increase in the number and size of plaques with age, in both regions. Scale bar: 100 μm. Inserts: Confocal images of swollen, dystrophic ChAT- (in **A** and **C**) or 5-HT-(in **B**) immunofluorescent axons (in red) in the immediate vicinity of thioflavin-positive Aβ plaques (green), in the hippocampus or cerebral cortex of 6, 12 and 18 month-old $hAPP_{SW,IND}$ mice. Note the much smaller, fine varicose, normal looking fibers in the neighboring neuropil. Scale bars: 10 μm

(inserts), double labeling with thioflavin-S (here in green) and ChAT- or serotonin-immunofluorescence (in red) revealed the presence of swollen and distorted ACh and 5-HT axons in the immediate vicinity of plaques, at all three ages. These dystrophic axons contrasted with the much thinner and discrete varicose fibers in the neighboring neuropil.

At 6 months of age, there were no measurable changes in the density of ChAT- or 5-HT-immunostained axons in either hippocampus or cerebral cortex. In 12–14 month-old hAPP mice, however, a significant ACh denervation became noticeable in the hippocampus alone, and in the absence of any 5-HT denervation

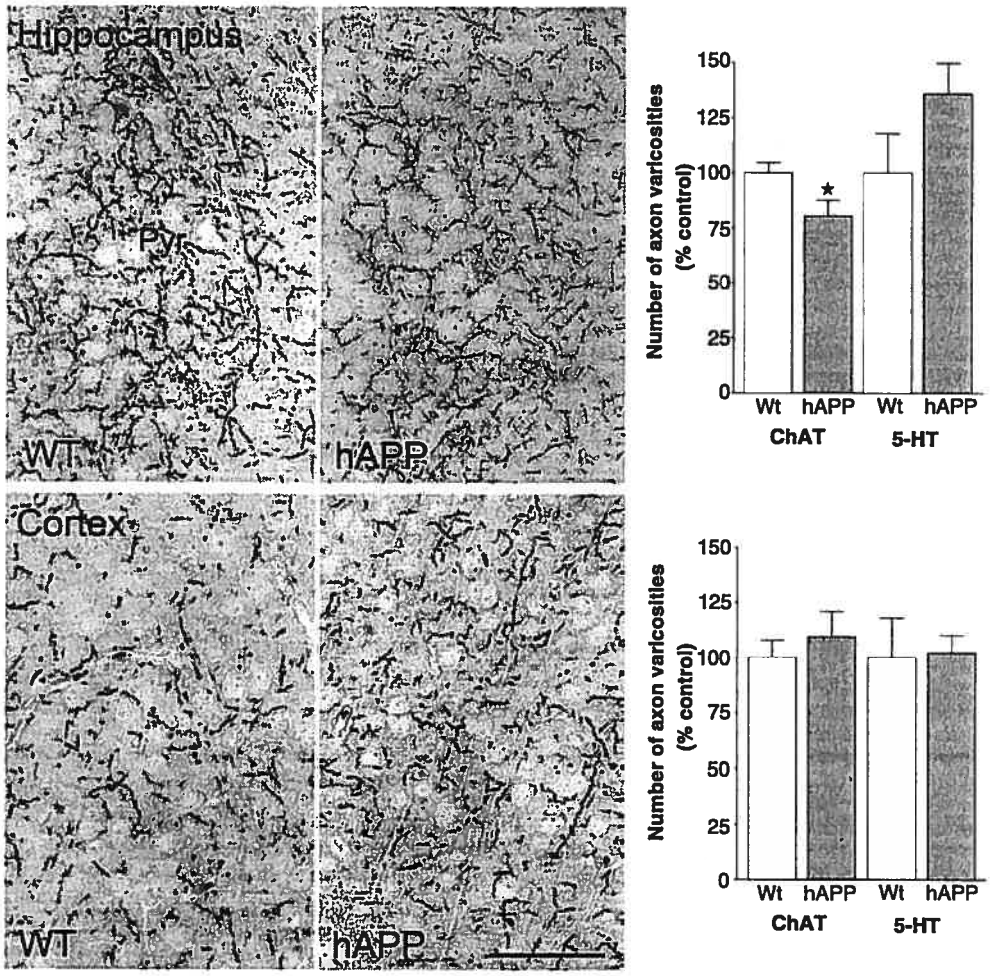


**Fig. 4.** Photomicrographs of the ChAT-immunostained innervation in hippocampus (top) and parietal cortex (bottom), in semi-thin sections from 12/14 month-old $hAPP_{SW,IND}$ (hAPP) and wild-type (WT) mice. Scale bar: 50 μm. Note the decreased density of axon varicosities in the stratum pyramidale (Pyr) of CA3 in the transgenics compared to WT, but lack of change in the cortex. The adjacent bar graphs represent the relative number of ChAT- and 5-HT-immunostained axon varicosities in both regions (means ± SEM from 4–6 mice in each group). The only statistically significant difference between transgenics and WT is the reduction in density of the ACh innervation in hippocampus (*$p < 0.05$ by Student $t$ test)

in either region (Fig. 4). Quantitative estimates of immunostained varicosities in two micrometer-thick sections revealed a 23% loss of ChAT-immunostained axon varicosities in the CA3 region of the dorsal hippocampus.

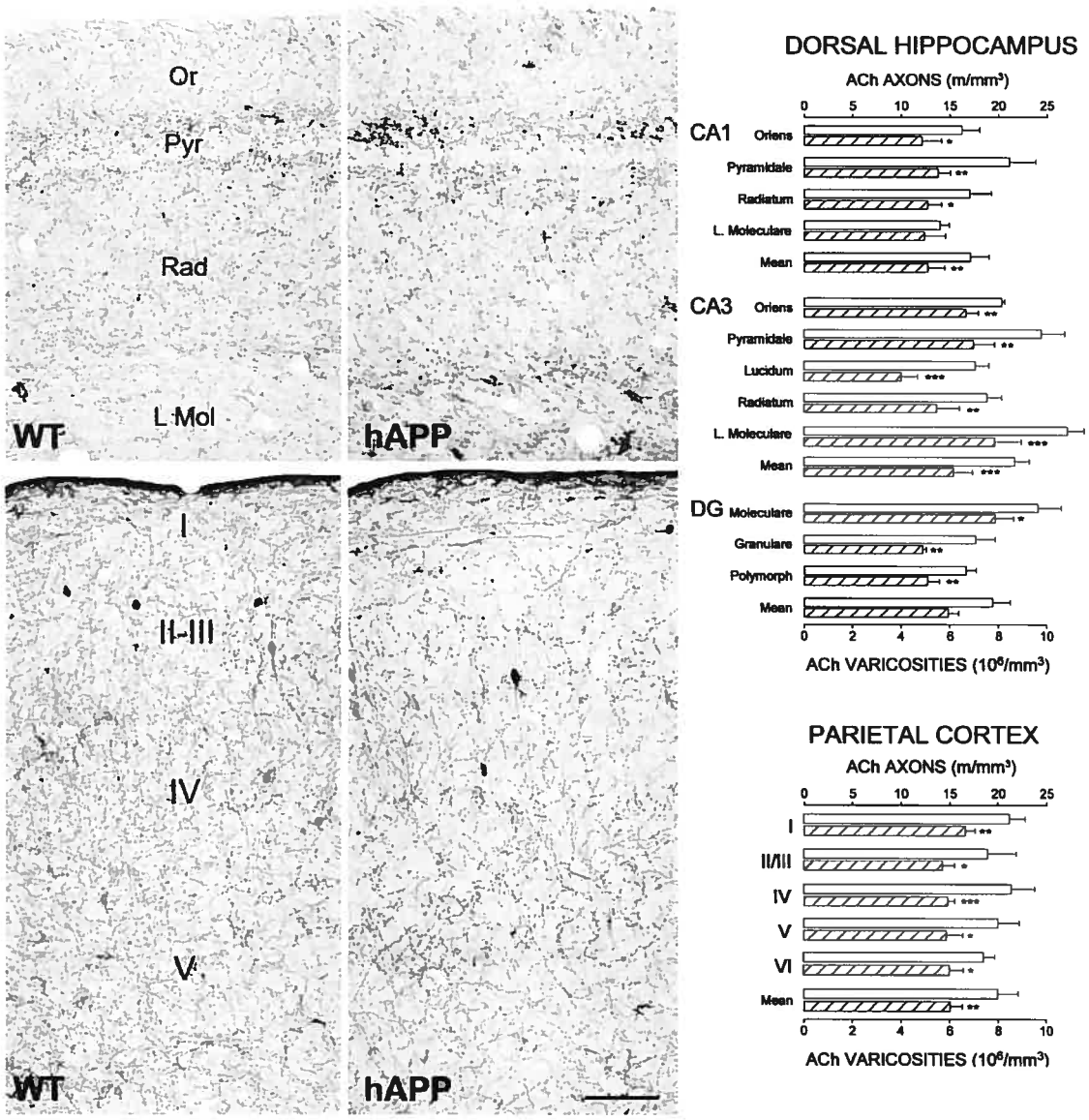


**Fig. 5.** Low-power photomicrographs illustrating the decrease in density of ACh innervation in CA1 of the dorsal hippocampus (top) and the parietal cortex (bottom) of 18 month-old, wild type (**A**, **C**) and $hAPP_{SW,IND}$ transgenic mice (**B**, **D**). The decrease is apparent in all hippocampal and cortical layers. Same abbreviations as in Fig. 1. Scale bar: 100 μm. The adjacent bar graphs represent the laminar and regional (mean) densities of ChAT-immunostained axons and varicosities in CA1, CA3 and DG of dorsal hippocampus, and layers I–VI of parietal cortex, in the WT (clear bars) versus $hAPP_{SW,IND}$ mice (hatched bars). Means ± SEM from 4 mice in each group, in meters of axons and/or millions of axon varicosities per $mm^3$. $^*p<0.05$, $^{**}p<0.01$, and $^{***}p<0.001$ by one-way ANOVA followed by Student *t*-test

In 18 month-old transgenic mice, the ACh denervation was apparent not only in hippocampus but also in the parietal cortex, as illustrated in Fig. 5. The quantitative estimate of ChAT-immunostained axon length and number of axon varicosities at 18 months showed an average decrease of 26% in the parietal cortex. In the hippocampus, the average decrease was in the order of 24%, hence not significantly greater than that at 12–14 months. These ACh denervations were widespread, all layers being equally affected in both regions. Thus, there was no relationship between the number of plaques and the location and severity of the ACh denervation. The 5-HT innervation was entirely spared, at least up to 18 months, in terms of the density of its immunostained axon network.

It was concluded from this study that, in addition to a local, plaque dependent, neurotoxic effect on ACh and serotonin axons, and presumably every other type of axon terminals (Diez et al., 2000), there is a cholinotoxicity in the hAPP mouse brain, leading to selective hippocampal and cortical ACh denervations. The widespread distribution and time course of this effect suggest that it is plaque independent and could be caused by an overload of soluble Aβ. In vitro, non aggregated forms of Aβ have been shown to specifically affect several aspects of ACh neurotransmission, including high affinity choline uptake, synthesis rate and release of ACh (for review, Kar et al., 1998; Dolezal and Kasparova, 2003; Kar and Quirion, 2004). It has also been demonstrated that RN46A cells which differentiate into a ACh phenotype in presence of neurotrophic factors are highly sensitive to soluble Aβ peptide, whereas differentiation of these cells into a 5-HT phenotype yields a population resistant to the same treatment (Olesen et al., 1998).

An ACh denervation of the severity and extent documented in the $hAPP_{SW,IND}$ mouse could indeed account for the cognitive dysfunctions in Alzheimer brain. Hence, even though the $hAPP_{SW,IND}$ transgenic mouse lacks some cardinal features of Alzheimer's disease, notably neurofibrillary tangles and neuronal losses, it might prove particularly useful as an animal model for investigating the biological mechanisms of the Aβ cholinotoxicity as well as the efficacy of vaccines or of other therapeutic measures aimed at the neuroprotection of ACh neurons.

## Acknowledgements

C. Cozzari of the University of Rome, and B. K. Hartman at the University of Minnesota, gave us the exquisitely sensitive monoclonal antibody against whole rat ChAT that made these studies possible. The hAPP transgenic mouse breeders came from the laboratory of L. Mucke. K. C. Watkins provided technical assistance with the electron microscopy. These studies were supported by grants NRF 3544 (L.D.) and MOP 53334 (E.H.) from the Canadian Institute of Health Research and the Alzheimer Society of Canada (E.H.).

## References

Amaral DG, Kurz J (1985) An analysis of the origins of the cholinergic and noncholinergic septal projections to the hippocampal formation of the rat. J Comp Neurol 240: 37–59

Auld DS, Kornecook TJ, Bastianetto S, Quirion R (2002) Alzheimer's disease and the basal forebrain cholinergic system: relations to beta-amyloid peptides, cognition, and treatment strategies. Prog Neurobiol 68: 209–245

Aucoin J-S, Aznavour N, Tong X-K, Buttini M, Descarries L, Hamel E (2004) Selective cholinergic denervation in a mouse model of Alzheimer's disease. (submitted)

Aznavour N, Mechawar N, Descarries L (2002) Comparative analysis of cholinergic innervation in the dorsal hippocampus of adult mouse and rat: a quantitative immunocytochemical study. Hippocampus 12: 406–417

Aznavour N, Mechawar N, Watkins KC, Descarries L (2003) Fine structural features of the acetylcholine innervation in the developing neostriatum of rat. J Comp Neurol 460: 280–291

Aznavour N, Tong X-K, Aucoin J-S, Descarries L, Hamel E (2003) Neurotoxicity of β-amyloid and selective, age-dependent loss of cholinergic fibers in the hippocampus and cerebral cortex of the PDAPP mouse. Program No 842.7. 2003 Abstract Viewer/Itinerary Planner. Society for Neuroscience, Washington, DC (online)

Beach TG, Kuo YM, Spiegel K, Emmerling MR, Sue LI, Kokjohn K, Roher AE (2000) The cholinergic deficit coincides with Abeta deposition at the earliest histopathologic stages of Alzheimer disease. J Neuropathol Exp Neurol 59: 308–313

Beaudet A, Sotelo C (1981) Synaptic remodeling of serotonin axon terminals in rat agranular cerebellum. Brain Res 206: 305–329

Bierer LM, Haroutunian V, Gabriel S, Knott PJ, Carlin LS, Purohit DP, Perl DP, Schmeidler J, Kanof P, Davis KL (1995) Neurochemical correlates of dementia severity in Alzheimer's disease: relative importance of the cholinergic deficits. J Neurochem 64: 749–760

Boncristiano S, Calhoun ME, Kelly PH, Pfeifer M, Bondolfi L, Stalder M, et al. (2002) Cholinergic changes in the APP23 transgenic mouse model of cerebral amyloidosis. J Neurosci 22: 3234–3243

Bronfman FC, Moechars D, Van Leuven F (2000) Acetylcholinesterase-positive fiber deafferentation and cell shrinkage in the septohippocampal pathway of aged amyloid precursor protein London mutant transgenic mice. Neurobiol Dis 7: 152–168

Buttini M, Yu G-Q, Shockley K, Huang Y, Jones B, Masliah E, et al. (2002) Modulation of Alzheimer-like synaptic and cholinergic deficits in transgenic mice by human apolipoprotein E depends on isoform, aging, and overexpression of amyloid β peptides but not on plaque formation. J Neurosci 22: 10539–10548

Coleman PD, Flood DG, West MJ (1987) Volumes of the components of the hippocampus in the aging F344 rat. J Comp Neurol 266: 300–306

Davies P, Maloney AJ (1976) Selective loss of central cholinergic neurons in Alzheimer's disease. Lancet 2: 1403

Descarries L (1998) The hypothesis of an ambient level of acetylcholine in the central nervous system. J Physiol Paris 92: 215–220

Descarries L, Mechawar N (2000) Ultrastructural evidence for diffuse transmission by monoamine and acetylcholine neurons of the central nervous system. Prog Brain Res 125: 27–47

Descarries L, Gisiger V, Steriade M (1997) Diffuse transmission by acetylcholine in the CNS. Prog Neurobiol 53: 603–625

Descarries L, Mechawar N, Aznavour N, Watkins KC (2004) Structural determinants of the roles of acetylcholine in cerebral cortex. Prog Brain Res 145: 45–58

Diez M, Koistinaho J, Kahn K, Games D, Hökfelt T (2000) Neuropeptides in hippocampus and cortex in transgenic mice overexpressing V717F beta-amyloid precursor protein – initial observations. Neuroscience 100: 259–286

Dodart JC, Mathis C, Saura J, Bales KR, Paul SM, Ungerer A (2000) Neuroanatomical abnormalities in behaviorally characterized APP(V717F) transgenic mice. Neurobiol Dis 7: 71–85

Dolezal V, Kasparova J (2003) Beta-amyloid and cholinergic neurons. Neurochem Res 28: 499–506

Eckenstein F, Baughman RW (1987) Cholinergic innervation in cerebral cortex. In: Jones EG, Peters A (eds) Cerebral cortex, vol 6. Further aspects of cortical function, including hippocampus. Plenum Press, New York, pp 129–160

Fine A, Hoyle C, Maclean CJ, Levatte TL, Baker HF, Ridley RM (1997) Learning impairments following injection of a selective cholinergic immunotoxin, ME20.4 IgG-saporin, into the basal nucleus of Meynert in monkeys. Neuroscience 81: 331–343

Franklin KBJ, Paxinos G (1997) The mouse brain in stereotaxic coordinates. Academic Press, San Diego

Gage FH, Björklund A, Stenevi U (1983) Reinnervation of the partially deafferented hippocampus by compensatory collateral sprouting from spared cholinergic and noradrenergic afferents. Brain Res 268: 27–37

Games D, Adams D, Alessandrini R, Barbour R, Berthelette PBC, Carr T, et al. (1995) Alzheimer-type neuropathology in transgenic mice overexpressing V717F beta-amyloid precursor protein. Nature 373: 523–527

German DC, Yazdani U, Speciale SG, Pasbakhsh P, Games D, Liang CL (2003) Cholinergic neuropathology in a mouse model of Alzheimer's disease. J Comp Neurol 462: 371–381

Geula C, Mesulam MM (1996) Systematic regional variations in the loss of cortical cholinergic fibers in Alzheimer's disease. Cereb Cortex 6: 165–177

Gisiger V, Stephens HR (1988) Localization of the pool of G4 acetylcholinesterase characterizing fast muscles and its alteration in murine muscular dystrophy. J Neurosci Res 19: 62–78

Gorenstein C, Gallardo KA, Robertseon RT (1991) Molecular forms of acetylcholinesterase in cerebral cortex and dorsal thalamus of developing rats. Brain Res Dev Brain Res 61: 271–276

Hasselmo ME, McGauthy J (2004) High acetylcholine levels set circuit dynamics for attention and encoding and low acetylcholine levels set dynamics for consolidation. Prog Brain Res 145: 207–231

Hernandez D, Sugaya K, Qu T, McGowann E, Duff K, McKinney M (2001) Survival and plasticity of basal forebrain cholinergic systems in mice transgenic for presenilin-I and amyloid precursor protein mutant genes. Mol Neurosci 12: 1377–1384

Jaffar S, Counts SE, Ma SY, Dadko E, Gordon MN, Morgan D, Mufson EJ (2001) Neuropathology of mice carrying mutant APP(swe) and/or PS1 (M146L) transgenes: alterations in the p75(NTR) cholinergic basal forebrain septohippocampal pathway. Exp Neurol 170: 227–243

Kar S, Quirion R (2004) Amyloid beta peptides and central cholinergic neurons: functional interrelationship and relevance to Alzheimer's disease pathology. Prog Brain Res 145: 261–274

Kar S, Issa AM, Seto D, Auld DS, Collier B, Quirion R (1998) Amyloid beta-peptide inhibits high-affinity choline uptake and acetylcholine release in rat hippocampal slices. J Neurochem 70: 2179–2187

Klingner M, Apelt J, Kumar A, Sorger D, Sabri O, Steinbach J, Scheunemann M, Schliebs R (2003) Alterations in cholinergic and non-cholinergic neurotransmitter receptor densities in transgenic Tg2576 mouse brain with beta-amyloid plaque pathology. Int J Dev Neurosci 21: 357–369

Koh S, Loy R (1989) Localization and development of nerve growth factor-sensitive rat basal forebrain neurons and their afferent projections to hippocampus and neocortex. J Neurosci 9: 2999–3018

Krnjević K, Silver A (1966) Acetylcholinesterase in the developing forebrain. J Anat 100: 63–89

Luth HJ, Apelt J, Ihunwo AO, Arendt T, Schliebs R (2003) Degeneration of beta-amyloid-associated cholinergic structures in transgenic APP SW mice. Brain Res 977: 16–22

Makuch R, Baratta J, Karaelias LD, Lauterborn JC, Gall CM, Yu J, Robertson RT (2001) Arrival of afferents and the differentiation of target neurons: studies of developing cholinergic projections to the dentate gyrus. Neuroscience 104: 81–91

Masliah E, Sisk A, Mallory M, Games D (2001) Neurofibrillary pathology in transgenic mice overexpressing V717F beta-amyloid precursor protein. J Neuropathol Exp Neurol 60: 357–368

McKinney M, Coyle JT, Hedreen JC (1983) Topographic analysis of the innervation of the rat neocortex and hippocampus by the basal forebrain cholinergic system. J Comp Neurol 217: 103–121

Mechawar N, Cozzari C, Descarries L (2000) Cholinergic innervation in adult rat cerebral cortex: a quantitative immunocytochemical description. J Comp Neurol 428: 305–318

Mechawar N, Watkins KC, Descarries L (2002) Ultrastructural features of the acetylcholine innervation in the developing parietal cortex of rat. J Comp Neurol 443: 250–258

Mesulam MM (1998) Some cholinergic themes related to Alzheimer's disease: synaptology of the nucleus basalis, location of m2 receptors, interactions with amyloid metabolism, and perturbations of cortical plasticity. J Physiol (Paris) 92: 293–298

Mesulam MM, Mufson EJ, Wainer BH, Levey AI (1983) Central cholinergic pathways in the rat: an overview based on an alternative nomenclature (Ch1–Ch6). Neuroscience 10: 1185–1201

Miki T, Harris SJ, Wilce P, Takeuchi Y, Bedi KS (2000) Neurons in the hilus region of the rat hippocampus are depleted in number by exposure to alcohol during early postnatal life. Hippocampus 10: 284–295

Mucke L, Masliah E, Yu G-Q, Mallory M, Rockenstein EM, Tatsuno G, Hu K, Kholodenko D, Johnson-Wood K, McConlogue L (2000) High-level neuronal expression of a beta 1–42 in wild-type human amyloid protein precursor transgenic mice: synaptotoxicity without plaque formation. J Neurosci 20: 4050–4058

Mufson EJ, Ma SY, Dills J, Cochran EJ, Leurgans S, Wuu J, Bennett DA, Jaffar S, Gilmor ML, Levey AI, Kordower JH (2002) Loss of basal forebrain P75(NTR) immunoreactivity in subjects with mild cognitive impairment and Alzheimer's disease. J Comp Neurol 443: 136–153

Nyakas C, Luiten PG, Spencer DG, Traber J (1987) Detailed projection patterns of septal and diagonal band efferents to the hippocampus in the rat with emphasis on innervation of CA1 and dentate gyrus. Brain Res Bull 18: 533–545

Olesen OF, Dago L, Mikkelsen JD (1998) Amyloid beta neurotoxicity in the cholinergic but not in the serotonergic phenotype of RN46A cells. Mol Brain Res 57: 266–274

Palop JJ, Jones B, Kekonius L, Chin J, Yu GQ, Raber J, Masliah E, Mucke L (2003) Neuronal depletion of calcium-dependent proteins in the dentate gyrus is tightly linked to Alzheimer's disease-related cognitive deficits. Proc Natl Acad Sci USA 100: 9572–9577

Reinikainen KJ, Soininen H, Riekkinen PJ (1990) Neurotransmitter changes in Alzheimer's disease: implications to diagnostics and therapy. J Neurosci Res 27: 576–586

Rye DB, Wainer BH, Mesulam MM, Mufson EJ, Saper CB (1984) Cortical projections arising from the basal forebrain: a study of cholinergic and noncholinergic components employing combined retrograde tracing and immunohistochemical localization of choline acetyltransferase. Neuroscience 13: 627–643

Semba K (2004) Phylogenetic and ontogenetic aspects of the basal forebrain cholinergic neurons and their innervation of the cerebral cortex. Prog Brain Res 145: 3–43

Semba K, Fibiger HC (1988) Time of origin of cholinergic neurons in the rat basal forebrain. J Comp Neurol 269: 87–95

Shi SR, Key ME, Kalra KL (1991) Antigen retrieval in formalin-fixed, paraffin-embedded tissues: an enhancement method for immunohistochemical staining based on microwave over heating of tissue sections. J Histochem Cytochem 39: 741–748

Shinotoh H, Namba H, Fukushi K, Nagatsuka S, Tanaka N, Aotsuka A, Ota T, Tanada S, Irie T (2000) Progressive loss of cortical acetylcholinesterase activity in association with cognitive decline in Alzheimer's disease: a positron emission tomography study. Ann Neurol 48: 194–200

Soghomonian JJ, Doucet G, Descarries L (1987) Serotonin innervation in adult rat neostriatum. I. Quantified regional distribution. Brain Res 425: 85–100

Swanson LW (1992) Brain maps: structure of the rat brain. Elsevier, Amsterdam

Tong XK, Hamel E (1999) Regional cholinergic denervation of cortical microvassels and nitric oxide synthase-containing neurons in Alzheimer's disease. Neuroscience 92: 163–175

Umbriaco D, Watkins KC, Descarries L, Cozzari C, Hartman BK (1994) Ultrastructural and morphometric features of the acetylcholine innervation in adult rat parietal cortex: an electron microscopic study in serial sections. J Comp Neurol 348: 351–373

Umbriaco D, Garcia S, Beaulieu C, Descarries L (1995) Relational features of acetylcholine, noradrenaline, serotonin and GABA axonal varicosities in the stratum radiatum of adult rat hippocampus (CA1). A comparative electron microscopic analysis. Hippocampus 5: 605–620

Whitehouse PJ, Price DL, Struble RG, Clark AW, Coyle JT, Delon MR (1982) Alzheimer's disease and senile dementia: loss of neurons in the basal forebrain. Science 215: 1237–1239

Wong TP, Debeir T, Duff K, Cuello AC (1999) Reorganization of cholinergic terminals in the cerebral cortex and hippocampus in transgenic mice carrying mutated presenilin-1 and amyloid precursor protein transgenes. J Neurosci 19: 2706–2716

Woolf NJ (1991) Cholinergic systems in mammalian brain and spinal cord. Progr Neurobiol 37: 475–524

Authors' address: L. Descarries, MD, Department of Pathology and Cell Biology, Faculty of Medicine, Université de Montréal, Pavillon Roger Gaudry, R-523, S-534 or N-535, 2900 boulevard Édouard-Montpetit, Montreal QC, Canada H3C 3J7, [redacted]

**Annexe 3**

# DIFFUSE (VOLUME) TRANSMISSION

Publié en 2003

The Encyclopedia of Neuroscience. Adelman G and Smith BH, eds.
Amsterdam: Elsevier Science.

(L Descarries, N Aznavour)

# DIFFUSE (VOLUME) TRANSMISSION

Laurent DESCARRIES and Nicolas AZNAVOUR

Départements de pathologie et biologie cellulaire et de physiologie, and

Centre de recherche en sciences neurologiques, Université de Montréal;

## 1. *Introduction*

Chemical transmission (Elliott, 1905; Loewi, 1921) and the neuron theory (Cajal, 1954) are founding paradigms of the modern neurosciences (see also **Neurons** and **Neurotransmitters**). In the 1950's, the electron microscopic visualization of the motor endplate and of synapses between neurons led to the tenet that, in the central as well as the peripheral nervous system, these specialized zones of cellular contact were the exclusive site of chemical neurotransmission (see **Synapses**). There, upon arrival of a nerve impulse, a transmitter would be released «pre-synaptically» to act on receptors concentrated «post-synaptically» at the junctional interface (e.g., Fig. AB). The present article highlights the view that, in addition to such transmission taking place at synapses, neurons of the central as well as the peripheral nervous system are capable of broader transmission, to various cellular targets, through what has come to be known as diffuse or volume transmission (Fig. CD). Indeed, in the last thirty years, evidence has accumulated for a widespread, sustained and diversified transfer of information by

neurons and their transmitters, in addition to point-to-point, on-and-off, excitatory or inhibitory synaptic transmission (see also **Neuromodulation**).

The concept of diffuse transmission was initially proposed on the basis of electron microscope radioautographic observations on the serotonin and noradrenaline innervations in adult rat cerebral cortex (Descarries et al., 1975, 1977; Beaudet and Descarries, 1978). These nerve terminals (axonal boutons or varicosities) were then shown to often lack the plasma membrane specializations (junctional complexes) that are the hallmark of synapses. It was inferred from this unexpected finding that the transmitter released from such non junctional («non synaptic») terminals would diffuse in the extracellular space and reach relatively remote targets, to exert a variety of effects on vast cellular ensembles, in a relatively large tissue volume, later referred to as «a sphere of influence» (reviewed in Descarries et al., 1991).

This proposal had considerable merit. It accounted for some general, prolonged and/or indirect actions attributed to noradrenaline and serotonin in the cerebral cortex, and which came to be designated as «modulation», to distinguish them from classical, point-to-point, synaptic transmission. It also explained: i) the existence of so-called «presynaptic» effects of transmitters on their own release or that of other transmitters, which took place in the obvious absence of axo-axonic synapses (Vizi, 1984; Vizi and Labós, 1991); ii) the frequent mismatch between the anatomical distribution of many receptors for different transmitters and that of the corresponding innervations (Herkenham, 1987); and iii) actions of these and other transmitters on non neuronal targets, such as astrocytes and microvessels, endowed with the appropriate receptors but often remote from the corresponding release sites.

With time, different names came to be given to this type of neuronal communication: non-synaptic, extrajunctional, paracrine, diffuse or volume transmission. Many of its properties, as well as its implications for the understanding of normal and abnormal brain function and pharmacotherapeutics were the subject of extensive reviews (Agnati et al., 1992, 1995; Zoli et al., 1996, 1998, 1999; see also **Non synaptic diffusion neurotransmission**). This short article will focus on additional morphological and biochemical data pertaining to diffuse (volume) transmission, which expand this notion to most if not all transmitter-defined neuronal systems in vertebrate central nervous system (CNS) and enlarge its functional significance.

## 2. *Ultrastructural evidence for diffuse transmission*

There is now incontrovertible electron microscopic evidence that many of the so-called axon terminals, boutons or varicosities issued from a variety of transmitter-defined neurons in mammalian CNS lack the junctional membrane specializations (junctional complexes) that are the hallmark of synapses. In recent years, most of this information has been obtained after immunocytochemical labeling with specific antibodies against the neurotransmitters themselves or their biosynthetic enzymes, or else against the specific membrane transporters ensuring their reuptake. In some of these studies, efforts were made to examine the immunostained axon terminals in serial as well as single thin sections for electron microscopy, allowing scrutiny of most if not their entire volume and direct determination of the frequency with which they made a synaptic junction (synaptic incidence). In other instances, such estimates were derived from a linear transformation of the relationship between the observed frequency of junctions and the number of thin

sections available for examination. A third approach was to extrapolate the synaptic incidence from the frequency of junctions in single thin sections by means of a stereological formula which took into account the average size of varicosity profiles, the length of visible junctions and the thickness of the sections (Beaudet and Sotelo, 1981). The validity of this formula has since been verified on a large population of varicosities which were examined both in serial sections and as a random sampling of single thin sections (Umbriaco et al., 1994).

In either type of study, the initial data on the largely asynaptic nature of the monoamine innervations of cerebral cortex has been confirmed, and extended to a greater number of cortical areas and different species, including monkey and human (reviewed in Smiley, 1996; Descarries and Mechawar, 2000). The histamine innervation of cerebral cortex (Takagi et al., 1986), as well as its cholinergic innervation (Umbriaco et al., 1994), were also shown to be predominantly asynaptic. The frequency with which the varicosities for a given monoamine innervation do make synapse was found to vary between cortical regions and among species for a given region. In rat neocortex, the dopamine stands out as the most synaptic (Séguéla et al., 1988); the noradrenaline innervation is the least (Séguéla et al., 1990), and the serotonin intermediate (Séguéla et al., 1989). The same could hold true in monkey (Smiley, 1996; Aoki et al., 1998), but there could be major differences between rat and human, as the only available figure for the human cortical dopamine innervation is very low (5-10% of the varicosities) (Smiley et al., 1992), whereas that for the cholinergic innervation is relatively high (67%) (Smiley et al., 1997).

Similar data are also available for the monoamine innervations in many other brain regions including the spinal cord, and the acetylcholine innervation in hippocampus and neostriatum (for a recent review, see Descarries and Mechawar, 2000). It is noteworthy that none of the monoamine or acetylcholine innervations in CNS has ever been described as entirely asynaptic. Moreover, from all available data, it seems that both synaptic and asynaptic varicosities are present on the same axons, so that this morphological feature cannot serve to distinguish subpopulations of neurons using a given transmitter. There is also increasing data to indicate that the largely asynaptic character of the monoamine and acetylcholine innervations is an innate feature of these systems, since it is already present during development (Latsari et al., 2002; Mechawar et al., 2002; Aznavour et al., 2003). Interestingly, in the case of the cholinergic system, it has been demonstrated for both neurons of projection (cerebral cortex) and interneurons (neostriatum).

These data stand in sharp contrast with all currently available electron microscopic evidence regarding the amino acid systems (GABA, glutamate-aspartate, glycine). Whether as interneurons or projection neurons, these amino acid neurons appear to be entirely synaptic and often display more than a single synaptic junction per axon terminal (e.g., Umbriaco et al., 1995). As for the peptidergic neurons in CNS, they have not been systematically examined to determine the synaptic frequency of their nerve terminals. It is most likely, however, that many will be found to be predominantly asynaptic and others entirely synaptic, in view of the frequent co-localization of the neuropeptides not only with GABA, but also with other canonical transmitters including

the monoamines and acetylcholine (see **Chemical neuroanatomy with special reference to coexistence of multiple messenger molecules**).

3. ***Extrasynaptic distribution of receptors and transporters***

One of the strongest argument in favour of diffuse (volume) transmission has always been the existence of mismatches between the anatomical distribution of certain transmitter-defined systems, and the localization of the receptors for the corresponding transmitters (Herkenham, 1987; Jansson et al., 2001). Among innumerable examples, one of the most striking is the dense innervation of the rat substantia nigra by substance P containing terminals, in the total absence of the main receptor (NK1) for this peptide in this brain region (Ribeiro-Da-Silva et al., 2000), implying diffusion of the peptide to act at considerable distance from its release sites. Mismatches have also been demonstrated at the electron microscopic level. For example, somatostatin sst2A receptors have been shown to be present on the plasma membrane of numerous dendrites and/or axon terminals in rat brain regions that are only sparsely innervated by this neuropeptide (Dournaud et al., 1998). In fact, an increasing number of immuno-electron microscopic studies indicates that plasma membrane receptors for the monoamines, ACh, and each of the amino acid transmitters and neuropeptides are localized at extrasynaptic sites on neuronal somata, dendrites, axons and axon terminals, and/or glia and microvessels (e.g., serotonin 5-HT1A and 5-HT1B receptors, Riad et al., 2000 ). Similarly, the plasma membrane transporters ensuring the reuptake of monoamines, as well as those for choline, GABA and glutamate, have been shown to be mostly extrasynaptic, on the

various parts of the corresponding neurons (e.g., serotonin transporter, Tao-Cheng et al. 1999).

There are no reasons to doubt the functionality of these extrasynaptic membrane receptors (and transporters). Some of them (e.g., serotonin 5-HT1A autoreceptors) have indeed been shown to internalize rapidly into the somato-dendritic cytoplasm upon the administration of a selective agonist (Riad et al., 2001), or after an increase in the ambient concentration of the transmitter after blockade of its reuptake (e.g., serotonin, Descarries and Riad, 2003). In this latter situation, the internalization of the receptors also attests to the functionality of the membrane transporters that are similarly located on the cell bodies and dendrites of the same neurons.

It is beyond the scope of this short article to review the data on GABA, glutamate and glycine receptors. However, because of the increasing evidence for extrasynaptic spillover of these amino acid transmitters in mammalian CNS (Isaacson et al., 1993; Kullmann, 2000), it seems to be no longer justified to restrict the diffuse (volume) transmission paradigm to only those neurons that are endowed with predominantly asynaptic axon terminals.

4. *Ambient level of transmitter*

The spread of various molecules, including dopamine, serotonin, neuropeptides, cytokines and growth factors, has now been documented in intact brain tissue following in vivo administration (e.g., dopamine, Kehr et al., 2000). This has led to an interesting hypothesis to complement the diffuse (volume) transmission paradigm, at least for brain regions rich in one and/or the other of the monoamine and acetylcholine innervations (Descarries et al., 1995). According to this hypothesis, spontaneous and evoked release from these mostly asynaptic nerve terminals and spillover from the synaptic ones would permanently maintain a low level of transmitter throughout the extracellular space. Reuptake and enzymatic degradation of the monoamines would primarily serve to keep their ambient level within physiological limits, rather than totally remove them from the extracellular space (and synaptic clefts), and a similar role would be ascribed to acetylcholinesterase (AChE) in the CNS. Indeed, in mammalian brain, this enzyme is now known to predominantly consist of the tetrameric G4 molecular isoform (Gorenstein et al., 1991) which, in skeletal muscle, is mainly concentrated outside and around endplates, in contrast with the A12 form which contributes to the rapid removal of ACh from synaptic clefts (Gisiger and Stephens, 1988; for detailed discussion, see Descarries et al., 1997). In many parts of the CNS, resting levels of the monoamines or acetylcholine in the nanomolar range have been measured by microdialysis. Such concentrations are consistent with the high affinities of many of the monoamine or acetylcholine receptor subtypes.

## 5. *Clinical implications*

Much remains to be known about the cellular and molecular mechanisms that govern diffuse (volume) transmission in the brain, either in normal or disease states. It may be speculated that the low ambient levels of transmitter permanently maintained in normal CNS regulate the expression and/or functional state of various subtypes of high affinity receptors located on the neurons releasing the corresponding transmitter (autoreceptors) or on other neurons (heteroreceptors), as well as glial cells and microvessels. Changes in this ambient level, affecting these widely distributed receptors, could mediate many of the morphogenetic effects of transmitters during development, and neuronal plasticity in the mature state. They could also play a major role in the behavioral effects of drugs acting on the monoamine transporters, the choline transporter, or AChE, for example.

The existence of the ambient level of transmitter could indeed account for some of the beneficial effects of substitution and pharmacological therapies, or of grafts of non-neuronal cells engineered to release transmitters, which obviously take place in the absence of restored synaptic connectivity. It could also explain why some of the motor or cognitive deficits respectively attributed to losses of dopamine or ACh neurons might become clinically manifest only when a major proportion of such terminals (release sites) have disappeared and even low background levels can no longer be maintained.

## *References*

Agnati LF, Bjelke B, Fuxe K (1992): Volume transmission in the brain. Do cells communicate solely through synapses? A new theory proposes that information also flows in the extracellular space. *Am Sci* 80: 362-374

Agnati LF, Zoli M, Strömberg I, Fuxe K (1995): Intercellular communication in the brain: wiring versus volume transmission. *Neuroscience* 3: 711-726

Aoki C, Venkatesan C, Go CG, Forman R, Kurose H (1998): Cellular and subcellular sites for noradrenergic action in the monkey dorsolateral prefrontal cortex as revealed by the immunocytochemical localization of noradrenergic receptors and axons. *Cerb Cortex* 8: 269-277.

Aznavour N, Mechawar N, Watkins KC, Descarries L (2003): Fine structural features of the acetylcholine innervation in the developing neostriatum of rat. *J Comp Neurol* 467: xxx-xxx

Beaudet A, Descarries L (1978): The monoamine innervation of rat cerebral cortex: synaptic and non synaptic relationships. *Neuroscience* 3: 851-860

Beaudet A, Sotelo C (1981): Synaptic remodeling of serotonin axon terminals in rat agranular cerebellum. *Brain Res* 206: 305-329

Cajal, SR (1954): *Neuron Theory or Reticular Theory? Objective Evidence of the Anatomical Unity of Nerve Cells.* Madrid: Consejo Superior de Investigaciones Cientificas

Descarries L, Mechawar N (2000): Ultrastructural evidence for diffuse transmission by monoamine and acetylcholine neurons of the central nervous system. In: *Volume Transmission Revisited, Prog Brain Res Vol 125,* Agnati LF, Fuxe K, Nicholson C and Siková E, eds, Amsterdam: Elsevier, pp 27-47

Descarries L, Riad M (2003): Acute treatment with fluoxetine internalizes 5-HT1A autoreceptors in the nucleus raphe dorsalis of rat. *6th World Congr Neurosci IBRO,* Prague, Czech Republic

Descarries L, Beaudet A, Watkins KC (1975): Serotonin nerve terminals in adult rat neocortex. *Brain Res* 100: 563-588

Descarries L, Watkins KC, Lapierre Y (1977): Noradrenergic axon terminals in the cerebral cortex of rat. III. Topometric ultrastructural analysis. *Brain Res* 133: 197-222

Descarries L, Séguéla P, Watkins KC (1991): Nonjunctional relationships of monoamine axon terminals in the cerebral cortex of adult rat. In: *Volume Transmission in the Brain: Novel Mechanisms for Neural Transmission,* Fuxe K and Agnati LF, eds, New York: Raven Press, pp 53-62

Descarries L, Umbriaco D, Contant C, Watkins KC (1995): A new hypothesis of acetylcholine (ACh) function in densely ACh-innervated regions of the brain. *IVth IBRO World Congr Neurosci Abstr* A3.15, p 101

Descarries L, Gisiger V, Steriade M (1997): Diffuse transmission by acetylcholine in the CNS. *Prog Neurobiol* 53: 603-625

Dournaud P, Boudin H, Schonbrunn A, Tannenbaum GS, Beaudet A (1998): Interrelationships between somatostatin sst2A receptors and somatostatin-containing axons in rat brain: evidence for regulation of cell surface receptors by endogenous somatostatin. *J Neurosci* 18: 1056-1071

Elliott TR (1905): The action of adrenalin. *J Physiol (Lond)* 32:401-467

Gisiger V, Stephens HR (1988): Localization of the pool of G4 acetylcholinesterase characterizing fast muscles and its alteration in murine muscular dystrophy. *J Neurosci Res* 19: 62-78

Gorenstein C, Gallardo KA, Robertson RT (1991): Molecular forms of acetylcholinesterase in cerebral cortex and dorsal thalamus of developing rats. *Dev Brain Res* 61: 271-276

Herkenham M (1987): Mismatches between neurotransmitter and receptor localizations in brain: observations and implications. *Neuroscience* 23: 1-38

Isaacson JS, Solis JM, Nicoll RA (1993): Local and diffuse synaptic actions of GABA in the hippocampus. *Neuron* 10: 165-175

Jansson A, Descarries L, Cornea-Hébert V, Riad M, Vergé D, Bancila M, Agnati LF, Fuxe K (2001) Transmitter-receptor mismatches in central dopamine, serotonin and neuropeptide systems. Further evidence for volume transmission. In: *The Neuronal Environment: Brain Homeostasis in Health and Disease,* Walz W, ed, Totowa: Humana Press, pp 83-108

Kehr J, Höistad, Fuxe K (2000) Diffusion of radiolabeled dopamine, its metabolites and mannitol in the rat striatum studied by dual-probe microdialysis. In *Volume*

*Transmission Revisited, Prog Brain Res Vol 125,* Agnati LF, Fuxe K, Nicholson C and Siková E, eds, Amsterdam: Elsevier, pp 179-190

Kullmann DM (2000) Spillover and synaptic cross talk mediated by glutamate and GABA in the mammalian brain. In: *Volume Transmission Revisited, Prog Brain Res Vol 125,* Agnati LF, Fuxe K, Nicholson C and Siková E, eds, Amsterdam: Elsevier, pp 339-351

Latsari M, Dori I, Antonopoulos J, Chiotelli M, Dinopoulos A (2002): The noradrenergic innervation of the developing and mature visual and motor cortex of the rat brain: a light and electron microscopic immunocytochemical analysis. *J Comp Neurol* 445: 145-158

Loewi O (1921) Über humorale Übertragbarkeit der Herznervenwirkung. *Plugers Arch Ges Physiol* 189: 239-242

Mechawar N, Watkins KC, Descarries L (2002): Ultrastructural features of the acetylcholine innervation in the developing parietal cortex of rat. *Neuroscience* 111: 83-94

Riad M, Garcia S, Watkins KC, Jodoin N, Doucet É, Langlois X, El Mestikawy S, Hamon M, Descarries L (2000): Somatodendritic localization of 5-HT1A and preterminal axonal localization of 5-HT1B serotonin receptors in adult rat brain. *J Comp Neurol* 417: 181-194

Riad M, Watkins KC, Doucet E, Hamon M, Descarries L (2001): Agonist-induced internalization of serotonin-1A receptors in the dorsal raphe nucleus (autoreceptors) but not hippocampus (heteroreceptors). *J Neurosci* 21: 8378-8386

Ribeiro-Da-Sylva A, McLeod AL, Krause JE (2000) Neurokinin receptors in the CNS. In: *Peptide Receptors, Part 1, Handbook of Chemical Neuroanatomy Vol 16,* Quirion R, Björklund A, Hökfelt T, eds, Amsterdam: Elsevier, pp 195-240

Séguéla P, Watkins KC, Descarries L (1988): Ultrastructural features of dopamine axon terminals in the anteromedial and suprarhinal cortex of adult rat. *Brain Res* 442: 11-22

Séguéla P, Watkins KC, Descarries L (1989): Ultrastructural relationships of serotonin axon terminals in the cerebral cortex of the adult rat. *J Comp Neurol* 289: 129-142

Séguéla P, Watkins KC, Geffard M, Descarries L (1990): Noradrenaline axon terminals in adult rat neocortex: an immunocytochemical analysis in serial thin sections. *Neuroscience* 35: 249-264

Smiley JF (1996): Monoamines and acetylcholine in primate cerebral cortex: what anatomy tells us about function. *Rev Brasil Biol* 56 (Suppl 1): 153-164

Smiley JF, Williams SM, Szigeti K, Goldman-Rakic PS (1992): Light and electron microscopic characterization of dopamine-immunoreactive axons in human cerebral cortex. *J Comp Neurol* 32: 325-335

Smiley JF, Morrell F, Mesulam M-M (1997): Cholinergic synapses in human cerebral cortex: an ultrastructural study in serial sections. *Exp Neurol* 144: 361-368

Takagi H, Miroshima Y, Matsuyama T, Hayashi H, Watanabe T, Wada H (1986) Histaminergic axons in the neostriatum and cerebral cortex of the rat: a correlated light and electron microscopic immunocytochemical study using histidine decarboxylase as a marker. *Brain Res* 364: 155-168

Tao-Cheng JH, Zhou FC (1999): Differential polarization of serotonin transporters in axons versus soma-dendrites: an immunogold electron microscopy study. *Neuroscience* 94: 821-830

Umbriaco D, Watkins KC, Descarries L, Cozzari C, Hartman BK (1994) Ultrastructural and morphometric features of the acetylcholine innervation in adult rat parietal cortex : an electron microscopic study in serial sections. *J Comp Neurol* 348: 351-373

Umbriaco D, Garcia S, Beaulieu C, Descarries L (1995): Relational features of acetylcholine, noradrenaline, serotonin and GABA axon terminals in the stratum radiatum of adult rat hippocampus (CA1). *Hippocampus* 5: 605-620

Vizi ES (1984): *Non-synaptic Interactions Between Neurons : Modulation of Neurochemical Transmission.* Chichester: John Wiley

Vizi ES, Lábos E (1991): Non-synaptic interactions at presynaptic level. *Progr Neurobiol* 37: 145-163

Zoli M, Agnati LF (1996): Wiring and volume transmission in the central nervous system: the concept of closed and open synapses. *Prog Neurobiol* 49: 363-380

Zoli M, Torri C, Ferrari R, Jansson A, Zini I, Fuxe K, Agnati LF (1998): The emergence of the volume transmission concept. *Brain Res Rev* 26: 136-147

Zoli M, Jansson A, Syková E, Agnati LF, Fuxe K (1999): Volume transmission in the CNS and its relevance for neuropsychopharmacology. *Trends Pharm Sci* 20: 142-150

## *Further Reading*

Nieuwenhuys R (2000): Comparative aspects of volume transmission, with sidelight on other forms of intercellular communication. In: *Volume Transmission Revisited, Prog Brain Res Vol 125,* Agnati LF , Fuxe K, Nicholson C and Siková E, eds, Amsterdam: Elsevier, pp 49-126.

## Figure legend

Electron microscope radioautographs of tritiated serotonin ([$^3$H]5-HT)-labeled axon terminals (varicosities) in the rat cerebral cortex (A,C), and their corresponding diagrammatic representations (B,D). These figures contrast the former, traditional view of synaptic transmission (A,B) with the newer concept of diffuse (volume) transmission and ambient level of transmitter (C,D). In AB, the serotonin terminal (decorated with silver grains in A, colored in B) is in synaptic contact with an underlying dendrite (postsynaptic density between asterisks in A). In the traditional view, the receptors were confined to the postsynaptic junctional zone (small red triangles in B). In CD, two labeled serotonin varicosities, presumably belonging to the same axon, do not form synapses. According to the diffuse transmission paradigm, the transmitter released by such varicosities diffuses in the extracellular space to reach receptors (small red triangles in D) distributed on a variety of cellular targets. Moreover, a low ambient level of transmitter is maintained throughout the extracellular space. as, astrocyte; av, axon varicosity; d, dendrite; sp, dendritic spine. X 30 000. Scale bar (in C): 0.5 μm.

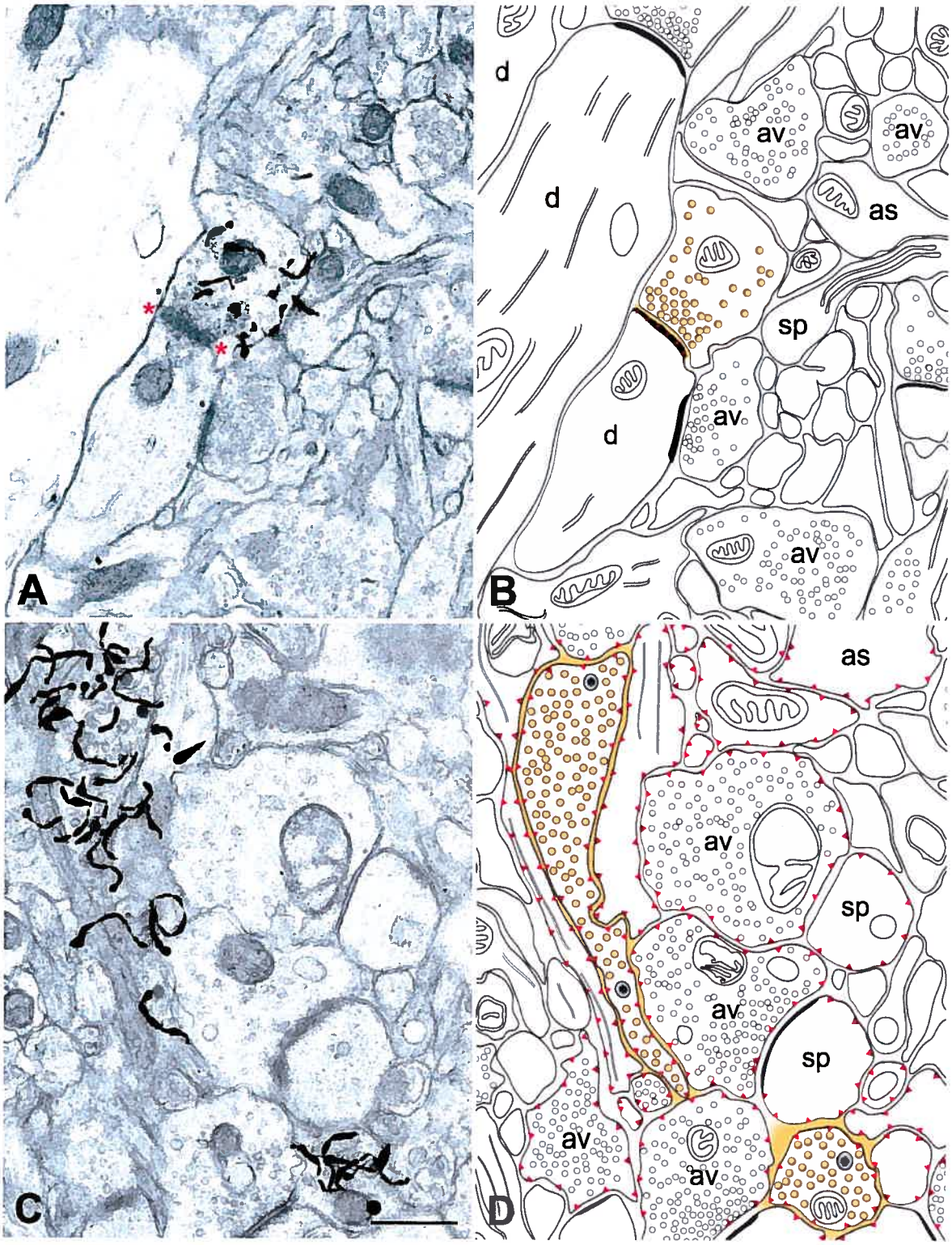
A
B
C
D
d
d
d
av
av
av
av
av
av
av
av
as
as
sp
sp
sp

# DIFFUSE (VOLUME) TRANSMISSION

Laurent DESCARRIES and Nicolas AZNAVOUR

Départements de pathologie et biologie cellulaire et de physiologie, and

Centre de recherche en sciences neurologiques, Université de Montréal,

2900, boul. Edouard-Montpetit, Montréal, Québec, Canada H3C 3J7

***Keywords:*** central nervous system, neurotransmitter,

diffuse (volume) transmission, synaptic transmission, monoamines, acetylcholine, amino

acid transmitters, neuropeptides

Correspondence: Laurent DESCARRIES M.D.
Département de pathologie et biologie cellulaire
Université de Montréal
CP 6128, Succursale Centre-ville
Montréal, QC, Canada H3C 3J7

tel. (514) 343-7070
fax (515) 343-5755
[redacted]

# STRUCTURAL DETERMINANTS OF THE ROLES OF ACETYLCHOLINE IN CEREBRAL CORTEX

Laurent DESCARRIES, Naguib MECHAWAR, Nicolas AZNAVOUR and Kenneth C. WATKINS

Departments of Pathology and Cell Biology and of Physiology,
and Centre de recherche en sciences neurologiques, Faculté de médecine,
Université de Montréal, Montréal, Québec, Canada H3C 3J7

Running title : **ACh in cerebral cortex**

Correspondence: Laurent Descarries m.d.
Département de pathologie et biologie cellulaire
Université de Montréal
C.P. 6128, Succ. Centre-ville
Montréal (Québec), Canada
H3C 3J7

Tel (514) 343-7070
Fax (514) 343-5755

E-mail: laurent.descarries@umontreal.ca

**Annexe 4**

# SELECTIVE CHOLINERGIC DENERVATION, INDEPENDENT FROM OXIDATIVE STRESS, IN A MOUSE MODEL OF ALZHEIMER'S DISEASE

Sous presse dans le journal *Neuroscience*

(JS Aucoin, P Jiang, N Aznavour, XK Tong, M Buttini, L Descarries, E Hamel)

*Neuroscience* xx (2005) xxx

# SELECTIVE CHOLINERGIC DENERVATION, INDEPENDENT FROM OXIDATIVE STRESS, IN A MOUSE MODEL OF ALZHEIMER'S DISEASE

J.-S. AUCOIN,[a] P. JIANG,[a] N. AZNAVOUR,[b] X.-K. TONG,[a] M. BUTTINI,[c] L. DESCARRIES[b] AND E. HAMEL[a]*

[a]*Complex Neural Systems, Department of Neurology and Neurosurgery, Montreal Neurological Institute, McGill University, 3801 University Street, Room 748, Montréal, QC, Canada H3A 2B4*

[b]*Départements de Pathologie et Biologie Cellulaire et de Physiologie, and Centre de Recherche en Sciences Neurologiques, Faculté de Médecine, Université de Montréal, QC, Canada H3C 3J7*

[c]*Gladstone Institute of Neurological Disease, San Francisco, CA 94141, USA*

**Abstract—Alzheimer's disease (AD) is characterized by increases in amyloid-β (Aβ) peptides, neurofibrillary tangles, oxidative stress and cholinergic deficits. However, the selectivity of these deficits and their relation with the Aβ pathology or oxidative stress remain unclear. We therefore investigated amyloidosis-related changes in acetylcholine (ACh) and serotonin (5-HT) innervations of hippocampus and parietal cortex by quantitative choline acetyltransferase (ChAT) and 5-HT immunocytochemistry, in 6, 12/14 and 18 month-old transgenic mice carrying familial AD-linked mutations ($hAPP_{Sw,Ind}$). Further, using manganese superoxide dismutase (MnSOD) and nitrotyrosine immunoreactivity as markers, we evaluated the relationship between oxidative stress and the ACh deficit in 18 month-old mice. Thioflavin-positive Aβ plaques were seen in both regions at all ages; they were more numerous in hippocampus and increased in number (>15-fold) and size as a function of age. A majority of plaques exhibited or were surrounded by increased MnSOD immunoreactivity, and dystrophic ACh or 5-HT axons were seen in their immediate vicinity. Counts of immunoreactive axon varicosities revealed significant decreases in ACh innervation, with a sparing of the 5-HT, even in aged mice. First apparent in hippocampus, the loss of ACh terminals was in the order of 20% at 12/14 months, and not significantly greater (26%) at 18 months. In parietal cortex, the ACh denervation was significant at 18 months only, averaging 24% across the different layers. Despite increased perivascular MnSOD immunoreactivity, there was no evidence of dystrophic ACh varicosities or their accentuated loss in the perivascular area. Moreover, there was virtually no sign of tyrosine nitration in ChAT nerve terminals or neuronal cell bodies. These data suggest that aggregated Aβ exerts an early, non-selective and focal neurotoxic effect on both ACh and 5-HT axons, but that a selective, plaque- and oxidative stress-independent diffuse cholinotoxicity, most likely caused by soluble Aβ assemblies, is responsible for the hippocampal and cortical ACh denervation.** 

**Key words: amyloid precursor protein (APP), acetylcholine, inflammation, amyloid, manganese SOD, neurodegeneration.**

Increased brain levels of amyloid-β (Aβ) peptides and their deposition in neuritic plaques and cerebral blood vessels (cerebral amyloid angiopathy, CAA), neurofibrillary tangles, oxidative stress and neuronal deficits are prominent neuropathological features of Alzheimer's disease (AD; Kalaria, 1997; Auld et al., 2002; Hardy and Selkoe, 2002; Huang et al., 2004). It is not yet clear, however, whether the extensive loss of neurons and pre-synaptic terminals observed in AD is one of the primary features of this disease or a consequence of the Aβ pathology. The acetylcholine (ACh) neurons in basal forebrain, which provide major inputs to the hippocampus and neocortex, are among the most precociously and severely affected in AD (Davies and Maloney, 1976; Whitehouse et al., 1982; Tong and Hamel, 1999; Beach et al., 2000; Mufson et al., 2002), and the resulting ACh deficits in these regions have been correlated with memory and cognitive impairments (Bierer et al., 1995; Shinotoh et al., 2000; Auld et al., 2002). There are indications that the serotonin (5-hydroxytryptamine, 5-HT) system, which is implicated in various aspects of cognition (Steckler and Sahgal, 1995; Buhot et al., 2000), could also be affected at relatively early stages in AD (Porter et al., 2000). At later stages, several neurotransmitter systems appear to be disturbed (Chan-Palay et al., 1986; Mufson et al., 1993). Interestingly, recent evidence suggests that the CAA may contribute more than Aβ plaques to cognitive loss (Pfeifer et al., 2002), and oxidative stress has been identified as an important accompanying factor in the Aβ pathology (Pappolla et al., 1998; Smith et al., 1998).

Most identified familial forms of AD (FAD) are caused by dominant mutations in genes encoding the amyloid precursor protein (APP) or the presenilin 1 or 2 (PS1 or PS2), all of which resulting in increased production of APP-derived Aβ peptides (Hardy, 1997; Selkoe, 1997; Price and Sisodia, 1998). In transgenic mouse models of AD that overexpress mutated forms of the human APP (hAPP), neuritic plaques, reactive gliosis, loss of synaptophysin-immunoreactive presynaptic terminals, and alterations in the innervation of various CNS regions have been reported (Games et al., 1995; Hsiao et al., 1996; Sturchler-Pierrat et al., 1997; Hsia et al.,

*Corresponding author. Tel: +1-514-398-8928; fax: +1-514-398-8106.
[redacted]

*Abbreviations:* Aβ, amyloid β; ACh, acetylcholine; [redacted], Alzheimer's disease; APP, amyloid precursor protein; CAA, cerebral amyloid angiopathy; ChAT, choline acetyltransferase; DAB, 3,3′-diaminobenzidine; FAD, familial form of Alzheimer's disease; $hAPP_{Sw,Ind}$, human amyloid precursor protein carrying familial AD-linked Swedish and Indiana mutations; MnSOD, manganese superoxide dismutase; PFA, paraformaldehyde; PS-1 or PS-2, presenilin 1 or presenilin 2; 5-HT, 5-hydroxytryptamine, serotonin.

0306-4522/05$30.00+0.00 
doi:10.1016/j.neuroscience.2004.11.047

1999; Mucke et al., 2000; Lewis et al., 2001). Some mice also exhibit synaptic transmission deficits and major behavioral/cognitive impairments (Hsiao et al., 1996; Chapman et al., 1999; Hsia et al., 1999; Larson et al., 1999; Chen et al., 2000; Palop et al., 2003). Cholinergic alterations of varying severity and magnitude have been documented in hAPP transgenic mice depending on age, mutations (hAPP±PS mutations) and brain areas (cortex, hippocampus) investigated (Wong et al., 1999; Bronfman et al., 2000; Apelt et al., 2002; Boncristiano et al., 2002; Buttini et al., 2002; German et al., 2003; Klingner et al., 2003). However, the selectivity of these changes, as well as their regional progression and relation with the amyloidosis or oxidative stress, remains unclear.

In the present study, we investigated the selectivity and severity of an eventual loss of ACh and 5-HT innervation in the hippocampus and parietal cortex of $hAPP_{Sw,Ind}$ transgenic mice at different ages, its temporal relationship with the Aβ pathology, and its association with oxidative stress. Quantitative immunocytochemical and cytochemical data were obtained on the density of choline acetyltransferase (ChAT) and 5-HT-immunostained innervations and number of neuritic plaques in the hippocampus and parietal cortex of wild type and transgenic mice aged 6, 12/14 and 18 months. Further, to gain insights into the pathological mechanisms leading to neuronal degeneration, we achieved simultaneous visualization of ChAT or 5-HT terminals and Aβ plaques, or the oxidative stress markers manganese superoxide dismutase (MnSOD) and nitrotyrosine which are both upregulated in AD brains (Furuta et al., 1995; Pappolla et al., 1992; Smith et al., 1997). Some of these results have been reported in abstract form (Descarries et al., 2002; Aznavour et al., 2003).

## EXPERIMENTAL PROCEDURES

### Animals

Experiments were approved by the Animal Ethics Committee of the respective institutions, and abided by the guidelines of the Canadian or American Council for Animal Care aimed at minimizing the number of animals used and their suffering. We used hAPP transgenic mice overexpressing the FAD-linked mutations $hAPP_{Sw,Ind}$ carrying the $670/671_{KM\rightarrow NL}$ (Sw) double mutation and the $717_{V\rightarrow F}$ mutation (Ind; line J20; Mucke et al., 2000). Mice were screened for transgene expression by Touchdown PCR with specific sense (5′-GGTGAGTTTGTAAGTGATGCC) and antisense (5′ TCTTCTTCTTCCACCTCAGC) hAPP primers, using tail extracted DNA (Games et al., 1995). Heterozygous transgenic founders were backcrossed with nontransgenic C57BL/6 mice. The study was performed on transgenic mice and their littermate controls (body weight: 40±10 g) aged 6, 12/14 and 18 months.

### Tissues and cyto/immunocytochemical labelings

Mice (16 wild-type and 16 transgenic) were anesthetized with sodium pentobarbital (65–80 mg/kg, i.p.) and perfused through the heart with 25 ml of ice-cold saline, followed by 250–300 ml of 4% paraformaldehyde (PFA) in 0.1 M phosphate buffer (50 mM, pH 7.4). Brains were rapidly removed, post-fixed overnight in PFA (4 °C) and either immediately cut on a vibratome (Leica, Montréal, QC, Canada) and sections stored at −20 °C in cryoprotectant solution (Vaucher and Hamel, 1995) until immunostaining, or cryoprotected (30% sucrose), frozen and stored at −80 °C until freezing microtome sectioning. The dorsal hippocampus and primary somatosensory (Par1) cortex were sampled in 20 μm-thick transverse sections between stereotaxic planes interaural A 1.5 and 1.98 mm (Franklin and Paxinos, 1997; Fig. 1). To confirm the specificity of primary antibodies not previously used by us (MnSOD, Aβ42 and nitrotyrosine), some sections were processed without these before incubation with secondary antibodies.

*ChAT, 5-HT, MnSOD and/or vascular (PECAM-1) immunostainings.* In initial experiments, free-floating frozen sections from 12/14 month-old wild-type and $hAPP_{Sw,Ind}$ mice ($n$=6 per group) were processed for ChAT or 5-HT immunocytochemistry, as previously described (Tong and Hamel, 1999). Sections were incubated (24 h, room temperature) either with goat anti-ChAT (1:500; Chemicon, Temecula, CA, USA) or rabbit anti-5-HT antibody (1:10,000; ImmunoStar, Hudson, WI, USA), then with biotinylated rabbit anti-goat or goat anti-rabbit secondary antibody (1.5 h; 1:200; Vector, Burlingame, CA, USA), and the reaction revealed with the ABC method (ABC Kit; Vectastain Elite; Vector; 1.25 h) and detected (1.5 min) with a 0.05% solution of 3,3′-diaminobenzidine (DAB; Sigma) activated with 0.005% $H_2O_2$. One of triplicate sections was mounted on slides, while the CA3 region of hippocampus and parietal cortex of the other two sections were resin-embedded and cut on an ultramicrotome in 2 μm-thick semithin sections (Tong and Hamel, 2000) for quantitative analysis of axon varicosities (see below).

To further assess the onset, evolution and selectivity of the ACh denervation, a method allowing for quantification of immunostained axon length and varicosity number (Mechawar et al., 2000; Aznavour et al., 2002) was used. Vibratome-cut sections from 6 month-old and 18 month-old wild-type mice and an equivalent number of $hAPP_{Sw,Ind}$ mice ($n$=4) were processed for ChAT immunocytochemistry (Aznavour et al., 2002), or for 5-HT immunostaining after antigen retrieval (Shi et al., 1991). Sections were incubated overnight with 2 μg/ml of monoclonal anti-ChAT antibody (B. K. Hartman, University of Minneapolis, USA) or rabbit 5-HT antibody (as above). Immunostaining was detected with the ABC method by incubation (2 h) with biotinylated horse anti-mouse or goat anti-rabbit secondary antibody (Vector; 1/200), the ABC kit (1.2 h), and detection (1.5 min) with $H_2O_2$-activated DAB (5-HT) or $H_2O_2$-activated DAB supplemented with 0.01% $CoCl_2$, 0.01% $NiSO_4$, 0.01% $(NH_4)_2SO_4$ (ChAT).

Other vibratome-cut sections from 18 month-old wild type and $hAPP_{Sw,Ind}$ mice ($n$=3–6 per group) were immunostained for MnSOD (a marker of increased production of the free radical superoxide; Pappolla et al., 1992), or double-immunolabeled for ChAT and MnSOD, ChAT and nitrotyrosine (a marker of peroxynitrite-mediated oxidative stress; Crow and Ischiropoulas, 1996; Smith et al., 1997), or for ChAT and the endothelial cell marker PECAM-1. For MnSOD, following overnight incubation with a rabbit anti-MnSOD (1:400; Stressgen, Victoria, BC, Canada), sections were incubated (1.5 h) with a goat anti-rabbit IgG (Vector), the ABComplex (1.25 h), and the reaction visualized with the slate gray reagent (gray precipitate, SG kit; Vector). For ChAT and MnSOD, ChAT was detected in first position with goat anti-ChAT (1:500; Chemicon) and DAB (brown precipitate), prior to MnSOD immunodetection with the SG reagent. For ChAT and PECAM-1 double-immunostaining, ChAT was detected in the first position prior to overnight incubation with a rat anti-PECAM-1 antibody (CD31, 1/200; BD Biosciences, San Diego, CA, USA) followed (2 h) by anti-rat IgG (1:200; Vector). Both reactions were detected with DAB as there is no overlap between neuronal ChAT and vascular CD-31 immunoreactivities, the latter being used to highlight blood vessel contours. Sections were then resin-embedded for semithin sectioning. For ChAT and nitrotyrosine double-immunofluorescence, sections were incubated overnight with goat anti-ChAT (1:500; Chemicon) and mouse anti-nitrotyrosine (1:1000; Upstate, Lake Placid, NY, USA) primary antibodies, respectively detected with Cy3- and Cy2-conjugated affiniPure species-specific secondary antibodies (1:200; Jackson ImmunoResearch,

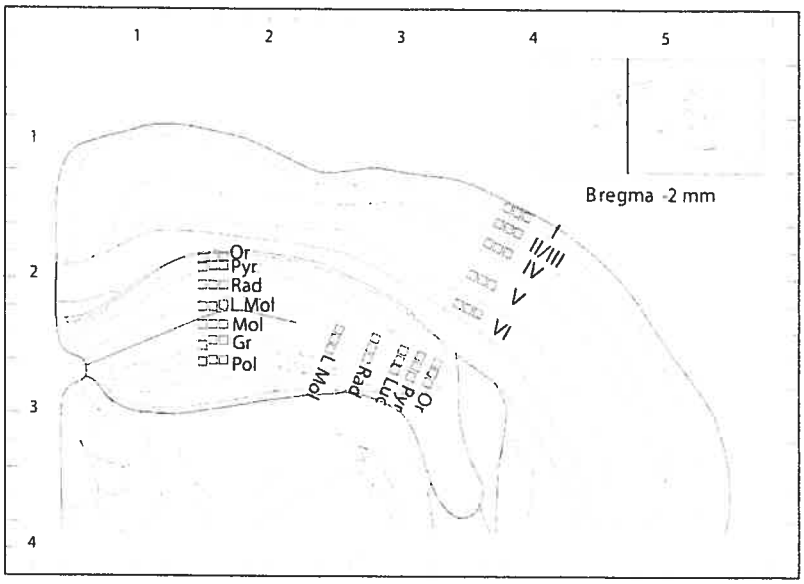


**Fig. 1.** Hippocampal and neocortical regions selected for quantitative analysis of the ACh and 5-HT innervations at a transverse mouse brain level approximately-2 mm to bregma (41). In 6 and 18 month-old mice, measurements of the density of ChAT- and 5-HT-immunostained axons were obtained from the different layers of three sectors of the dorsal hippocampus (CA1, CA3 and dentate gyrus) and of the primary somatosensory (Par1) area of parietal cortex, as schematized by the short rows of small square sampling windows (see Experimental Procedures for details). In 12/14 month-old mice, ChAT- and 5-HT-immunostained axon varicosities were counted directly on semithin sections from the stratum pyramidale (Pyr) and the stratum radiatum (Rad) of CA3, respectively, and from layers IV of the parietal cortex. Abbreviations for hippocampal strata: Gr, granulare; L Mol, lacunosum moleculare; Luc, lucidum; Mol, moleculare; Or, oriens; Pol, polymorph; Pyr, pyramidale; Rad, radiatum. The scaled is in millimeters.

West Grove, PA, USA). Sections were observed under confocal microscopy (Zeiss LSM 510; Zeiss, Jena, Germany) using simultaneous double channel visualization with emission intensities of 488 nm (Cy2) and 543 nm (Cy3).

*Aβ plaques staining combined or not with ChAT or 5-HT immunofluorescence.* Sections from all $hAPP_{Sw,Ind}$ and wildtype mice were stained (8 min) for amyloid with Thioflavin-S (Sigma; Wyss-Coray et al., 1997). The number of Aβ neuritic plaques in dorsal hippocampus and parietal cortex (up to the rhinal sulcus) was counted on a Leitz Aristoplan microscope equipped for epifluorescence with an FITC filter. Counts (two to three sections/mouse) were obtained from both regions in both hemispheres, averaged and expressed as number of plaques per region. Additionally, sections from two to three transgenic mice in each age group were used to examine the relationships between neuritic plaques and MnSOD, ChAT or 5-HT immunoreactivities by fluorescence immunocytochemistry (as above, but detected with Cy3-labeled secondary antibodies) followed by Thioflavin-S staining of Aβ plaques on immunostained sections already mounted on slides. In some 18 month-old $hAPP_{Sw,Ind}$ mice ($n$=3), Aβ plaques were simultaneously visualized with a specific antibody against $Aβ_{1-42}$ (rabbit anti-Aβ42, 1:200; Biosource, Camarillo, CA, USA) detected with a Cy3-labeled secondary antibody, followed by co-staining for Thioflavin-S. Other sections were immunostained for ChAT and Aβ42, by detecting ChAT (Chemicon) in first position with Cy3-labeled secondary antibody, followed by Aβ42 immunodetection with Cy2-labeled secondary antibody. All immunofluorescence-labeled sections were examined under confocal microscopy as described above.

*Quantification of ACh and 5-HT innervations.* The number of ChAT or 5-HT-immunostained varicosities were counted from three or more semithin sections per region in each 12/14 month-old wild-type or $hAPP_{Sw,Ind}$ mouse. Immunostained varisosities, defined as small punctate dilations 0.5 μm or more in transverse diameter (Umbriaco et al., 1994), were counted by two independent observers directly on photomicrographs from the CA3 region of dorsal hippocampus or the parietal cortex (layers IV and V), printed at a final magnification of 410×. In view of their respective distribution, hippocampal ChAT terminals were counted in the stratum pyramidale and 5-HT terminals in the stratum radiatum, using a transparent grid overlay (Geula and Mesulam, 1989; Tong and Hamel, 2000). Counts of varicosities (obtained from areas of approximately 60,000 $\mu m^2$ in hippocampus and 125,000 $\mu m^2$ in the cortex) from all sections in each region, and from each observer, were averaged and expressed as percent change from control mice. The size of ChAT varicosities in hippocampus was also measured on these photomicrographs, using a video camera, a frame grabber and the appropriate software (MCID/M4-Image Analysis System; Imaging Research, ON, Canada).

In 6 and 18 month-old mice, digitized images of ChAT- and/or 5-HT-immunostained axons were obtained at the selected levels (Fig. 1) with a RT Color camera (Diagnostic Instruments, Inc., Sterling Heights, MI, USA) mounted on a Leitz Diaplan microscope equipped with SPOT RT Software (v3.1; Diagnostic Instruments installed on a PC computer). Length measurements of these respective immunostained axon networks were determined in both regions, using a semi-computerized method as previously described (Mechawar et al., 2000; Aznavour et al., 2002). A total hippocampal area of 90,000 $\mu m^2$ and cortical area of 37,500 $\mu m^2$ was sampled in each mouse. Using a stereological formula (Soghomonian et al., 1987), the data were expressed as average density of axons ($m/mm^3$) for each layer and region. For ACh innervation, a further step was carried out to express its density in number of ChAT-immunostained axon varicosities per $mm^3$ of tissue. The average number of varicosities (defined as above) per unit length of immunostained axon was counted directly at the light microscope (×1000), on 50 axon segments from the different layers of the three hippocampal sectors and parietal cortex of wild-type and $hAPP_{Sw,Ind}$ mice (total of 800 counts). As the aver-

age number of varicosities per unit length of axon was fixed (four per 10 μm of axon), the density of axons could be arithmetically converted to density of varicosities.

To ensure that tissue volume changes would not bias the density measurements, the surface area of dorsal hippocampus and thickness of parietal cortex were determined by means of the same image analysis system in ChAT-immunostained sections from six wild-type and six transgenic 18-month-old mice.

Cortical perivascular ChAT varicosities (touching blood vessel walls in layers II–IV immunodetected with CD31 antibody; Tong and Hamel, 2000) were counted in double-immunostained semithin sections (two to three sections/mouse) from 18 month-old mice ($n$=6 wild-type and $n$=6 transgenic mice). Digitalized color pictures (Nikon Coolpix 4500 camera mounted on the Leitz Aristoplan microscope) covering a tissue area of approximately 3000 $\mu m^2$ were used for the analysis (Metamorph software, version 6.13; Universal Imaging Corp., Downingtown, PA, USA). Perivascular terminals were expressed per μm of vessel perimeter in the corresponding tissue sections.

### ChAT enzyme activity in the medial septum

ChAT activity was measured in the medial septum of 12/14 month-old $hAPP_{Sw,Ind}$ ($n$=15) and wildtype ($n$=12) mice as described (Buttini et al., 2002). Tissues extracts were obtained by sonication (diluted 1:20 wet w/v in 50 mM Tris/0.2% Triton buffer), followed by centrifugation. Supernatants were collected, protein levels determined (bicinchoninic acid assay; Pierce, Rockford, IL, USA), and diluted to 50 μl (50 mM Tris/0.5 M sodium-phosphate buffer, pH 7.0) before incubation (37 °C, 30 min) with 50 μl reaction buffer (0.4 M NaCl, 80 μg/ml eserine, 12 mM choline chloride, 10 μg/ml albumin, and 0.05 μCi $^{14}$C-labeled acetylCoA in Na-phosphate buffer). Reactions were stopped with ice-cold $H_2O$ (500 μl), samples loaded onto columns of Dowex 1X-A resin (Bio-Rad, Hercules, CA, USA), washed (2× with 600 μl $H_2O$), and effluents collected for counting on a Beckman scintillation counter. ChAT activity over that determined in boiled (5 min) tissue extracts was calculated and expressed as nanomoles/mg protein/h.

### Statistical analysis

Statistical comparisons of the laminal or regional density of ACh and 5-HT innervations in the cortex and hippocampus were performed by one-way ANOVA followed by two-tailed Student's $t$-test. Changes in innervation densities (ACh and 5-HT) or ChAT activity in 12/14 month-old mice, and perivascular ChAT terminals in 18 month-old mice were assessed by Student's $t$-test. A $P<0.05$ was considered significant.

## RESULTS

### ACh and 5-HT innervations in wild-type mouse hippocampus and parietal cortex

In keeping with earlier reports in mouse (Wong et al., 1999; Aznavour et al., 2002), fine varicose ChAT-immunostained fibers pervaded all layers of the dorsal hippocampus and parietal cortex, as illustrated here in an 18 month-old wild-type mouse (Fig. 2A, C). ChAT-positive cell bodies were rare in hippocampus (not shown), and the overall regional density of the ACh innervation was comparable (15–20 m of axons per $mm^3$ of tissue) between CA1, CA3 and DG (Fig. 2A; see Figs. 4–6). In parietal cortex, ChAT-positive neurons were present (Fig. 2C), and the mean density of innervation was comparable across all layers and similar to that in the most densely innervated hippocampal layers

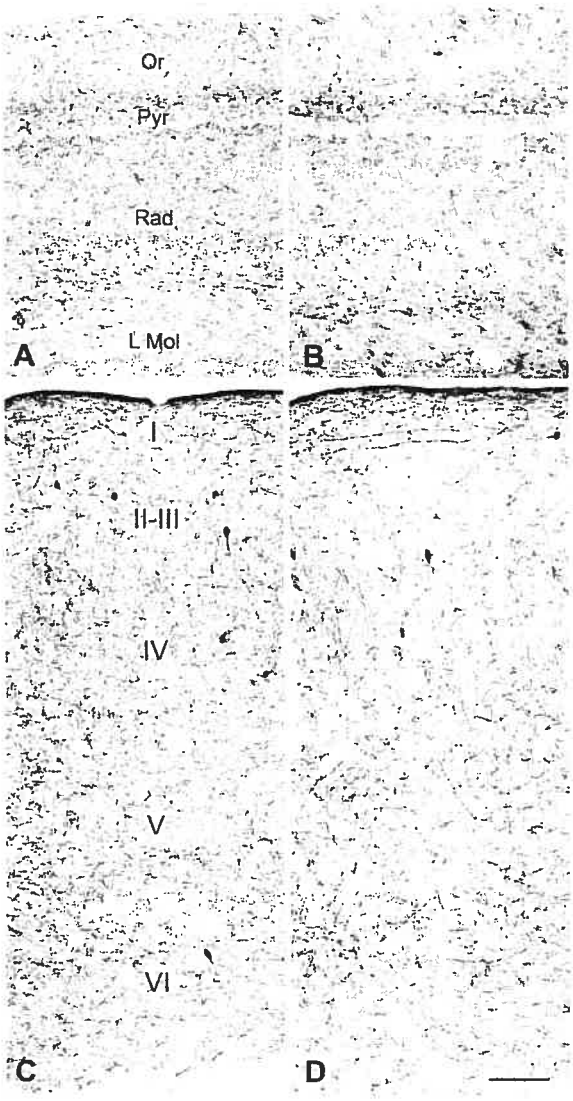


**Fig. 2.** Low-power photomicrographs illustrating the ACh (ChAT-immunostained) innervation pattern in CA1 of the dorsal hippocampus (top) and parietal cortex (bottom) of 18 month-old, wild type (A, C) and $hAPP_{Sw,Ind}$ transgenic mice (B, D). The decrease in density of the innervation in the transgenic mouse is apparent in all hippocampal and neocortical layers (see Fig. 6 for quantitative data). Scale bar=100 μm (in D).

(Fig. 2B, Figs. 4–6). The density of ACh innervation did not decrease in hippocampus or parietal cortex between 6 and 18 months of age (quantified in Figs. 4 and 6).

5-HT-immunoreactive axons were also distributed as previously reported, in both hippocampus and parietal cortex (Fujimiya et al., 1986; Donovan et al., 2002; data not shown). In hippocampus, the highest laminar densities of 5-HT innervation were in the stratum lacunosum moleculare of CA1 and CA3, and the lowest (8–9 vs approximately 4 m of axons per $mm^3$ of tissue, respectively) in the strata pyramidale and the stratum granulare of DG. In parietal cortex, the density of 5-HT innervation was highest

in layer I, at almost 10 m of axons per $mm^3$ of tissue. In both regions, the density of 5-HT axons and varicosities was clearly less than that of the ACh innervation (see Figs. 4 and 6).

### Aβ plaques, oxidative stress, and ChAT or 5-HT innervation in $hAPP_{Sw,Ind}$ mouse

All transgenic mice showed Thioflavin-S positive Aβ plaques in hippocampus, corpus callosum and cerebral cortex (Fig. 3, top panels), as well as in several pial and intracortical blood vessels (not shown). The plaques varied in number and size depending on mouse and age, being small and sparse in 6 month-old mice, and increasing in size, but mainly in number, with age. They were consistently more numerous in hippocampus than parietal cortex (approximately 50% at 6 and 12/14 months and approximately 20% at 18 months). They were also abundant in posterior cingulate and frontoparietal areas (Fig. 3, top panels). Compared with 6 months, their number increased almost seven-fold in both hippocampus and parietal cortex at 12/14 months, and more than 20-fold at 18 months (histogram in Fig. 3). There were no Thioflavin-S positive amyloid deposits in the brain or cerebrovascular tissue of wild-type littermate control mice at any age.

In $hAPP_{Sw,Ind}$ mice of all age groups, dystrophic, swollen and distorted ChAT- and 5-HT-immunofluorescent neurites were present in the immediate vicinity or within the core of Thioflavin-S stained Aβ plaques (Fig. 3, middle panels). Strikingly, even in the younger mice when rare and mainly small punctuate plaques could be detected, a proportion of these were surrounded or penetrated by abnormal ChAT- and 5-HT-immunoreactive varicose fibers (Fig. 3, 6 month panels). With increasing age, the increased number and size of plaques translated into a more frequent appearance of associated dystrophic terminals. Except for a minority of plaques, Thioflavin-S and Aβ42-positive Aβ plaques were equivalent in location (>90%), but could vary in size and extent depending on marker; Thioflavin-S positive plaques were easier to locate and exhibited a larger surface area (Fig. 3, bottom panel). A vast majority of Aβ42-immunostained plaques were invaded by dystrophic terminals as shown here for ChAT (Fig. 3, bottom panel). Thioflavin-S positive Aβ plaques either exhibited MnSOD immunostaining or were unstained in their core but surrounded by MnSOD immunoreactive material (Fig. 3; see also Fig. 7A, B insets). MnSOD-positive plaques were similarly invaded or surrounded by dystrophic ChAT varicosities (Fig. 3). Normal looking nerve terminals coursing through the tissue could be seen to become abnormally large and dysmorphic when approaching or penetrating Thioflavin-, Aβ42- or MnSOD-stained Aβ plaques (Fig. 3).

### Selective, age-dependent loss of ChAT innervation in $hAPP_{Sw,Ind}$ mice

The quantitative analysis of ChAT- and 5-HT-immunostained axon density in $hAPP_{Sw,Ind}$ mice of the three age groups revealed a loss of ACh innervation that progressed regionally with age. In both hippocampus and parietal cortex, the density of ChAT-immunostained axon varicosities was unaltered at 6 months (Fig. 4). At 12/14 months, there was a significant decrease in the relative number of ChAT varicosities in the stratum pyramidale of CA3 (19.5±5.6%, $P<0.05$), but not in the parietal cortex (Fig. 5A, B and 5E, F, and left bottom panels). As also shown in Fig. 5 (right bottom graphs), the average size of hippocampal ChAT varicosities remained unchanged, but ChAT activity in the medial septum was significantly decreased by comparison to wild-type littermate controls (23.4±3.6%, $P<0.01$).

At 18 months, comparable decreases in ACh innervation density (24–26%, $P<0.05$–$0.001$) were measured in both hippocampus and parietal cortex (compare Fig. 2B, D with 2A, C, and see Fig. 6). More specifically, the mean number of ChAT varicosities was reduced to 5.8 million/$mm^3$ in hippocampus and 6.3 million/$mm^3$ in parietal cortex, compared with corresponding values of 7.8 and 8.3 million/$mm^3$ in littermate controls (Fig. 6). In both regions, all layers appeared to be similarly affected (Fig. 6). This decrease in ChAT axons and varicosities occurred in the absence of any significant change in either the overall surface area of hippocampus (2.09±0.13 vs 2.01±0.22 $mm^2$ in wild-type and transgenic, respectively) or thickness of parietal cortex (0.91±0.06 vs 0.92±0.05 mm in wild-type and transgenic, respectively). Also, once established, there was no apparent progression in the ACh deficit, as illustrated by the comparable severity of denervation at 12/14 and 18 months in the CA3 region (stratum radiatum) of hippocampus (19.5±5.6% vs 28±5.9%, $P=0.34$).

In contrast to this progressive ACh denervation in hippocampus and then parietal cortex, there were no significant differences in density of 5-HT-immunostained varicose fibers between wild-type and transgenic mice in either the stratum radiatum of CA3 and layers IV–V of the parietal cortex at 12/14 months (Fig. 5), or across the different layers of the three hippocampal sectors and of parietal cortex at 18 months (Fig. 6).

### Oxidative stress and loss of ChAT-immunoreactive varicose fibers

Another striking finding of the present study was an upregulation of MnSOD immunoreactivity in both hippocampus and parietal cortex of 18 month-old $hAPP_{Sw,Ind}$ mice (Fig. 7). In addition to the granular neuronal labeling seen in wild-type littermates, consistent with mitochondrial localization of this antioxidant enzyme (Lindenau et al., 2000), 18 month-old $hAPP_{Sw,Ind}$ mice displayed plaque-associated MnSOD immunoreactivity (Fig. 7A, inset; see also Fig. 3) and, more notably, increased perivascular MnSOD-immunostained small punctate structures around some penetrating, intracortical and intrahippocampal blood vessels. In some mice, perivascular rims and cuffs of MnSOD immunoreactivity were salient (Fig. 7A). ChAT-immunostained varicosities within these perivascular areas were intermingled with MnSOD positive elements, but were not dystrophic or abnormal in appearance (Fig. 7B–D) except when located in the immediate vicinity of MnSOD immunoreactive plaques (Fig. 7B, inset).

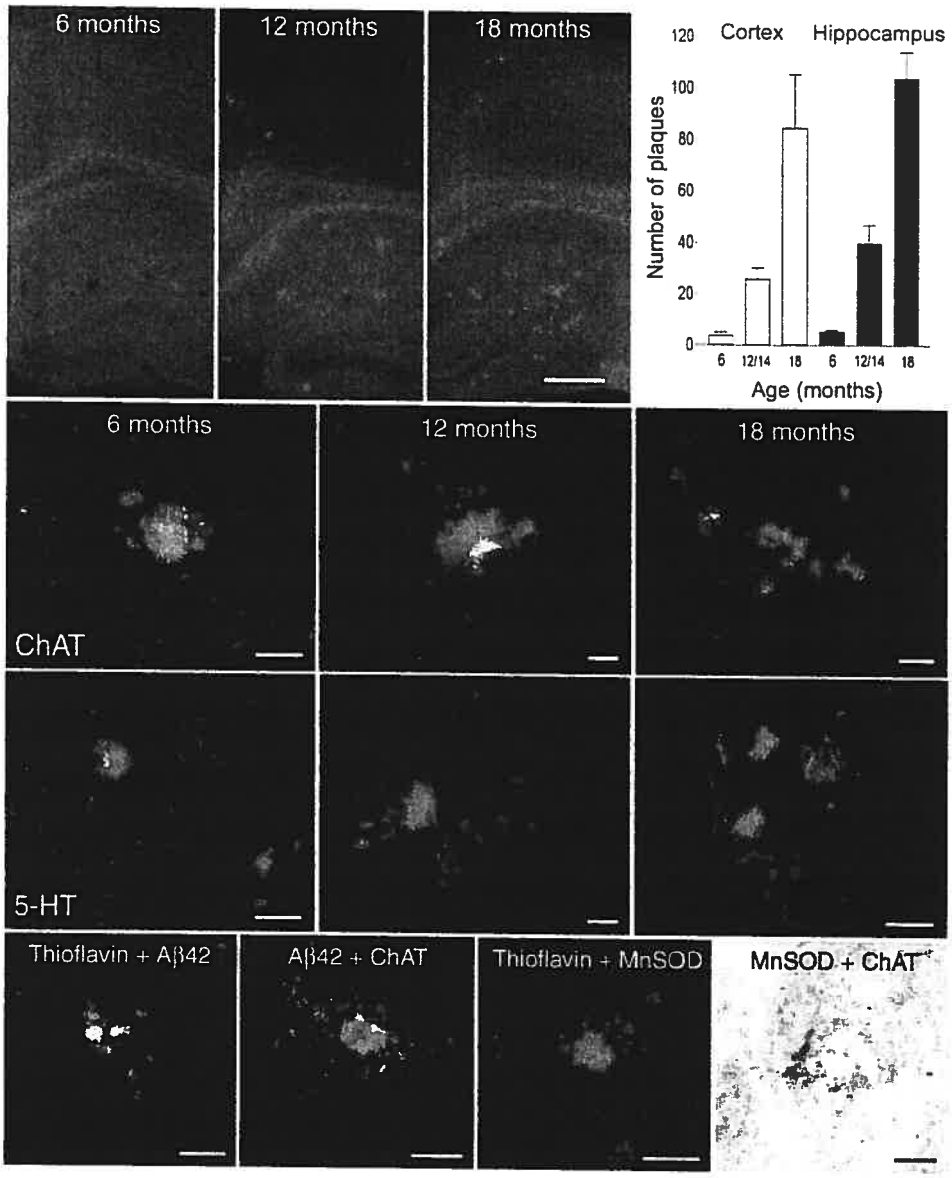


**Fig. 3.** Top panels: age-dependent increase in the number of Thioflavin-positive neuritic plaques in the hippocampus and parietal cortex of 6, 12/14 and 18 month-old $hAPP_{Sw,Ind}$ mice. Scale bar=50 μm. Right: bar graph showing the mean number of plaques per region for four to six mice in each age group. Middle panels: confocal pictures of dystrophic and swollen ChAT- or 5-HT-immunostained axons (red) in the immediate vicinity of Thioflavin-positive Aβ plaques (green) in the hippocampus or parietal cortex of 6, 12/14 and 18 month-old $hAPP_{Sw,Ind}$ mice. Scale bars=10 μm. Bottom panels: confocal pictures showing representative illustrations of the co-distribution of Thioflavin-S and Aβ42 immunostaining in plaques, the association of dystrophic ChAT-positive varicosities with a Aβ42-positive plaque, the presence of MnSOD immunoreactivity surrounding the core of a Thioflavin-positive Aβ plaque and, finally, light photomicrograph of ChAT immunostained varicose fibers (brown, DAB precipitate) within the outline of a MnSOD-immunoreactive plaque (gray, SG precipitate). Scale bars=20 μm, except for Thioflavin+MnSOD, 10 μm.

Despite such apparent increase in perivascular oxidative stress, quantitative analysis on semithin sections (Fig. 7E, F) showed that the loss of perivascular ChAT varicosities (3.22±0.46 vs 2.53±0.28 terminals/μm of vascular perimeter, ↓21%, n.s.) was comparable to that in the corresponding parenchyma (477.3±21.7 vs 409.3± 12.0 terminals/3000 $\mu m^2$, ↓14%, $P<0.05$). Additionally, peroxynitrite-mediated protein nitration was evidenced in $hAPP_{Sw,Ind}$ mice by increased intensity in nitrotyrosine immunostaining as compared with wild-type controls (not shown). Nitrotyrosine immunoreactivity could be seen in some neurons, but was prominent in glial cells distributed in plaque-like structures often associated with dystrophic ChAT varicose fibers (Fig. 7G) or diffusely throughout the neuropil (Fig. 7H). As such, the distribution pattern of nitrotyrosine immunoreactivity was totally distinct from that of ChAT-immunostained neuronal structures (Fig. 7H, I). Virtually no ChAT neuronal cell bodies or axonal varicos-

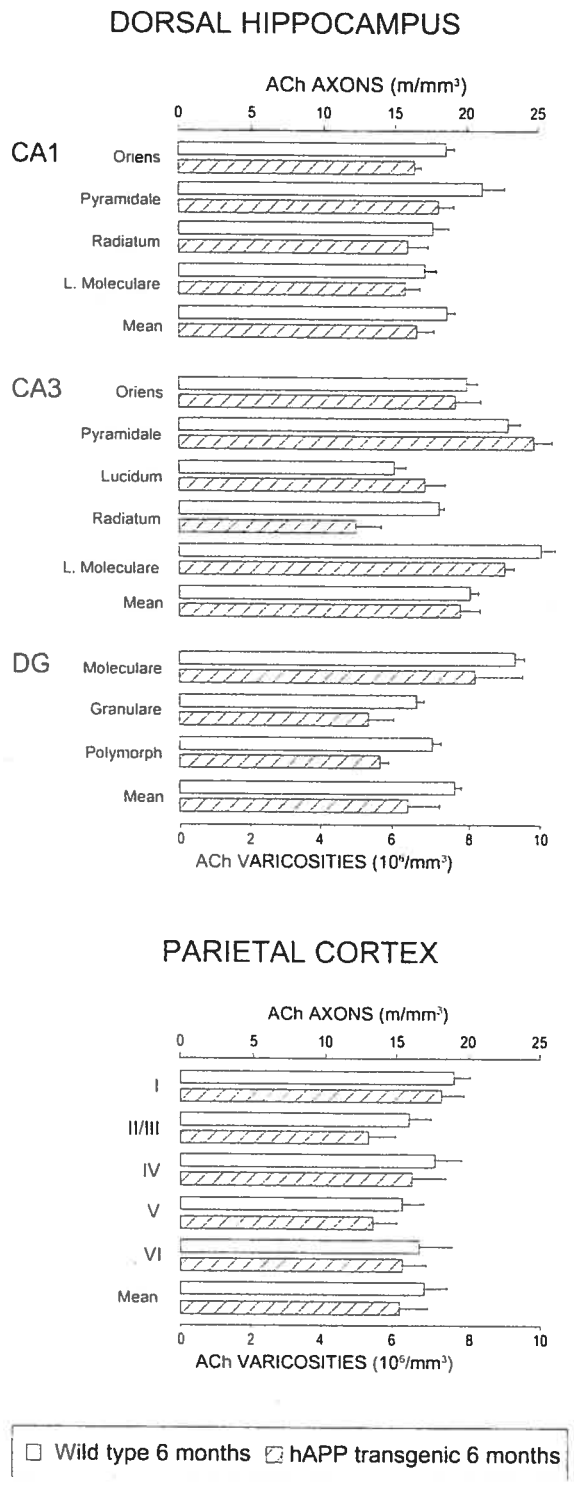


**Fig. 4.** Laminar and regional density of ChAT-immunostained axons and varicosities in dorsal hippocampus (CA1, CA3 and DG) and parietal cortex (layers I–VI) of 6 month-old wild-type and $hAPP_{Sw,Ind}$ mice. Data (means±S.E.M.) are from four mice in each group, and are expressed in meters of axons or millions of axon varicosities per $mm^3$. No statistically significant difference between wild-type and $hAPP_{Sw,Ind}$ transgenic mice, as analyzed by one-way ANOVA.

ities (2.7±0.7%, $n$=2743 ChAT varicosities counted) in cerebral cortex (Fig. 7J) or hippocampus showed sign of protein nitration.

## DISCUSSION

### Early and non-selective neurotoxicity of Aβ plaques in the $hAPP_{Sw,Ind}$ mouse

A first finding of this study was that neuritic plaques, as soon as they appeared, were locally neurotoxic to both ACh and 5-HT axons in $hAPP_{Sw,Ind}$ mouse brain. This was evidenced by the presence of swollen and distorted ChAT- and 5-HT-immunostained axons in the vicinity or within the core of plaques in 6 month-old mice, an age at which the plaques were still rare and minuscule, and when there was no measurable denervation. This clearly indicates that aggregated Aβ species exert a local, non-selective toxicity on neighboring neuronal elements. Another original finding was that, despite increased oxidative stress in brain of $hAPP_{Sw,Ind}$ mice, substantiated by upregulation of MnSOD immunoreactivity in the vicinity of both Aβ plaques and blood vessels, and of nitrotyrosine immunostaining in glial cells around plaques and in the neuropil, ChAT terminals were dystrophic only when associated with plaques, not preferentially affected around blood vessels, and did not, nor did ChAT neuronal perikarya in cortex, show sign of peroxynitrite-mediated oxidative damage. These findings foster the neurotoxic role of Aβ deposits and, further, suggest that oxidative stress per se is not cholinotoxic. Finally, the Aβ-associated local neuronal degeneration did not appear to be related to the subsequent widespread ACh denervation, since only ACh axons, and not the 5-HT, were eventually lost with age.

Such lack of selectivity in the neurotoxicity of Aβ deposits *in vivo* agrees with previous reports albeit in aged (12–23 months) transgenic mouse models of AD, showing swollen and distorted neurites around Aβ plaques that could be labeled not only with ACh markers (AChE; Sturchler-Pierrat et al., 1997; Bronfman et al., 2000; Boncristiano et al., 2002); vAChT (Wong et al., 1999); p75 (Jaffar et al., 2001); ChAT (Hernandez et al., 2001; German et al., 2003; Luth et al., 2003), but also for tyrosine hydroxylase or for different neuropeptides (Diez et al., 2000; Tomidokoro et al., 2000). As the electrophysiological properties of distorted neurites crossing through Aβ plaques are altered in AD (Knowles et al., 1999), our finding imply that there could be focal impaired neuronal functions resulting from these abnormal neurites at an early stage of the disease process. An important contributor to aggregated Aβ neurotoxicity is probably the highly fibrillogenic $Aβ_{1-42}$, as it is the form primarily but not exclusively increased in neuritic plaques of transgenic hAPP mice (Sturchler-Pierrat et al., 1997; Hsia et al., 1999; Mucke et al., 2000; Klein et al., 2001; Klingner et al., 2003), and in those of AD brains (Roher et al., 1993; Selkoe, 1997; Hardy and Selkoe, 2002). This is in accord with the robust overlap seen here between Thioflavin-S and Aβ42-positive plaques. Several mechanisms responsible for the neurotoxicity of aggregated Aβ have been proposed: $[Ca^{2+}]$ dysregulation (Mattson et al.,

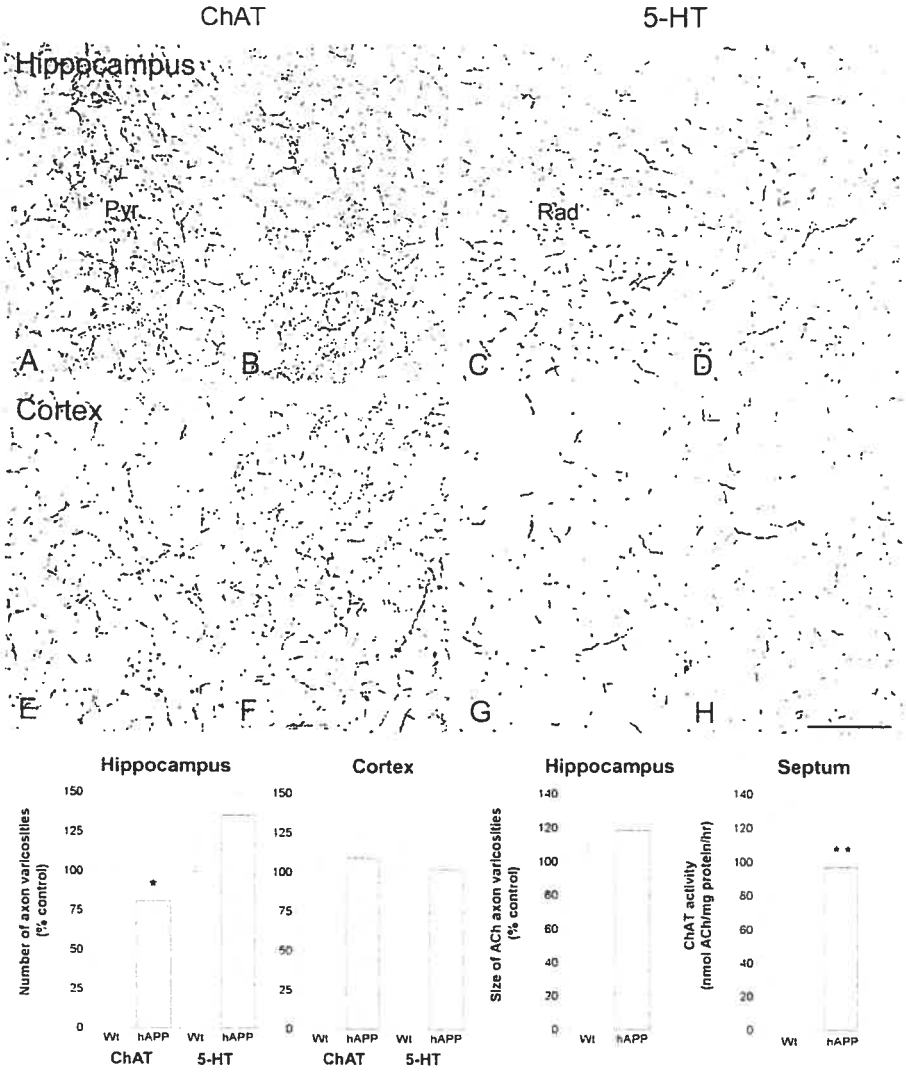


**Fig. 5.** The top panels (A–H) depict the ChAT- and 5-HT-immunostained innervations in CA3 of hippocampus and layers IV–V of the parietal cortex, as visualized in semi-thin sections from 12/14 month-old wild-type controls (A, C, E, G) and their littermate $hAPP_{Sw,Ind}$ mice (B, D, F, H). Note the decreased density of axon varicosities in the stratum pyramidale (Pyr) of CA3 of the transgenic mouse (compare A to B), but lack of change in the neocortex (E, F). In contrast, there was no significant change in either region (Rad, stratum radiatum) in sections immunostained for 5-HT (C, D, G, H). Scale bar=50 μm. The graphs at bottom represent the relative number of ChAT- and 5-HT-immunostained axon varicosities in both regions, the size of ChAT-immunostained axon varicosities in hippocampus, and measurements of ChAT activity in the medial septum of the same mice. Means±S.E.M. from four to six mice in each group, except for ChAT activity which was measured in 12 and 15 wild type and $hAPP_{Sw,Ind}$ mice, respectively. * $P<0.05$ and ** $P<0.01$ by Student's *t*-test.

1993; Palop et al., 2003), increased neurofibrillary tangles formation (Gotz et al., 2001) and tau phosphorylation (Zheng et al., 2002), electrostatic membrane interaction or persistent binding and activation of cell surface receptors (Yankner, 1996; Hertel et al., 1997), apoptosis (Estus et al., 1997) and, more recently, enhanced local inflammation (Luth et al., 2003) or oxidative stress (Pappolla et al., 1998; Smith et al., 1998; Huang et al., 2004).

In this respect, we found increased MnSOD and nitrotyrosine immunoreactivities and hence, oxidative stress, within and around Aβ plaques, in proximity of brain vessels or in microglial cells in $hAPP_{Sw,Ind}$ mice. Such findings were in keeping with earlier reports of plaque-associated MnSOD-positive material in AD brains (Pappolla et al., 1992; Furuta et al., 1995). They corroborate observations in other APP transgenic mice of increased vascular (Paris et al., 2000; Park et al., 2004) or Aβ deposits-associated (Smith et al., 1998) oxidative stress, and protein nitration in glial cells-attributed to excessive NO production by activated glia (Rodrigo et al., 2004). The upregulated MnSOD perivascular cuffs seen here in $hAPP_{Sw,Ind}$ mice were also remarkably similar to those in rats with lipopolysaccharide-induced endothelial cell activation, and found to encompass endothelial, neuronal and glial elements (Ruetzler et al., 2001). However, despite such signs of increased oxidative stress in aged $hAPP_{Sw,Ind}$ mice, we found no evi-

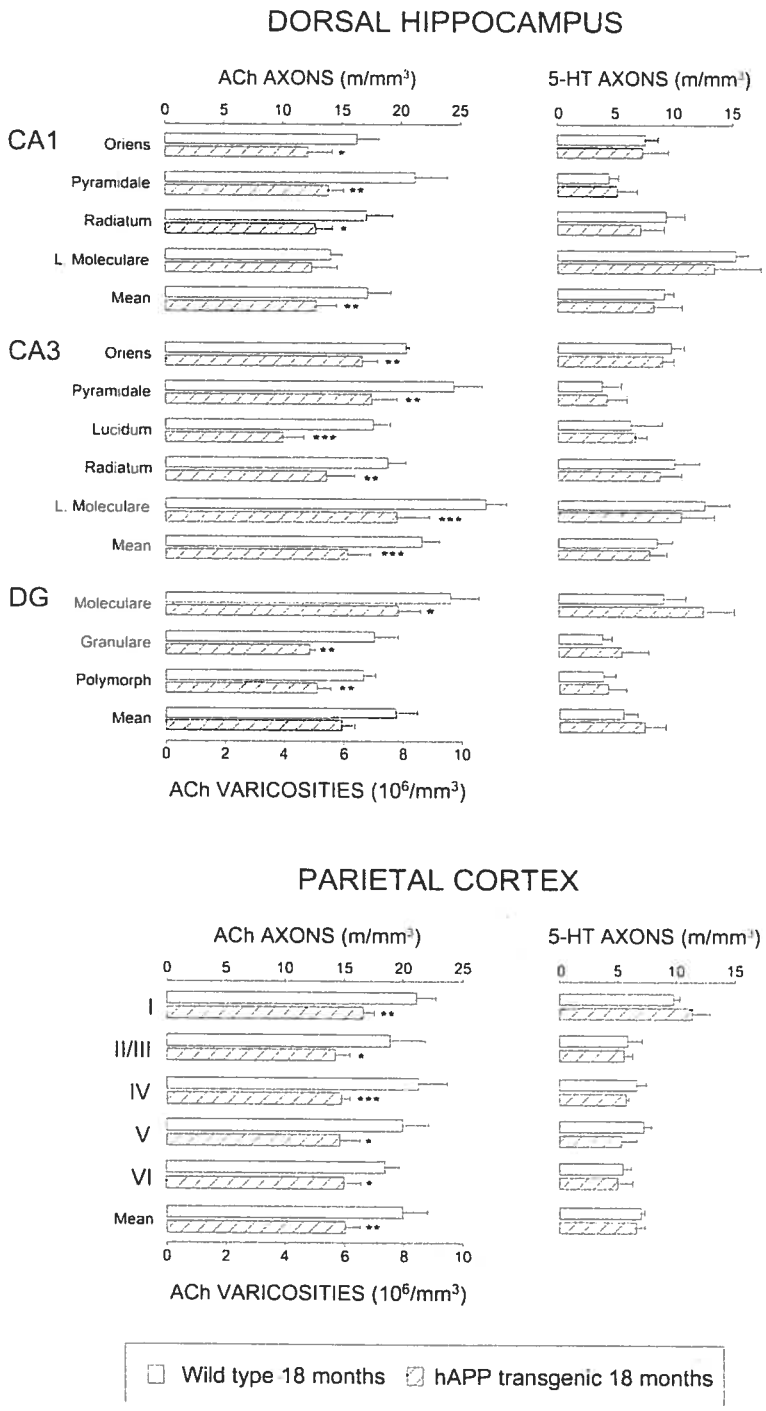


**Fig. 6.** Laminar and regional density of ChAT-immunostained axons and varicosities (left), and of 5-HT-immunostained axons (right), in dorsal hippocampus (CA1, CA3 and DG) and parietal cortex (layers I–VI) of 18 month-old wild-type and $hAPP_{Sw,Ind}$ mice. Data (means±S.E.M.) are from four mice in each group, and are expressed in meters of axons and/or millions of axon varicosities per $mm^3$. Statistically significant differences between wild-type and $hAPP_{Sw,Ind}$ mice are designated by asterisks. * $P<0.05$, ** $P<0.01$, and *** $P<0.001$ by one-way ANOVA followed by Student's *t*-test.

dence for enhanced ACh denervation in perivascular areas or for peroxynitrite-mediated oxidative damage in ChAT varicosities or neuronal perikarya. Indeed, dystrophic ChAT fibers were strictly found in association with Thioflavin-, Aβ42-, MnSOD- or nitrotyrosine-positive plaques. Together, these findings support a role for oxidative stress in the neurotoxicity of aggregated $A\beta_{1-42}$ (Butterfield and Bush, 2004), and further indicate that oxidative stress per se—independent

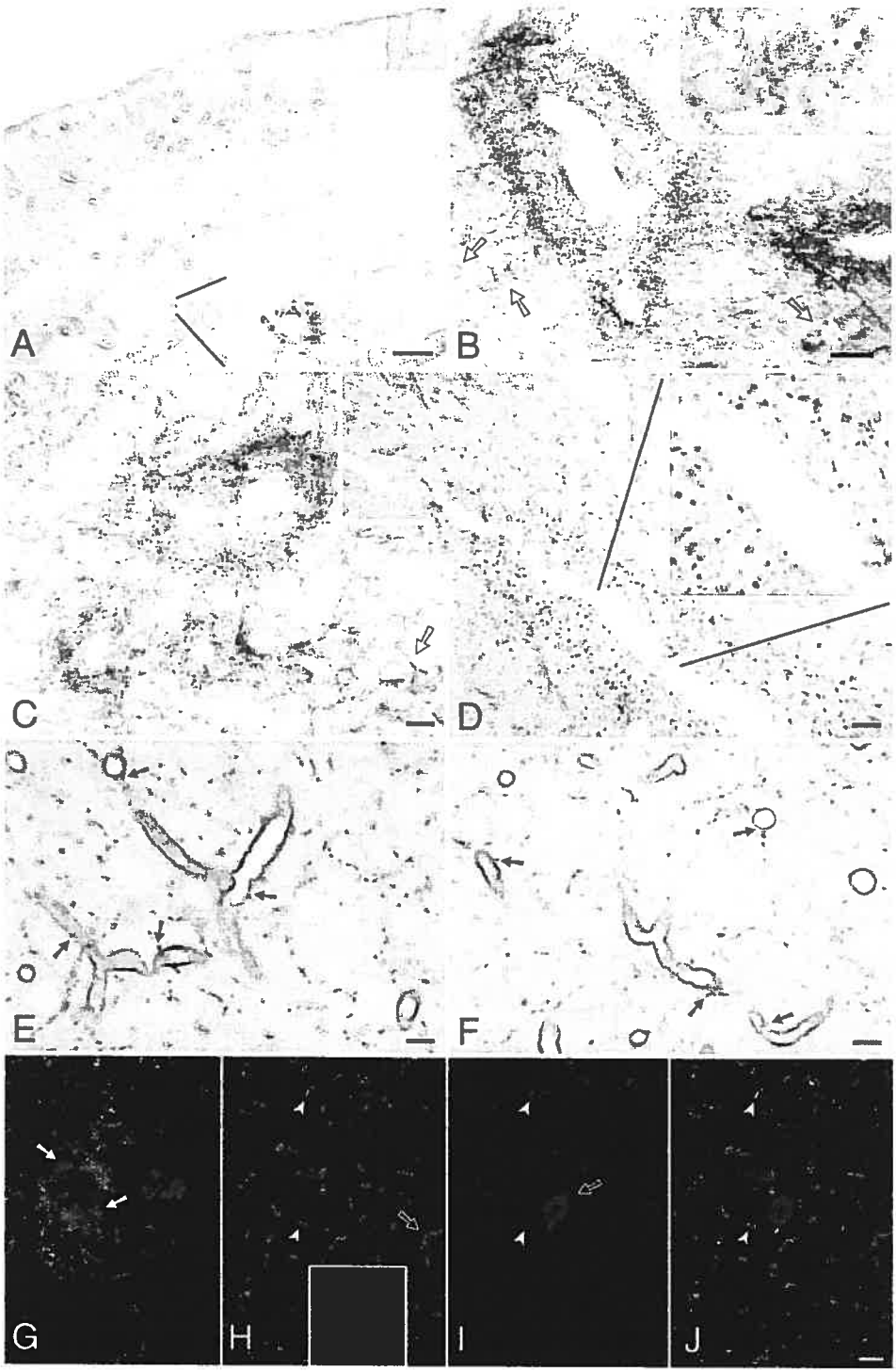


**Fig. 7.** MnSOD and nitrotyrosine immunoreactivities in 18 month-old $hAPP_{Sw,Ind}$ mice. In hippocampus and cerebral cortex (A), strong MnSOD-immunoreactivity is distributed in rims around penetrating and intraparenchymal blood vessels, as well as in association with plaques (bottom inset). Scale bar=250 μm. In MnSOD and ChAT double-immunostained thick (B, C) and semithin (D) sections, MnSOD immunoreactivity (gray/black) is seen in neurons (arrows in B and C) and in small punctuate structures around blood vessels through which normal ChAT varicose fibers (brown) are coursing. ChAT varicosities are dystrophic when approaching MnSOD-positive plaques (inset in B), but normal in size and appearance within perivascular rims where they are intermingled with MnSOD-positive elements (D), as better appreciated at a higher magnification (inset in D). Semithin sections from wild-type (E) and $hAPP_{Sw,Ind}$ (F) mice double-immunostained for ChAT and CD31 showing that perivascular ChAT varicosities (small

from aggregates of Aβ—is not implicated in the selective and widespread ACh denervation occurring uniformly throughout the neocortex and hippocampus of $hAPP_{Sw,Ind}$ mice.

### Selective and progressive cholinergic denervation in the $hAPP_{Sw,Ind}$ mouse

The most striking finding of the present study was the selective and progressive decrease in ACh innervation density, which first involved the hippocampus at 12/14 months (20%), and then the parietal cortex at 18 month (25% in both regions). There was no direct relationship between the age-dependent increase in the number of plaques and the decrease in the density of ChAT positive axonal varicosities in hippocampus and parietal cortex. Only a small increase (20% to 26%, n.s.) in the ACh deficit was measured in hippocampus between 12/14 and 18 months, while there was a 2.6-fold increase in the number of plaques. Moreover, the ACh denervation was selective in that, even in the oldest $hAPP_{Sw,Ind}$ mice, the density of 5-HT innervation was maintained despite the presence of dystrophic 5-HT axons in the immediate vicinity of plaques. The sparing of 5-HT innervation observed here *in vivo* agrees with previous reports of an apparent resistance of 5-HT neurons to Aβ toxicity *in vitro* (Gschwind and Huber, 1995). It has also been shown that neurotrophic factor-induced differentiation of RN46A cells into an ACh phenotype results in a cell population highly sensitive to Aβ peptide, whereas the differentiation of these cells into the 5-HT phenotype yields a population unaffected by Aβ treatment (Olesen et al., 1998). These observations clearly point to a selective alteration of the ACh system in $hAPP_{Sw,Ind}$ mice, which develops independently of the focal non-selective neurotoxicity associated with Aβ neuritic plaques.

Previous studies have reported cholinergic deficits in different transgenic mouse models of AD. For example, Klingner and colleagues (2003) reported an approximately 30% decrease in vesicular choline uptake or ACh transporter (vAChT) in cortex and/or hippocampus of 17 month-old $hAPP_{Sw}$ mice with high levels of both soluble and fibrillar Aβ. Wong and colleagues (1999) reported a 20% decrease in the density of vAChT-immunostained axon varicosities in the frontal cortex of 8 month-old $hAPP_{Sw}$/$PS1_{M146L}$ double transgenic mice, which displayed extensive Aβ neuritic plaques (see also Jaffar et al., 2001). Likewise, Boncristiano and colleagues (2002) measured a 29% loss of AChE-labeled axons in the neocortex of 24 month-old APP23 mice that also exhibited a considerable number of neuritic plaques. Here, the ubiquitous distribution of the cholinergic denervation contrasting with the focal distribution of Aβ plaques can be viewed as a further indication that Aβ plaques are not primarily responsible for this ACh deficit. Also, at variance with the focal dystrophic changes in ChAT and 5-HT terminals, which were already present around plaques 6 months, the cholinergic denervation became apparent only at 12/14 months in the hippocampus and 18 months in the parietal cortex, further downgrading aggregated Aβ and plaque-associated oxidative stress as causal mechanisms. Additionally, our findings of no progression in the cholinergic deficit in hippocampus with age together with previous studies of a similar extent of ACh denervation (20–30%) between regions, ages (8–24 months) and different hAPP transgenic mouse models (Wong et al., 1999; Jaffar et al., 2001; Boncristiano et al., 2002; Klingner et al., 2003) clearly point to a plateau in the progression of this degenerative process in transgenic mice. This would be compatible with the reported stabilization (or even slight decrease) in soluble Aβ species levels in brain and cerebrospinal fluid of these mice due to increased sequestration into plaques between 9 and 23 months (Kawarabayashi et al., 2001).

In keeping with the hypothesis of a cholinotoxicity of soluble Aβ (Lue et al., 1999; McLean et al., 1999; Hardy and Selkoe, 2002; Klein et al., 2001), an important cortical ACh deficit has recently been shown to occur in homozygous 4 month-old $hAPP_{Ind}$ mice, at a time when these mice exhibit high levels of Aβ but minimal plaque load (German et al., 2003). Our findings together with these previous observations strongly suggest that soluble Aβ, including its amorphous, non-congophilic protofibrils and small oligomers not readily detected here with either Thioflavin-S or Aβ42 antibody, might be causing the cholinotoxicity. Among possible mechanisms, soluble Aβ has been shown to increase choline fluxes in PC12 cells (Allen et al., 1997), to bind with high affinity to nicotinic ACh receptors (Wang et al., 2000), and to affect the high affinity choline uptake and the rate of ACh synthesis and release (Kar et al., 1998; for review, Dolezal and Kasparova, 2003). The latter would be consistent with the decrease (23%) in ChAT activity measured here in the medial septum of 12/14 month-old $hAPP_{Sw,Ind}$ mice, or in the medial septum, hippocampus or neocortex of other APP transgenic mouse models (Bronfman et al., 2000; Boncristiano et al., 2002; German et al., 2003).

## CONCLUSIONS

Our study shows that the plaque-associated, non-selective neurodegeneration and the diffuse, selective ACh denervation detected here in $hAPP_{Sw,Ind}$ transgenic mice are independent events, most likely secondary to increased levels of aggregated and soluble forms of Aβ peptides,

arrows) in $hAPP_{Sw,Ind}$ mice are not more severely affected than those in the neuropile (see text for data), despite increased perivascular MnSOD immunoreactivity as depicted in A–D. In double-immunofluorescence-stained sections for ChAT (Cy3, red) and nitrotyrosine (Cy2, green), nitrotyrosine immunoreactivity is localized in glial cells distributed into plaque-like structures (G) often associated with swollen and dystrophic ChAT terminals (arrows in G). In the neuropil, nitrotyrosine immunoreactivity (H) is primarily distributed in microglial cells (open arrow in H) and their processes while ChAT immunostaining (I) is restricted to neuronal cell bodies (open arrow) and numerous axonal varicosities, with virtually no sign (<3%; see text) of tyrosine nitration (J; merge is yellow). Arrowheads in H–J point to varicosities that co-localize ChAT and nitrotyrosine. Scale bars=50 μm in B, and 10 μm for all other panels. Negative controls are shown for MnSOD (top inset in A) and nitrotyrosine (inset in H) immunocytochemistry.

respectively. Our results also indicate that oxidative stress is not a primary factor in the diffuse ACh deficit. In view of the selectivity and regional progression of this ACh denervation in hippocampus, and later appearance in parietal cortex, this animal model could prove particularly useful to investigate the biological mechanisms of Aβ amyloid cholinotoxicity, as well as the efficacy of vaccines or other therapeutic measures aimed at protecting ACh neurons.

*Acknowledgments—We thank Dr. L. Mucke (Gladstone Inst of Neurological Disease and Dept of Neurology, UCSF, CA, USA) for the $hAPP_{Sw,Ind}$ transgenic mouse breeders, and Drs. C. Cozzari (Rome, Italy) and B. K. Hartman (Minneapolis, MN, USA) for their generous gift of monoclonal anti-ChAT antibody. We are also grateful to Mrs. N. Serluca and A. Yanes for technical support, Drs. T. Yeo and F. Longo (VA San Francisco Medical Center and Dept of Neurology, UCSF) for help with the ChAT assay, and Ms L. Michel for secretarial assistance. This study was supported by grants MOP 53334 (E.H.) and NRF 3544 (L.D.) from the Canadian Institute of Health Research, as well as a research grant from the Alzheimer Society of Canada (E.H.).*

## REFERENCES

Allen DD, Galdzicki Z, Brining SK, Fukuyama R, Rapoport SI, Smith QR (1997) Beta-amyloid induced increase in choline flux across PC12 cell membranes. Neurosci Lett 234:71–73.

Apelt J, Ashok J, Schliebs R (2002) Impairment of cholinergic neurotransmission in adult and aged transgenic Tg2576 mouse brain expressing the Swedish mutation of human β-amyloid precursor protein. Brain Res 953:17–30.

Auld DS, Kornecook TJ, Bastianetto S, Quirion R (2002) Alzheimer's disease and the basal forebrain cholinergic system: relations to beta-amyloid peptides, cognition, and treatment strategies. Prog Neurobiol 68:209–245.

Aznavour N, Mechawar N, Descarries L (2002) Comparative analysis of cholinergic innervation in the dorsal hippocampus of adult mouse and rat: a quantitative immunocytochemical study. Hippocampus 12:406–417.

Aznavour N, Tong XK, Aucoin J-S, Descarries L, Hamel E (2003) Neurotoxicity of beta-amyloid and selective, age-dependent loss of cholinergic fibers in the hippocampus and cerebral cortex of the PDAPP mouse. Program No. 842.7. 2003 Abstract Viewer/Itinerary Planner. Washington, DC: Society for Neuroscience. Online.

Beach TG, Kuo YM, Spiegel K, et al (2000) The cholinergic deficit coincides with Abeta deposition at the earliest histopathologic stages of Alzheimer disease. J Neuropathol Exp Neurol 59:308–313.

Bierer LM, Haroutunian V, Gabriel S, et al (1995) Neurochemical correlates of dementia severity in Alzheimer's disease: relative importance of the cholinergic deficits. J Neurochem 64:749–760.

Boncristiano S, Calhoun ME, Kelly PH, et al (2002) Cholinergic changes in the APP23 transgenic mouse model of cerebral amyloidosis. J Neurosci 22:3234–3243.

Bronfman FC, Moechars D, Van Leuven F (2000) Acetylcholinesterase-positive fiber deafferentation and cell shrinkage in the septohippocampal pathway of aged amyloid precursor protein London mutant transgenic mice. Neurobiol Dis 7:152–168.

Buhot MC, Martin S, Segu L (2000) Role of serotonin in memory impairment. Ann Med 32:210–221.

Butterfield DA, Bush AI (2004) Alzheimer's amyloid β-peptide (1–42): involvement of methionine residue 35 in the oxidative stress and neurotoxicity properties of this peptide. Neurobiol Aging 25:563–568.

Buttini M, Yu G-Q, Shockley K, et al (2002) Modulation of Alzheimer-like synaptic and cholinergic deficits in transgenic mice by human apolipoprotein E depends on isoform, aging, and overexpression of amyloid β peptides but not on plaque formation. J Neurosci 22:10539–10548.

Chan-Palay V, Lang W, Haesler U, Kohler C, Yasargil G (1986) Distribution of altered hippocampal neurons and axons immunoreactive with antisera against neuropeptide Y in Alzheimer's-type dementia. J Comp Neurol 248:376–394.

Chapman PF, White GL, Jones MW, et al (1999) Impaired synaptic plasticity and learning in aged amyloid precursor protein transgenic mice. Nat Neurosci 2:271–276.

Chen G, Chen KS, Knox J, et al (2000) A learning deficit related to age and β-amyloid plaques in a mouse model of Alzheimer's disease. Nature 408:975–979.

Crow JP, Ischiropoulas H (1996) Detection and quantification of nitrosative residues in proteins: in vivo marker of peroxynitrite. Methods Enzymol 269:185–194.

Davies P, Maloney AJ (1976) Selective loss of central cholinergic neurons in Alzheimer's disease. Lancet 2:1403.

Descarries L, Aznavour N, Aucoin J-S, Buttini M, Mucke L, Hamel E (2002) Loss of cholinergic innervation in the cerebral cortex and hippocampus of transgenic mice overexpressing V717F beta-amyloid precursor protein. Program No. 295.17. 2002 Abstract Viewer/Itinerary Planner. Washington, DC: Society for Neuroscience. Online.

Diez M, Koistinaho J, Kahn K, Games D, Hokfelt T (2000) Neuropeptides in hippocampus and cortex in transgenic mice overexpressing V717F β-amyloid precursor protein-initial observations. Neuroscience 100: 259–286.

Dolezal V, Kasparova J (2003) β-Amyloid and cholinergic neurons. Neurochem Res 28:499–506.

Donovan SL, Mamounas LA, Andrews AM, Blue ME, McCasland JS (2002) GAP-43 is critical for normal development of the serotonergic innervation in forebrain. J Neurosci 22:3543–3552.

Estus S, Tucker HM, van Rooyen C, et al (1997) Aggregated amyloid-β protein induces cortical neuronal apoptosis and concomitant "apoptotic" pattern of gene induction. J Neurosci 17:7736–7745.

Franklin KBJ, Paxinos G (1997 )The mouse brain in stereotaxic coordinates. San Diego: Academic Press.

Fujimiya M, Kimura H, Maeda T (1986) Postnatal development of serotonin nerve fibers in the somatosensory cortex of mice studied by immunohistochemistry. J Comp Neurol 246:191–201.

Furuta A, Price DL, Pardo CA, et al (1995) Localization of superoxide dismutases in Alzheimer's disease and Down's syndrome neocortex and hippocampus. Am J Pathol 146:357–367.

Games D, Adams D, Alessandrini R, et al (1995) Alzheimer-type neuropathology in transgenic mice overexpressing V717F β-amyloid precursor protein. Nature 373:523–527.

German DC, Yazdani U, Speciale SG, Pasbakhsh P, Games D, Liang C-L (2003) Cholinergic neuropathology in a mouse model of Alzheimer's disease. J Comp Neurol 462:371–381.

Geula C, Mesulam M (1989) Special properties of cholinesterases in the cerebral cortex of Alzheimer's disease. Brain Res 498:185–189.

Gotz J, Chen F, van Dorpe J, Nitsch RM (2001) Formation of neurofibrillary tangles in P3011 tau transgenic mice induced by Abeta 42 fibrils. Science 293:1491–1495.

Gschwind M, Huber G (1995) Apoptotic cell death induced by beta-amyloid 1–42 peptide is cell type dependent. J Neurochem 65: 292–300.

Hardy J (1997) The Alzheimer family of diseases: many etiologies, one pathogenesis? Proc Natl Acad Sci USA 94:2095–2097.

Hardy J, Selkoe DJ (2002) The amyloid hypothesis of Alzheimer's disease: progress and problems on the road of therapeutics. Science 297:353–356.

Hernandez D, Sugaya K, Qu T, McGowann E, Duff K, McKinney M (2001) Survival and plasticity of basal forebrain cholinergic systems in mice transgenic for presenilin-I and amyloid precursor protein mutant genes. Mol Neurosci 12:1377–1384.

Hertel C, Terzi E, Hauser N, Jakob-Rotne R, Seelig J, Kemp JA (1997) Inhibition of the electrostatic interaction between beta-amyloid

peptide and membranes prevents beta-amyloid-induced toxicity. Proc Natl Acad Sci USA 94:9412–9416.

Hsia AY, Masliah E, McConlogue L, et al (1999) Plaque-dependent disruption of neural circuits in Alzheimer's disease mouse models. Proc Natl Acad Sci USA 96:3228–3233.

Hsiao K, Chapman P, Nilsen S, et al (1996) Correlative memory deficits, Abeta elevation, and amyloid plaques in transgenic mice. Science 274:99–102.

Huang X, Moir RD, Tanzi RE, Bush AI, Rogers JT (2004) Redox-active metals, oxidative stress, and Alzheimer's disease pathology. Ann NY Acad Sci 1012:153–163.

Jaffar S, Counts SE, Ma SY, et al (2001) Neuropathology of mice carrying mutant APP(swe) and/or PS1 (M146L) transgenes: alterations in the p75(NTR) cholinergic basal forebrain septohippocampal pathway. Exp Neurol 170:227–243.

Kalaria RN (1997) Cerebrovascular degeneration is related to amyloid-β protein deposition in Alzheimer's disease. Ann NY Acad Sci 826: 263–271.

Kar S, Issa AM, Seto D, et al (1998) Amyloid β-peptide inhibits high-affinity choline uptake and acetylcholine release in rat hippocampal slices. J Neurochem 70:2179–2187.

Kawarabayashi T, Younkin LH, Saido TC, et al (2001) Age-dependent changes in brain, CSF, and plasma amyloid β protein in the Tg2576 transgenic mouse model of Alzheimer's disease. J Neurosci 21:372–381.

Klein WL, Krafft GA, Finch CE (2001) Targeting small Aβ oligomers: the solution to an Alzheimer's disease conundrum? Trends Neurosci 24:219–224.

Klingner M, Apelt H, Kumar A, et al (2003) Alterations in cholinergic and non-cholinergic neurotransmitter receptor densities in transgenic Tg2576 mouse brain with β-amyloid plaque pathology. Int J Dev Neurosci 21:357–369.

Knowles RB, Wyart C, Buldyrev SV, et al (1999) Plaque-induced neurite abnormalities: implications for disruption of neural networks in Alzheimer's disease. Proc Natl Acad Sci USA 96:5274–5279.

Larson J, Lynch G, Games D, Seubert P (1999) Alterations in synaptic transmission and long-term potentiation in hippocampal slices from young and aged PDAPP mice. Brain Res 840:23–35.

Lewis J, Dickson DW, Lin WL, et al (2001) Enhanced neurofibrillary degeneration in transgenic mice expressing mutant tau and APP. Science 293:1487–1491.

Lindenau J, Noack H, Possel H, Asayama K, Wolf G (2000) Cellular distribution of superoxide dismutases in the rat CNS. Glia 29:25–34.

Lue L-F, Kuo Y-M, Roher AE, et al (1999) Soluble amyloid β peptide concentration as a predictor of synaptic change in Alzheimer's disease. Am J Pathol 155:853–862.

Luth HJ, Apelt J, Ihunwo AO, Arendt T, Schliebs R (2003) Degeneration of beta-amyloid-associated cholinergic structures in transgenic APP SW mice. Brain Res 977:16–22.

Mattson MP, Tomaselli KJ, Rydel RE (1993) Calcium-destabilizing and neurodegenerative effects of aggregated beta-amyloid peptide are attenuated by basic FGF. Brain Res 621:35–49.

McLean CA, Cherney RA, Fraser FW, et al (1999) Soluble pool of Aβ amyloid as a determinant of severity of neurodegeneration in Alzheimer's disease. Ann Neurol 46:860–866.

Mechawar N, Cozzari C, Descarries L (2000) Cholinergic innervation in adult rat cerebral cortex: a quantitative immunocytochemical description. J Comp Neurol 428:305–318.

Mucke L, Masliah E, Yu G-Q, et al (2000) High-level neuronal expression of Aβ 1–42 in wild-type human amyloid protein precursor transgenic mice: synaptotoxicity without plaque formation. J Neurosci 20:4050–4058.

Mufson EJ, Cochran E, Benzing W, Kordower JH (1993) Galaninergic innervation of the cholinergic vertical limb of the diagonal band (Ch2) and bed nucleus of the stria terminalis in aging, Alzheimer's disease and Down's syndrome. Dementia 4:237–250.

Mufson EJ, Ma SY, Dills J, et al (2002) Loss of basal forebrain P75 (NTR) immunoreactivity in subjects with mild cognitive impairment and Alzheimer's disease. J Comp Neurol 443:136–153.

Olesen OF, Dago L, Mikkelsen JD (1998) Amyloid β neurotoxicity in the cholinergic but not in the serotonergic phenotype of RN46A cells. Mol Brain Res 57:266–274.

Palop JJ, Jones B, Kekonius L, et al (2003) Neuronal depletion of calcium-dependent proteins in the dentate gyrus is tightly linked to Alzheimer's disease-related cognitive deficits. Proc Natl Acad Sci USA 100:9572–9577.

Pappolla MA, Chyan YJ, Omar RA, et al (1998) Evidence of oxidative stress and in vivo neurotoxicity of beta-amyloid in a transgenic mouse model of Alzheimer's disease: a chronic paradigm for testing antioxidant therapies in vivo. Am J Pathol 152:871–877.

Pappolla MA, Omar RA, Kim KS, Robakis NK (1992) Immunohistochemical evidence of oxidative stress in Alzheimer's disease. Am J Pathol 140:621–628.

Paris D, Town T, Mori T, Parker TA, Humphrey J, Mullan M (2000) Soluble β-amyloid mediate vasoactivity via activation of a pro-inflammatory pathway. Neurobiol Aging 21:183–197.

Park L, Anrather J, Forster C, Kazama K, Carlson GA, Iadecola C (2004) Aβ-induced vascular oxidative stress and attenuation of functional hyperemia in mouse somatosensory cortex. J Cereb Blood Flow Metab 24:334–342.

Pfeifer LA, White LR, Ross GW, Petrovitch H, Launer LJ (2002) Cerebral amyloid angiopathy and cognitive function: the HAAS autopsy study. Neurology 58:1587–1588.

Porter RJ, Lunn BS, Walker LLM, Gray JM, Ballard CG, O'Brien JT (2000) Cognitive deficit induced by acute tryptophan depletion in patients with Alzheimer's disease. Am J Psychiatry 157:638–640.

Price DL, Sisodia SS (1998) Mutant genes in familial Alzheimer's disease and transgenic models. Annu Rev Neurosci 21:479–505.

Rodrigo J, Fernández-Vizarra P, Castro-Blanco S, et al (2004) Nitric oxide in the cerebral cortex of amyloid-precusor protein (SW) Tg2576 transgenic mice. Neuroscience 128:73–89.

Roher AE, Lowenson JD, Clarke S, et al (1993) Beta-amyloid-(1–42) is a major component of cerebrovascular amyloid deposits: implications for the pathology of Alzheimer disease. Proc Natl Acad Sci USA 90:10836–10840.

Ruetzler CA, Furuya K, Takeda H, Hallenbeck JM (2001) Brain vessels normally undergo cyclic activation and inactivation: evidence from tumor necrosis factor-α, heme oxygenase-1, and manganese superoxide dismutase immunostaining of vessels and perivascular brain cells. J Cereb Blood Flow Metab 21: 244–252.

Selkoe DJ (1997) Alzheimer's disease: genotypes, phenotypes, and treatments. Science 275:630–631.

Shi SR, Key ME, Kalra KL (1991) Antigen retrieval in formalin-fixed, paraffin-embedded tissues: an enhancement method for immunohistochemical staining based on microwave oven heating of tissue sections. J Histochem Cytochem 39:741–748.

Shinotoh H, Namba H, Fukushi K, et al (2000) Progressive loss of cortical acetylcholinesterase activity in association with cognitive decline in Alzheimer's disease: a positron emission tomography study. Ann Neurol 48:194–200.

Smith MA, Hirai K, Hsiao K, et al (1998) Amyloid-β in Alzheimer transgenic mice is associated with oxidative stress. J Neurochem 20:2212–2215.

Smith MA, Harris PLR, Sayare LM, Beckman JS, Perry G (1997) Widespread peroxynitrite-mediated damage in Alzheimer's disease. J Neurosci 17:2653–2657.

Soghomonian JJ, Doucet G, Descarries L (1987) Serotonin innervation in adult rat neostriatum: I. Quantified regional distribution. Brain Res 425:85–100.

Steckler T, Sahgal A (1995) The role of serotonergic-cholinergic interactions in the mediation of cognitive behaviour. Behav Brain Res 67:165–199.

Sturchler-Pierrat C, Abramowski D, Duke M, et al (1997) Two amyloid precursor protein transgenic mouse models with Alzheimer disease-like pathology. Proc Natl Acad Sci USA 94:13287–13292.

Tomidokoro Y, Harigaya Y, Matsubara E, et al (2000) Impaired neurotransmitter systems by Aβ amyloidosis in APPSW transgenic mice overexpressing amyloid β protein precursor. Neurosci Lett 292:155–158.

Tong XK, Hamel E (1999) Regional cholinergic denervation of cortical microvessels and nitric oxide synthase-containing neurons in Alzheimer's disease. Neuroscience 92:163–175.

Tong XK, Hamel E (2000) Basal forebrain nitric oxide synthase (NOS)-containing neurons project to microvessels and NOS neurons in the rat neocortex: cellular basis for cortical blood flow regulation. Eur J Neurosci 12:2769–2780.

Umbriaco D, Watkins KC, Descarries L, Cozzari C, Hartman BK (1994) Ultrastructural and morphometric features of the acetylcholine innervation in adult rat parietal cortex: an electron microscopic study in serial sections. J Comp Neurol 348:351–373.

Vaucher E, Hamel E (1995) Cholinergic basal forebrain neurons project to cortical microvessels in the rat: electron microscopic study with anterogradely transported *Phaseolus vulgaris* leucoagglutinin and choline acetyltransferase immunocytochemistry. J Neurosci 15:7427–7441.

Wang HY, Lee DH, D'Andrea MR, Peterson PA, Shank RP, Reitz AB (2000) beta-Amyloid (1–42) binds to alpha7 nicotinic acetylcholine receptor with high affinity: implications for Alzheimer's disease pathology. J Biol Chem 275:5626–5632.

Whitehouse PJ, Price DL, Struble RG, Clark AW, Coyle JT, Delon MR (1982) Alzheimer's disease and senile dementia: loss of neurons in the basal forebrain. Science 215:1237–1239.

Wong TP, Debeir T, Duff K, Cuello AC (1999) Reorganization of cholinergic terminals in the cerebral cortex and hippocampus in transgenic mice carrying mutated presenilin-1 and amyloid precursor protein transgenes. J Neurosci 19:2706–2716.

Wyss-Coray T, Masliah E, Mallory M, et al (1997) Amyloidogenic role of cytokine TGF-β 1 in transgenic mice and in Alzheimer's disease. Nature 389:603–606.

Yankner BA (1996) Mechanisms of neuronal degeneration in Alzheimer's disease. Neuron 16:921–932.

Zheng WH, Bastianetto S, Mennicken F, Ma W, Kar S (2002) Amyloid beta peptide induces tau phosphorylation and loss of cholinergic neurons in rat primary septal cultures. Neuroscience 115:201–211.

*(Accepted 30 November 2004)*

**Annexe 5**

# STRUCTURAL DETERMINANTS OF THE ROLES OF ACETYLCHOLINE IN THE CEREBRAL CORTEX

Publié en 2004

*Progress in Brain Research* 145: 45-58

(L. Descarries, N Mechawar, N Aznavour, KC Watkins KC)

## INTRODUCTION

The various roles attributed to acetylcholine (ACh) in mammalian cerebral cortex span across all levels of observation and knowledge at which the CNS may be studied. As illustrated by the different chapters in this book, cortical ACh has been implicated in elementary processes such as corticogenesis, neuronal excitability, shaping of receptive fields and the control of microcirculation, but also in more global functions, such as waking and sleep, attention, memory, learning, and even conscious experience. Accordingly, in humans, dysregulations of cholinergic neurons and properties have been identified in numerous neurological and psychiatric diseases, and sometimes held responsible for their occurrence and/or manifestations, raising hopes of therapies that might be better targetted and more efficient in a near future.

In general terms, it is therefore a real challenge for contemporary neuroscience to elucidate the different mechanisms underlying the many actions of ACh in cerebral cortex; notably how this neuromodulator participates in the processing of information and in the development of this part of the brain. This endeavor obviously requires a detailed knowledge of the structural and ultrastructural features of the cortical ACh innervation. For this reason, and to set the stage for current and future research, this chapter reviews the results of light and electron microscopic immunocytochemical studies, carried over the last ten years in our laboratory, which have provided basic information on the

regional distribution and relational features of the cortical ACh innervation in both the adult and the postnatal rat neocortex. Similar data are currently being acquired in the hippocampus. Our most recent observations indicate that, at least in neocortex, the ACh innervation develops early, and rapidly reaches the relatively dense laminar and regional densities measured in the adult. Moreover, we have established that this ACh innervation is largely non synaptic, not only in the adult but also throughout development.

## ACh INNERVATION IN CEREBRAL CORTEX AND HIPPOCAMPUS: GENERAL ORGANIZATION

As also described and illustrated in Chapters I (see also Wolff, 1991), the intricate network of varicose ACh axons pervading the mammalian neocortex and hippocampus arises mainly from magnocellular neurons in the basal forebrain (Rye et al., 1984; Saper, 1984). All areas and layers of the neocortex receive an ACh projection from a subpopulation of neurons in the substantia innominata-nucleus basalis complex, named Ch4 by Mesulam (Mesulam et al., 1983). The hippocampal ACh innervation originates mostly from cell bodies located in the septal nucleus and vertical limb of the diagonal band of Broca, i.e. Ch1 and Ch2 (McKinney et al., 1983; Rye et al., 1984; Amaral and Kurz, 1985; Nyakas et al., 1987; Woolf, 1991). It is currently estimated that there are some 7-9 thousand Ch4 neurons on each side of the rat brain (Rye et al., 1984; Gritti et al, 1993), versus some 400 in Ch1/Ch2 (Schwegler et al., 1996). In rodents at least, both regions also

receive an intrinsic ACh innervation from scattered bipolar interneurons, which has been estimated to account for about 20% of ACh axon terminals in neocortex (Eckenstein and Baughman, 1987), and 5-10% in hippocampus (Gage et al., 1983; Eckenstein and Baughman, 1987). In rat neocortex, these choline acetyltransferase (ChAT)-expressing interneurons are also known to synthesize GABA and VIP (Chédotal et al., 1994; Bayraktar et al., 1997).

The ACh cortical input may therefore be considered as having a dual origin, from both extrinsic (projection) and intrinsic neurons. This input can also be viewed as a system exerting its influence indirectly, through other cortical afferent systems, as exemplified by the dense ACh projections from the midbrain and pontine tegmentum to thalamocortical relay nuclei (Steriade et al., 1988; see Woolf, 1991, and Chapters 4 and 11). Moreover, the ACh projections from the midbrain to Ch4, and probable influence of the latter on cortical ACh interneurons (Porter et al., 1999) are suggestive of important interactions between the different ACh neuron groups. We will now review some of the basic structural determinants of ACh function in both neocortex and hippocampus.

## REGIONAL AND LAMINAR DISTRIBUTION OF THE ACh INNERVATION IN THE MATURE CORTEX AND HIPPOCAMPUS

In their light microscopic description of the distribution of ChAT-immunolabeled axons in the different cortical areas of the rat cerebral cortex, Lysakowski et al., (1989) reported a total of 13 different patterns of ACh innervation that were generally correlated to functionally similar cortical areas. However, none of the different ChAT antibodies available at that time allowed for a complete detection of the ACh axon network, prerequisite to a quantitative analysis of its distributional features. It is only in 1990 that an antibody against whole rat brain ChAT became available, that was sensitive enough to achieve a full visualization of the fine ACh varicose axons throughout the CNS of different mammalian species (Cozzari et al., 1990). As labeling of ACh axons with this antibody could be shown to be maximal in vibratome sections of perfusion-fixed brain, it became posssible to quantitate their regional and laminar distribution in adult rat cerebral cortex (Mechawar et al., 2000).

In transverse sections like those in Fig. 1, we used a semi-computerized light microscopic method to measure the actual length of the ChAT-immunoreactive axon network contained within the full thickness of transverse sections from the frontal (Fr1), parietal (Par1) and occipital (Oc1) neocortex (for technical details, see Mechawar et al., 2000). The number of varicosities (i.e. dilations > 0.5 microns in diameter) on these axons was counted directly under the light

microscope on axon segments randomly selected from every layer of each cortical region. Given that a constant ratio of 4 varicosities per 10 $\mu$m of axon was found throughout neocortex, the actual number of varicosities on the axon network could be directly derived from measurements of its length. Thus, the data could be expressed in two ways: 1) densities, i.e. axon length (in meters) and number of varicosities (in millions) per $mm^3$ of tissue; 2) axon length (in meters) and number of varicosities (in millions) under an arbitrary surface of 1 $mm^2$, to take into account the varying thickness of the layers and areas examined.

It was immediately apparent that the frontal cortex had the densest ACh innervation, followed by the occipital and the parietal cortex, with respective values of 5.4, 4.6 and 3.8 x $10^6$ varicosities/$mm^3$, as shown in Table 1 and Fig. 2. Because of the lesser thickness of the occipital cortex, the order changed between parietal and occipital for the values under 1 $mm^2$ of cortical surface. In the three areas, layers I and V were the most densely innervated, with respective inter-areal means of 5.3 and 5.0 x $10^6$ varicosities/$mm^3$. The least densely innervated layers were IV and VI of the primary sensory areas, with inter-areal means (Par1 and Oc1) of 3.4 and 3.8 x $10^6$ varicosities/$mm^3$, respectively. The laminar distributions were area specific, and characterized by uniformly high densities throughout frontal cortex, and lower densities in layers II/III, IV and VI of the parietal cortex, as well as in layers IV and VI of the occipital cortex (Fig. 2).

In hippocampus, the distribution of the ACh innervation was quantified in both mouse and rat (Aznavour et al., 2002). Values of regional (Table 1) and laminar

densities (Fig. 2) were obtained from three sectors of the dorsal hippocampus, CA1, CA3 and the dentate gyrus (DG). Again, the number of varicosities per unit length of ACh axon was fixed at 4 per 10 mm, allowing to express the data as both densities of axons and densities of varicosities. The salient features were regional densities even higher than in neocortex, ranging from 4.9 million in CA1 to 6.2 million in CA3 of rat, for a regional average of 5.9 million, compared to 4.6 million in the neocortex. There were few differences between rat and mouse hippocampal ACh innervations, the only significant one being a slightly lower interareal density in CA1 of rat, accounted for by relatively low values in its stratum radiatum and lacunosum moleculare.

## ULTRASTRUCTURAL FEATURES OF THE ACh INNERVATION IN ADULT NEOCORTEX AND HIPPOCAMPUS

We have described the ultrastructural features of the ACh innervation in both the primary somatosensory cortex (Par 1) (Umbriaco et al., 1994) and CA1 stratum radiatum of adult rat (Umbriaco et al., 1995). In the parietal cortex, an extensive examination of the intrinsic and relational features of the ACh (ChAT-immunostained) axon varicosities was carried out in serial as well as single thin sections. Among other findings, this thorough analysis revealed that, in all layers of the parietal cortex, only a small fraction of all ACh varicosities were endowed with a junctional complex, i.e. a straightening of apposed membranes with or without postsynaptic thickening on either side of a slightly widened extracellular

space. In general, the cortical ACh varicosities were relatively small, averaging 0.57 $\mu$m in diameter. Those bearing a synaptic junction were slightly but significantly larger than their non synaptic counterparts (0.67 $\mu$m in diameter). The junctional complexes formed by these terminals were single, occupied a small fraction of the total surface of varicosities ( 3%), and were almost always symmetrical (99%).

As shown in Table 2, the percentages of synaptic ACh varicosities that were then found in the various layers of Par1 were 10%, 14%, 11%, 21% and 14%, respectively, for an interlayer mean of 14%, and a true average of 16%, when taking into account the various thickness of the different layers. In hippocampus, ACh varicosities displayed similar ultrastructural features, with an average diameter of 0.6 $\mu$m and a synaptic incidence of 7%, as extrapolated for whole varicosities from the very low proportion (3%) observed to form synaptic contact in single thin sections (Umbriaco et al., 1995). In both neocortex and hippocampus, ACh synapses were always made with dendrites, either branches or spines. In cerebral cortex, enough synaptic ACh varicosities were seen to conclude that 75% percent were in contact with dendritic branches and only 25% with spines (Umbriaco et al., 1994). Combined with the above-mentionned quantified data, these average synaptic proportions gave us the actual number of synaptic and non synaptic ACh varicosities, as well as the number of synaptic varicosities in contact with dendritic branches or spines in cerebral cortex (Table 2). It is clear from these values that the synaptic ACh varicosities represent a

very small minority of all synapses in cortex or hippocampus, something in the order of 1 per 1500 synaptic terminals. This relative paucity of cortical ACh synapses should however not be taken to represent a lesser influence of ACh in cortical tissue, as discussed below.

Subsequent investigations in other laboratories have confirmed that a vast majority of cortical ACh varicosities in rat cortex are asynaptic, with reported estimates of 14% and 9% for the frontoparietal and entorhinal region, respectively (Chédotal et al., 1994; Vaucher and Hamel, 1995). The value of 66% recently reported by Turrini et al. (2001) for layer V of rat parietal cortex after labeling with the vesicular ACh transporter was presumably the result of a sampling bias, as suggested by a significantly larger size of the profiles examined in that particular study.

It is interesting to note that a thourough ChAT-immunocytochemical study of the cortical ACh innervation has also been performed in the prefrontal cortex of adult rhesus monkey (Mrzljak et al., 1995). These authors found that among 100 serially sectioned ChAT-immunoreactive varicosities at the border of layers II and III, only 44% made synaptic contact. Again, small dendritic shafts represented the most frequent synaptic target (70%). Fifty-six percent of the cortical ACh varicosities were without any visible junctional specialization, even if frequently juxtaposed to dendrites or spines receiving asymmetrical synapses. More recently, Smiley et al. (1997) carried out a similar study on two samples of human anterior temporal lobe removed at surgery. Sixty-seven percent of 42

varicosities sampled in layers I and II were then observed to be endowed with small but identifiable synaptic specializations. It remains to be determined whether such variations of synaptic incidence in cortex reflect sampling biases, regional differences or species differences. Unfortunately, there are at present no such data on the proportion of synaptic ACh varicosities in primate or human hippocampus.

## REGIONAL AND LAMINAR DISTRIBUTION OF THE ACh INNERVATION IN THE DEVELOPING NEOCORTEX

The development of the cortical ACh innervation was recently described between birth (P0) and postnatal day 32 (P32) in the frontal, parietal and occipital areas of rat, using the same approach as in the adult (>P60) (Mechawar and Descarries, 2001). The main findings of this study were that this innervation develops rapidly and much earlier than previously suspected. This was apparent even without quantification. As illustrated in the original article, immunostained ACh fibers, capped with growth cones, were already visible in the cortical subplate of the three regions at birth. These fibers, initially few in number, had invaded the cortical plate and marginal zone by P4, the age at which faintly immunoreactive interneurons were first detected. Rapid ingrowth and proliferation generated and adult-like distribution of axons that was already apparent at P8. Adult densities of branched varicose axons were apparently reached by postnatal day sixteen in the parietal area, while development continued

until the end of the first month for the frontal area and even later for the occipital area.

Another basic finding was that, in addition to the lenghtening and branching of ACh axons, a third parameter characterized this growing innervation. Between P4 and P16, the number of axon varicosities per unit lenght of axon increased steadily in all layers and areas, from 2 per 10 $\mu$m at P4 to 4 at P16, the adult ratio.

Fig. 3 depicts the growth of the ACh innervation in the three neocortical regions at the different postnatal ages examined. Again, both the density of varicosities (left) and their number under 1 $mm^2$ of cortical surface (right) are presented. The curves describe the time course of the growth in each layer and in the full thickness of each cortex. As may be observed for the three regions, the first two weeks are the period of fastest growth for each layer, and the temporal profile of growth is similar in every layer. There is no overproduction of fibers or varicosities at any age, only a steady increase until adult values are reached by 1 month. The curves for the frontal, parietal and occipital region are similar, except for a slightly slower, more protracted development in the occipital cortex.

## ULTRASTRUCTURAL FEATURES OF THE ACh INNERVATION IN THE DEVELOPING CORTEX

The intrinsic and relational features of ACh varicosities in the developing cortex were examined in single sections from the parietal (Par1) region at postnatal ages P8, P16 and P32 (Mechawar et al., 2002). Fig. 4 shows some examples of ChAT-immunostained varicosities, asynaptic or synaptic, at the three postnatal ages. On average, these varicosities were of similar size throughout development, with an average diameter of 0.48 $\mu$m, and area of 0.16 $\mu m^2$, significantly smaller than in the adult (0.52 $\mu$m and 0.23 $\mu m^2$; Umbriaco et al., 1994). Interestingly, the proportion of ACh varicosity profiles containing mitochondria increased gradually with age, from 21% at 8 days to 61% in the adult. As in adult, the vast majority of synaptic varicosities displayed symmetrical junctional complexes, which averaged 0.29 $\mu$m in length and were exclusively made with dendritic branches (71%) and spines (29%). Among 300 single sectional profiles examined at each postnatal age, only a small fraction displayed a synaptic junction, yielding respective synaptic incidences of 13.2% (P8), 15.6% (P16) and 22.2% (P32) for whole varicosities, a proportion not significantly different from the adult (16%). It was clear that the low frequency of synapses was characteristic of ACh varicosities as soon as they formed, as also reported recently for the noradrenaline innervation in the developing frontal and occipital cortex of rat (Latsari et al., 2002).

Since the proportion of synaptic ACh varicosities was stable during development, it could be inferred that the number of cortical ACh synapses had already reached its adult value by the end of the second week, at least in the parietal cortex. It could then be estimated at about 0.55 million per $mm^3$, and 1.0 million under 1 $mm^2$ of cortical surface (P16), compared to 0.53 and 1.23 million in the adult (>P60).

## FUNCTIONAL PROPERTIES OF THE ACh INNERVATION IN THE MATURE AND THE DEVELOPING CORTEX

These studies reveal major organizational features of the ACh innervations in cerebral cortex and hippocampus that should be determining their role(s) both in the adult and during development. First is their widespread distribution and abundance. As documented in Table 4, our quantitative data indicate that the ACh innervation is the densest neuromodulatory input to both neocortex and hippocampus. In neocortex, its average density of axon varicosities is more than four times higher than that of the noradrenaline (Audet et al., 1988) and a little higher than that of the serotonin innervation (Audet et al., 1989). In hippocampus, the average density of ACh varicosities is almost threefold that of the noradrenaline (Oleskevich et al., 1989) and more than twofold that of the serotonin innervation (Oleskevich and Descarries, 1990).

The ubiquity and density of the ACh input to cerebral cortex and hippocampus is consistent with the well documented involvement of ACh in numerous functional

processes, such as the modulation of sensory information (Sillito and Kemp, 1983; Donoghue and Carroll, 1987; Lamour et al., 1988; McKenna et al., 1988; Rasmusson and Dykes, 1988), plasticity of sensory maps (Metherate et al., 1988; Tremblay et al., 1990; Juliano et al., 1991; Kilgard and Merzenich, 1998; see chapter 10), control of microcirculation (Armstrong, 1986; Elhusseiny and Hamel, 2000; see chapter 12), learning (Rigdon and Pirch, 1986; Pirch et al., 1992; Fine et al., 1997; Miranda and Bermudez-Rattoni, 1999) and memory (Hasselmo et al., 1992; see also chapter 15). The richness of the ACh input to cortex can also be related to the more global effects attributed to ACh in wakefulness and sleep (Richter and Crossland, 1949; Jasper and Tessier, 1971; Jiménez-Capdeville and Dykes, 1996; see chapter 11), cortical activation (Krnjevic and Phillis, 1963a,b; Mitchell, 1963; Celesia and Jasper, 1966; Buzsàki et al., 1988; Metherate et al., 1992; see chapter 13), attention (Voytko et al., 1994; Gill et al., 2000), and even conscious awareness (Perry et al., 1999; see also chapter 20).

The mechanisms underlying these numerous functions are only beginning to be unraveled. For instance, the induction of low-amplitude, fast (20-40 Hz) oscillations in neocortex by *in vivo* nucleus basalis stimulation is thought to underlie the cortical activating properties of ACh (Metherate et al., 1992; Cox et al., 1994; Steriade et al., 1996; see also chapters 10 and 13). Such oscillations are viewed by some as reflecting the synchronous activity of widely distributed neuronal ensembles (Steriade and Amzica, 1996), which in turn would bind the separately processed features of a stimulus (for review, see Engel and Singer,

2001). The recent finding that nucleus basalis stimulation also elicits 40 Hz oscillations in the visual cortex has further prompted the hypothesis that ACh is crucial for the temporal binding of visual stimuli (W. Singer, personal communication). Of course, this does not preclude that other modulatory systems, differentially afferented and ubiquitously distributed in the cortex, might operate in concert to achieve the binding of information from various sources.

It has also been proposed that the involvement of ACh in learning and memory formation is rooted in its ability to differentially modulate the processing of afferent and efferent information (Hasselmo and Schnell, 1994; Kimura et al., 1999; Kimura, 2000; see also chapter 15). Interestingly, the respective laminar distributions of the ACh innervation in primary motor and primary sensory neocortex (Mechawar et al., 2000), as well as in dorsal hippocampus (Aznavour et al., 2002), are consistent with this hypothesis.

A second feature of obvious functional consequences is the predominantly asynaptic nature of the cortical and hippocampal ACh innervations, as first demonstrated in adult rat parietal cortex (Umbriaco et al., 1994) and stratum radiatum of CA1 (Umbriaco et al., 1995). It is generally assumed that such innervations exert many of their effects by diffuse transmission, in addition to synaptic transmission (Descarries et al., 1997; Descarries and Mechawar, 2000). Considering the density of ACh innervation in both neocortex and hippocampus, it is likely that much of the ACh released from their predominantly asynaptic ACh

varicosities reaches muscarinic and nicotinic receptors by diffusion in the extracellular space. To date, several immunocytochemical reports on the subcellular localization of muscarinic or nicotinic receptor subunits in cerebral cortex or hippocampus have underlined the fact that both receptor subtypes are mainly found at extrasynaptic locations (e.g. Hill et al., 1993; Mrzljak et al., 1998; Lubin et al., 1999; Rouse et al., 2000; see also chapters 3 and 7).

Because of the high density and predominantly asynaptic nature of the ACh axon varicosities, we have also proposed that in richly ACh-innervated regions such as cortex and hippocampus, as well as in neostriatum, a low ambient level of ACh might be permanently maintained in the extracellular space, and capable of influencing nicotinic and muscarinic receptors distributed on a variety of neighboring elements, including endothelial cells (Fig. 5; Descarries et al., 1997; Descarries, 1998). This hypothesis is consistent with the basal levels of extracellular ACh measured in cerebral cortex by microdialysis (e.g. Nilsson et al., 1990; Kosasa et al., 1999). It is also consistent with the fact that most of the acetylcholinesterase in the CNS is of the tetrameric globular form (G4). This isoform, which is found extrasynaptically at the neuromuscular junction (Gisiger and Stephens, 1988), is secreted by nerve terminals in the CNS and thus thought to regulate levels of ACh diffusing in the extracellular space (see Descarries et al., 1997). The existence of an ambient level of ACh and its functional impact in cortex and hippocampus could also account for the fact that heavy losses of cholinergic neurons (and hence of ACh innervation) must be occur in Alzheimer's

disease before it becomes clinically manifest (e.g. Whitehouse et al., 1982; see also chapter 22).

A third, previously unsuspected feature of the cortical ACh innervation, is its early and rapid development. Early, because we could observe ingrowing ChAT-immunoreactive axons in the cortical subplate on the very day of birth, almost two weeks sooner than reported in earlier ChAT-immunocytochemical investigations (Dori and Parnavelas, 1989; Gould et al., 1991; see also chapter 1). The precocity of this innervation is consistent with the expression of several parameters of ACh function in the embryonic and early postnatal neocortex (e.g. Aubert et al., 1996), and the various roles assigned to ACh in corticogenesis. However, the relatively high concentrations of ACh measured in rat neocortex at birth (Coyle and Yamamura, 1976) remain to be explained. They are difficult to reconcile with the existence of only few, scarcely distributed, unbranched ChAT-immunoreactive fibers observed in this brain region at birth (Mechawar and Descarries, 2001), even if these fibers are already capable of ACh release (Pedata et al., 1983). It is unlikely that this discrepancy reflects a transient synthesis of ACh by other cortical elements (e.g. glial cells), since ChAT protein or mRNA have never been detected at "ectopic" locations in developing cortex (Gould et al., 1991; Ibanez et al., 1991; Mechawar and Descarries, 2001). Perhaps the absence of a fully mature (and impermeable) blood-brain barrier until the end of the first postnatal week in rodents allows for the penetration and

diffusion in cortex of non-neuronal ACh synthesized in the placenta or in peripheral organs (for review on non-neuronal ACh, see Wessler et al., 1998).

In addition to demonstrating the speed with which the ACh innervation is formed in the developing neocortex, our quantitative study revealed a new parameter of ACh axon growth, i.e. the increase in number of varicosities per unit length of axon, which takes place in the first two weeks. During this period, if broken down to a single basalo-cortical neuron, the speed of axon growth may then be estimated at 2 cm of axon and 9000 varicosities per day, i.e. almost 1 mm of axon and 400 varicosities per hour.

Our ultrastructural study in postnatal rat indicated that diffuse transmission by ACh might apply to the developing as well as the adult cortex. Indeed, the intrinsic and relational features of ACh varicosities in the developing somatosensory area were adult-like throughout its postnatal development (Mechawar et al., 2002). The low proportion of synapses made by cortical ACh neurons may be considered as an innate feature, since it does not show significant age- or area-related variations, as also being observed in an ongoing study of the cholinergic innervation in the developing neostriatum (Aznavour et al., 2003). Also noteworthy is the fact that this proportion remains stable at a time when the varicosities are forming and greatly increasing in number along axons. It makes it unlikely that transient, "instructive" synapses are being established by the growing ACh neurons.

Even though the subcellular distribution of ACh receptors in the developing cortex has not yet been determined, functional receptors of both the nicotinic and muscarinic families are known to be expressed by cortical cells in the late embryonic and early postnatal periods (Ostermann et al., 1995; Zoli et al., 1995; Aubert et al., 1996; Ma et al., 2000; see also chapter 1). Thus, diffuse transmission and an ambient level of ACh, as discussed above, could participate in the many roles attributed to ACh during corticogenesis (Bear and Singer, 1986; Broide et al., 1996; Zhu and Waite, 1998; Aramakis et al., 2000; Peinado, 2000). This again raises the question as to the source(s) of the high concentrations of ACh measured in the cortex during the perinatal period, and how this ACh might be involved in corticogenesis? One might also ask if distinct or complementary functions are then being subserved by the synaptic versus asynaptic ACh varicosities? Which trophic factors/molecular cues guide the early and rapid growth of the cortical ACh innervation and the establishment and maintenance of its laminar- and area-specific distribution during the postnatal period and adult life? Answering these questions would undoubtedly provide useful information from both the fundamental and clinical standpoints.

The studies altogether convey a new image of the ACh neurons innervating the cerebral cortex or hippocampus. Early tracing experiments had shown the widespread (and probably overlapping) distribution of the axonal arborization of individual nucleus basalis neurons innervating the cerebral cortex (McKinney et al., 1983). On the basis of the present data, unitary ACh neurons may be calculated

to project 0.5 to 1 meter of axon endowed with 200 000 and 500 000 varicosities in cerebral cortex and hippocampus, respectively (Mechawar et al., 2000; Aznavour et al., 2002). In adult rat cortex alone, this adds up to a staggering total of 7.6 km of ACh axons bearing more than 3 billion varicosities. Such numbers together with the largely asynaptic nature of ACh axon varicosities suggest that these neurons are ideally shaped to exert diverse and widespread influences in vast expanses of cortex.

Acknowledgements

These studies were supported by grant MT-3544 to L.D., from the Medical Research Council of Canada (MRC), now grant NRF 3544 from the Canadian Institutes for Health Research. N.M. held a Research Studentship from MRC, and N.A. is recipient of a Ph.D. studentship from the Groupe de recherche sur le système nerveux central (FCAR) at the Université de Montréal. The authors are grateful to Costantino Cozzari and Boyd K. Hartman for their generous gift of ChAT antibody. They also thank Jean Léveillé and Gaston Lambert for photographic work.

## References

Amaral, D.G. and Kurz, J. (1985) An analysis of the origins of the cholinergic and noncholinergic septal projections to the hippocampal formation of the rat. *J. Comp. Neurol.*, 240: 37-59.

Aramakis, V.B., Hsieh, C.Y., Leslie, F.M. and Metherate, R. (2000) A critical period for nicotine-induced disruption of synaptic development in rat auditory cortex. *J. Neurosci.*, 20: 6106-6116.

Armstrong, D.M. (1986) Ultrastructural characterization of choline acetyltransferase-containing neurons in the basal forebrain of rat: Evidence for a cholinergic innervation of intracerebral blood vessels. *J. Comp. Neurol.*, 250: 81-92.

Aubert, I., Cécyre, D., Gauthier, S. and Quirion, R. (1996) Comparative ontogenic profile of cholinergic markers, including nicotinic and muscarinic receptors, in the rat brain. *J. Comp. Neurol.*, 369: 31-55.

Audet, M.A., Doucet, G., Oleskevich, S. and Descarries, L. (1988) Quantified regional and laminar distribution of the noradrenaline innervation in the anterior half of the adult rat cerebral cortex. *J. Comp. Neurol.*, 274: 307-318.

Audet, M.A., Descarries, L. and Doucet, G. (1989) Quantified regional and laminar distribution of the serotonin innervation in the anterior half of adult rat cerebral cortex. *J. Chem. Neuroanat.*, 2: 29-44.

Aznavour, N., Mechawar, N. and Descarries, L. (2002) Comparative analysis of cholinergic innervation in the dorsal hippocampus of adult mouse and rat: a quantitative immunocytochemical study. *Hippocampus*, 12: 206-217.

Aznavour, N., Mechawar, N., Watkins, K.C. and Descarries, L. (2003) Fine structural features of the acetylcholine innervation in the developing neostriatum of rat. *J Comp Neurol* 460: 280-291.

Bayraktar, T., Staiger, J.F., Acsady, L., Cozzari, C., Freund, T.F. and Zilles, K. (1997) Co-localization of vasoactive intestinal polypeptide, γ-aminobutyric acid and choline acetyltransferase in neocortical interneurons of the adult rat. *Brain Res.*, 757: 209-217.

Bear, M.F. and Singer, W. (1986) Modulation of visual cortical plasticity by acetylcholine and noradrenaline. *Nature*, 320: 172-176.

Broide, R.S., Robertson, R. T. and Leslie, F.M. (1996) Regulation of $\alpha_7$ nicotinic acetylcholine receptors in the developing rat somatosensory cortex by thalamocortical afferents. *J. Neurosci.*, 16: 2956-2971.

Buzsàki, G., Bickford, R.G., Ponomareff, G., Thal, L.J., Mandel, R. and Gage, F.H. (1988) Nucleus basalis and thalamic control of neocortical activity in the freely moving rat. *J. Neurosci.*, 8: 4007-4026.

Celesia, G.G. and Jasper, H.H. (1966) Acetylcholine released from cerebral cortex in relation to state of activation. *Neurology*, 16: 1053-1063.

Chédotal, A., Cozzari, C., Faure, M.P., Hartman, B.K. and Hamel, E. (1994) Distinct choline acetyltransferase (ChAT) and vasoactive intestinal polypeptide (VIP)

bipolar neurons project to local blood vessels in the rat cerebral cortex. *Brain Res.*, 646: 181-193.

Cox, C.L., Metherate, R. and Ashe, J.H. (1994) Modulation of cellular excitability in neocortex: muscarinic receptor and second messenger-mediated actions of acetylcholine. *Synapse*, 16: 123-136.

Coyle, J.T. and Yamamura, H.I. (1976) Neurochemical aspects of the ontogenesis of cholinergic neurons in the rat brain. *Brain Res.*, 118: 429-440.

Cozzari, C., Howard, J. and Hartman, B. (1990) Analysis of epitopes on choline acetyltransferase (ChAT) using monoclonal antibodies (Mabs). *Soc. Neurosci. Abstr.*, 16: 200.

Descarries, L. (1998) The hypothesis of an ambient level of acetylcholine in the central nervous system. *J. Physiol. (Paris)*, 92: 215-220.

Descarries, L. and Mechawar, N. (2000) Ultrastructural evidence for diffuse transmission by monoamine and acetylcholine neurons of the central nervous system. *Progr. Brain Res.*, 125: 27-47.

Descarries, L., Gisiger, V. and Steriade, M. (1997) Diffuse transmission by acetylcholine in the CNS. *Progr. Neurobiol.*, 53: 603-625.

Donoghue, J.P. and Carroll, K.L. (1987) Cholinergic modulation of sensory responses in rat primary somatic sensory cortex. *Brain Res.*, 408: 367-371.

Dori, I. and Parnavelas, J. G., (1989) The cholinergic innervation of the rat cerebral cortex shows two distinct phases in development. *Exp. Brain Res.*, 76: 417-423.

Eckenstein, F. and Baughman R.W. (1987) Cholinergic innervation in cerebral cortex. In E.G. Jones and A. Peters (Eds.), *Cerebral Cortex. Further Aspects of Cortical Function, Including Hippocampus*, Vol. 6, Plenum Press, New York, pp. 129-160.

Elhusseiny, A. and Hamel, E. (2000) Muscarinic, but not nicotinic, acetylcholine receptors mediate a nitric oxide-dependent dilation in brain cortical arterioles: a possible role for the M5 receptor subtype. *J. Cereb. Blood Flow Metab.*, 20: 298-305.

Engel, A.K. and Singer, W. (2001) Temporal binding and the neural correlates of sensory awareness. *Trends Cog. Sci.*, 5: 16-25.

Fine, A., Hoyle, C., Maclean, C.J., Levatte, T.L., Baker, H.F. and Ridley, R.M. (1997) Learning impairments following injection of a selective cholinergic immunotoxin, ME20.4 IgG-saporin, into the basal nucleus of Meynert in monkeys. *Neuroscience*, 81: 331-343.

Gage, F.H., Björklund, A., Stenevi, U. (1983) Reinnervation of the partially deafferented hippocampus by compensatory collateral sprouting from spared cholinergic and noradrenergic afferents. *Brain Res.*, 268: 27-37.

Gill, T.M., Sarter M. and Givens B. (2000) Sustained visual attention performance-associated prefrontal neuronal activity: evidence for cholinergic modulation.

*J. Neurosci.*, 20: 4745-4757.

Gisiger, V. and Stephens, H.R. (1988) Localization of the pool of $G_4$ acetylcholinesterase characterizing fast muscles and its alteration in murine muscular dystrophy. *J. Neurosci. Res.*, 19: 62-78.

Gould, E., Woolf, N.J. and Butcher, L.L. (1991) Postnatal development of cholinergic neurons in the rat: I. Forebrain. *Brain Res. Bull.*, 27:767-789.

Gritti, I., Mainville, L. and Jones, B.E. (1993) Codistribution of GABA- with acetylcholine-synthesizing neurons in the basal forebrain of the rat. *J. Comp. Neurol.*, 329: 438-457.

Hasselmo, M.E. and Schnell, E. (1994) Laminar selectivity of the cholinergic suppression of synaptic transmission in rat hippocampal region CA1: computational modeling and brain slice physiology. *J. Neurosci.*, 14: 3898-3914.

Hasselmo, M.E., Anderson, B.P. and Bower, J.M. (1992) Cholinergic modulation of cortical associative memory function. *J. Neurophysiol.*, 67: 1230-1246.

Hill, J.A., Zoli, M., Bourgeois, J.-P. and Changeux, J.-P. (1993) Immunocytochemical localization of a neuronal nicotinic receptor: the β2-subunit. *J. Neurosci.*, 13: 1551-1568.

Ibanez, C.F., Ernfors, P. and Persson, H. (1991) Developmental and regional expression of choline acetyltransferase mRNA in the rat central nervous system. *J. Neurosci. Res.*, 29:163-171.

Jasper, H.H. and Tessier, J. (1971) Acetylcholine liberation from cerebral cortex during paradoxical (REM) sleep. *Science*, 172: 601-602.

Jiménez-Capdeville, M.E., Dykes, R.W. (1996) Changes in cortical acetylcholine release in the rat during day and night : differences between motor and sensory areas. *Neuroscience*, 71: 567-579.

Juliano, S.L., Ma, W. and Eslin, D. (1991) Cholinergic depletion prevents expansion of topographic maps in somatosensory cortex. *Proc. Natl Acad. Sci. USA*, 88: 780-784.

Kilgard, M.P. and Merzenich, M.M. (1998) Cortical map reorganization enabled by nucleus basalis activity. *Science*, 279: 1714-1718.

Kimura, F. (2000) Cholinergic modulation of cortical function: a hypothetical role in shifting the dynamics in cortical network. *Neurosci. Res.*, 38: 19-26.

Kimura, F., Fukuda, M. and Tsumoto, T. (1999) Acetylcholine suppresses the spread of excitation in the visual cortex revealed by optical recording : possible differential effect depending on the source of input. *Eur. J. Neurosci.*, 11: 3597-3609.

Kosasa, T., Kuriya, Y. and Yamanishi, Y. (1999) Effect of donepezil hydrochloride (E2020) on extracellular acetylcholine concentration in the cerebral cortex of rats. *Jpn. J. Pharmacol.*, 81: 216-22.

Krnjevic, K. and Phillis, J.W. (1963a) Acetylcholine-sensitive cells in the cerebral cortex. *J. Physiol. (London)*, 166: 296-327.

Krnjevic, K. and Phillis, J.W. (1963b) Pharmacological properties of acetylcholine-sensitive cells in the cerebral cortex. *J. Physiol. (London)*, 166: 328-350.

Lamour, Y., Dutar, P., Jobert, A. and Dykes, R.W. (1988) An iontophoretic study of single somatosensory neurons in rat granular cortex serving the limbs: a laminar analysis of glutamate and acetylcholine effects on receptive-field properties. *J. Neurophysiol.*, 60: 725-750.

Latsari, M., Dori, I., Antonopoulos, J., Chiotelli, M. and Dinopoulos, A. (2002) Noradrenergic innervation of the developing and mature visual and motor cortex of the rat brain: a light and electron microscopic immunocytochemical analysis. *J. Comp. Neurol.*, 445: 145-158.

Lubin, M., Erisir, A. and Aoki, C. (1999) Ultrastructural immunolocalization of the α7 nAChR subunit in guinea pig medial prefrontal cortex. *Ann. NY Acad. Sci.*, 868: 628-632.

Lysakowski, A., Wainer, B.H., Bruce, G. and Hersh, L.B. (1989) An atlas of the regional and laminar distribution of choline acetyltransferase immunoreactivity in rat cerebral cortex. *Neuroscience*, 28: 291-336.

Ma, W., Maric, D., Li, B.-s., Hu, Q., Andreadis, J.D., Grant, G.M., Liu, Q.-Y., Shaffer, K.M., Chang, Y.H., Zhang, L., Pancrazio, J.J., Pant, H.C., Stenger, D.A. and Barker, J.L. (2000) Acetylcholine stimulates cortical precursor cell proliferation *in vitro* via muscarinic receptor activation and MAP kinase phosphorylation. *Eur. J. Neurosci.*, 12: 1227-1240.

McKenna, T.M., Ashe, J.H., Hui, G.K. and Weinberger, N.M. (1988) Muscarinic agonists modulate spontaneous and evoked unit discharge in auditory cortex of cat. *Synapse*, 2: 54-68.

McKinney, M., Coyle, J.T. and Hedreen, J.C. (1983) Topographic analysis of the innervation of the rat neocortex and hippocampus by the basal forebrain cholinergic system. *J. Comp. Neurol.*, 217: 103-121.

Mechawar, N. and Descarries, L. (2001) The cholinergic innervation develops early and rapidly in the rat cerebral cortex: a quantitative immunocytochemical study. *Neuroscience*, 108: 555-567.

Mechawar, N., Cozzari, C. and Descarries, L. (2000) Cholinergic innervation in adult rat cerebral cortex: a quantitative immunocytochemical description. *J. Comp. Neurol.*, 428: 305-318.

Mechawar, N., Watkins, K.C. and Descarries, L. (2002) Ultrastructural features of the acetylcholine innervation in the developing parietal cortex of rat. *J. Comp. Neurol.*, 443: 250-258.

Mesulam, M.M., Mufson, E.J., Wainer B.H. and Levey A.I. (1983) Central cholinergic pathways in the rat: an overview based on an alternative nomenclature (Ch1-Ch6). *Neuroscience*, 10: 1185-1201.

Metherate, R., Tremblay, N. and Dykes, R.W. (1988) Transient and prolonged effects of acetylcholine on responsiveness of cat somatosensory cortical neurons. *J. Neurophysiol.*, 59: 1253-1276.

Metherate, R., Cox, C.L. and Ashe, J.H. (1992) Cellular bases of neocortical activation: modulation of neural oscillations by the nucleus basalis and endogenous acetylcholine. *J. Neurosci.*, 12: 4701-4711.

Miranda, M.I. and Bermúdez-Rattoni, F. (1999) Reversible inactivation of the nucleus basalis magnocellularis induces disruption of cortical acetylcholine release and acquisition, but not retrieval, of aversive memories. *Proc. Natl Acad. Sci. USA*, 96: 6478-6482.

Mitchell, J.F. (1963) The spontaneous and evoked release of acetylcholine from the cerebral cortex. *J. Physiol. (London)*, 165: 98-116.

Mrzljak, L., Pappy, M., Leranth, C. and Goldman-Rakic, P.S. (1995) Cholinergic synaptic circuitry in the macaque prefrontal cortex. *J. Comp. Neurol.*, 357: 603-617.

Mrzljak, L., Levey, A.I., Belcher, S. and Goldman-Rakic, P.S. (1998) Localization of the m2 muscarinic acetylcholine receptor protein and mRNA in cortical neurons of the normal and cholinergically deafferented rhesus monkey. *J. Comp. Neurol.*, 390: 112-132.

Nilsson, O.G., Kalén, P., Rosengren, E. and Björklund, A. (1990) Acetylcholine release in rat hippocampus as studied by microdialysis is dependent on axonal impulse flow and increases during behavioral activation. *Neuroscience*, 36: 325-328.

Nyakas, C., Luiten, P.G., Spencer, D.G. and Traber, J. (1987) Detailed projection patterns of septal and diagonal band efferents to the hippocampus in the rat

with emphasis on innervation of CA1 and dentate gyrus. *Brain Res. Bull.*, 18: 533-545.

Oleskevich, S. and Descarries, L. (1990) Quantified distribution of the serotonin innervation in adult rat hippocampus. *Neuroscience*, 34: 19-33.

Oleskevich, S., Descarries, L. and Lacaille, J.C. (1989) Quantified distribution of the noradrenaline innervation in the hippocampus of adult rat. *J. Neurosci.*, 9: 3803-3815.

Ostermann, C.-H., Grunwald, J., Wevers, A., Lorke, D. E., Reinhardt, S., Maelicke, A. and Schröder, H. (1995) Cellular expression of $\alpha$4 subunit mRNA of the nicotinic acetylcholine receptor in the developing rat telencephalon. *Neurosci. Lett.*, 192: 21-24.

Pedata, F., Slavikova, J., Kotas, A. and Pepeu, G. (1983) Acetylcholine release from rat cortical slices during postnatal development and aging. *Neurobiol. Aging*, 4: 31-35.

Peinado, A. (2000) Traveling slow waves of neural activity: a novel form of network activity in developing neocortex. *J. Neurosci.*, 20: RC54 (1-6).

Perry, E., Walker, M., Grace, J. and Perry, R. (1999) Acetylcholine in mind: A neurotransmitter correlate of consciousness. *Trends Neurosci.*, 22: 273-280.

Pirch, J.H., Turco, K. and Rucker, H.K. (1992) A role for acetylcholine in conditioning-related responses of rat frontal cortex neurons: microiontophoretic evidence. *Brain Res.*, 586: 19-26.

Porter, J.T., Cauli, B., Tsuzuki, K., Lambolez, B., Rossier, J. and Audinat, E. (1999) Selective excitation of subtypes of neocortical interneurons by nicotinic receptors. *J. Neurosci.*, 19: 5228-5235.

Rasmusson, D.D. and Dykes, R.W. (1988) Long-term enhancement of evoked potentials in cat somatosensory cortex by co-activation of the basal forebrain and cutaneous receptors. *Exp. Brain Res.*, 70: 276-286.

Richter, D. and Crossland, J. (1949) Variation in acetylcholine content of the brain with physiological state. *Am. J. Physiol.*, 159: 247-255.

Rigdon, G.C. and Pirch, J.H. (1986) Nucleus basalis involvement in conditioned neuronal responses in the rat frontal cortex. *J. Neurosci.*, 6: 2535-2542.

Rouse, S.T, Edmunds, S.M., Yi, H., Gilmor M.L. and Levey A.I. (2000) Localization of M2 muscarinic acetylcholine receptor protein in cholinergic and non-cholinergic terminals in rat hippocampus. *Neurosci. Lett.* 284: 182-186.

Rye, D.B., Wainer, B.H., Mesulam, M.-M., Mufson, E.J. and Saper, C.B. (1984) Cortical projections arising from the basal forebrain: a study of cholinergic and noncholinergic components employing combined retrograde tracing and immunohistochemical localization of choline acetyltransferase. *Neuroscience*, 13: 627-643.

Saper, C.B. (1984) Organization of the cerebral cortical afferent systems in the rat. II. Magnocellular basal nucleus. *J. Comp. Neurol.*, 222: 313-342.

Schwegler, H., Boldyreva, M., Linke, R., Wu, J., Zilles, K. and Crusio, W.E. (1996) Genetic variation in the morphology of the septo-hippocampal cholinergic and

GABAergic systems in mice: II. Morpho-behavioral correlations. *Hippocampus*, 6: 535-545.

Sillito, A.M. and Kemp, J.A. (1983) Cholinergic modulation of the functional organization of the cat visual cortex. *Brain Res.*, 289: 143-155.

Smiley, J.F., Morrell, F. and Mesulam, M.-M. (1997) Cholinergic synapses in human cerebral cortex: an ultrastructural study in serial sections. *Exp. Neurol.*, 144: 361-368.

Steriade, M. and Amzica, F. (1996) Intracortical and corticothalamic coherency of fast spontaneous oscillations. *Proc. Natl. Acad. Sci. USA* 93:2533-2538.

Steriade, M., Paré, D., Parent, A. and Smith, Y. (1988) Projections of cholinergic and non-cholinergic neurons of the brainstem core to relay and associational thalamic nuclei in the cat and macaque monkey. *Neuroscience* 25:47-67.

Steriade, M., Amzica, F. and Contreras, D. (1996) Synchronization of fast (30-40Hz) spontaneous cortical rhythms during brain activation. *J. Neurosci.* 16:392-417.

Tremblay, N., Warren, R.A. and Dykes, R.W. (1990) Electrophysiological studies of acetylcholine and the role of the basal forebrain in the somatosensory cortex of the cat. II. Cortical neurons excited by somatic stimuli. *J. Neurophysiol.*, 64: 1212-1222.

Turrini, P., Casu, M.A., Wong, T.P., De Koninck, Y., Ribeiro-Da-Silva, A. and Cuello, A.C. (2001) Cholinergic nerve terminals establish classical synapses in the rat cerebral cortex: synaptic pattern and age-related atrophy. *Neuroscience.*,

105: 277-285.

Umbriaco, D., Watkins, K.C., Descarries, L., Cozzari C. and Hartman, B.K. (1994) Ultrastructural and morphometric features of the acetylcholine innervation in adult rat parietal cortex. An electron microscopic study in serial sections. *J. Comp. Neurol.,* 348: 351-373.

Umbriaco, D., Garcia, S., Beaulieu, C. and Descarries, L. (1995) Relational features of acetylcholine, noradrenaline, serotonin and GABA axon terminals in the stratum radiatum of adult rat hippocampus (CA1). *Hippocampus*, 5: 605-620.

Vaucher, E. and Hamel, E. (1995) Cholinergic basal forebrain neurons project to cortical microvessels in the rat: electron microscopic study with anterogradely transported *Phaseolus vulgaris* leucoagglutinin and choline acetyltransferase immunocytochemistr. *J. Neurosci.,* 15: 7427-7441.

Voytko, M.L., Olton, D.S., Richardson, R.T., Gorman, L.K., Tobin, J.R., Price, D.L. (1994) Basal forebrain lesions in monkeys disrupt attention but not learning and memory. *J. Neurosci.*, 14: 167-186.

Wessler, I., Kirkpatrick, C.J. and Racké, K. (1998) Non-neuronal acetylcholine, a locally acting molecule, widely distributed in biological systems: expression and function in humans. *Pharmacol. Ther.*, 77: 59-79.

Whitehouse, P.J., Price, D.L., Clark, A.W., Coyle, J.T. and DeLong, M.R. (1981) Alzheimer disease : evidence for selective loss of cholinergic neurons in the nucleus basalis. *Ann. Neurol.*, 10: 122-126.

Woolf, N.J. (1991) Cholinergic systems in mammalian brain and spinal cord. *Progr.*

*Neurobiol.*, 37: 475-524.

Zhu, X.O. and Waite, P.M.E. (1998) Cholinergic depletion reduces plasticity of barrel field cortex. *Cereb. Cortex*, 8: 63-72.

Zoli, M., Le Novère, Hill Jr., J.A. and Changeux, J.-P. (1995) Developmental regulation of nicotinic ACh receptor subunit mRNAs in the central and peripheral nervous system. *J. Neurosci.*, 15: 1912-1939.

## Figure legends

**Figure 1** Low power micrographs illustrating the laminar distribution of ACh (ChAT-immunopositive) fibers in transverse sections from three neocortical areas: frontal, primary motor, Fr1; parietal, primary somatosensory, Par 1; occipital, primary visual, Oc1. Narrow strips from adjacent Nissl-stained sections, which helped to delinetate the cortical layers, are also shown. In each area, small, fusiform, bipolar cholinergic interneurons, with their vertically oriented dendrites, are scattered in layers II-VI, amidst the intricate network of fine varicose fibers pervading the entire cortical thickness. In the lower part of layer VI, immediately above the callosal radiations, smooth and thicker, transversely oriented fibers are also visible. (Reproduced with permission from Mechawar et al., 2000).

**Figure 2** Densities of ACh axons (A) and axon varicosities (B) in the different layers (I-VI) of the frontal (Fr1), parietal (Par1) and occipital (Oc1) neocortex and the dorsal hippocampus (CA1, CA3 and DG) of adult rat. Mean values (± s.e.m) from five and six rats in cortex and hippocampus, respectively. The data are expressed in density of ACh axons (upper scale) and density of axon varicosities (lower scale), as the number of axon varicosities per unit lenght of axons was stable in all regions at 4 per 10 μm. The layers showing statistically significant differences are linked by hooks, with asterisks in front of the differing layer(s). * $p < 0.005$ (cortex); ** ($p < 0.01$) and *** ($p < 0.001$) (hippocampus) indicate

significant differences between layers by Student t test. (Modified from Mechawar et al., 2000, and Azanavour et al., 2002).

**Figure 3** Temporal profile of laminar and regional densities of ACh innervation in the frontal, parietal and occipital neocortex, at different postnatal ages (P4 - P32) and in the adult. Means from 3 rats per age, except at P60 (n = 5). Data for the different layers (I, II/III or II/IV, V and VI) and the whole cortex (I-VI) are expressed as densities (left graphs) and number of ACh axon varicosities under 1 $mm^2$ of cortical surface (right graphs), as explained in the text. (Modified from Mechawar and Descarries, 2001).

**Figure 4A-F** Electron micrographs of asynaptic (A,C,E) and synaptic (B,D,F) ACh axon varicosities from rat parietal cortex, at postnatal ages P8 (A-B), P16 (C-D) and P32 (E-F). These ChAT-immunostained profiles are identified as axon varicosities by their content in aggregated synaptic vesicles, often associated with a mitochondrion. The two ACh varicosities at P8 (A, B) are from layers VI and V, respectively. The one in B makes a symmetrical synaptic junction (between thin arrows) on a dendritic branch (upper d). Both the ACh varicosities at P16 are from layer VI. In C, the non synaptic ACh profile is juxtaposed to the base of a dendritic trunk (dt). The synapse made by the ACh varicosity in D (between thin arrows) is again symmetrical and made with a dendritic branch (d). The two ACh varicosities at P32 are from layer V. The one in E is juxtaposed to a dendritic branch (d), below, and a neuronal cell body (N), above. The synapse made by the

varicosity in F is of the perforated type, asymmetrical, and made with a dendritic spine which also receives two other synaptic varicosities ($V_2$ and $V_3$), unlabeled. Scale bar (in F): 0.5 $\mu$m. (Reproduced with permission from Mechawar et al., 2002).

**Figure 5** Schematic representation of a non synaptic ACh axon terminal (varicosity) in the cerebral cortex (see Fig. 1A in Descarries et al.,1997), from which ACh (in blue) has been released to diffuse in the extracellular space and contribute to a low ambient level of ACh around a variety of neighboring cellular elements. The extracellular space has been widened for illustrating purposes. ACh receptors, many of which are located extrasynaptically on diverse potential targets, are represented by small red triangles. as, astrocyte; av, axon varicosity; d, dendrite; n, neurite; sp, dendritic spine.

## Table 1

**REGIONAL DISTRIBUTION OF THE ACh INNERVATION IN ADULT RAT CEREBRAL CORTEX AND HIPPOCAMPUS**

| | NEOCORTEX | | | DORSAL HIPPOCAMPUS | | |
|---|---|---|---|---|---|---|
| | Frontal | Parietal | Occipital | CA1 | CA3 | DG |
| Axons | | | | | | |
| density ($m/mm^3$) | 13.0 | 9.9 | 11.0 | 12.2 | 16.2 | 15.6 |
| length under 1 $mm^2$ (m) | 26.7 | 19.7 | 15.3 | - | - | - |
| Varicosities | | | | | | |
| density ($10^6/mm^3$) | 5.4 | 3.8 | 4.6 | 4.9 | 6.6 | 6.2 |
| number under 1 $mm^2$ ($10^6$) | 11.1 | 7.7 | 6.4 | - | - | - |

Data from Mechawar et al. (2000) and Aznavour et al. (2002), as explained in the text.

**Table 2**

**SYNAPTIC AND ASYNAPTIC ACh AXON VARICOSITIES IN ADULT RAT**

**PARIETAL CORTEX AND DORSAL HIPPOCAMPUS**

| | PARIETAL CORTEX | | | | | | DORSAL HIPPOCAMPUS | |
|---|---|---|---|---|---|---|---|---|
| Layer | I | II-III | IV | V | VI | *I-VI* | CA1: stratum radiatum | |
| Synaptic incidence | 10% | 14% | 11% | 21% | 14% | *16%* | 7% | |
| Varicosities under 1 $mm^2$ ($10^6$) | | 0.69 | 1.05 | 0.70 | 2.82 | 2.44 | 7.70 | 0.93 |
| asynaptic | 0.62 | 0.90 | 0.62 | 2.23 | 2.10 | *6.47* | 0.87 | |
| synaptic | 0.07 | 0.15 | 0.08 | 0.59 | 0.34 | *1.23* | 0.06 | |

Synaptic incidence as estimated in Umbriaco et al. (1994) for cortex, and Umbriaco et al., (1995) for hippocampus. Data on the number of varicosities under 1 $mm^2$ from Mechawar et al. (2000) for cortex, and Aznavour et al. (2002) for hippocampus.

## Table 3

**SYNAPTIC AND ASYNAPTIC ACh AXON VARICOSITIES IN THE DEVELOPING PARIETAL CORTEX OF RAT**

| Age | P4 | P8 | P16 | P32 |
|---|---|---|---|---|
| Synaptic incidence | - | 13.2% | 15.6% | 22.2% |
| Varicosities under 1 $mm^2$ ($10^6$) | 0.40 | 2.0 | 6.6 | 8.3 |
| asynaptic | - | 1.7 | 5.6 | 6.5 |
| synaptic | - | 0.3 | 1.0 | 1.8 |

Synaptic incidence as estimated in Mechawar et al. (2002). Data on the number of varicosities under 1 $mm^2$ from Mechawar and Descarries (2001).

## Table 4

**DENSITY OF MODULATORY INPUTS TO ADULT RAT CEREBRAL CORTEX AND HIPPOCAMPUS**

| | NEOCORTEX | | | DORSAL HIPPOCAMPUS | | |
|---|---|---|---|---|---|---|
| | ACh | NA | 5-HT | ACh | NA | 5-HT |
| Synaptic incidence | 14% [1] | 17% [2] | 38% [3] | 7% [4] | 16% [5] | 22% [6] |
| Number per $mm^3$ ($10^6$) | 4.60 [7] | 1.05 [8] | 4.55 [9] | 5.9 [10] | | 2.0 [11] |
| | 2.65 [12] | | | | | |
| asynaptic | 4.0 | 0.87 | 2.82 | 5.5 | 1.28 | 2.07 |
| synaptic | 0.6 | 0.18 | 1.73 | 0.4 | 0.32 | 0.58 |

Values of synaptic incidence are from [1] the parietal cortex (Umbriaco et al., 1994); [2,3] the frontal (Fr1), parietal (Par1) and occipital (Oc1) cortex (Séguéla et al., 1989, 1990); [4,5] the stratum radiatum of CA1 (Umbriaco et al., 1995) ; [6] CA1, CA3 and DG (Oleskevich et al., 1991; Umbriaco et al., 1995). Numbers of varicosities per $mm^3$ are

from the frontal, parietal, and occipital cortex (Mechawar et al., 2000); [8,9] the frontal and parietal cortex (Audet et al., 1988, 1989); [10,11,12] CA1, CA3 and DG (Oleskevich et al, 1989; Oleskevich and Descarries, 1990; Aznavour et al., 2002).

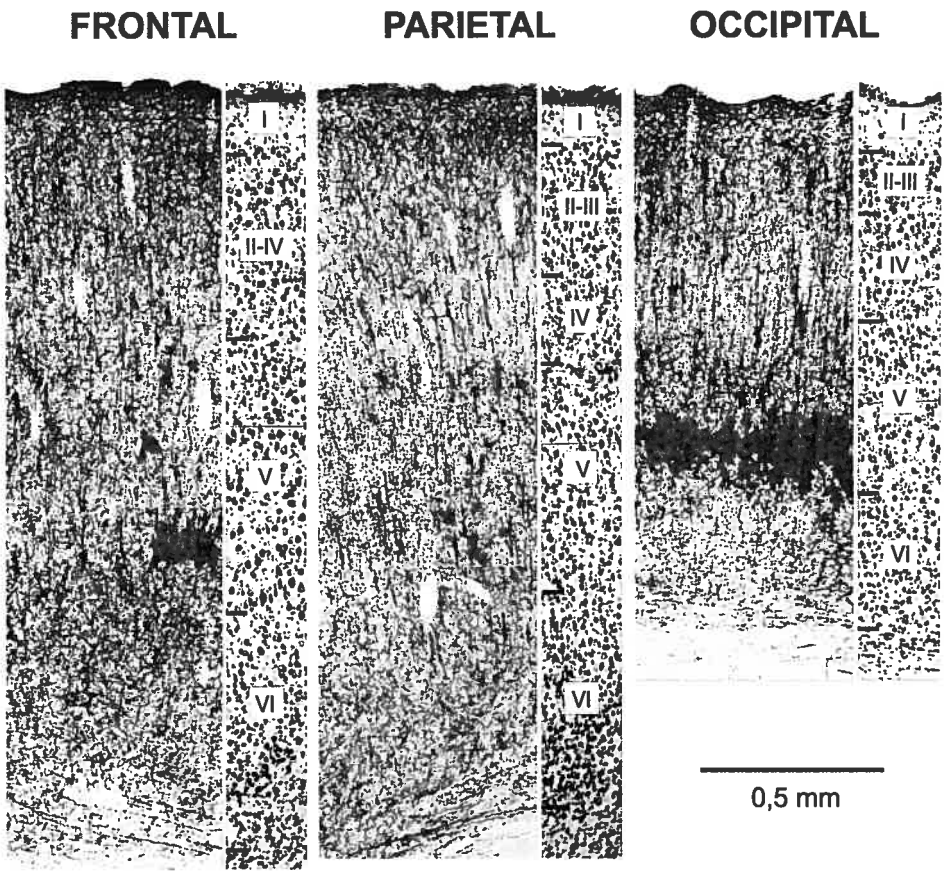
FRONTAL
PARIETAL
OCCIPITAL
I
II-IV
V
VI
I
II-III
IV
V
VI
I
II-III
IV
V
VI
0,5 mm

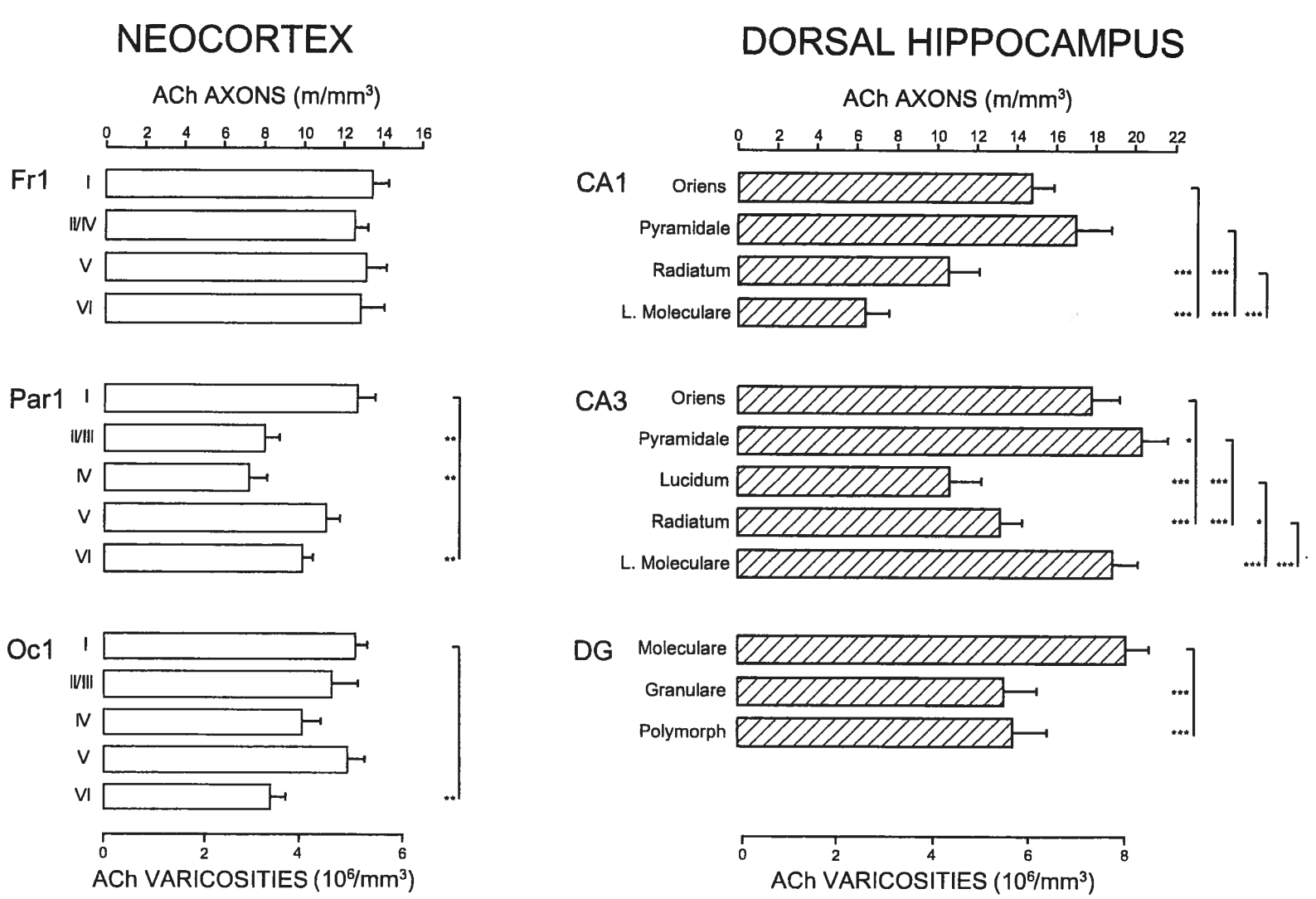
NEOCORTEX
ACh AXONS (m/mm³)
0 2 4 6 8 10 12 14 16
Fr1
I
II/IV
V
VI
Par1
I
II/III
IV
V
VI
**
**
**
Oc1
I
II/III
IV
V
VI
**
0 2 4 6
ACh VARICOSITIES (10⁶/mm³)
DORSAL HIPPOCAMPUS
ACh AXONS (m/mm³)
0 2 4 6 8 10 12 14 16 18 20 22
CA1
Oriens
Pyramidale
Radiatum
L. Moleculare
***
***
***
***
***
***
CA3
Oriens
Pyramidale
Lucidum
Radiatum
L. Moleculare
*
***
***
***
***
*
***
***
DG
Moleculare
Granulare
Polymorph
***
***
0 2 4 6 8
ACh VARICOSITIES (10⁶/mm³)

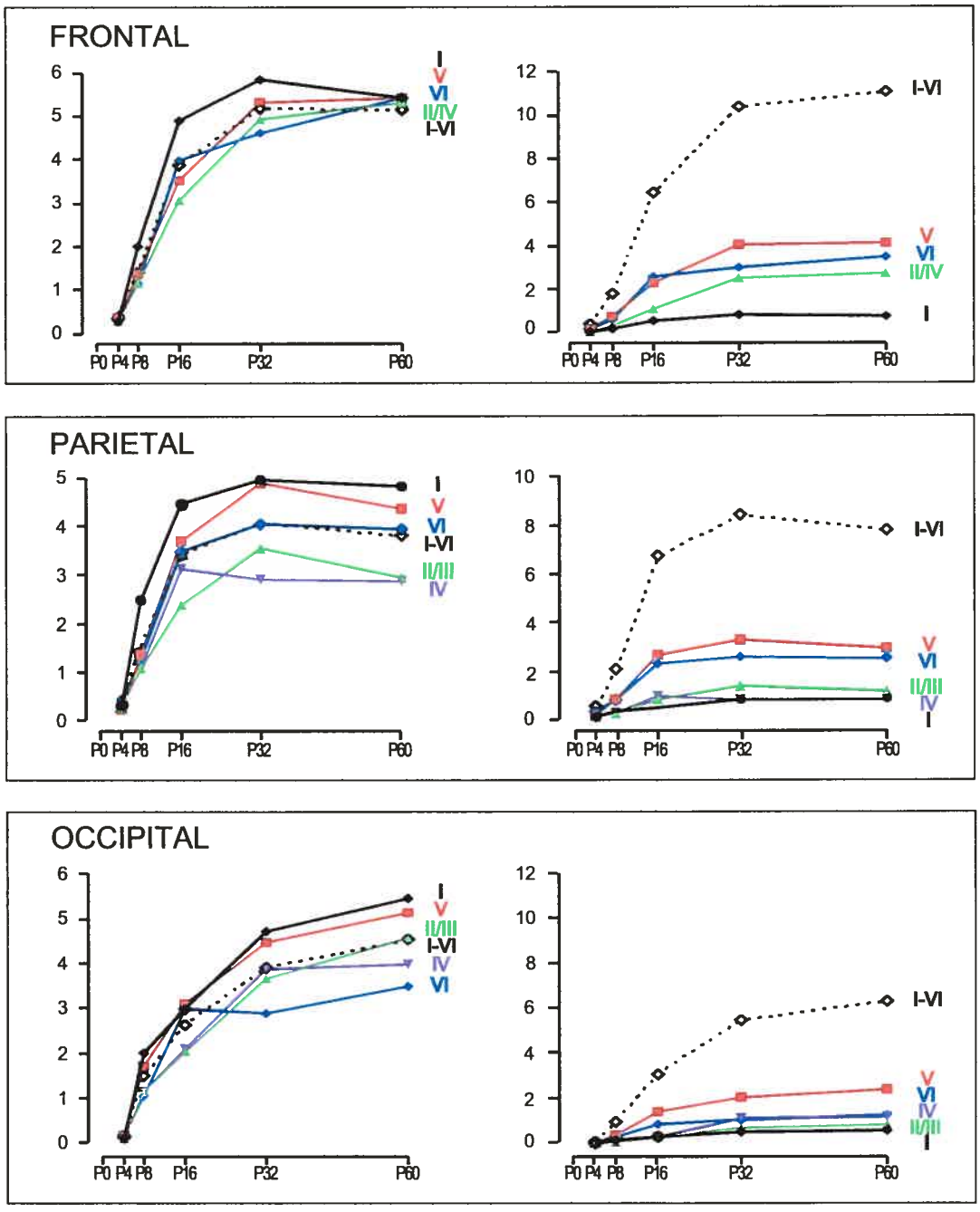
Density (10⁶/mm³)
N under 1 mm² (10⁶)
FRONTAL
PARIETAL
OCCIPITAL
I
V
VI
II/IV
I-VI
II/III
IV
P0 P4 P8 P16 P32 P60

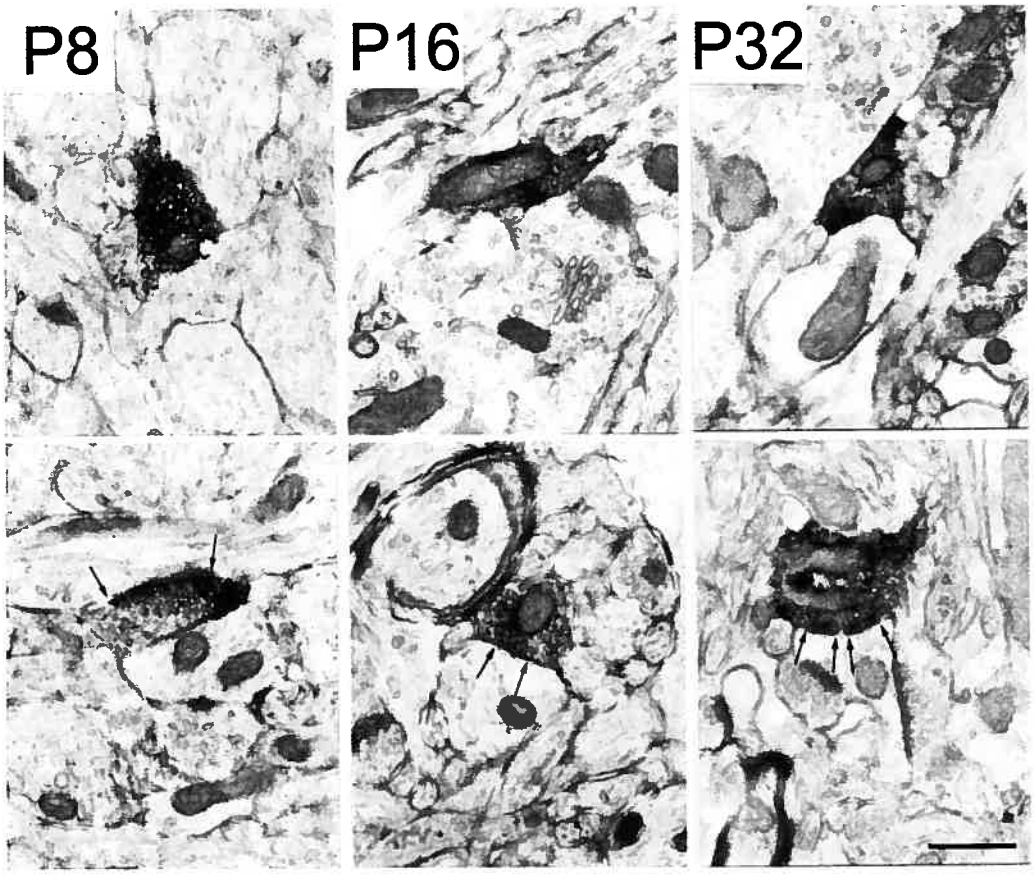
P8
P16
P32

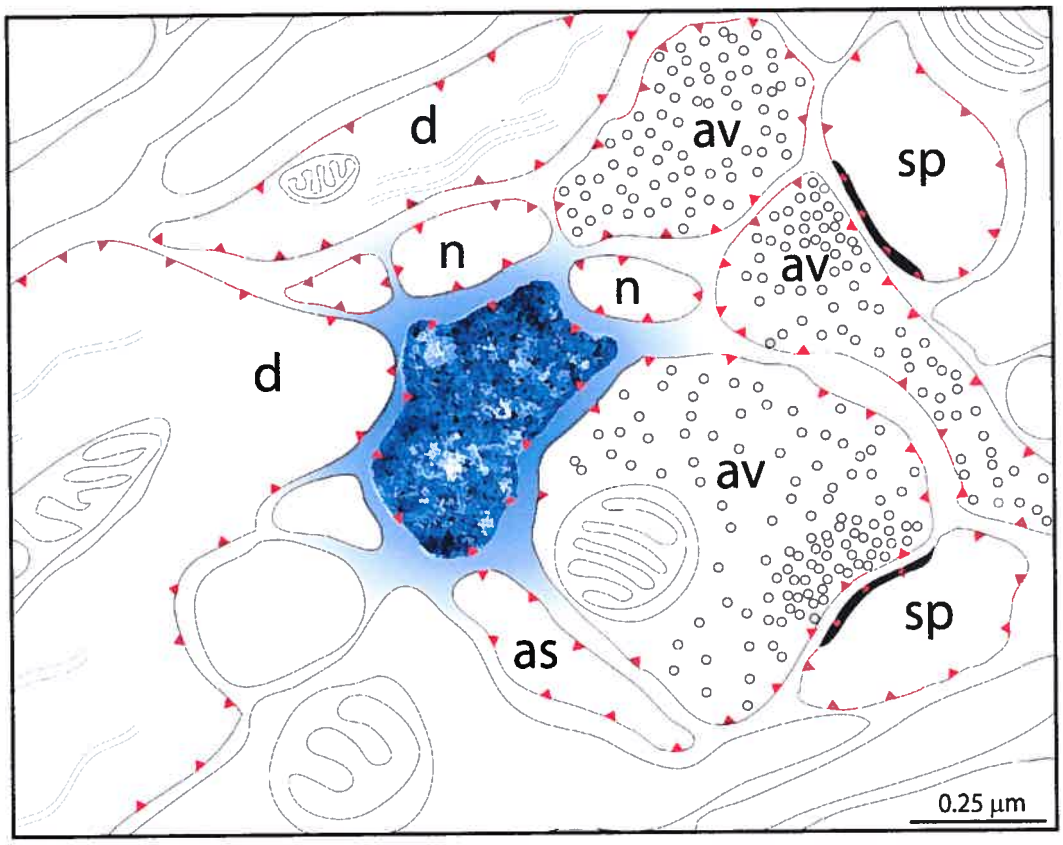
d
av
sp
n
n
av
d
av
sp
as
0.25 µm